Novel Polymer Electrolyte Nano-Composite Membranes for Fuel Cell Applications

by

Hadis Zarrin

A thesis
presented to the University of Waterloo
in fulfillment of the
thesis requirement for the degree of
Doctor of Philosophy
in
Chemical Engineering

Waterloo, Ontario, Canada, 2014

AUTHOR'S DECLARATION

This thesis consists of material all of which I authored or co-authored: see Statement of Contributions included in the thesis. This is a true copy of the thesis, including any required final revisions, as accepted by my examiners.

I understand that my thesis may be made electronically available to the public.

Statement of Contributions

Chapter 4 is based on published work by Jun et al. Jun et al. entitled “Functionalized Titania Nanotube Composite Membranes for High Temperature Proton Exchange Membrane Fuel Cells” in International Journal of Hydrogen Energy (2011), 36, 10, 6073-6081, and is reproduced with permission from the International Journal of Hydrogen Energy. The thesis author's specific contributions to this paper were to synthesize and fabricate the nano-composite membrane, conduct the electrochemical impedance spectroscopy (EIS) measurements, run some parts of physicochemical characterization tests including water uptake and TGA, prepare the final plots and results, write the final manuscript and respond to the comments of reviewers. This work and journal paper preparation was conducted with direction from the project supervisors who are co-authors on the publication. The post-doc fellow, Yu Jun aided with the main idea development and performing most of physicochemical characterization tests including XRD, XPS, FT-IR, and TEM.

Chapter 5 is based on published work by Zarrin et al. entitled “Functionalized Graphene Oxide Nanocomposite Membrane for Low Humidity and Intermediate Temperature PEMFCs” in Journal of Physical Chemistry C (2011), 115, 20774-20781, and is reproduced with permission from the Journal of Physical Chemistry C. The thesis author's specific contributions to this paper were to synthesize and fabricate nano-composite membrane, conduct EIS measurements, run most of physicochemical characterization tests, prepare all plots and results, write the final manuscript and respond to the comments of reviewers. This work and journal paper preparation was conducted with direction from the project supervisors who are co-authors on the publication. Yu Jun aided with the synthesis and

performed some of physicochemical characterization tests. Drew Higgins assisted in editing the manuscript.

Chapter 6 is based on published work by Zarrin et al. entitled “High Durable PEK-based Anion Exchange Membrane for Elevated Temperature Alkaline Fuel Cells” in Journal of Membrane Science (2012), 394-395, 193-201, and is reproduced with permission from the Journal of Membrane Science. The thesis author's specific contributions to this paper were to synthesize and fabricate the anion exchange membrane (AEM), conduct EIS measurements, run all of physicochemical characterization tests, prepare all plots and results, write the final manuscript and respond to the comments of reviewers. This work and journal paper preparation was conducted with direction from the project supervisors who are co-authors on the publication. Jason Wu assisted in editing the manuscript.

Chapter 7 is based on published work by Zarrin et al. entitled “High performance porous polybenzimidazole membrane for alkaline fuel cells” in International Journal of Hydrogen Energy (2014), 39, 32, 18405-18415, and is reproduced with permission from the International Journal of Hydrogen Energy. The thesis author's specific contributions to this paper were to synthesize and fabricate the AEM, conduct EIS measurements, run all of physicochemical characterization tests, prepare all plots and results, write the final manuscript and respond to the comments of reviewers. This work and journal paper preparation was conducted with direction from the project supervisors who are co-authors on the publication. Gaopeng Jiang aided with testing the single AEMFC performance. Grace Lam helped to conduct alkaline stability tests.

Chapter 8 is based on submitted work by Zarrin et al. to ACS Nano Journal. The thesis author's specific contributions to this paper were to synthesize and fabricate the nano-composite AEM, conduct EIS measurements, run all of physicochemical characterization tests, prepare all plots and results, write the final manuscript and respond to the comments of reviewers. This work and journal paper preparation was conducted with direction from the project supervisors who are co-authors on the publication. Ms. Jing Fu aided with testing the single AEMFC performance. Mr. Gaopeng Jiang assisted in running some of physicochemical characterization tests. Ms. Skylar Yoo helped the first author to conduct EIS measurements for alkaline durability tests.

Abstract

Fuel cells are electrochemical devices which have been established to lead in the transition to clean energy technology and will become the energy efficient power source of the future. Among all the fuel cell systems, anion exchange membrane fuel cells (AEMFCs) and solid polymer electrolyte membrane fuel cells (PEMFCs) are qualified of achieving high power densities (>l W cm^{-2}) that is required for many applications. Mainly, operation of AEMFCs and PEMFCs at higher temperatures (100-130 °C) would considerably enhance their kinetic performance over the current lower temperature operation technologies. However, due to the type of materials used in each fuel cell there is an associated set of challenges including cost and lifetime which require innovative engineering solutions. One of the important challenges is the fabrication of a cost effective solid electrolyte with high efficiency and durability for both PEMFCs and AEMFCs.

Concerning PEMFCs, the state of the art perfluorosulfonic acid (PFSA) membrane (Dupont Nafion®) has high ionic conductivity and good mechanical and chemical stability. However, its high performance and durability is limited to the operational conditions (e.g., temperature, humidity, and pH). In the case of AEMFCs, the dilemma between high ionic conductivity and physicochemical stability for membranes is an important issue, i.e., maximizing one will minimize the other. Thus, for both PEMFCs and AEMFCs, there is a desire to develop a solid electrolyte material capable of maintaining both ion-conductivity and durability at the same time for various operational conditions, especially elevated temperature conditions.

The main goal of this research project has been the design and fabrication of novel nano-composite electrolyte membranes that fulfills all the aforementioned requirements for a cost effective solid electrolyte membrane in both PEMFCs and AEMFCs. To accomplish this, different approaches have been effectively integrated and improved by understanding and combination of organic chemistry, electrochemistry, chemical engineering and nano-materials science. Hygroscopic nano-fillers made of titanium oxide nanotubes (TiO_2-NT) or graphene oxide (GO) nanosheets were first functionalized with highly ion-conductive groups, and then composed with the commercial membrane or another type of polymeric backbone. The latter was morphologically modified to favor higher electrolyte and water absorption capacity. Combining the benefits of a nano-filler with a morphologically modified polymer electrolyte effectively led to the development of a highly ion-conductive, water-retentive, and durable electrolyte membrane. Electrochemical, thermal, physical and chemical properties of proposed membranes were tested, analyzed and reported by various characterization methods. For PEMFC applications, the developed nano-composite PFSA membranes demonstrated significant ion conductivity and single fuel cell performance improvement (~4 times) over commercial PEM at the humidity of 30 % and temperature of 120 °C. For AEMFCs, the selected nano-filler (e.g., GO) composed with morphologically modified polymer (e.g., porous polybenzimidazole) notably increased both performance and durability of AEMs in harsh alkaline conditions. This work offered promising solid electrolyte replacements synthesized by simple and cost effective techniques, able to meet the fuel cell market demands.

Acknowledgements

I would like to express my gratitude and appreciation to my supervisors: Dr. Zhongwei Chen and Dr. Michael Fowler for their continual support and guidance. Both were tremendous mentors whose directions and encouragement during all these years allowed me to grow.

Natural Science and Engineering Research Council (NSERC) and University of Waterloo are also appreciated for the funding of this research.

I want to thank all of my friends and colleagues at the department of chemical engineering of University of Waterloo for all their help, support, and valuable hints.

In the end, I would like to extend my heartfelt appreciation to my lovely husband, Kaveh, and my parents for their endurance, support, and encouragements especially during difficult times. Moreover, I like to appreciate the help and support of my in-laws during years of PhD studies.

Dedication

This thesis is dedicated to my incredibly wonderful husband, Kaveh, whose wholehearted love, wisdom and unwavering support constantly encouraged me when the tasks seemed arduous and insurmountable. This thesis and the pursuit of my goals would not have been possible without you.

Table of Contents

List of Figures

List of Tables

Chapter 1
Introduction

1.1 Overview and Objectives

Since utilizing fossil fuels for power has led to many negative consequences including climate change, urban air pollution, depletion of resources, and energy security concerns, the interest in alternative clean energy technologies has arisen during the past decades. Among them, fuel cells are established to become one of the main power sources of the future which are clean and energy-efficient. A fuel cell is an electrochemical device (a galvanic cell) which converts free energy of a chemical reaction into electrical energy (electricity) such that the byproducts are only heat and water/steam if hydrogen and air are used as the reactants. The heart of fuel cells is a membrane electrode assembly (MEA) consisting of an ion-conductive liquid or solid electrolyte, catalyst layers (CLs), and gas diffusion layers (GDLs). Generally, there are five different types of fuel cells which are categorized based on different factors including the electrolyte type and the operating temperature (explained in section 2.1.3) [1-8]. Among all the fuel cell systems, alkaline fuel cells (AFCs) and solid polymer electrolyte membrane fuel cells (PEMFCs) are qualified of achieving high power densities (> 1 W cm^{-2}) required for portable, automobile and stationary applications [9].

The very popular PEMFCs functioning in an acidic environment uses a proton exchange membrane (PEM) as the electrolyte and hydrogen as the fuel. The principal advantages of PEMFCs involve high electrical efficiencies (up to 60%), high energy densities, and zero emissions [10]. Alkaline Fuel Cells (AFCs) were first described in the beginning of twentieth century which can operate from 40 to 200 °C using concentrated potassium hydroxide (KOH)

solution as the electrolyte. Since KOH does not freeze at temperatures close to 0 °C, it is kinetically more workable with an AFC rather than that with a PEMFC. More importantly, AFC do not require expensive noble metal catalysts employed for PEMFCs. At 25 °C, the thermodynamic voltage for the AFC is 1.23 V and the theoretical energy conversion efficiency reaches 83%, exhibiting very high electrical efficiency [11]. However, due to the type of applied materials, each type of aforementioned fuel cells has its own set of challenges including cost, performance and lifetime which require innovative engineering solutions.

For both PEMFCs and AFCs, one of the important challenges is to fabricate a cost effective solid electrolyte with high performance efficiency (i.e., ion conduction) and durability at relevant operating conditions. Concerning PEMFCs, the state-of-the-art solid electrolyte is the expensive perfluorosulfonic acid or PFSA (e.g. Nafion®) membrane functioning only in the presence of liquid water which restricts the fuel cell operating temperature to about 80 °C. On the contrary, in order to have (i) faster kinetic in CLs, (ii) higher cell performance, and (iii) enhanced water management, PEMFCs are favorably desired to operate at elevated temperatures (e.g., 120 °C) and reduced relative humidity (RH < 100 %) [6, 9, 12, 13]. As a result of PFSA deficiency at temperatures approaching the boiling point of water (100 ˚C), it is extremely required to substitute PFSA based electrolyte with a water-retentive membrane maintaining the high performance and durability of PEMFCs at temperatures higher than 80 °C and low RH in the feed stream of gases. In the case of AFCs, the most conventional used electrolyte is concentrated potassium hydroxide (KOH) solution. Nonetheless, other than leakage, the major drawback of using liquid KOH is the absorbance of existing CO_2 in air which would react with the mobile anions, i.e.,

hydroxide (OH^-), and converts them to undesired bicarbonate/carbonate (CO_3^{2-}/HCO_3^-) anions under the carbonation process [11, 14-16]. This leads to failure of the membrane. In order to avoid such deficiency, the KOH solution could be substituted with an alkaline anion exchange membrane (AEM), while keeping the electrokinetic advantages of AFCs. While the advance anion exchange membrane fuel cell (AEMFC) systems combine the advantages of AFC and PEMFC, some problems and challenges are still remained to commercialize this technology, including lack of high ion conduction, poor mechanical properties and low chemical stabilities in an alkaline environment.

Several strategies have been employed to enhance the performance and durability of PEMFC and AEMFC systems through the improvement of chemical structure and functionality of PEM and AEM, respectively. Traditional approaches used in solid electrolyte development generally consist of either: **(i)** composing a hygroscopic nano-filler (e.g., ZrO_2 [17], SiO_2 [17, 18], TiO_2 [17, 19], Zeolite [20, 21]) with the state-of-the-art polymeric membrane, i.e., PFSA or Nafion®, or **(ii)** employing other types of polymeric matrices [22-30] possessing different ion-conductive channels or groups with enhanced chemical stability, ion conductivity, and water-retention properties. Each of these individual approaches has demonstrated some success in improving ion conduction and operational durability. However, the ionic conductivity and durability are inversely correlated to each other, i.e., maximizing one will minimize the other. Thus, the development of PEM and AEM materials possessing both high ion conductivity and physicochemical stability is highly desired.

The main goal of this PhD research has been the design and fabrication of novel nano-composite electrolyte membranes that fulfills all the aforementioned requirements for a cost

effective solid electrolyte membrane in both PEMFCs and AEMFCs. To accomplish this, the abovementioned approaches have been effectively integrated and improved by understanding and combination of organic chemistry, electrochemistry, chemical engineering and nano-materials science. Hygroscopic nano-fillers were first functionalized with highly ion-conductive groups, then composed with the commercial PEM (i.e., Nafion®) [31, 32] or other types of polymeric backbones for AEMs [33-35]. The latter can be morphologically modified to favor higher electrolyte and water absorption capacity (e.g., with a porous structure) [33-35]. Combining the benefits of a nano-filler with a morphologically modified polymer electrolyte can effectively lead to the development of highly ion-conductive, water-retentive, and durable solid electrolytes at various operational conditions. This will offer promising ion-conducting membrane replacements synthesized by simple and cost effective techniques, able to meet the fuel cell market demands. Thus, the three principal stages of this PhD study have been **(1)** the fabrication of sulfunic-acid functionalized nano-composite PFSA membranes for PEMFCs, **(2)** the synthesis of novel or modified AEMs with high hydroxide conductivity and durablity for AEMFCs, and then **(3)** the development of a novel quaternary-ammonium functionalized nano-composite AEM for AEMFCs.

1.2 Thesis Layout

This thesis is composed of 9 chapters. The first chapter describes the motivation and objectives of the overall study with the thesis layout. The second chapter reviews the fuel cell technology, especially PEMFCs and AEMFCs, along with their advantages and challenges. Then, different developed types of ion conducting polymer electrolytes and their properties for both PEMs and AEMs are described. Chapter 3 provides the methodology of applied

experimental routes along with the necessary characterization tests to evaluate the performance of proposed PEMs and AEMs. Chapters 4 to 8 consist of materials all of which I authored or co-authored as the principle lead author (please refer to Statement of Contributions included in this thesis).

Chapter 4 is based on published work by Jun et al. [1] and is reproduced with permission from the International Journal of Hydrogen Energy. In this Chapter the sulfonic acid-functionalized titania nanotube/Nafion composite membrane was introduced as a highly proton conductive PEM at high temperature and low humidity operating conditions for PEMFCs. The thesis author's specific contributions to this paper were to synthesize and fabricate the nano-composite membrane, conduct the electrochemical impedance spectroscopy (EIS) measurements, run some parts of physicochemical characterization tests including water uptake and TGA, prepare the final plots and results, write the final manuscript and respond to the comments of reviewers. This work and journal paper preparation was conducted with direction from the project supervisors who are co-authors on the publication. The post-doc fellow, Yu Jun aided with the main idea development and performing most of physicochemical characterization tests including XRD, XPS, FT-IR, and TEM.

Chapter 5 is based on published work by Zarrin et al. [2] and is reproduced with permission from the Journal of Physical Chemistry C. In this Chapter sulfonic acid-functionalized graphene oxide nanosheet/Nafion composite membrane was fabricated and tested in high temperature PEMFCs. Like the first work described in Chapter 4 [31], incorporation of graphene oxide nanosheets into the matrix of PFSA significantly enhanced

the proton conductivity and the single cell MEA performance at elevated temperatures and low RH. The thesis author's specific contributions to this paper were to synthesize and fabricate nano-composite membrane, conduct EIS measurements, run most of physicochemical characterization tests, prepare all plots and results, write the final manuscript and respond to the comments of reviewers.

Chapter 6 is based on published work by Zarrin et al. [3] and is reproduced with permission from the Journal of Membrane Science. In this Chapter quaternary ammonium poly ether ketone (QAPEK-OH) membrane was designed and fabricated for AEMFCs application. The QAPEK-OH exhibited high thermal, mechanical and chemical stabilities at elevated temperatures. The thesis author's specific contributions to this paper were to synthesize and fabricate the AEM, conduct EIS measurements, run all of physicochemical characterization tests, prepare all plots and results, write the final manuscript and respond to the comments of reviewers.

Chapter 7 is based on published work by Zarrin et al. [4] and is reproduced with permission from the International Journal of Hydrogen Energy. In this Chapter to further improve the anion conductivity and durability of AEMs, the attention was concentrated on polybenzimidazole (PBI) polymer as a stable backbone for AEMs. In this work porosity was introduced into PBI creating more open paths as well as higher surface area for ion transfer and the absorption of an electrolytic solution. The alkali-doped porous PBI exhibited excellent physicochemical stability, anion conductivity and AEMFC performance. The thesis author's specific contributions to this paper were to synthesize and fabricate the AEM,

conduct EIS measurements, run all of physicochemical characterization tests, prepare all plots and results, write the final manuscript and respond to the comments of reviewers.

Chapter 8 is based on submitted work by Zarrin et al. to the ACS Nano Journal. In this chapter in order to fulfill the ultimate goal described before, porous PBI (pPBI) was selected as a highly stable and durable polymeric backbone for electrolyte membrane. Then, graphene oxide nanosheets were nominated as the nano-sized filler with high surface which was functionalized with quaternary ammonium groups (QAFGO). The nano-composite QAFGO/pPBI exhibited outstanding ion conductivity, physicochemical stability, and AEMFC performance, having promising potential to be employed as a reliable AEM for AEMFCs at various operating conditions. The thesis author's specific contributions to this paper were to synthesize and fabricate the nano-composite alkaline electrolyte membrane (AEM), conduct EIS measurements, run all of physicochemical characterization tests, prepare all plots and results, write the final manuscript and respond to the comments of reviewers.

Chapter 9 summarizes the conclusions reached about the topic and delivers recommendations for future work.

Chapter 2
Background

2.1 Fuel Cell Technology

Fuel cells are established to lead in the clean energy technology and become the power source of the future. Since utilizing fossil fuels for power has led to many negative consequences, the interest in fuel cells has arisen during the past decades. Some of these include CO_2 emissions contributing to climate change, urban air pollution, and energy security issues associated with the location of petroleum resources. Therefore, new power generation technologies such as fuel cells are required which are clean and energy efficient [1-8].

Fuel cells are electrochemical devices which convert chemical energy sources (often H_2 or H_2-containing fuels and O_2 from air) directly to electricity, heat and water, presenting enhanced efficiency over current means of energy conversion [2, 3, 36, 37]. Since hydrogen and oxygen gases are electrochemically converted into water, fuel cells are more appealing than heat engines in converting fuels to electrical energy. High efficiency ("two to three times more efficient than an internal combustion engine (ICE)"), quiet operation and no undesirable emissions (if hydrogen is the fuel) are basically named as the main advantages of fuel cells over ICEs. Moreover, the produced power can be more environmental friendly if the hydrogen is gained from renewable or nuclear energy sources such that no climate change emissions occur [38].

2.1.1 General Structure of a Fuel Cell

In general, fuel cells are composed of electrodes (i.e., anode and cathode with catalyst), electrolyte (solid or liquid), gas diffusion layers (GDL), bipolar plates/interconnects and sometimes gaskets for sealing the stack and preventing leakage of gases. All of these components are arranged in a stack which the repeated stacks are linked in either series or parallel format to produce the appropriate voltage and current (**Figure 2-1**). The electrodes contain catalyst and must be able to conduct both ions and electrons, as well as allowing for the transport of reactant gases. The optimal properties for the catalyst layers include hydrophilicity, thinness, uniformity, and the appropriate ratio of solubilized format of ion conducting electrolyte and supported catalyst. The latter is necessary to make the thin film catalyst layers which are cast from "inks" comprising a supported catalyst and solubilized ionomer. In fact, using the solubilized fashion of the ion conducting electrolyte bind the thin film catalyst structure together [39, 40]. GDLs aid both the distribution of the reactants to and the removal of the products from the surface of electrodes, as well as electron conduction and mechanical support. The optimal properties for the GDLs are achieved by changing their hydrophobic materials. In a typical fuel cell, gaseous fuels, hydrogen or hydrogen containing fuels (e.g., methanol) and an oxidant (i.e., oxygen from air) continuously enter the anode (negative electrode) and the cathode (positive electrode), respectively. Anodic catalyst layers activate the hydrogen oxidation reaction (HOR), and cathodic catalysts vitalize the oxygen reduction reaction (ORR). Platinum for low temperature fuel cells and nickel for higher temperature fuel cells are the most common metals for catalyst layers. Individually, both anode and cathode comprise porous gas diffusion layers, containing highly electron-

conductive substances without any ion conduction (e.g., porous graphite thin layers) which transport electrons and distribute reactant gases. Conversely, the applicable materials for the electrolyte, which divides the two electrodes, are extremely ion-conductive (have theoretically zero electron conductivity) and thereby, complete the cell electric circuit such that the produced electrons, which cannot pass through the electrolyte, flow through an external circuit (i.e., a motor or other electric load) which consumes the generated power by the cell.

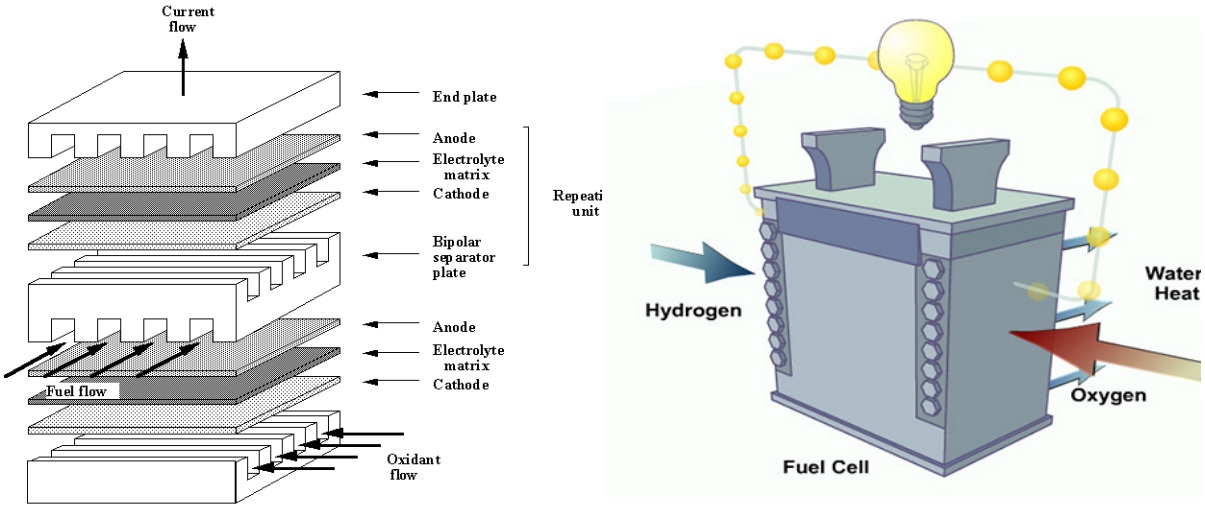

Figure 2-1. Simplified Fuel Cell Schematic [41].

The transport direction of the charge specie (positive or negative ion) through the electrolyte can be different, depending on the type of the fuel cell (**Figure 2-2**, also see section 2.1.3), which plays a part in the position change of water production and removal. The electrolyte not only conducts the ionic charge between the electrodes, but also transports dissolved reactants to the electrode. Moreover, it acts as a physical block to restrain the fuel and oxidant gas streams from being mixed in a direct manner leading to combustion. The

bipolar plates (or interconnects) are in charge of collecting the produced electrical current along with the distribution and separation of reactive gases in a fuel cell stack [37, 42].

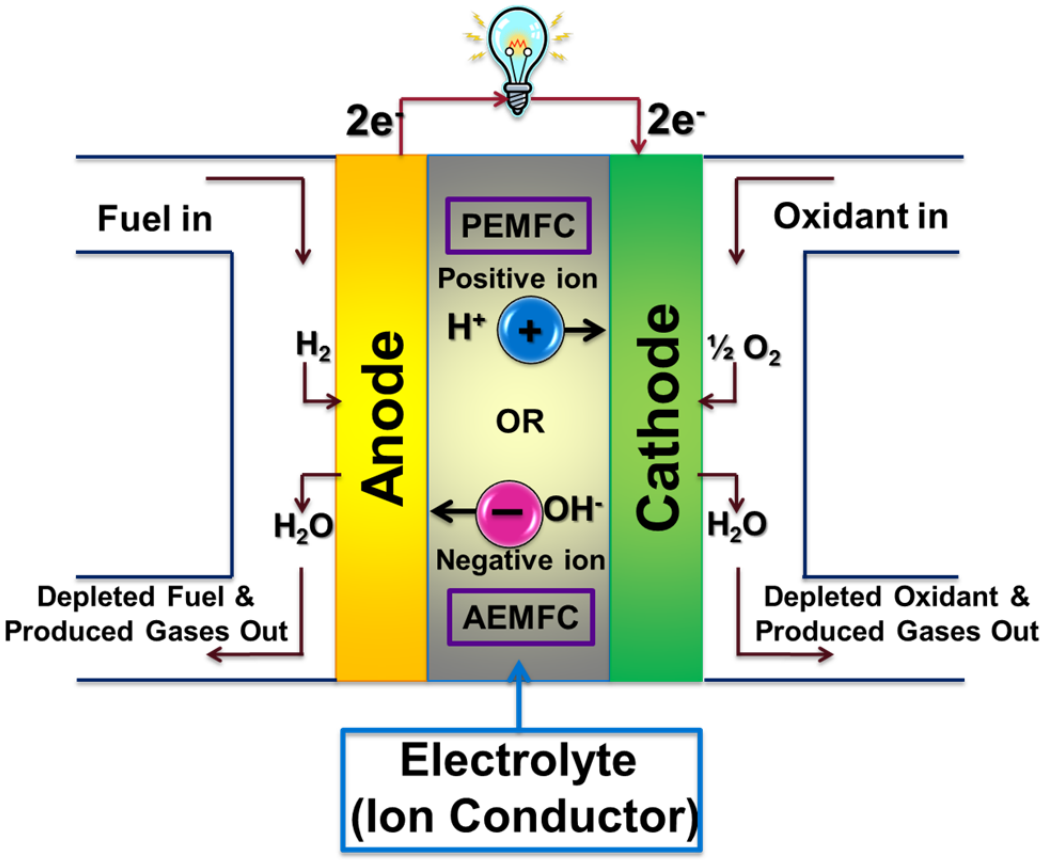

Figure 2-2. A schematic representation of a fuel cell with the reactant/product components and the ion conduction flow directions through the cell.

2.1.2 Advantages and Limitations

In principal, the main characteristic of fuel cells is *high efficiency* since it is not restricted by Carnot Law efficiency. In fuel cells the energy is directly converted to the power which generally makes them more efficient than piston or turbine based internal combustion engines (ICEs). Thereby, the small systems can be as efficient as large ones which are very

essential in the case of using small local power generating systems for combined heat and power (CHP) systems. Fuel cells with a combined cycle and/or cogeneration can be efficient as high as 55-65% whereas the efficiency of ICE systems is up to about 40-45% [2, 8, 37, 42]. *Increased range* is another advantage of fuel cells which is especially advantageous for applications that are energy-limited. They do not need to be recharged and refueled quickly. For example, power for portable devices is limited; therefore, constant recharging is necessary to keep a device working. *Simplicity* of fuel cell system extends its potential application as a significant technology. As there are no moving parts in fuel cell systems except an air blower and hydrogen recirculation pump, they are very quiet and thereby, more reliable than ICEs or gas turbine power plant. This feature is of great significance in both portable power devices and local power generation in CHPs [2, 42]. *Low emissions* at point of use are one of the most important characteristics of fuel cells. When hydrogen is used as the fuel, the by-product is pure water, denoting that a fuel cell can be 'zero emission' in practice. In other words, the emissions of NO_2, NO_3, SO_2, and CO_2 are emitted in a fuel cell system and therefore, urban air pollution and ground source ozone levels defects, acid rain and global warming issues are not contributed to. This principal advantage is of great importance, as there is a need to decrease and eliminate vehicle emissions within cities.

For all types of fuel cells, the most considerable disadvantage is the cost, due to the requirement for materials with specific qualities. For instance, platinum and PFSA are the most common used materials for catalyst layers and electrolytic membrane, respectively. However, there is an ongoing need to develop lower cost alternatives to these materials for commercialization. Another big disadvantage could be the preference of using hydrogen as a

fuel for which there is no production and distribution systems currently in place. Moreover, catalyst degradation and electrolyte poisoning will occur over time if another fuel besides hydrogen is fed into the fuel cell system (or CO contamination in the hydrogen) which by degrees results in the overall efficiency decrease. On the other hand, the fact that hydrogen is the favorite fuel in fuel cells is an advantage. Fossil fuels supplies are limited and thus, hydrogen can become the principal world energy vector. Specifically hydrogen can be used to store energy (e.g. energy from intermitted renewable sources such as wind and solar, base load sources such as nuclear), and transport energy onboard vehicles and portable devices. Some other disadvantages of fuel cells could be its unfamiliarity for power industry, durability, and the lack of hydrogen infrastructure [2, 8, 37]. Another drawback refers to the desirable lifetime for fuel cell systems. For commercial portable and mobile devices a lifetime of around 5000 hrs and for stationary and power plant applications up to 40,000 hrs operations is required [11].

2.1.3 Types of Fuel Cells

There are various types of fuel cells which can be categorized according to different factors, such as the combination type of fuel and oxidant, external or internal fuel reforming, the type of electrolyte, the operating temperature, internal or external manifolds for feeding the reactants. The most common classification of fuel cells is based on the type of electrolyte used in the system, including (i) Polymer Electrolyte Membrane Fuel Cell (PEMFC) for transportation power generation, (ii) Direct Methanol Fuel Cells (DMFC) for portable power generation, (iii) Alkaline Fuel Cell (AFC) for producing electricity and drinking water for the space program and other applications if some technology challenges can be addressed (iv)

Phosphoric Acid Fuel Cell (PAFC), (v) Molten Carbonate Fuel Cell (MCFC), and (vi) Solid Oxide Fuel cell (SOFC) for stationary power generation applications which are listed in the order of relative operating temperature of ~80 °C, ~100 °C, ~200 °C, ~650 °C, and ~600-1000 °C, respectively (see **Table 2-1**). The operating temperature has a significant role in determining the physical, mechanical, chemical and thermal properties of substances used in the cell elements such as electrodes, electrolyte, interconnect and bipolar plates. For instance, 200 °C or lower is the proper temperature for aqueous electrolytes as they have high water vapor pressure and quick degradation at higher temperatures. In addition, the intensity of temperature dictates the type of the fuel and oxidant to be used in the system. The fuel could be pure hydrogen, gaseous or gasified hydrocarbons (natural gas, biogas, sewage gas, coal mine gas, methane containing gas mixtures), synthesis gases (mixtures of hydrogen and carbon monoxide) and as oxidant both pure oxygen and air are used. As an example, the Low-Temperature Fuel Cells (LTFC) such as PEMFC and AFC with aqueous or polymeric electrolytes, which are used in most practical applications, are restricted to hydrogen fuel; while, in High-Temperature Fuel Cells (HTFC) such as MCFC and SOFCs, CO and even CH_4 are allowed to be fed as the fuel, because of the inherently fast electrode kinetics, potential for internal reforming, and the lesser need for high catalytic activity at high temperature [2, 37, 42].

Table 2-1. Different types of fuel cells based on the type of electrolyte and operating temperature.

Temperature range class	Fuel Cell	Electrolyte	Temperature (°C)
Low Temperature (LT)	AFC	• Liquid potassium hydroxide (KOH) – Basic environnement • Anion exchange polymeric membrane	• 100 (Old designs) • 23-70 (New designs)
	PEMFC	Polymer electrolyte membrane – acidic environnement	80 – lower
High Temperature (HT)	PAFC	Liquid phosphoric acid	200 – higher
	MCFC	Molten carbonate salt mix. suspended in $LiAlO_2$	650 – high
	SOFC	Hard & non-porous ceramic compound	1000 – high

2.1.4 Performance of Fuel Cells

In general, a fuel cell performance is estimated by a polarization curve. The polarization in fuel cells is defined as the voltage drop from the open circuit voltage (OCV) due to the generation of electrical current. Voltage drop, often called overpotential, is mainly resulted from the losses associated with current flow, electrodes and external connections, kinetic limitations of the electrode reactions, and mass transfer limitations of reactants at the electrode surfaces [2, 43]. Overpotentials in the polarization curves can be divided into three regions including (i) an activation loss (η_{act}) region, (ii) a pseudo-linear ohmic loss or IR-loss (η_{ohm}) region, and (iii) a mass transfer limited (η_{conc}) region which indicate what material characteristics or components have been degraded [2]. **Equation 2-1** shows the total

sum of overpotentials (η) which is evaluated as the difference of the real cell voltage (E) and the ideal equilibrium potential (E^0), called Nernst potential.

$$\eta = E - E^0 \qquad \textbf{Equation 2-1}$$

As an example, the typical polarization curve (voltage as a function of current density) as well as the power density of PEMFCs, operating at 70 $^{\circ}$C without backpressure, are shown in **Figure 2-3.** In theory, the overall electrochemical reaction of a single PEMFC produces 1.23 V ideal equilibrium potential at 25 °C room temperature and 1 atm pressure. Therefore, it is expected that the OCV, which is the cell potential under no current flow, reach E^o. However, internal currents caused by inefficiencies in the cell such as leakage of H_2 from anode side to cathode side, and platinum (Pt) catalyst oxidation, are believed to lower the OCV below E^o. Therefore, the practically highest achievable OCV for a single fuel cell approximately exists between 0.95-1 V [43, 44].

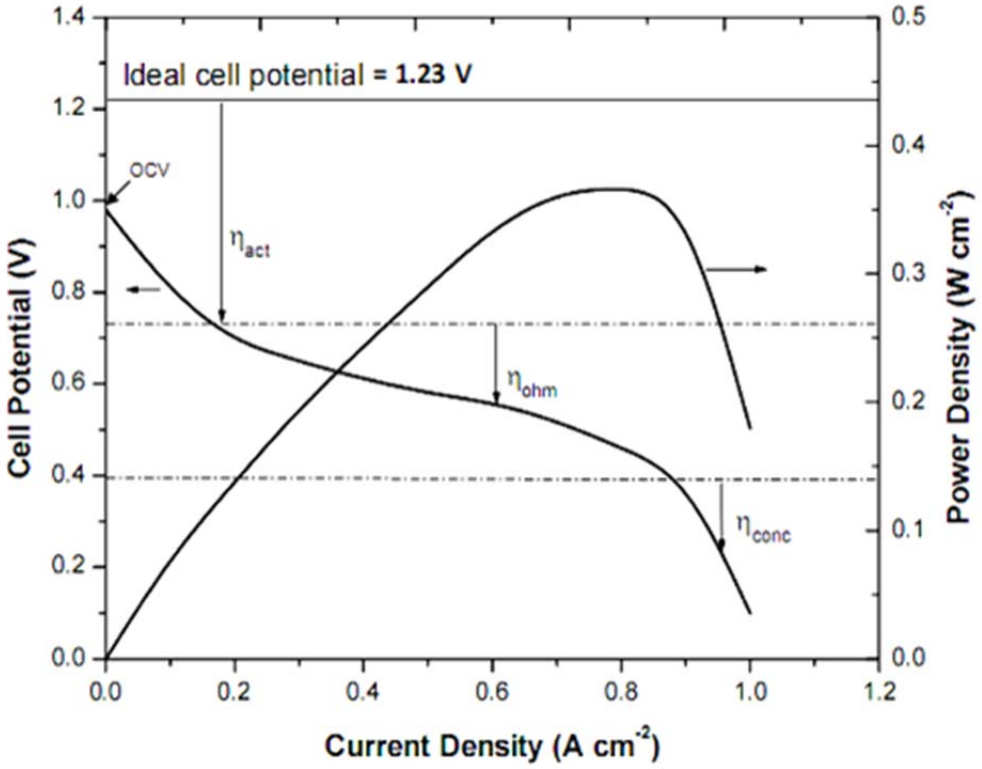

Figure 2-3. Polarization and power density curves of a PEMFC operating at 70 °C [43].

During the fuel cell operation, the real cell potential (E) relies on several factors such as temperature, pressure, and the mole fraction of the reactants [37]. The Nernst equation is a relationship between the cell potential and these variables as expressed in **Equation 2-2**.

$$\Delta E = \Delta E^0 - \frac{RT}{2F}\ln\left(\frac{a_{H_2O}}{a_{H_2}\,a_{O_2}{}^{1/2}}\right) \qquad \textbf{Equation 2-2}$$

where R is the universal gas constant, T is the absolute temperature, F is Faraday's constant, and a_{H_2O}, a_{H_2} and $a_{O_2}{}^{1/2}$ are the activities of water, hydrogen and oxygen, respectively.

The maximum cell voltage value is achieved at the OCV condition where there is no current flow. At low current densities, the polarization curve is governed by the activation

overpotential, which is resulted from the kinetics of charge transfer reactions across interfaces and displays the amount of activation energies when the rate of reactions increase to the required extent by the current. This depends on the type of reactions and catalyst materials (e.g., platinum in PEMFCs), reactant activities, electrolyte material (acidic/alkaline), electrode microstructure, temperature and current density. Activation overpotential of ORR at the cathode is much larger than the overpotential of HOR in anode such that the anode activation overpotential is often neglected in calculations [44, 45]. For instance in PEMFCs, the activation overpotential at the cathode from the ORR is related to platinum surface area ($A_{Pt,el}$), platinum loading (L_{ca}), current and exchange current density (i_o) as well as the fuel cell current (i) which can be expressed by **Equation 2-3** [2].

$$\eta_{act} = \frac{RT}{n\alpha F} ln\left[\frac{i}{10 \cdot \left(L_{ca} A_{Pt,el}\right) \cdot i_o}\right] \qquad \textbf{Equation 2-3}$$

where n is the number of electron transferred and α is the transfer coefficient (taken to be 0.5).

After the fast voltage drop in activation overpotential region, fuel cell polarization exhibits pseudo-linear behavior at intermediate current densities which is due to the ohmic overpotential resulting from the resistance of fuel cell components. Bulk materials and interfaces between components display an inherent resistance to electron flow along with the electrolyte materials which represent resistance to transport of ions (e.g., resistance to proton conduction in PEMFCs). The amount of ohmic overpotential (η_{ohm}) is dependent on the total current (I) and cell resistance (R), and can be expressed as:

$$\eta_{ohm} = IR = jr$$ **Equation 2-4**

According to **Equation 2-4** the ohmic loss can be also expressed in terms of area or volume specific current density (*j*) and resistance (*r*), respectively. This approach is useful when calculating contributions to *IR*-loss from individual components. The largest part of the cell resistance amount is typically attributed to the electrolyte resistance to ionic current [44].

The third region of polarization curve is assigned to the mass transfer overpotential which occurs at high current density. When current density reaches a specific level, voltage loss caused by mass transfer sluggishness starts as the reactants cannot be quickly supplied to the active catalyst sites of electrode [2]. Because, under high current densities, the kinetic of the electrode reactions is so high that the transport of the reactants to the active catalyst sites limits the rate at which the fuel cell must operate. In order to express the mass transfer loss, an empirical equation (**Equation 2-5**) is applied which gives a good fit to the results and appears to be quite widely used in the fuel cell measurements [43].

$$\eta_{conc} = m \cdot \exp(nI)$$ **Equation 2-5**

where *m* and *n* are constants and *I* is the total current of the cell. *m* is typically about 3×10^{-5} V, and n is about 8×10^{-3} $cm^2\,mA^{-1}$.

2.1.5 Applications

High efficiency, cleanliness, inherent modularity and scalability of fuel cells as well as its high reliability as an energy supply, makes this technology be employed in a wide range of applications including batteries, automotive electrical propulsion systems, power stations, small apparatus (e.g., laptops, consumer electronics), units in spacecrafts and aircrafts,

Combined Heat and Power (CHP) units or tri-generation units (combined heat, power, cooling energy) and Auxiliary Power Units (APU) [4, 8]. Broadly, all of aforementioned applications can be categorized into three general groups, namely (i) portable devices, (ii) transportation systems, and (iii) stationary (**Figure 2-4**).

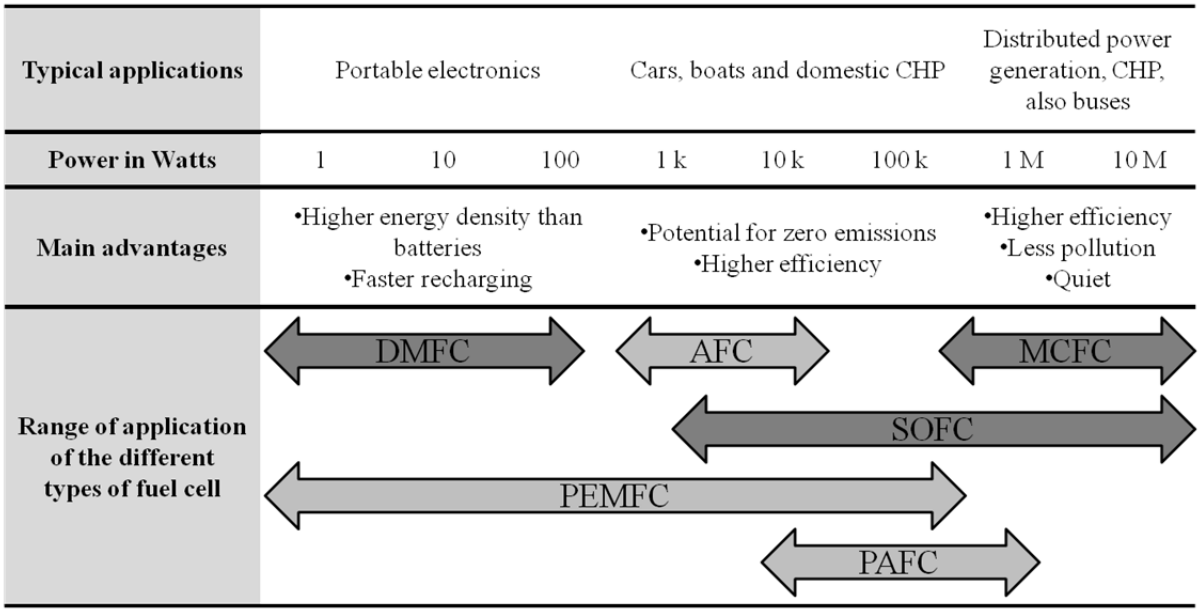

Figure 2-4. A summary of applications and main advantages of different types of fuel cells (redrawn from reference[2]).

2.2 Polymer Electrolyte Membrane Fuel Cells (PEMFCs)

2.2.1 General Structure of PEMFCs

A PEMFC stack is composed of a Polymer Electrolyte Membrane (PEM) electrolyte, anodic and cathodic electrodes containing catalyst (required for the electrochemical reactions) and gas diffusion layers, bipolar and flow field plates, gaskets and end plates. However, the key component of a fuel cell is the combination of the PEM with anode and cathode electrodes

which are pressed together with GDL (**Figure 2-5**), and is called the Membrane Electrode Assembly (MEA). Accordingly, aforementioned stack has many cells with MEAs sandwiched between bipolar and flow field plates and just one pair of end plates. Oxidization of the hydrogen takes place on the anode which produces protons and free electrons. In PEMFCs, by applying specific materials, protons can keep their ionic state by traveling from one molecule to another through the electrolyte. Therefore, the released protons move from the anode to the cathode via a polymeric electrolyte membrane, and the free electrons are attracted to conductive materials and carried to the cathode by traveling through an external circuit. On the cathode, oxygen is reduced and reacts with arrived protons and electrons, producing water and heat which must be continuously removed from the system; otherwise, some performance issues may occur for PEMFC specifically associated with water management. All aforementioned electrochemical reactions for a PEMFC are shown in **Figure 2-5** [10, 26, 37, 42, 46-50].

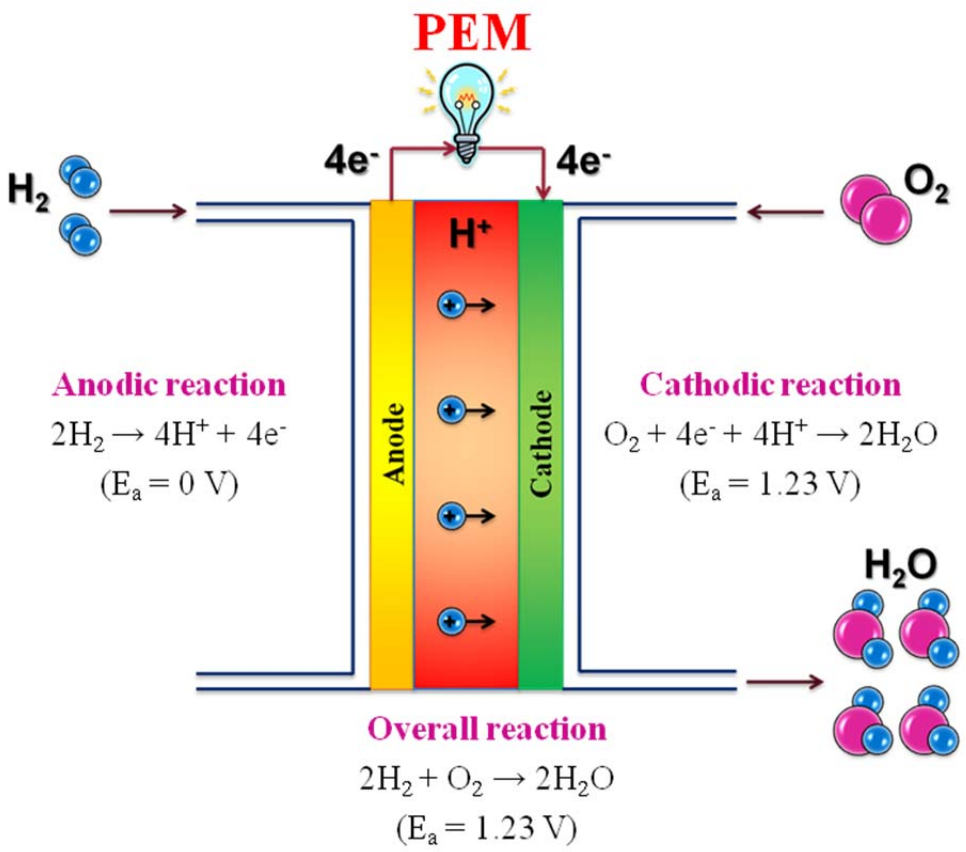

Figure 2-5. A PEMFC scheme with relevant electrochemical reactions.

2.2.2 Characteristics and Challenges

The principal advantages of PEMFCs involve high electrical efficiencies (up to 60 %), high energy densities, and low emissions. One of the main disadvantages and challenges is related to the proton conducting electrolytes which limit PEMFCs to be commercialized. The state-of-the-art PEM electrolyte is based on perfluorosulfonic acid (PFSA) polymeric membrane (often the commercial Nafion^{TM} polymer is used). Expensive PFSA membranes (**Figure 2-6**) conduct protons only in the presence of liquid water in the membrane which restricts the fuel cell operating temperature to about 80 °C without pressurization, causing low fuel cell

performance due to slow electrode kinetics and limited CO tolerance. Operation of PEMFCs at high temperatures (100-130 °C) would considerably enhance its performance by (i) speeding up the electrode reaction kinetics (mainly ORR), (ii) simplifying the water management and heat removal, (iii) improving the electrocatalyst CO tolerance, and (iv) limiting the excessive precious platinum (Pt) metal catalyst requirement. At temperatures approaching the boiling point of water (100 ˚C), PFSA exhibits a drastic ionic conductivity loss from the membrane structure (due to the evaporation of water in the membrane) which hinders the PEMFC to operate at temperatures higher than 80 ˚C and/or reduced relative humidity (RH < 100 %). In addition, the mechanical and dimensional stability of the polymer chains can be diminished at high temperatures as a result of the relatively low glass transition temperature of PFSA (140 °C). Another issue for PFSA membranes above 100 °C is the decrease of electrochemical surface area of the electrodes because of the electrolyte expansion with hydration within the catalyst layers which closes reactant pathway pores. Therefore, to accomplish the commercialization of PEMFCs, it is essential to develop novel proton exchange membranes for elevated temperature systems [10, 22-31, 46, 47, 50].

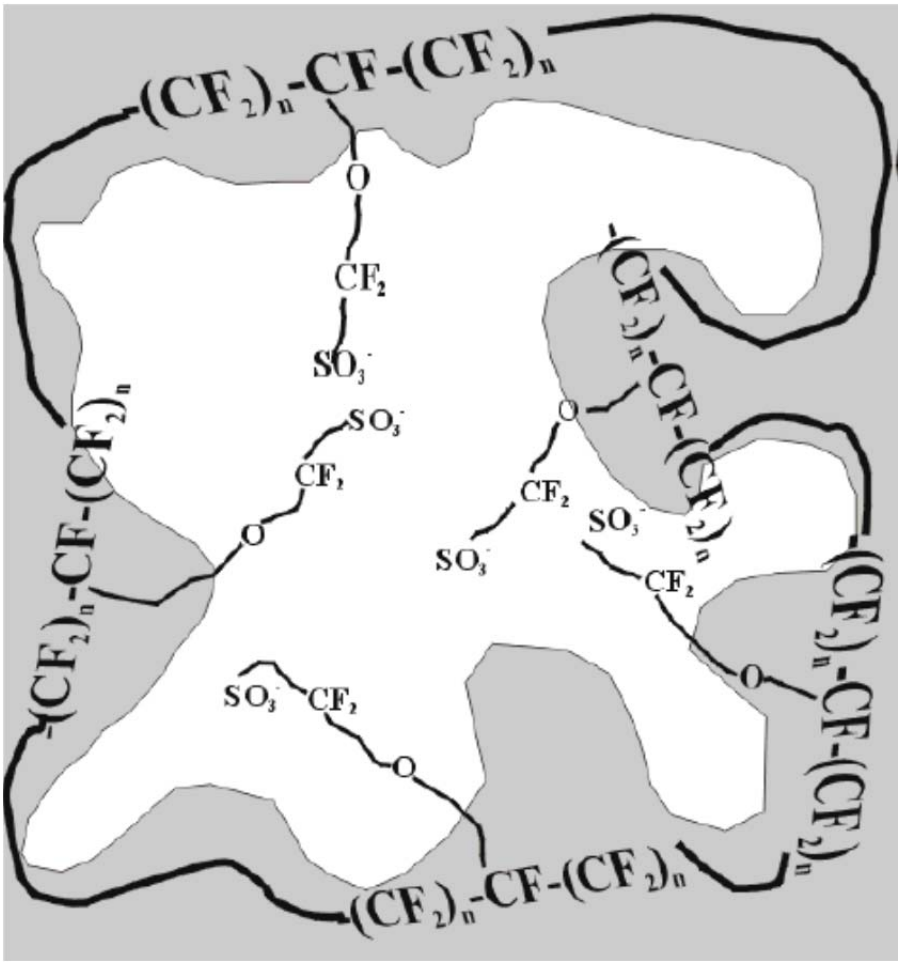

Figure 2-6. The chemical structure of proton conductive Nafion™ membranes showing three different regions: the hydrophobic polytetrafluoroethylene (PTFE) backbone, the hydrophilic ionic zone, and the intermediate region [50].

2.2.3 Types of Acid Electrolytes Membranes for PEM

According to literature, many Solid Polymer Electrolyte (SPE) membranes have been proposed for both acid and alkaline fuel cell applications. In general, SPEs are divided into two categories of (i) ion-solvating polymers (ISPs) and (ii) polyelectrolytes which are distinguished by the model of ion conduction within the polymeric structure. ISPs are solid membranes in which the ions are conducted based on the migration of cations or anions

through the membranes. The polymer involves electronegative heteroatoms (e.g., oxygen, nitrogen, sulfur or phosphorus), interacting with the cations of the ionic salt by means of a donor-acceptor link. For instance, Polybenzimidazole (PBI) is the most commonly used ISP in PEMFCs. PBI has excellent thermal, chemical and mechanical stability. It is cheaper and has much lower permeability for hydrogen when compared to Nafion^{TM} (i.e., a polyelectrolyte). However, blank PBI is an electronic and ionic insulator, which becomes an excellent ionic conductor when it is doped in proper conditions, although the stability of the 'doping' has yet to be demonstrated. In polyelectrolytes the ionic functional groups (e.g., sulphonate, carboxylate or quaternary ammonium) are grafted on the backbone of polymer chain and the ion conduction is accomplished by the counter-ion. The most common and important example of polyelectrolyte is the aforementioned Nafion^{TM} membrane (based on PFSA structure) in PEMFCs [15].

One way to overcome the temperature limitations of the current polyelectrolyte material (i.e., PFSA, Nafion^{TM}), while preserving other advantages, is incorporating some water retentive fillers (e.g., ceramic components) into the structure of PFSA, producing organo-inorganic composite membranes. Another way is to design a new structure of ion conductive SPE membrane which meets all the requirements, including high ion conductivity, satisfactory mechanical property and thermal and chemical stability.

Organo–inorganic hybrid composite materials are considered as promising substances for many applications owing to the distinctive combination of the functionality existed in the organic part with the physico-chemical stability of the inorganic ingredient. Because, along the low cost and high ion conductivity, the thermal, chemical and mechanical stability of the

membrane electrolyte is a crucial challenge for its application in a fuel cell. Organic-inorganic nano-composite membranes have been explored to be used in low-temperature fuel cells. To generate nano-composite membranes, the sol–gel method (explained in section **Error! Reference source not found.**) is normally employed [15, 51]. Some research efforts have been devoted to develop organic-inorganic hybrid composite membranes to be applied in PEMFCs at elevated operating temperatures [19-21, 52-56]. Incorporation of hygroscopic inorganic nanomaterials such as zirconia (ZrO_2), silica (SiO_2), titania (TiO_2), phosphorous pentoxide (P_2O_5) and Zeolite onto the backbone of PFSA has shown to be a potential replacement for Nafion at high temperatures, due to their good water retention and effect on the membrane stability enhancement [19, 20, 53, 57-64]. However, the proton conductivity of these hybrid membranes is still low, when compared to bare PFSA membranes. It is believed that this is mainly due to the incorporation of inorganic fillers which agglomerate at higher concentrations, increasing the block properties of the PFSA membrane [19]. In order to increase the proton conductivity, functionalization of hybrid membranes with sulfonic acid groups can improve the protons movement, by increasing the water retention ability and helping better homogeneous dispersion of fillers onto the hydrophilic sites of the PFSA, compared to non-functionalized ones [54, 64-66].

2.3 Alkaline Fuel Cells (AFCs)

For the first time, Alkaline Fuel Cells (AFCs) were described in the beginning of twentieth century; after the achievement to apply the aqueous potassium hydroxide (KOH) as the electrolyte in fuel cells. In AFCs, basically, ions in an alkaline electrolyte (typically 6 M

KOH solution [16]) travel from cathode to anode, in a reverse direction when compared to PEMFCs. The anodic and cathodic reactions in an AFC are:

Anode: $H_2 + 2OH^- \rightarrow 2H_2O + 2e$-

Cathode: $O_2 + 2H_2O + 4e^- \rightarrow 4OH^-$

Operating temperatures in AFCs are low, varying from 20 to 90 °C, for which, KOH is a proper electrolyte. Since KOH does not freeze at temperatures close to 0 °C, it is kinetically more workable with an AFC rather than that with a PEMFC. At 25 °C, the thermodynamic voltage for the AFC is 1.23 V and the theoretical energy conversion efficiency reaches 83%, exhibiting very high electrical efficiency. This is mainly due to faster oxygen kinetics in an alkaline solution other than that in an acidic medium in PEMFCs [11].

2.3.1 Drawbacks of AFCs

According to literature, the existence of carbon dioxide (CO_2) in air causes a problem for AFCs [11]. As normally the used alkaline solution electrolyte in AFCs is highly concentrated (i.e., 6 M KOH solution), it could extremely absorb CO_2 from the air such that it would react with the mobile hydroxide (OH^-) ion and converts it to bicarbonate/carbonate (CO_3^{2-}/HCO_3^-) anions under the carbonation process [14-16].

$CO_2 + 2OH^- \rightarrow CO_3^{2-} + H_2O$

$CO_2 + OH^- \rightarrow HCO_3^-$

As the mobility of $CO_3^{2-/}HCO_3^-$ is slower than OH^-, it results in OH^- ion conductivity decrease through the electrolyte. But, the major problem of carbonates (i.e., K_2CO_3) is their low solubility. When the carbonate content of electrolyte increases, it starts to be precipitated

and then, fills the micro-porous areas (e.g., gas diffusion layers) on the anode to the extent that the electrodes would not be able to operate properly, leading to the leakage of electrolyte solution from the system. To solve this failure, complex and costly accessories and power supply are needed. For example, the CO_2 can be removed from the air by applying some filters at the air entrance on the anode side (i.e., use of pure oxygen) or the KOH electrolyte can be renewed frequently (e.g. a rolling electrolyte that moves through the cell and then out the cell to cleaning bath) to reform carbonates to hydroxide. Therefore, the system is generally limited to use pure oxygen on the cathode side [14-16].

2.3.2 Transformation from Liquid Alkaline Fuel Cells (AFCs) to Solid Anion Exchange Membrane Fuel Cells (AEMFCs)

To conquer the aforementioned difficulties, the solid polymer electrolytes (SPE) in PEMFCs were modeled to be applied in AFCs. First of all, the polymeric property simplifies light and compact devices to be fabricated, resulting in the increase of volume-specific and weight-specific efficiency of the electrochemical devices (e.g., a fuel cell, a battery, or an electrolyser). Second, it is believed that substituting alkaline Anion Exchange Membranes (AEMs) for an alkali can help to resolve the problem of the carbonate formation, while keeping the electrokinetic advantages of AFCs. Because in AEMs, the cations are immobilized on the polymer chain and are not able to precipitate solid crystals of carbonate. To enable ion conduction, the basic positively charged polymer structure in AEM contains detached anions which function as the charge carrier. Usually, a Quaternary Ammonium (QA) group, $-NR_3^+$, is attached onto the polymeric chain, and the anion (OH^-) is ionized in the aqueous phase of the polymer. In practice, only when AEMFCs are at the open circuit

condition (i.e., no actual reaction happens at the electrodes), the CO_2 absorption from the air occurs. If the cathode has to be opened to air all the time (i.e., self-breathing mode), the OH^- in the AEM polyelectrolyte may be fully transformed to CO_3^{2-}/HCO_3^- by gradually taking CO_2 from the air. However, the main ion carrier would still be the OH^- while the cell is discharging, because when 1 mole of O_2 is reduced at the cathode, 4 moles of OH^- are produced and traveled through the AEM to the anode. As in the air the molar ratio between O_2 and CO_2 is 700, the OH^- produced under the ORR would still be much higher than the CO_2 sucked from the air. Therefore, in discharging conditions, the detached anion in the AEM polyelectrolyte would be essentially OH^-. Like in AFCs, OH^- ions travel from the cathode to the anode in AEMFCs, opposed to H^+ transport direction in PEMFC. The variation mode of ion conduction causes two modifications in a fuel cell system. First, the water (H_2O) is produced at the anode side of AEMFC rather than at the cathode as in PEMFC (**Figure 2-7**) which is transported from the cathode to the anode by electro-osmotic forces. Therefore, the water management regime is changed and simplified which keeps the cathode away from a flooding problem which can be experience by PEMFC. Second, H_2O is a vital reactant for the ORR in AEMFC, rather than just doing the humidification job for the air in PEMFC. Alkaline nature of the electrolyte in AEMFC allows non-precious metal oxides to be applied as catalyst layers instead of precious platinum (Pt) as in acidic PEMFC; thus, the cost of the system can be notably reduced. For the ORR at the cathode, Ag and such complex metal oxides as MnO_2 could be employed, and Ni-based catalysts are suitable for HOR at the anode. Other important superiorities of AFCs using AEMs over regular AFCs with alkali electrolytes are (i) no liquid electrolyte weeping or leaking, (ii) decreased alcohol

crossover if run on say methanol, and (iii) potentially reduced corrosion [14, 16] as there is no caustic liquid electrolyte. A schematic drawing of an AEMFC is shown in **Figure 2-7**.

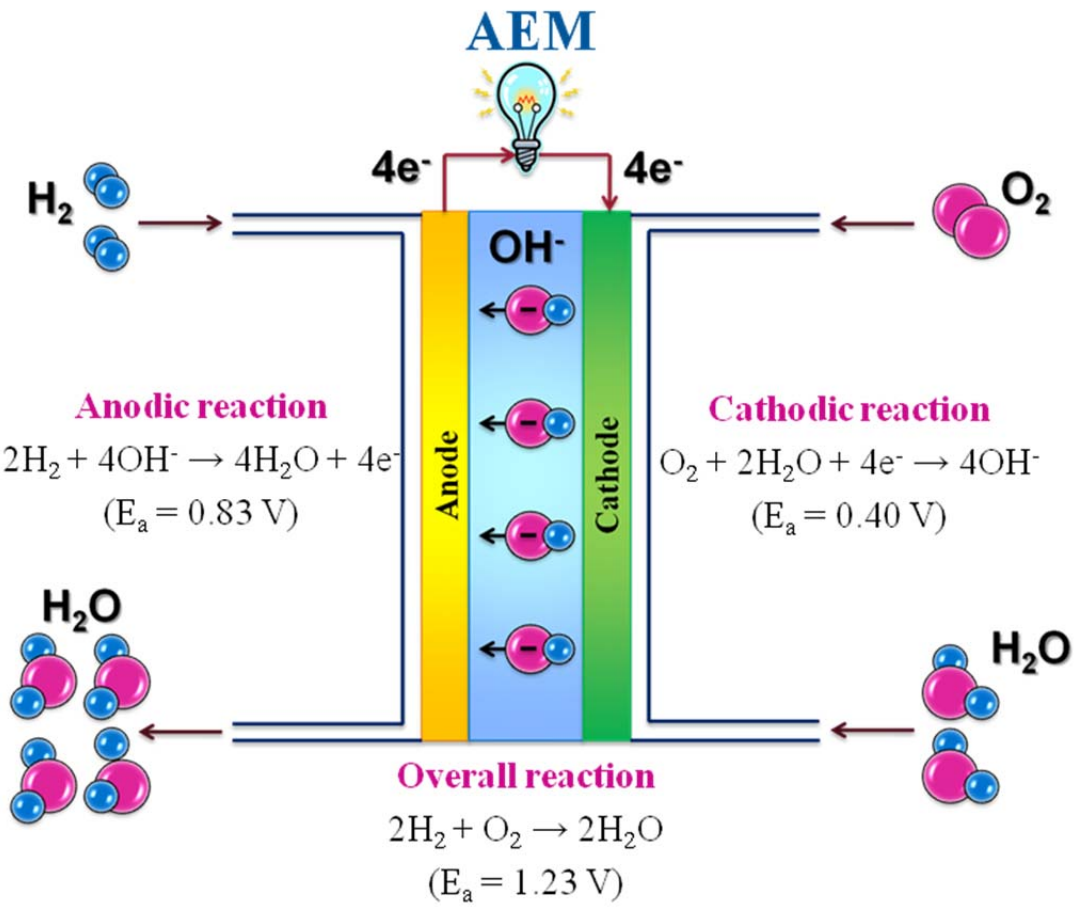

Figure 2-7. An AEMFC scheme with relevant electrochemical reactions

2.3.3 Requirements and Challenges to Develop Anion Exchange Membranes (AEMs)

While the advance AEMFC system combines the advantages of AFC and PEMFC, some problems and challenges are still remained to commercialize this technology. The primary challenge of an AEMFC derives from the lack of high performance AEMs which could accomplish all the necessities of fuel cell applications. Most commercial AEMs are made of

quaternary ammonium polystyrene which is mainly used in water processing. Nevertheless, they cannot be employed in fuel cells due to low and insufficient thermal, chemical and mechanical stability. Distinctively, flexible thin polymeric membranes are hard to achieve from the rigid polystyrene backbone, and the grafted QA functional group on polystyrene degrade at 40–60 °C. In fuel cell applications, polymer electrolytes should be operated at temperatures about 100 °C, and are required to be used in two modes of (i) solution and (ii) membrane. A polymer electrolyte requires acting as a solution (i.e., to make an 'ink' with the catalyst materials) to make a three-dimensional catalyst/electrolyte interface by being impregnated into the micro-pores of the electrodes. To function as a membrane, the polymer electrolyte film is expected to have adequate mechanical property, i.e., being both strong and flexible with a thin thickness (a few tens of micrometers). As well as the acceptable mechanical property requirement for polymer electrolytes, their chemical characteristics have a direct effect on the performance of a fuel cell. First, the ion-exchange capacity (IEC) is an identifying key factor for the ionic conductivity of a polymer electrolyte. To achieve a satisfactory performance, the ionic conductivity of 10^{-2} S cm^{-1} is mandatory for alkaline AEMs. To have a durable fuel cell, the chemical and thermal stability of the polymer electrolyte need to be significantly sufficient. All of the aforementioned requirements, i.e., satisfactory mechanical strength, high chemical and thermal stability, high ionic conductivity, and solubility, are all challenging for developing AEMs to be applied in fuel cells. Naturally, the mobility of OH^- is just 1/3 of that of H^+; thereby, in comparison to the acidic PEMs, the IEC of AEMs has to be raised to a higher level, yet, increasing the IEC always results in a decrease in the mechanical strength of the polymer membrane. Thus, the

ionic conductivity and the mechanical property have to be optimized and balanced in practice. Another challenge for AEMs is the alkaline stability of the QA functional groups, especially at elevated temperatures, which are extremely sensitive to the local chemical environment. Essentially, alkaline instability is due to the displacement of the QA group by the highly nucleophile OH^- anions through (i) a direct nucleophillic displacement and/or (ii) a Hofmann degradation reaction when β-hydrogen (β-H) at the alkyl chain of the QA group exist [14, 16].

2.3.4 Types of Alkaline Electrolyte Membranes for AEMs

Based on the type of chemical structure and composition in the main polymer chain, the thus far synthesized AEMs can be classified into three groups:

(i) membranes based upon aromatic fragments in the polymer main chain (e.g., polyphenylenes and polyheteroarylenes);

(ii) membranes based upon polymers with an aliphatic main chain (e.g., perfluorinated polymers and heterochains such as polyether); and,

(iii) composite organo-inorganic membranes

2.3.4.1 AEMs Based on Aromatic Structure

Polymer electrolyte membranes composed of aromatic constituents possess high thermal and chemical stability which makes them suitable to be employed for fuel cells operating in the range of 100-200 °C. Among them, polyarylenes (e.g., polyphenylenes (PPE), blends of chloroacetylated polyphenylene oxide (CPPO) and bromomethylated PPO (BPPO), etc.) and polyheteroarylenes (e.g., aromatic polyimides (PI), polybenzimidazoles (PBI), polyether

ketones (PEK), polyether sulfones (PES), polyethers (PE), etc.) are widely used for the production of membranes in fuel cells. **Table 2-2** shows the characteristics such as Ion Exchange Capacity (IEC), water uptake and ion conductivity for AEMs made of aforementioned aromatic structures. The fully aromatic polymers have notably high chemical stability (e.g., Homo-/co-polymer of PPE in **Table 2-2**). In the case of the presence of large bulky groups in the polymer backbone, higher ion conductivities are expected to achieve, due to the creation of non-close packed polymer chains. In comparison with homo-polymers, co-polymers possess higher water uptake and ion conductivity which can be assigned to their "more clearly defined diphilicity", leading to a "co-operative hydration effect" [67]. Moreover, the amount of hydration depends on the value of the IEC which is in the ranges of 25-45 mEq g^{-1} for the homopolymers and 32-37 mEq g^{-1} for the copolymers. By comparing the OH^- conducting membranes (AEMs) with H^+ conducting ones (PEMs), it is thought that the morphology of the polymer has a significant effect on the transport properties of the membranes. In contrast to PEMs, the production method of the AEM does not let the ion groups form separated phase domains. Generally, a phase-separated structure boosts the rate of ion transport, howbeit the water diffusion is slower and because of hydration by the sulfone groups, its bonding is much stronger in comparison with AEMs. Producing AEMs with higher conductivity (close to 10^{-1} Scm^{-1}, as in the proton-conducting membranes) are hindered by the relatively weak basicity of the QA groups and the low mobility of OH^- ions, in comparison with protons [68]. Furthermore, if the concentration of KOH is increased over a particular amount, the ammonium groups could be substituted by hydroxyls which results in the decrease of the conductivity.

Table 2-2. Characteristics of AEMs Based on Aromatic Structure

Aromatic AEM	Chemical Structure	IEC ($mEq \cdot g^{-1}$)	Water Uptake (%)	Ion-conductivity at 25 °C ($S\ cm^{-1}$)	Ref.
PPE (Homo-polymer)	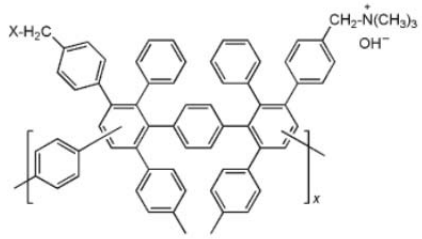	0.93-1.57	42-122	$(0.5\text{-}5)\cdot10^{-2}$	[67]
PPE (Co-polymer)	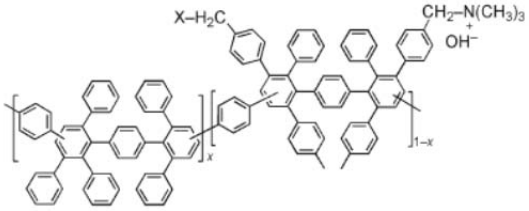	0.4-1.15	23-78	$(0.5\text{-}3)\cdot10^{-2}$	[67]
PES	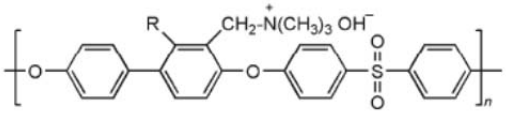	0.69-1.89	20-99	$1\cdot10^{-3}$ – $3.6\cdot10^{-2}$	[68]
PEK	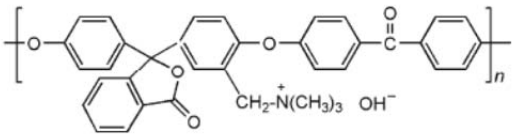	0.11	<5	$1.6\cdot10^{-3}$	[69]
PI	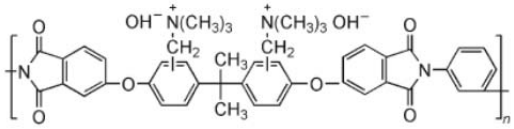	0.983	43.1	$2.28\cdot10^{-3}$	[70]
PBI	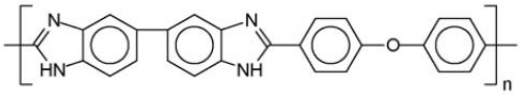	-	-	$0.5\cdot10^{-5}$ $1\cdot10^{-1}$ (at 70-90 °C)	[71]
CPPO/BPPO	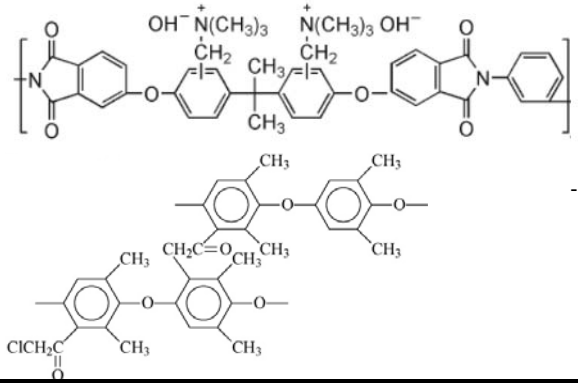	-	-	$2.2\cdot10^{-2}$ – $3.2\cdot10^{-2}$	[72]

2.3.4.2 AEMs Based on Aliphatic Backbone

AEMs composed of apliphatic components can be divided into two groups of (i) fluorinated and (ii) unfluorinated aliphatic polymers. The idea of applying aliphatic fluorinated polymers for AEMs has been borrowed from the PFSA structure in PEMs such that among AEMs, fluorinated polymers (tetrafluoroethylene with hexafluoropropylene (FEFP) and tetrafluoroethylene–ethylene copolymer (FEET)) show the great potential for the use as AEM in alkaline fuel cells (**Table 2-3**) [15, 51]. Nonetheless, both FEFP-based and FEET-based showed significantly lesser ion conductivities at lower relative humidity which makes them undesirable for fuel cell application. Clearly, the development of AEMs with high ion conductivities at low relative humidity conditions is one of the requirements to approach the commercialization of AEMFCs commercialization [73]. Furthermore, the fluorinated polymers have disadvantages such as the complicated preparation procedures and thus the high material cost. Therefore, some researchers commenced to develop cheaper unfluorinated polymeric AEMs [15, 51].

Among unfluorinated aliphatic polymers both "carbon-chain" (Polystyrene co-polymer with ethylene and butylenes (PSEB) [74], Quaternized Ammonium Polyvinyl Alcohol (QAPVA) [75] , Quaternized Chitosan (HACC) blended with QAPVA [76], etc.) and "hetero-chain" polymers (polyethers (PE) [77], the copolymer of epichlorohydrin and allyl glycidyl ether (PECH/AGH) [78], etc.) containing groups of ammonium bases in the side chain have been applied. To enhance the mechanical, thermal and chemical stability of AEMs, the polymer chains were cross-linked, or block copolymers were used. However, the increase of the degree of cross-linking results in more compact structure of the polymeric

membrane which narrows the hydroxide conducting channels and reduces the water uptake which could promote the ion conductivity.

Table 2-3. Characteristics of AEMs based on aliphatic structure

AEM	Chemical Structure	IEC ($mEq \cdot g^{-1}$)	Water Uptake (%)	Ion-conductivity at 25 °C ($S\ cm^{-1}$)	Ref.
FEFP	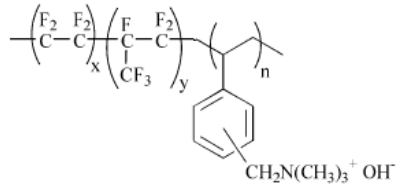	1.08	54	• $2.3 \cdot 10^{-2}$ (50 °C) • $1 \cdot 10^{-2}$ – $3.5 \cdot 10^{-2}$ (20-80 °C)	[79]
FEET	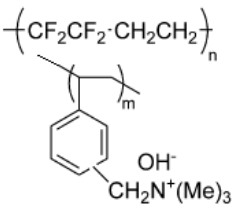	1.04 - 1.14	33-91	$3 \cdot 10^{-2}$	[80, 81]
PE	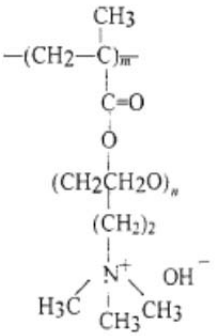	-	1.5 - 4.5	$5.4 \cdot 10^{-5}$ – $6.2 \cdot 10^{-3}$	[82]
PSEB	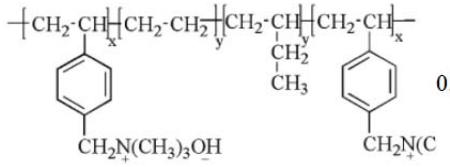	0.3	12	• $5.12 \cdot 10^{-3}$ (30 °C) • $9.93 \cdot 10^{-3}$ (80 °C)	[74]
PVA	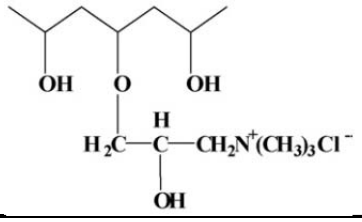	-	240	$7.34 \cdot 10^{-3}$ (30 °C)	[75, 76]

PECH/AGH	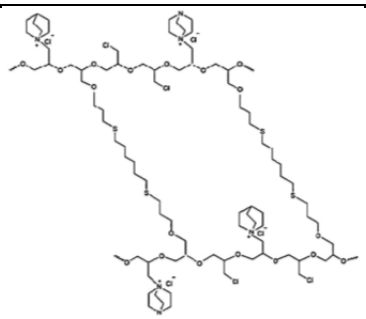	1.3	30-50	• $2.5 \cdot 10^{-3}$ (20 °C) • $1.3 \cdot 10^{-2}$ (60 °C)	[78, 83]
HACC / QAPVA		-	-	$1 \cdot 10^{-3} – 1 \cdot 10^{-2}$	[76]

2.3.4.3 Composite Organo–Inorganic AEMs

The main purpose of incorporating the inorganic fillers into the AEMs is to boost the ion conductivity, increase the thermal stability, and decrease the fuel (e.g., methanol) permeability [37]. Some of the aforementioned types of polymers (QAPVA and PPO) have been applied to create organo–inorganic composite AEMs through the sol–gel method. The organic polymers are composed of hydroxyl and QA groups in the salt form and combined with silicon-containing precursors such as tetraethoxysiloxane (TEOS) and/or phenyltriethoxysilane (EPh), followed by alkalinization of the obtained composite (**Table 2-4)** [72]. The presence of the hydroxyl groups assures covalent bonding of the organic and inorganic fillers during the heat treatment of the composite which has a significant effect on composite membrane properties. Increasing the incorporated amount of the inorganic filler (here the silicate phase) raises the IEC and water uptake, but, decreases the anion conductivity. This can be attributed to the increase of the bonded water content, which does not participate in anion transport [69]. Moreover, the decrease of anion

conductivity may be caused by the more compact structure of the formed organic-inorganic composite membrane [15, 51].

Table 2-4. Characteristics of organo-inorganic composite AEMs

AEM	Chemical Structure	Inorganic filler (wt.%)	IEC ($mEq \cdot g^{-1}$)	Water Uptake (%)	Ion-conductivity at 25 °C ($S\ cm^{-1}$)	Ref.
QAPVA/ TEOS composite	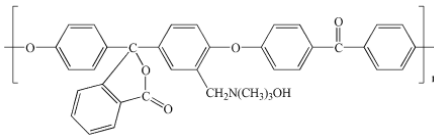	5, 10, 20	0.46 - 0.57	131 - 167	• (6.8-3.46)·10^{-3} (30°C) • 1.4·10^{-2} (60 °C, for 5 wt.% TEOS)	[69]
PPO/EPh composite	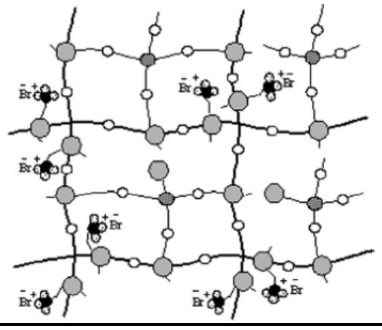	7.8	2 - 2.3	-	• 1.1·10^{-2} • 3.5·10^{-2} (60 °C)	[84]

Chapter 3
Experimental Studies and Characterization Techniques

Since the overall object of this work is to develop better membranes for fuel cell application, the required experimental procedures to make or modify electrolyte membranes followed by vital characterization tests including chemical, physical, thermal and electrochemical analysis are described in this chapter.

3.1 Experiment Procedures

3.1.1 Solution Casting Process

Solution casting process is a simple and low cost technique for isotropic membrane preparation. In this method, first, a solute is dissolved in a solvent to generate a casting solution and according to the desired membrane thickness the weight of the casting solution can be varied. Then the prepared solution is poured into a membrane-casting plate which is horizontally adjusted such that the casting solution is uniformly spread out into the plate. After, the top of the plate is covered with a watch glass and put into the convection oven to perform the heat treatment until the solvent in the casting solution is completely evaporated. The casting plate is then removed from the oven to be cooled down. After cooling, double deionized water (DDI H2O) is poured in the plate to loosen the membrane for being peeled off from the glass. Finally, the edges of the casted membrane are trimmed and by applying a standard preparation technique, the membrane is treated before starting any performance characterization tests [74, 85].

3.1.2 Chloromethylation and Quaternization

Regardless of the type of polymer applied to produce the AEM, the principal method of incorporation the quaternary ammonium (QA) groups into the compound is “polymer-like” conversions. The common polymer backbones for such a sequence of conversions are both polyheteroarylenes and polyphenylenes [68, 70, 75, 77, 86, 87] as well as the polymers with an aliphatic main chain with aromatic ringss in the side chain of the polymer [74]. The steps of this method involves (i) chloromethylation, (ii) quaternization of the created benzyl chloride constituents by a tertiary amine (e.g., triethylamine), and (iii) alkalinization of the produced salt in order to convert it into the base form (**Figure 3-1**). Chloromethylation is a vital step to identify the amount of ion-containing constituents grafted into the polymers. Normally, this stage is performed in a solution of chlorinated hydrocarbons [68, 70, 77, 86-89] and N-methyl-2-pyrrolidone (NMP) as the solvent [69]. Among chlorinated hydrocarbons, chloromethyl methyl ether (CMME) is the most common material for chloromethylation [69, 70, 77, 87, 88]. However, because of the toxic and carcinogenic nature of CMME, chloromethylation can be also realized with other solutions such as paraformaldehyde combined with HCl [69, 74, 89], chloromethyl octyl ether [86], and dimethoxymethane in conjunction with thionyl chloride [68]. The typical used catalysts for the chloromethylation reaction are $ZnCl_2$ [68-70, 77, 87, 89] and $SnCl_4$ [86]. Depending on the type of polymer backbone, the reaction temperature can be varied between 0 and 75 °C, and the reaction time between 75 and 137 hrs. Increase of the reaction time and temperature can result in cross-linking of the polymer chains [51].

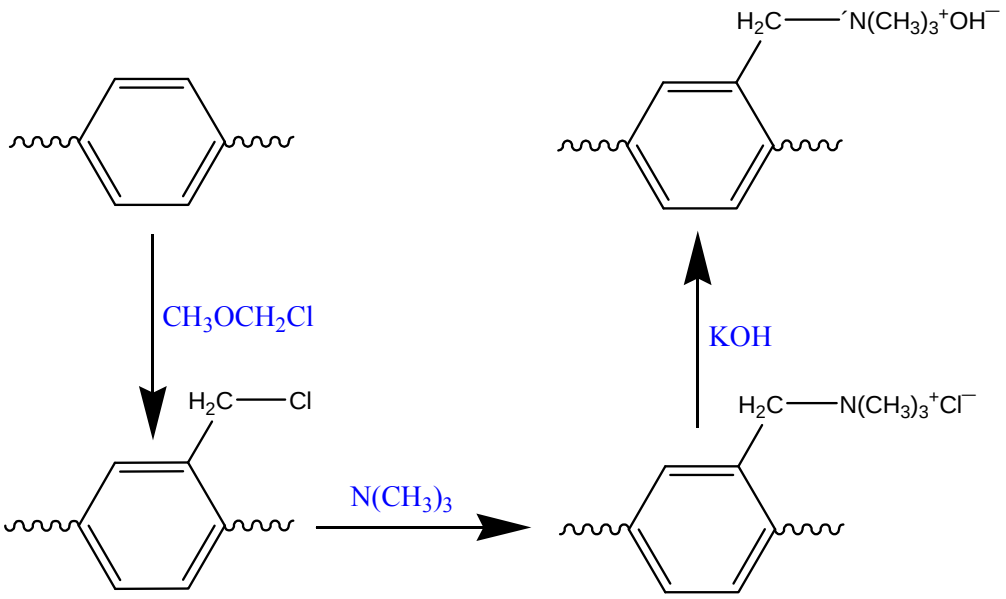

Figure 3-1. The general scheme of the insertion of the groups of quaternary ammonium bases into the polymers containing aromatic fragments.

3.2 Characterization Techniques

3.2.1 Elemental and Morphological Analysis

3.2.1.1 Fourier Transform Infrared (FT-IR) Spectroscopy

FT-IR spectroscopy is a very common-used method to recognize the molecular structures of organic compounds, mainly because it delivers significant amount of information and is fairly inexpensive and easy to perform. Advantages of FT-IR spectroscopy include:

(i) better signal-to-noise ratios; and,

(ii) the ability to record complete spectra in much shortest timescales.

Basically, the useful parts of the infrared (IR) region for the analysis of polymers have a wavelength ranging from 2500 to 16000 nm, with a corresponding frequency range from 1.9×10^{13} to 1.2×10^{14} Hz. The related photon energies of this range of the IR are from 1 to 15 kcal $mole^{-1}$ that are not big enough to excite electrons; yet, they are able to cause vibrational excitation of covalently bonded atoms and groups which can be stretched and bent. The characteristic of organic compounds is that they can go through a broad variety of vibrational motions of their constituent atoms, resulting in the absorbance of IR radiation related to the energy of the corresponding component vibration. Consequently, the existing bonds and functional groups in the polymer can be identified by comparing the absorptions positions in the IR spectrum with the characteristic absorption regions. However, it is not simple to explain absolutely the more precise features of IR spectra, such as those caused by alterations in tacticity. Such explanations are usually made on the basis of information obtained from other methods, especially nuclear magnetic resonance (NMR) spectroscopy (section **3.2.1.2**) which is the most powerful technique for identifying the detailed molecular structures of polymers [90].

3.2.1.2 Nuclear Magnetic Resonance (NMR) Spectroscopy

NMR is a physical phenomenon employed to explore the molecular properties of polymers by irradiating atomic nuclei in a magnetic field with radio waves. Both Hydrogen (H) and Carbon (C) NMR are widely used for conventional objectives such as polymer identification, proof of molecular structure and estimation of average co-polymer composition. Both utilize tetramethylsilane (TMS), $Si(CH3)_4$, as the reference compound. NMR spectroscopy, however, presents much greater scope than IR spectroscopy for clarifying the detailed

characteristics of molecular microstructure. NMR spectroscopy (especially C NMR) has the capability to give quantitative information on molecular microstructure properties which are not accessible through other techniques. These properties include (i) head-to-tail and head-to-head repeat unit linkages, (ii) the different types of repeat unit structures deriving from 1,3-diene monomers, (iii) isotactic and syndiotactic sequences of repeat units , and (iv) in co-polymers, the sequence distributions of the different repeat units present along the co-polymer chains [90].

3.2.1.3 X-Ray Photoelectron Spectroscopy (XPS)

In many applications, the key question is the chemical composition of the surface. XPS, also known as electron spectroscopy for chemical analysis (ESCA), is an experimental technique which is commonly used in these studies. In this method, the sample is irradiated with x-rays of known energy, thus causing emission of electrons by the photoelectric effect. The binding energy spectrum of these photoelectrons is recorded, and by analyzing the spectrum, the elements present within a few nanometers from the sample surface can be identified and their relative abundances can be determined. Moreover, in many cases also the different chemical states of the elements can be distinguished [91, 92].

3.2.1.4 X-Ray Diffraction (XRD)

XRD is a useful technique to describe the crystal structure of a material. It is based on well known Bragg's law on diffraction which states that when a sample is irradiated with monochromatic radiation, intensity maxima are observed in angles θ given by **Equation 3-1**.

$$\sin(\theta) = \frac{n\lambda}{2d}$$ **Equation 3-1**

where n, λ, d, and θ represent the order of the spectrum, the wavelength of the X-rays, the lattice spacing of the crystal, and the angle of incidence, respectively. In practice, the intensity of diffracted X-rays is recorded as a function of the angle, and the angles giving the intensity maxima are compared with a database containing the diffraction patterns of several structures. It is to be noted, however, that XRD cannot detect amorphous materials. Amorphous structures with poorly defined characteristics yield diffuse patterns, compared to the distinct intensity peaks obtained with crystalline materials [91, 92].

3.2.1.5 Scanning Electron Microscopy (SEM)

In SEM, an electron beam with a spot size of a few nanometers is scanned over the sample. The image is constructed so that the intensity of a given pixel is determined by the intensity of detected secondary and/or backscatters electrons corresponding to that point on the surface. Imaging with SEM is fast and easy but the resolution is typically lower. In addition, SEM produces no direct height information of the surface structures and is sometimes difficult to use with insulating samples [91].

3.2.1.6 Transmission Electron Microscopy (TEM)

Through TEM technique the objects can be seen to the order of a few angstroms (10^{-10} m). Small details in polymeric membranes can be studied down to near atomic levels. TEM operates on the same basic principles as the light microscope but uses electrons instead of

light. TEMs use electrons as “light source” and their much lower wavelength make it possible to get a resolution a thousand times better than with a light microscope [93].

3.2.2 Physical Properties

3.2.2.1 Mechanical Properties

Polymers are often thought of as being mechanically weak and their mechanical properties have consequently been somewhat ignored in the past. These days many polymers are used in structural engineering applications and are subjected to appreciable stresses. This increase in use has been due to several factors. One of the most important being that, although on an absolute basis their mechanical strength and stiffness may be relatively low compared with metals and ceramics, when the low density of polymers is taken into account their specific strength and stiffness become more comparable with those of conventional materials. Polymers melt at relatively low temperature and can be readily molded into quite intricate components using a single molding. The mechanical properties of polymer electrolytes can be considered in terms of the molecular deformation processes which occur. This approach has been facilitated by a better understanding of polymer structure [90].

3.2.2.2 Water Uptake (WU) and Ion Exchange Capacity (IEC)

The Water Uptake (WU) is a measurement which exhibits the capability of an ion conductive electrolyte membrane to retain the water. The speed and extent of membrane water uptake depend on the membrane’s viscoelastic mechanical properties, which are themselves dependent on membrane hydration, and increased hydration enhances membrane ion conductivity and fuel cell performance [75, 83]. To calculate WU, the desired membrane is

first immersed and saturated in deionized water at room temperature for 24 hrs. Then the wet membranes are taken out and weighed immediately after the water droplets are removed from the surface. Then, they are vacuum dried at 80 °C for 24 hrs, put into a plastic sealing bag immediately and weighed. Then, the WU can be determined from the following **Equation 3-2** [94, 95]

$$WU(\%) = \frac{W_{wet} - W_{dry}}{W_{dry}} \times 100 \qquad \textbf{Equation 3-2}$$

where WU (%), Wwet and Wdry are the water uptake by weight percentage, the weight of wet membrane and the weight of dry membrane respectively.

Ion Exchange Capacity (IEC) is a key property of an electrolyte membrane which determines how much ions can be exchanged per the weight of the membrane. Generally, IEC is recognized by a back titration method. At first, the samples are dried until the weight becomes constant. After, the membranes are soaked in a specific concentration of NaCl (e.g. 2 M) for 24 hrs to exchange sodium ions with existed protons in the membranes. Back titration is then accomplished with a standardized solution of NaOH and IEC values are calculated through the following **Equation 3-3** [96].

$$IEC = \frac{V_{NaOH} C_{NaOH}}{W_{dry}} \qquad \textbf{Equation 3-3}$$

where IEC is the ion exchange capacity (meq g^{-1}), V_{NaOH} the added titrant volume at the equivalent point (mL), C_{NaOH} is the molar concentration of the titrant, W_{dry} is the dry mass of the sample (g).

3.2.3 Thermal Properties

3.2.3.1 Thermal Gravimetric Analysis (TGA)

TGA is a continuous process to study the thermal degradation of polymeric materials which involves the measurement of sample weight as the reaction temperature is changed by means of a programmed rate of heating. Mass is lost if the substance contains a volatile fraction. Thus, the sample weight decreases slowly as reaction begins, then decreases rapidly over a comparatively narrow temperature range, and finally levels off as the reactant becomes spent [97].

3.2.3.2 Differential Scanning Calorimetry (DSC)

DSC analyzes thermal transitions occurring in polymer samples when they are cooled down or heated up under inert atmosphere (not based on a change in sample mass as in TGA). Melting and glass transition temperatures can be determined as well as the various transitions in liquid crystalline mesophases. Glass Transition is a method to characterize a property of a polymeric material. The glass transition is the temperature (Tg) where the polymer goes from a hard, glass like state to a rubber like state. DSC defines the glass transition as a change in the heat capacity as the polymer matrix goes from the glass state to the rubber state. This is a second order endothermic transition (requires heat to go through the transition) so in the DSC the transition appears as a step transition and not a peak such as might be seen with a melting transition. Most polymers have Tg's but technically its measurement depends on a crystalline transition so if a polymer is largely or totally amorphous in nature it may not have (or readily exhibit) a Tg [98].

3.2.4 Electrochemical Properties

3.2.4.1 Ion Conductivity Measurement via Electrochemical Impedance Spectroscopy (EIS)

In order to study the electrochemical performance of polymeric electrolyte membranes, their capability to transfer the ions (protons or hydroxides) must be evaluated. In this respect, EIS is the well-known technique to measure and analyze the materials in which ionic conduction strongly predominates. The ion conductivity is generally obtained from the measurement of resistivity of the ion-conductive membrane against the flow of alternating current (AC). These measurements are carried out at different AC frequencies and, thus, the name impedance spectroscopy was later adopted. The polarization, the distribution of chemical potential, and changes of electrode reaction should be considered in the measurement of resistivity with the current flow, which is classified into the two-terminal and four-terminal methods. The four-terminal method is usually used to measure the resistivity of ion conductors with low resistance, because of the reduced interfacial resistance and polarization, whereas the two-terminal method is restrictively applicable to the measurement of resistivity in material of high resistance (above 106 Ω), as the contribution for resistance of the lead itself is low enough to be neglected in the total resistance. The values of ion conductivities measured using the four-probe method were always higher (2-5 times) than those measured using the two-probe method at ambient humidity and temperature [99-102]. The ion conductivity of electrolyte membranes is measured in the longitudinal direction, and is calculated using **Equation 3-4** [102-105].

$$\sigma = \frac{L}{AR}$$ **Equation 3-4**

where σ, L, R, and A denote the ionic conductivity, sample length (or distance between the reference electrodes in the membrane), the resistance of the membrane), and the cross-sectional area of the membrane, respectively.

Chapter 4

Functionalized Titania Nanotube Composite Membranes for High Temperature Proton Exchange Membrane Fuel Cells

Chapter 4 is based on published work by Jun et al. [31] and is reproduced with permission from the International Journal of Hydrogen Energy. The thesis author's specific contributions to this paper were to synthesize and fabricate the nano-composite membrane, conduct the EIS measurements, run some parts of physicochemical characterization tests including water uptake and TGA, prepare the final plots and results, write the final manuscript and respond to the comments of reviewers. This work and journal paper preparation was conducted with direction from the project supervisors who are co-authors on the publication. The post-doc fellow, Yu Jun aided with the main idea development and performing most of physicochemical characterization tests including XRD, XPS, FT-IR, and TEM.

4.1 Introduction

Hydrogen as a storage and carrying medium of renewable energy resources, can be converted to electricity by using electrochemical energy converters like proton exchange membrane fuel cells (PEMFCs) [106]. Proton exchange membrane fuel cells (PEMFCs), also known as polymer electrolyte fuel cells, have emerged as promising power supply systems for stationary, vehicular, and portable applications [107, 108]. These devices are traditionally based on perfluoro-sulfonic acid membrane electrolytes, given the commercial name Nafion. However, Nafion membranes are restricted to operating temperatures below 100 ˚C. At temperatures approaching the boiling point of water, Nafion exhibits a drastic ionic

conductivity loss which hinders the PEMFC operation at temperatures higher than 80 ˚C and/or reduced relative humidity (RH < 100%). In addition, the mechanical and dimensional stability of the polymer chains can be diminished at high temperatures as a result of the relatively low glass transition temperature of Nafion [109, 110]. To achieve a timely, sustainable commercialization of PEMFC, the development of proton exchange membranes for high temperature operation is a necessity and has been receiving a great deal of attention. The ability to perform at high operation temperatures in the range of 100–130 °C is desirable in order to significantly boost PEMFC performance. This results from the enhancement of several important parameters including; i) electrode reaction kinetics (mainly the oxygen reduction reaction (ORR)), ii) carbon monoxide (CO) tolerance, and iii) simplified water and thermal management of the fuel cell system [13, 27, 109, 111].

To overcome the temperature limitations of the current electrolyte materials, several organic/inorganic hybrid membranes have become the focus of intense research recently [112, 113]. So far, many kinds of inorganic fillers, such as TiO_2, SiO_2, ZrO_2, zeolite nanoparticles as well as mesoporous silica (MCM41) have been employed for use in these organic/inorganic hybrid membranes for PEMFC applications at high temperatures [17, 114-127]. Such composite electrolytes have been proposed as potential replacements for Nafion in PEMFCs operating at a temperature range of 100–150 ˚C and/or low relative humidity. Because they have good water retention and enhance the membrane stability [111, 112, 128-130]. The proton conductivity of these hybrid membranes is still inferior when compared to recast Nafion membranes , which is believed to derive mainly from the increased barrier properties of the membranes, due to the incorporation of inorganic fillers (an increase in

inorganic particle agglomeration at higher concentrations of inorganic additives) [131, 132]. In order to increase the proton conductivity of these hybrid membranes, functionalized nanoparticles have been employed. After functionalization, the nanoparticles can display improved proton conductivity, the ability to hold more water and a more homogeneous dispersion among the hydrophilic sites of the Nafion, compared with non-functionalized nanoparticles [133-136]. Moreover, dimensionality plays a critical role in governing the properties of materials due to the different ways that electrons interact with nanostructures of varying dimensions (3-D, 2-D, 1-D and 0-D). Compared with 0-D nanostructures (i.e. nano-particles) and 2-D nanostructures (i.e. thin films), 1-D nanostructures (including nanotubes, nanowires and nanorods) are ideal for various potential applications such as composite materials, due to their unique electronic and structural properties [122, 137, 138]. Among them, nanotubes have attracted interest for potential application in high temperature PEMFCs, due to their distinct morphology, high-specific surface area, thermal stability and corrosion resistance [139-143]. Their 1-D nanostructure leads to higher water retention and it is proposed that they can produce a continuous channel to improve the proton conductivity [139, 140, 144-146]. Also, among all the previously mentioned nanostructured metal oxides, TiO_2-based nanotubes (TiO_2-NT) with a high specific surface area and ion-changeable capabilities have been considered for use in a variety of applications [140, 147-150]. Matos et. al. [147] employed TiO_2-NT in high temperature PEMFC Nafion composite membranes. Their results indicated that the addition of TiO_2-NT resulted in a decrease in the overall proton conductivity, attributed to the low conductivity of the nanotube additives within the Nafion matrix. An enhanced fuel cell performance however was observed at temperatures

greater than 120 °C, which can be attributed to the larger water retention capacity of TiO_2-NT which originates from their high specific surface area [147].

In this study, TiO_2-NT were functionalized by using 3-mercaptopropyltri-methoxysilane (MPTMS 98 wt.%) as a precursor for the formation of sulfonate groups. As shown in the schematic of **Figure 4-1**, these nanotubes have a high specific surface area and when combined result in highly ordered nanotube arrays which provide excellent pathways for protons. Moreover, functionalization can provide sulfonate groups which will serve to increase the proton conductivity of these materials. Therefore, by combining these two distinct advantages, functionalized TiO_2-NT (F- TiO_2-NT) has potential for application in high temperature PEMFCs. The structure and proton conductivity of F-TiO_2-NT and F-TiO_2NT/Nafion composite membranes were studied at high operating temperatures and low relative humidity in order to evaluate their advantages at high temperature PEMFCs. F-TiO_2-NT/Nafion composite membranes are presented as potential replacements for commercial Nafion membranes in high temperature PEMFCs.

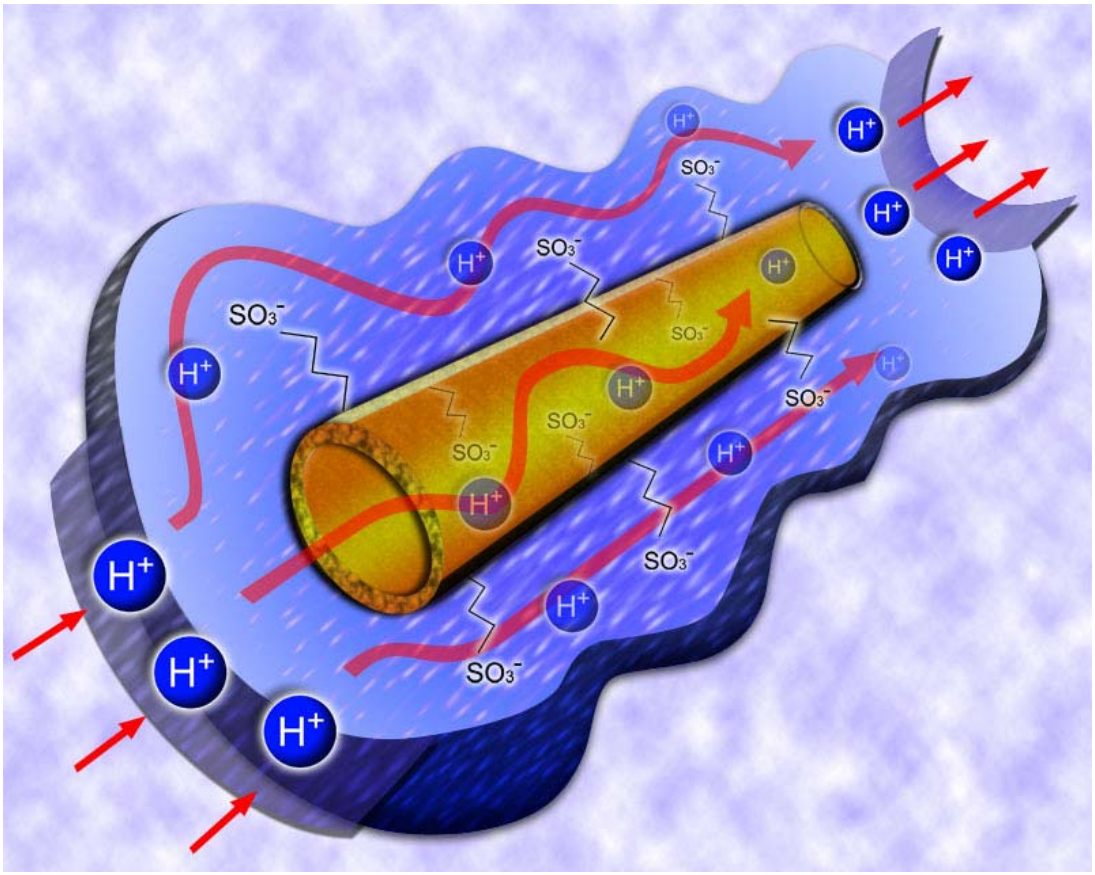

Figure 4-1. Schematic of proton conduction in F-TiO_2-NT/Nafion composite.

4.2 Experimental

4.2.1 Synthesis of the Titania Nanotubes

TiO_2-NT were prepared by the alkaline hydrothermal method [140, 144]. A brief description is outlined here. First, 0.9 g of titania nanoparticle (<25nm) was mixed with 120 mL of 10 M NaOH solution. The resulting mixture was stirred and ultrasonicated for several minutes before pouring the solution into a stainless steel/Teflon autoclave which was heated for 48

hrs at 140 ˚C. Finally, the solution was filtered with deionized water, washed with 40 mL of 0.1 M HCl and dried overnight.

4.2.2 Functionalization of TiO_2-NT

The functionalization of titania nanotubes was performed by using MPTMS as the sulfonic acid functional group precursor [145]. The reaction was carried out in toluene at a temperature of 110 ˚C under reflux conditions for 24 hrs, with 1:2:20 molar ratios of TiO_2-NT, MPTMS and toluene respectively. The mercapto groups grafted onto the TiO_2-NT were then oxidized to sulfonic acid groups by using 30 wt.% H_2O_2 solution at 25 ˚C for 24 hrs. The prepared samples were filtered and washed with ethanol and water to remove the precursor residue. Samples were dried overnight prior to characterization. For comparison, titania nanoparticles were also functionalized under the same procedure as mentioned above.

4.2.3 Membrane Fabrication

In order to cast the pure Nafion membrane, 15 wt.% Nafion solution was mixed with an appropriate amount of ethanol. The mixture was then sonicated in an ultrasonic bath for 30 min followed by heating at 60 ˚C until the liquid evaporated. Finally, it was heated for 2 hrs at 100 ˚C and for 1 hour at 140 ˚C.

F-TiO_2-NT/Nafion composite membrane was casted by mixing 5 wt.% F- TiO_2-NT with an appropriate amount of 15 wt.% Nafion solution and ethanol mixture. After, as same as the pure Nafion casting procedure, it was ultrasonicated for 30 min and heated at 60 ˚C until the liquid evaporated. Finally, it was heated at 100 ˚C for 2 hrs and then 140 ˚C for 1 h [113].

Both pure Nafion and F-TiO_2-NT/Nafion composite membranes were pretreated by boiling in a 3% H_2O_2 aqueous solution for 1 h, rinsed in boiling deionized water for 1 h, boiled in 0.5 M H_2SO_4 for 1 h, and finally rinsed again in deionized water before being tested [117].

4.2.4 Physical Characterization

The morphology of unmodified TiO_2-NT was examined by using transmission electron microscopy (TEM, JEM-100CX II). The specific surface areas of TiO_2-NT and F-TiO_2-NT were determined by the Brunauer-Emmett-Teller (BET) method. After functionalization, the F-TiO_2-NT was analyzed using Fourier transform infrared spectroscopy (FTIR, PerkinElmer-283B FT-IR Spectrometer) and X-ray diffraction (XRD, RigakuD/max2500v/pa, Cu Kα, 40 kV, 200mA, $8^{\circ}min^{-1}$). X-ray photoelectron spectroscopy (XPS, Thermal Scientific K-Alpha XPS spectrometer) was used to investigate the elemental composition and atomic configuration of TiO_2-NT. To probe the dehydration properties, Thermogravimetric analysis (TGA) of the unmodified and modified TiO_2-NT was performed on a TGA Q500 V20.10 Build 36 system in a temperature range from 50 to 700 °C at a heating rate of 10 °C/min in a N_2 atmosphere.

4.2.5 Water Uptake

In order to measure the water retention capability of the membranes, the Water Uptake (WU) was calculated. For this, they were first immersed and saturated in deionized water at room temperature for 24 hrs. Then the wet membranes were taken out and weighed immediately after the water droplets were removed from the surface. Then, they were vacuum dried at 80 °C for 24 hrs, put into a plastic sealing bag immediately and weighed. This experiment was

replicated 4 times for each membrane and the water uptake was determined from the following equation [151, 152]:

$$WU(\%) = \frac{W_{wet} - W_{dry}}{W_{dry}} \times 100 \qquad \textbf{Equation 4-1}$$

4.2.6 Proton Conductivity

The proton conductivity of TiO_2-NT, F-TiO_2-NT and titania nanoparticles were measured using a two-electrode setup under controlled temperature and degree of water saturation [153]. First, each of the powdered samples was individually loaded into a tube cell with a diameter of 1.6 mm in which the two electrodes are inserted from the top and bottom. Then, they were pressed for several hours. To attain water-saturated conditions (100 % humidity), the fixture was disassembled from the top and 20 μL of double deionized water was injected with a syringe onto the sample in each cell. The water was allowed to soak into the samples for 30 min. Then the top electrodes were replaced, the fixture was reassembled, and the sample cells were retorqued.

The proton conductivity of a pure Nafion membrane and a F-TiO_2-NT/Nafion composite membrane was measured using a four-electrode AC impedance method [104, 154] under various conditions of relative humidity and temperature. During measurements, the humidity was controlled by mixing water-saturated nitrogen gas with dry nitrogen gas, while the temperature was fixed at 80, 100 and 120 °C. On average, the needed equilibration time to reach the steady state for each relative humidity was 45 min.

The conductivity of all powdered samples and different membranes was then measured in the longitudinal direction, and was calculated using the following equation [104, 148, 154, 155]:

$$\sigma = \frac{L}{AR}$$ **Equation 4-2**

where σ, L, R, and A denote the ionic conductivity, sample length (or distance between the reference electrodes in the membrane), the resistance of the sample (or the membrane), and the cross-sectional area of the sample (or the membrane), respectively.

4.3 Results and Discussion

The TEM of TiO_2-NT is shown in **Figure 4-2**. Several TiO_2-NT are observed, displaying uniform outer diameters of approximately 5 nm. The BET surface area of titania nanoparticles (TiO_2-NP) was 186.5 m^2 g^{-1}, while that of titania nanotubes (TiO_2-NT) increased to 381.2 m^2 g^{-1} which would be advantageous for the application of the nanotubes in the structure of Nafion nanocomposite to boost the proton conductivity of the electrolyte membrane.

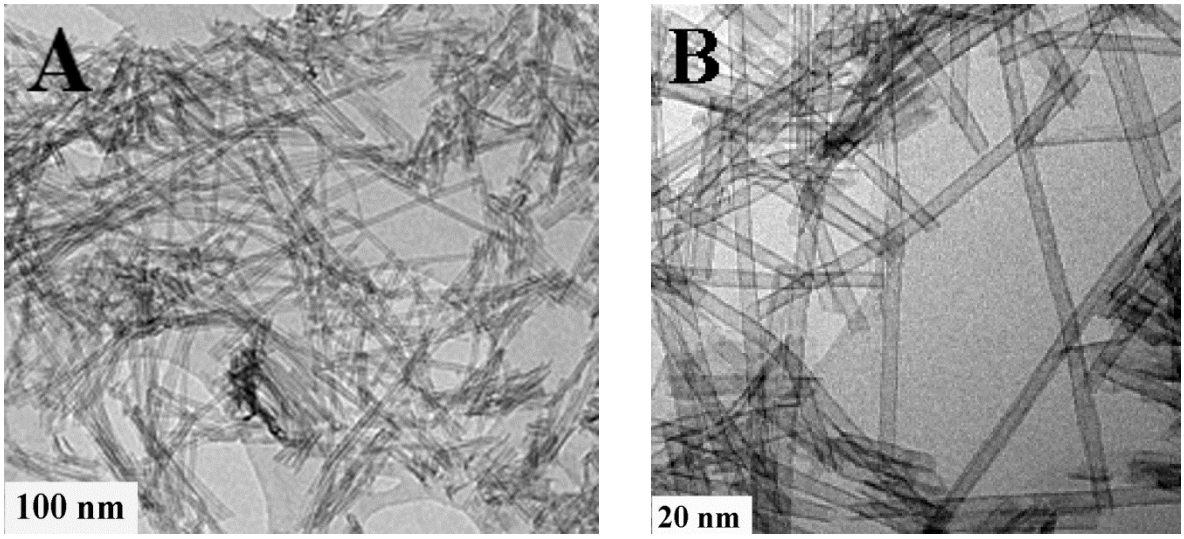

Figure 4-2. TEM image of TiO_2-NT at (A) low and (B) high resolutions.

The FT-IR spectra of the TiO_2-NT and F-TiO_2-NT are shown in **Figure 4-3**. The peaks at 669 cm^{-1} and 1634 cm^{-1} are attributed to the Ti-O-Ti and hydroxyl groups, respectively. By comparing the unmodified TiO_2-NT with F-TiO_2-NT, it can be observed that the sulfonic acid group shows a peak which is located at 1044 cm^{-1}. This analysis confirms the successful presence of the sulfonic acid group that has been grafted onto the TiO_2-NT.

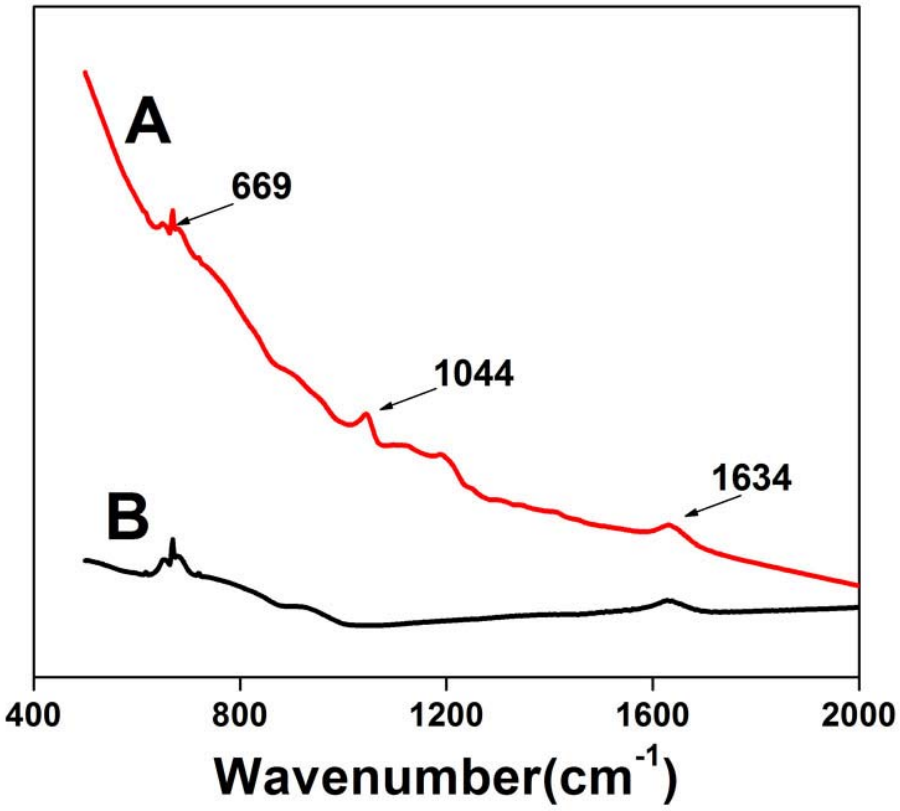

Figure 4-3. FT-IR spectra of (A) F-TiO_2-NT and (B) TiO_2-NT.

The XRD pattern of unmodified and functionalized TiO_2-NT is shown in **Figure 4-4**. The intensive diffraction peaks in this pattern can be attributed to the anatase phase of TiO_2 (JCPDS 89- 4921), corresponding to the (101), (004), (200), and (204) planes. It should be noted that there is a slight deviation between the unmodified and functionalized titania nanotubes at the (101) plane of TiO_2 anatase phase. This difference may be attributed to the functionalization which causes a shift in the crystalline structure.

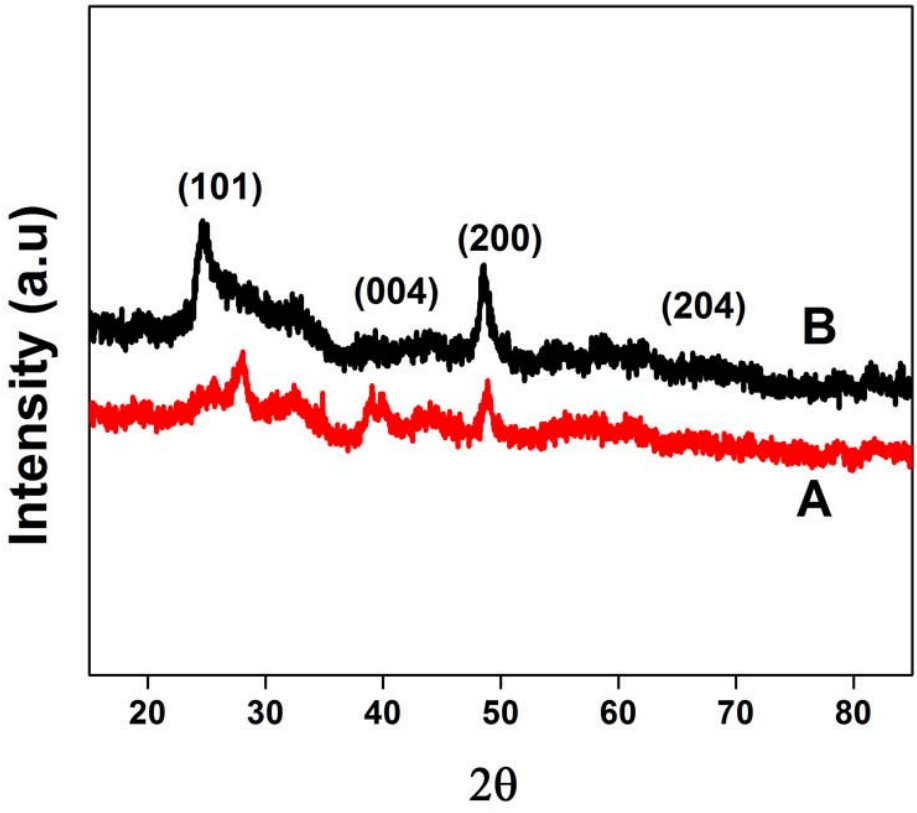

Figure 4-4. XRD of (A) F-TiO_2-NT and (B) TiO_2-NT.

The chemical composition of both unmodified and functionalized Titania nanotube (TiO_2 -NT and F-TiO_2-NT) were characterized by XPS measurements. Typical XPS patterns are presented in **Figure 4-5**. It can be seen that the TiO_2-NT and F-TiO_2-NT particles contain the Ti 2p and O 1s peaks of the titanium dioxide (Figures 4a and 4b). The spectrum of the F-TiO_2-NT particles also contains C 1s and S 2p peaks in addition to the Ti 2p and O 1s peaks, confirming the presence of the MPTMS surface modifier.

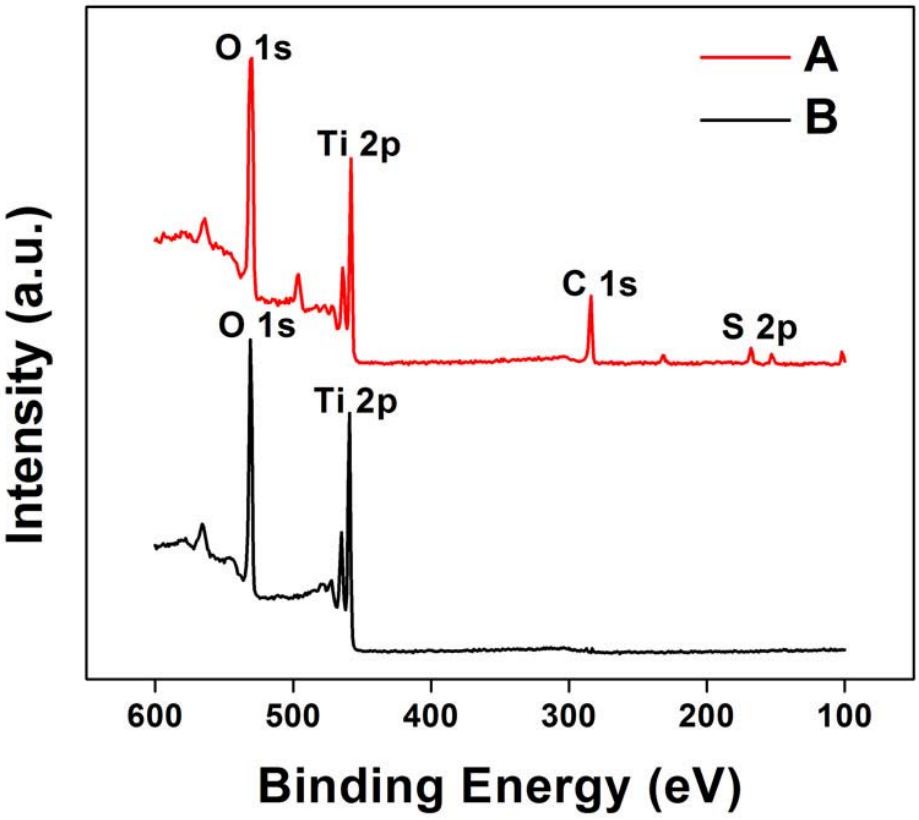

Figure 4-5. XPS survey spectra of (A) F-TiO_2-NTand (B) TiO_2-NT.

Figure 4-6 shows the TGA for F-TiO_2-NT and TiO_2-NT samples. For both membranes, the mass loss below 160 °C is due to the removal of water which is 14.3 % F-TiO_2-NT and 17.2 % for TiO_2-NT. This water may be present in the form of membrane hydration, or in the structure of acidic solid for F-TiO_2-NT. For the pristine TiO_2-NT no other weight loss is observed. However, the TGA graph for F-TiO_2-NT shows significant decomposition at 220 °C which can be attributed to the loss of functional groups in the sample [156, 157].

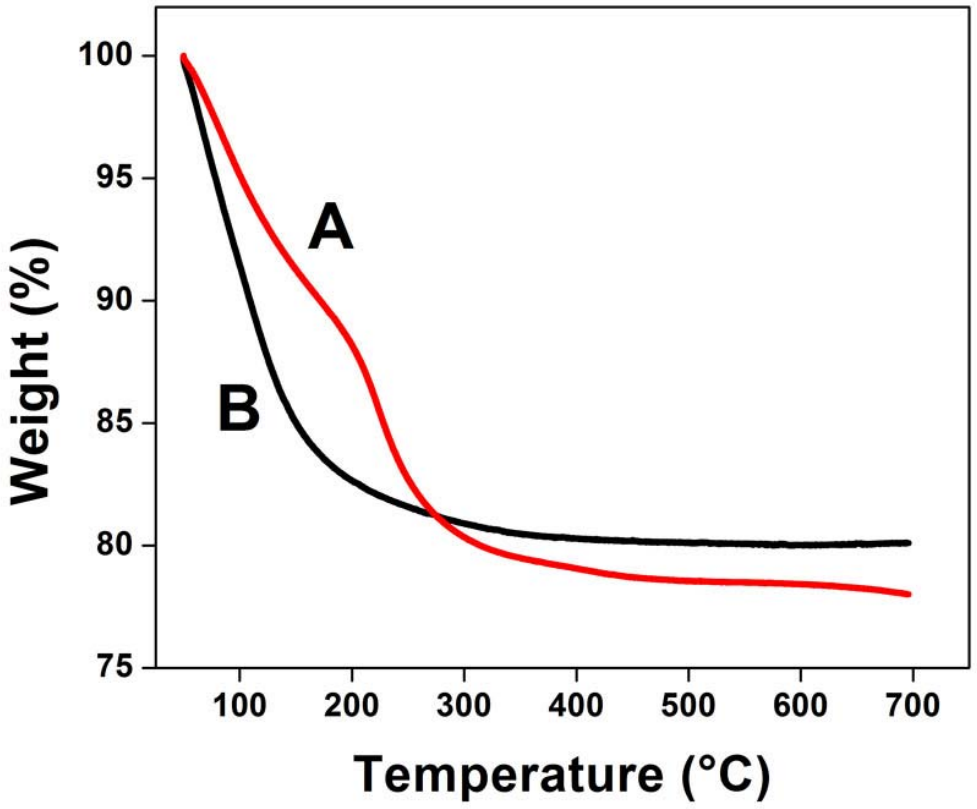

Figure 4-6. TGA of (A) F-TiO_2-NT and (B) TiO_2-NT.

In **Table 4-1**, the water uptake of 5 wt.% F-TiO_2-NT and 5 wt.% functionalized titania nanoparticle (F-TiO_2-NP) Nafion composite membranes are compared to recast and commercial Nafion 112. It is seen that the water uptake of F-TiO_2-NT/Nafion composite is about 7, 4 and 2 % higher than Nafion 112, recast Nafion and F-TiO_2-NP/Nafion, respectively. These results suggest that the one dimensional structure of nanotubes with high specific surface areas leads to higher water retention of Nafion composite membranes than

any other tested structure. This can be explained by the reduction of crystallinity and stronger interactions between the absorbed water and the network of the F-TiO_2-NT/Nafion membrane which results in enhancement of its proton conductivity. Specifically, when the membrane absorbs higher amount of water, the number of exchange sites available per cluster increases, resulting in an increment in the proton conductivity [158].

Table 4-1. Membrane water uptake values at 25 °C.

Type of membrane	Water uptake (%)	Standard Deviation
5 wt.% F-TiO_2-NT/Nafion	27.18	±0.2075
5 wt.% F-TiO_2-NP/Nafion	23.72	±0.3202
Recast Nafion	25.53	±0.2347
Nafion 112	20.19	±0.3294

Impedance spectroscopy is performed to investigate the conductivity of F-TiO_2-NT at different temperatures. Typical impedance spectra are shown in **Figure 4-7** in which the data exhibit high frequency, depressed semicircle, and the often observed low-frequency tail, indicative of ionic conductivity. The AC resistance of each sample is read from the high-frequency intercept of the semicircular arc with the real axis or by curve-fitting a semicircular arc to the data. From Figure 6, the F-TiO_2-NT at 20 ˚C exhibits a larger resistance than that at 80 ˚C.

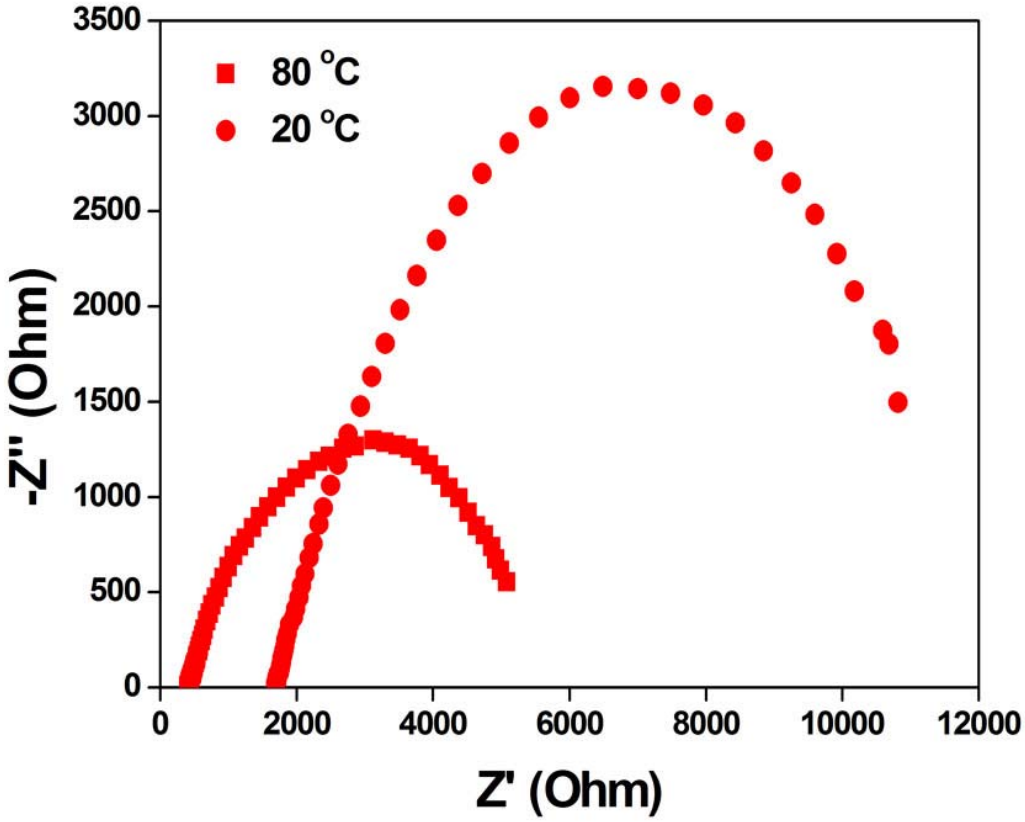

Figure 4-7. The Nyquist plot of the impedance spectrum of F-TiO_2-NT at (■) 80 °C and (●) 20 °C with 100% relative humidity.

Figure 4-8 shows the proton conductivity of the unmodified and functionalized TiO_2-NT at 100 % relative humidity and different temperatures. It can be seen that by raising the temperature from 20 ˚C to 80 ˚C the proton conductivity of TiO_2-NT has not considerably changed (~ 0.0011 S cm^{-1}). However, the conductivity of the F-TiO_2-NT has increased from 0.013 to 0.08 S cm^{-1} as a result of this temperature increase. It is believed that the sulfonic

acid groups have strongly affected this change. Thereby, this beneficial improvement can pave the way for significant enhancements in PEMFC efficiencies at higher temperatures.

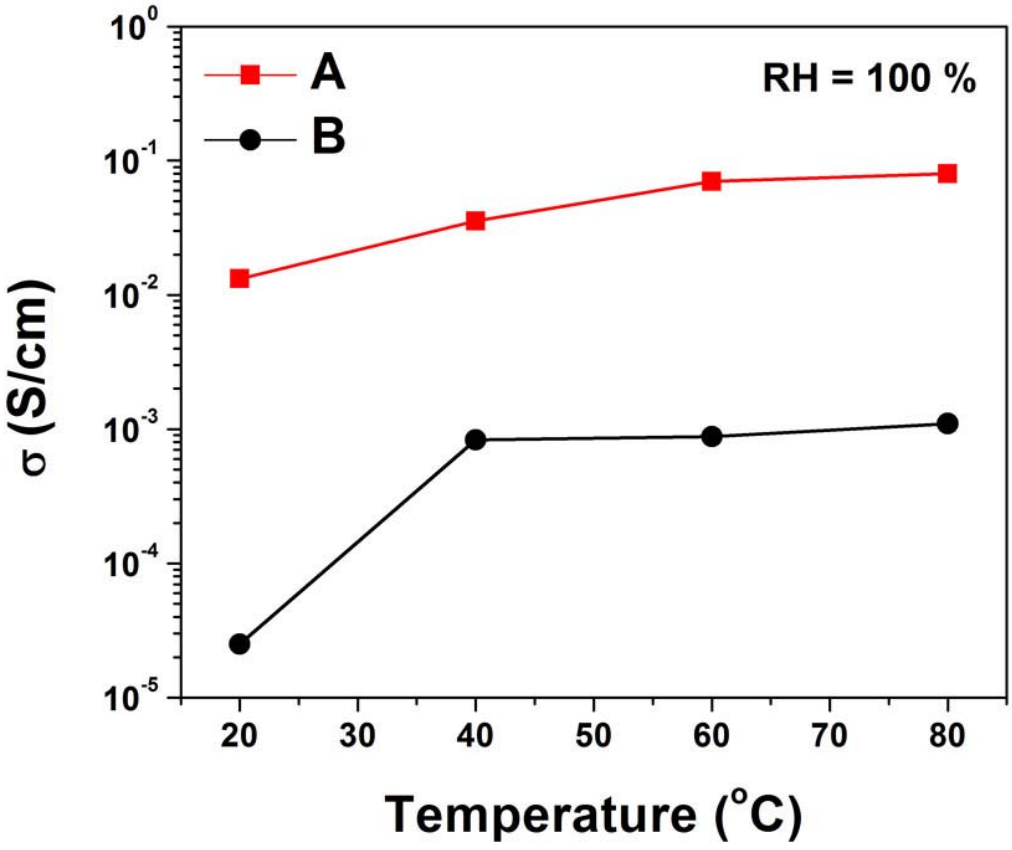

Figure 4-8. Proton conductivity of (A) F-TiO_2-NT and (B) TiO_2- NT at different temperatures and the relative humidity (RH) of 100%.

Figure 4-9 indicates that after functionalization the conductivity of TiO_2-NT (0.08 S cm^{-1}) is much higher than titania nanoparticles (0.03 S cm^{-1}) at 80 ˚C and 100 % humidity. This is due to the significantly higher specific surface area of the TiO_2-NT, that when functionalized,

can anchor a higher number of sulfuric acid groups compared to titania nanoparticles. Therefore, the F-TiO_2-NT shows a higher overall proton conductivity.

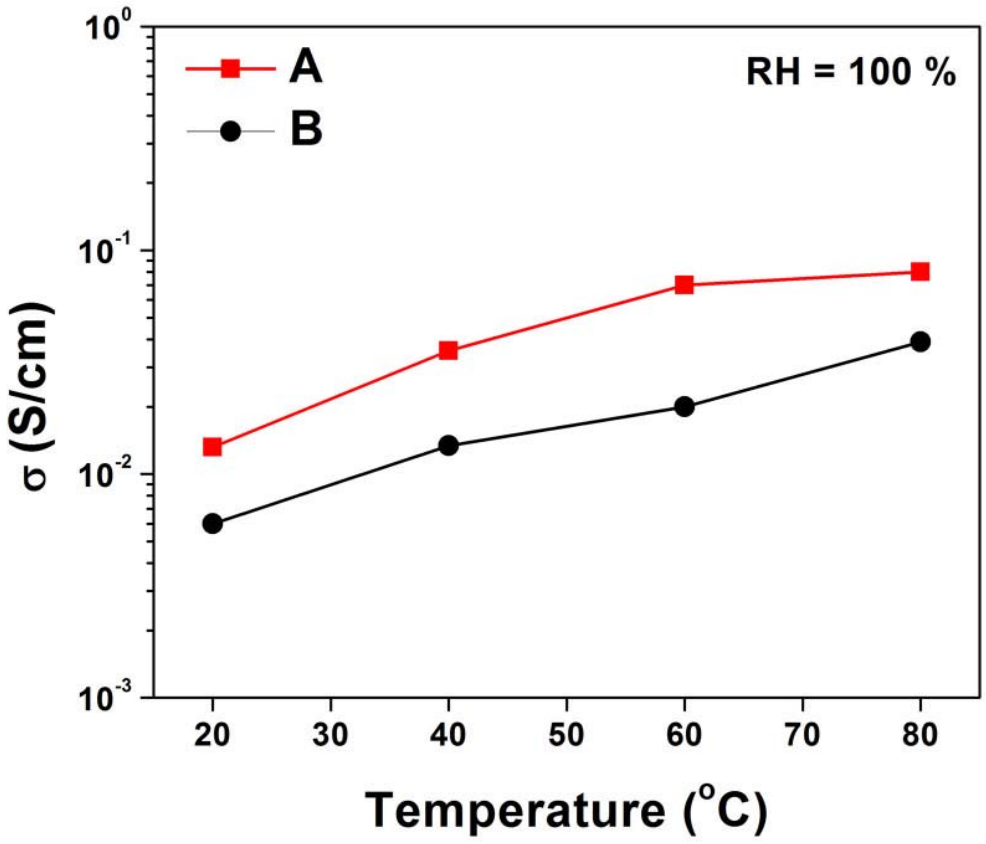

Figure 4-9. Proton conductivity of (A) F-TiO_2-NT and (B) F-TiO_2- NP at different temperatures and the relative humidity (RH) of 100%.

Figure 4-10 is the Arrhenius plot of the unmodified and functionalized TiO_2-NT, illustrating the temperature dependence of proton conductivity. It is seen that at 100 % relative humidity level, ion conductivities increased with increasing temperature, however,

that for F-TiO_2-NT was much higher compared to TiO_2-NT. Moreover, the conductivity of F-TiO_2-NT showed an Arrhenius behavior (**Equation 4-3**), while that of TiO_2-NT displayed some deviation from the trend. This shows that after functionalization, TiO_2-NT has high and relatively stable proton conductivity; i.e. the natural logarithm of conductivity for F-TiO_2-NT increases more linearly with temperature rise than that for non-functionalized TiO_2-NT. The natural logarithmic form of the Arrhenius equation is as follows:

$$\ln(\sigma) = \ln(A) - \frac{E_a}{RT} \qquad \textbf{Equation 4-3}$$

where σ, A, E_a, R and T represent ion conductivity, exponential prefactor, activation energy, gas constant and temperature, respectively. The activation energies of proton conduction in TiO_2-NT and F-TiO_2-NT were calculated to be 51.34 and 26.95 kJ mol^{-1}, respectively. As it is seen, there is a significant decrease in the activation energy of conductivity in F-TiO_2-NT, suggesting that the proton conduction is more facile with the presence of sulfonic acid groups in titania nanotubes which can enhance the transport of protons in composite membranes [159].

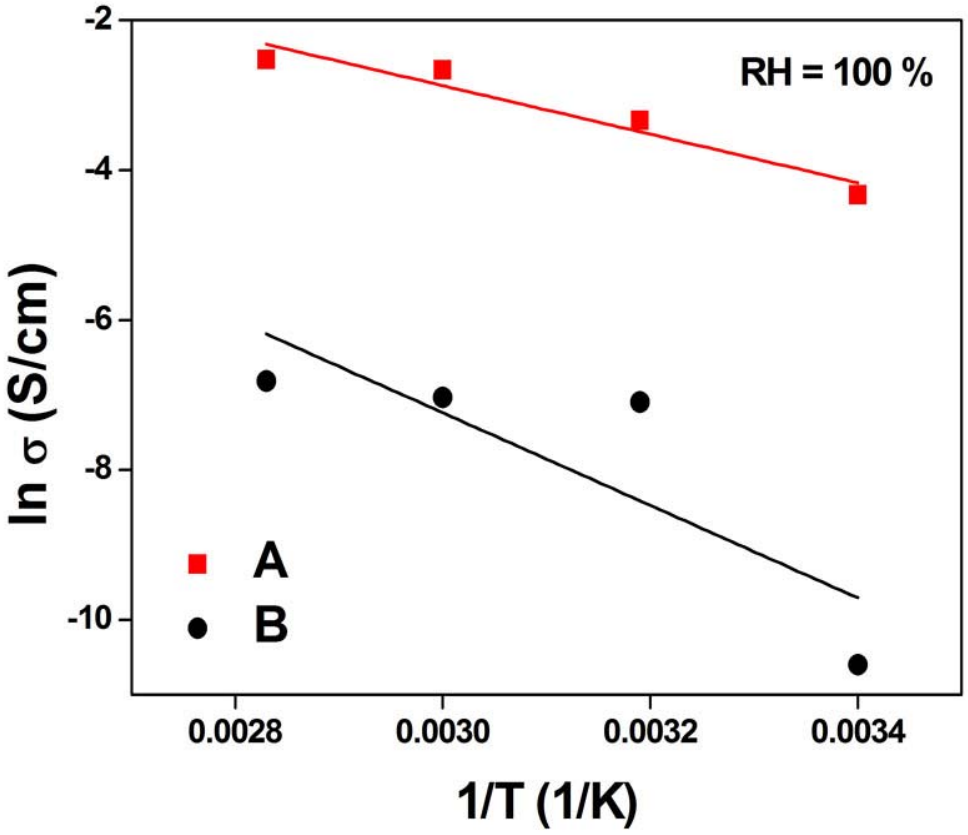

Figure 4-10. Arrhenius plot for the conductivity of (A) F-TiO_2-NT and (B) TiO_2-NT at 100% relative humidity.

So far it has been shown that after functionalization, the TiO_2-NT possesses very good proton conductivity. In order to ensure that this can be demonstrated for the F-TiO_2-NT/Nafion composite membrane, the proton conductivity of both pure Nafion and F-TiO_2-NT/Nafion composite membranes was measured at different relative humidity and temperature. **Figure 4-11 to Figure 4-13** show the membranes conductivity at 80 ˚C, 100 ˚C

and 120 ˚C. The relative humidity range was from 20 to 100% at 80 and 100 ˚C; and from 20 to 50 % at 120 ˚C. In all figures, it can be seen that at high relative humidity, both pure and composite Nafion membranes show good proton conductivity, where the conductivity of the composite membrane is always a little bit higher than the pure Nafion. However, at low relative humidity (20-40 %), the F-TiO_2-NT composite membrane shows better proton conductivity compared to the pure one. This difference becomes larger at higher temperatures, at 120 ˚C and 30 % relative humidity, the proton conductivity for F-TiO_2-NT/Nafion composite membrane is 0.067 S/cm, while pure Nafion is only 0.012 S/cm.

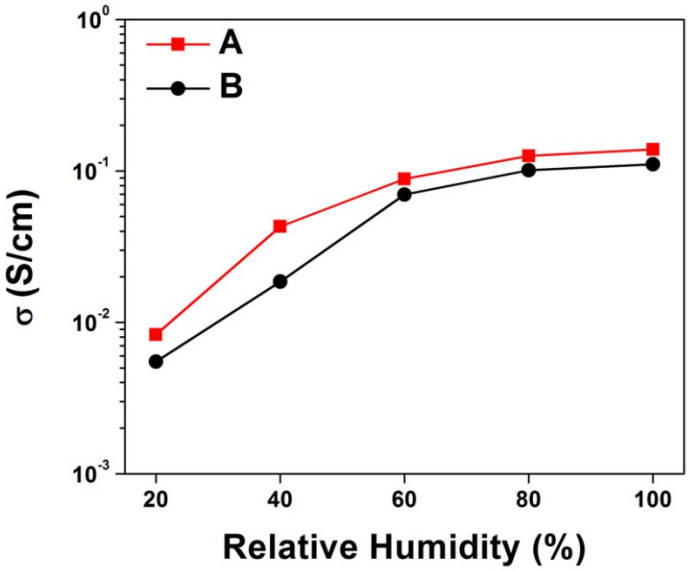

Figure 4-11. Proton conductivity of (A) F-TiO2-NT/Nafion composite membrane and (B) recast Nafion membrane at 80 °C.

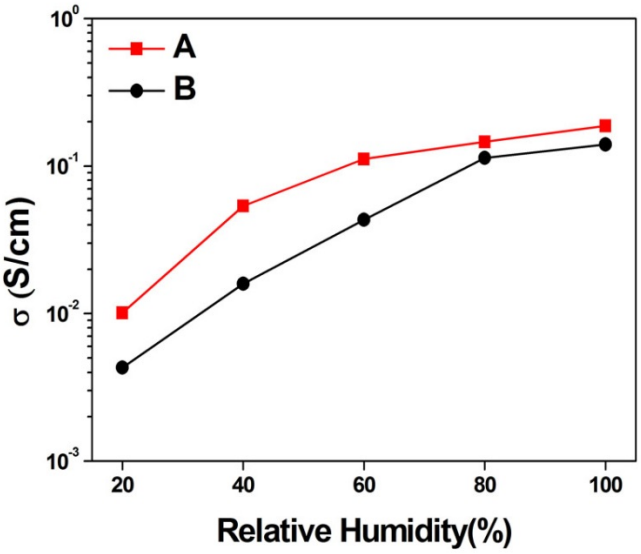

Figure 4-12. Proton conductivity of (A) F-TiO_2-NT/Nafion composite membrane and (B) recast Nafion membrane at 100 °C.

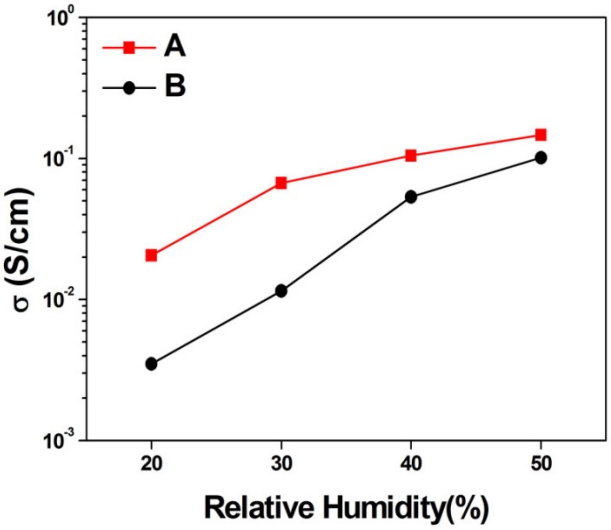

Figure 4-13. Proton conductivity of (A) F-TiO_2-NT/Nafion composite membrane and (B) recast Nafion membrane at 120 °C.

F-TiO_2-NT/Nafion composite membranes demonstrate a significant improvement over the unmodified one at low humidity and high temperature. The increase in conductivity can be attributed to the high specific area (greater number of protonated sites per unit mass of powder in the membrane) and good water retention of hydrophilic F-TiO_2-NT which result in higher conductivity comparing to the bare Nafion.

4.4 Conclusions

The sulfonic acid group was successfully grafted to the TiO_2-NT by using MPTMS as the sulfonic acid precursor. Proton conductivity tests indicated that the functionalized TiO_2-NT had a much higher conductivity than the unmodified one. At the temperature of 80 ˚C, the conductivity of F-TiO_2-NT was as high as 0.08 S/cm. By incorporating the F-TiO_2-NT into a Nafion membrane, the sulfonic acid groups of F-TiO_2-NT enhanced the conductivity of the composite membrane. The higher conductivity of F-TiO_2-NT increased the proton conductivity of the composite membrane at higher temperatures and low relative humidity compared to pure Nafion. At 120 ˚C and a relative humidity of 30 %, the proton conductivity for the composite membrane was 0.067 S/cm, whereas for a pure Nafion membrane a proton conductivity of only 0.012 S/cm was found. In conclusion, F-TiO_2-NT/Nafion composite membranes are presented as a potential proton exchange membrane replacement for high temperature PEMFC applications at low humidity values. Further investigations are still required in order to determine other important effects of F-TiO_2-NT/Nafion composite membranes at high temperature, including fuel cell testing.

Chapter 5

Functionalized Graphene Oxide Nanocomposite Membrane for Low Humidity and High Temperature Proton Exchange Membrane Fuel Cells

Chapter 5 is based on published work by Zarrin et al. [32] and is reproduced with permission from the Journal of Physical Chemistry C. The thesis author's specific contributions to this paper were to synthesize and fabricate nano-composite membrane, conduct EIS measurements, run most of physicochemical characterization tests, prepare all plots and results, write the final manuscript and respond to the comments of reviewers. This work and journal paper preparation was conducted with direction from the project supervisors who are co-authors on the publication. Yu Jun aided with the synthesis and performed some of physicochemical characterization tests. Drew Higgins assisted in editing the manuscript.

5.1 Introduction

Proton exchange membrane fuel cells (PEMFCs) are being developed intensively due to their great potential as environmentally benign energy conversion devices for transportation, residential and portable applications [107]. Operation of PEMFCs at high temperatures (above 100 °C) would significantly boost their performance by enhancing the electrode reaction kinetics, limiting the excessive precious metal (Pt) catalyst requirement, along with improving the electrocatalyst CO tolerance and allowing easier thermal and water management of the system [160]. However, high temperature operation of PEMFCs is not practical while using the state-of-the-art hydrated perfluorosulfonic acid membranes (PFSA,

under the commercial name of Dupont Nafion®); as they require strict humidification under temperatures above 80 °C due to the evaporation of water from the membrane structure [27, 111, 161-163]. Considerable research efforts have been devoted to developing organic-inorganic composite membranes able to operate at increased temperatures. Incorporation of hygroscopic inorganic nanomaterials [17, 31, 118, 164-168], such as ZrO_2, SiO_2, TiO_2, P_2O_5 and Zeolite nanoparticles, and TiO_2 nanotubes and nanowires into the structure of the PFSA has been demonstrated to result in composite membranes with promising proton conductivity at high temperature and low relative humidity [19, 132, 169-173].

Graphene oxide (GO), has been considered attractive for many applications owing to their unique thermal and mechanical properties [174-176]. Upon incorporation in PFSA, the unique structure and high surface area of the GO may provide more proton transport channels and hold more water, which could be beneficial for the improvement of the proton conductivity and mechanical properties of the membranes [176-178]. In the present work, the effects of functionalized graphene oxide (F-GO) nanosheets have been investigated as inorganic fillers in a Nafion composite membrane, fabricated by a simplistic solution casting method (**Figure 5-1**). The surface morphology, thermal stability, ion exchange capacity, water uptake and proton conductivity have been investigated. Moreover, the performance of these composite membranes have been investigated in high temperature PEMFCs at low relative humidity conditions and found to provide good performance, rendering this material as very promising materials for application in PEMFC operating at elevated temperatures.

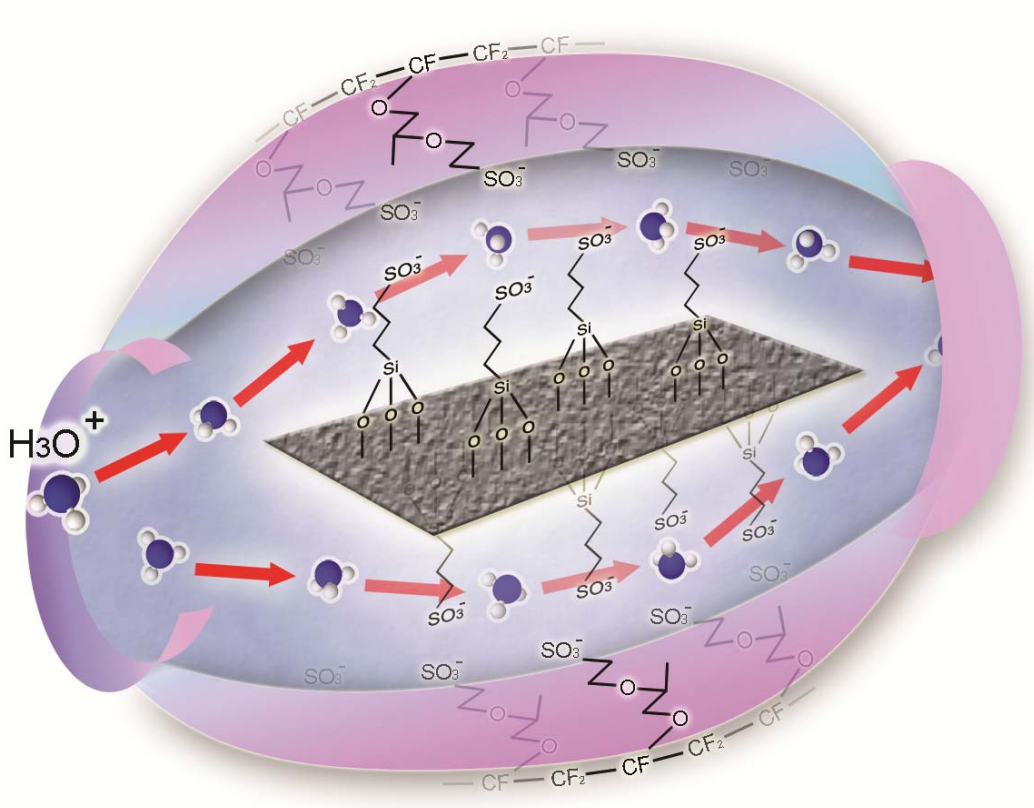

Figure 5-1. Schematic of proton conduction in F-GO/Nafion composite membrane.

5.2 Experimental Methods

5.2.1 Synthesis of Graphene Oxide (GO)

The graphene oxide (GO) nanosheets were produced from natural graphite flakes by the modified Hummer's method [176, 179, 180]. Graphite powder (2 g) and sodium nitrate ($NaNO_3$, 1 g) were combined in a round bottom flask. Concentrated sulphuric acid (H_2SO_4, 46 mL) was added while stirring in an ice bath at 0 °C. Potassium permanganate ($KMnO_4$, 6 g) was added very slowly because it is a strong oxidizing agent. The flask was removed from

the ice bath and stirred for 1 h at room temperature. The distilled de-ionized water (DDI, 92 mL) was added drop by drop. This step generates a large amount of heat and gas and needs to be done with extra care. After stirring for 30 min the reaction was diluted with warm DDI water (280 mL) and 30 % hydrogen peroxide (H_2O_2, 40 mL) was added to neutralize any remaining permanganate. The product was then filtered and washed with copious amounts 5 % hydrochloric acid (HCl). After which it was centrifuged, collected, and dried in an oven at 70 °C.

5.2.2 Functionalization of Graphene Oxide (F-GO) with Sulfonic Acid-Containing Groups

The functionalization of GO (F-GO) nanosheets was performed by using 3-mercaptopropyl trimethoxysilane (MPTMS) as the sulfonic acid functional group precursor [31, 181]. The reaction was carried out in toluene at a temperature of 110 ˚C under reflux conditions for 24 hrs, with 1:15:70 weight ratios of GO, MPTMS and toluene respectively. The mercapto groups grafted onto the GO nanosheets; then were oxidized to sulfonic acid groups by using 30 wt. % H_2O_2 solution at 25 ˚C for 24 hrs. The prepared samples were filtered and washed with ethanol and water to remove the precursor residue. Samples were dried overnight prior to characterization.

5.2.3 Casting F-GO/Nafion Nanocompposite Membrane

5 or 10 wt. % F-GO/Nafion composite membranes were casted by mixing 5 or 10 wt. % F-GO with an appropriate amount of Nafion® 1100 EW solution (5 %, DuPont) and ethanol. Then, the mixtures were ultrasonicated for 30 min and heated at 60 ˚C until the evaporation of half of the solution. Finally, it was heated at 100 ˚C for 2 hrs and then 140 ˚C for 1 h

[113]. Both pure Nafion and F-GO/Nafion composite membranes were pretreated by boiling in a 3 % H_2O_2 aqueous solution for 1 h, rinsed in boiling deionized water for 1 h, boiled in 0.5 M H_2SO_4 for 1 h, and finally rinsed again in deionized water before being tested [117].

5.2.4 Proton Conductivity Measurement

Proton conductivity of GO and F-GO powders was estimated by using a two-electrode setup [153]. First, each of the powdered samples was individually loaded into a tube cell with a diameter of 1.6 mm in which the two electrodes are inserted from the top and bottom. Then, they were pressed for several hours. To attain water-saturated conditions, the fixture was disassembled from the top and 20 μL of double deionized water was injected with a syringe onto the sample in each cell. The water was allowed to soak into the samples for 30 min. Then the top electrodes were replaced, the fixture was reassembled, and the sample cells were retorqued. Then, the proton conductivity was measured at 100 % relative humidity in different temperatures from 20 to 80 °C to probe the effect of sulfonic acid functionalization on GO ionic conductivity.

The proton conductivity of all membranes was obtained by four-electrode method using AC impedance spectroscopy [182] with potentiostat (CHI760D Model). The impedance is measured in the frequency range between 1 MHz and 0.1 Hz with perturbation voltage amplitude of 5 mV. The humidity was controlled by mixing water-saturated nitrogen gas with dry nitrogen gas, while the temperature was fixed at 80, 100 and 120 °C. This method avoids contact resistance effectively and the results are good reproducible in measurement. The proton conductivity (σ) of all powdered samples and membranes was then measured along the longitudinal direction, using the following equation [104, 154, 155]:

$$\sigma = \frac{L}{AR}$$ **Equation 5-1**

where σ, L, R, and A denote the ionic conductivity, sample length (or distance between the reference electrodes in the membrane), the resistance of the powder/membrane, and the cross-sectional area of the powder/membrane, respectively.

5.2.5 Water Uptake (WU) and Ion Exchange Capacity (IEC)

In order to measure the water retention capability of the membranes, the WU (%) was calculated. For this, the membranes were first immersed and saturated in deionized water at room temperature for 24 hrs. They were then taken out and weighed immediately after the water droplets were removed from the surface. Following this, they were vacuum dried at 80 $^{\circ}$C for 24 hrs, put into a plastic sealing bag immediately and weighed. The WU was determined from the following equation [151, 152]:

$$WU(\%) = \frac{W_{wet} - W_{dry}}{W_{dry}} \times 100$$ **Equation 5-2**

where WU (%), W_{wet} and W_{dry} are the water uptake by weight percentage, the weight of the wet membrane and the weight of the dry membrane, respectively.

IEC of each membrane was determined by a back titration method. At first, the samples were dried until the weight was constant, after which each sample was soaked in 0.2 M NaCl (50 mL) for 24 hrs to exchange sodium ions with protons in the composite membranes. Back titration was then accomplished with 0.01 M NaOH standardized solution and IEC values were calculated by the following equation [123]:

$$IEC = \frac{V_{NaOH} C_{NaOH}}{W_{dry}}$$ **Equation 5-3**

where IEC is the ion exchange capacity (meq g^{-1}), V_{NaOH} the added titrant volume at the equivalent point (mL), C_{NaOH} is the molar concentration of the titrant, W_{dry} is the dry mass of the sample (g).

5.2.6 Physico-chemical Characterization

The overall morphology of all samples was examined by using transmission electron microscopy (TEM, JEM-100CX II) and Scanning electron microscopy (SEM, LEO FESEM 1530). X-ray photoelectron spectroscopy (XPS, Thermal Scientific K-Alpha XPS spectrometer) was used to investigate the surface elemental composition and atomic configurations of both GO and F-GO. Fourier transform infrared spectroscopy (FTIR, PerkinElmer-283B FT-IR Spectrometer) was used for determinination of the functional groups present in the Nafion and F-GO/Nafion membranes.

5.2.7 MEA Fabrication and Testing

The performance of the 10 wt. % F-GO/Nafion and recast Nafion memebranes in a fuel cell setup was determined using a single cell MEA setup fabricated using a decal method as described elsewhere [183]. The electrocatalyst used in the anode and cathode was Pt/C (20 wt. %, E-TEK). Briefly, catalyst ink was prepared by mixing the catalyst with 5 % Nafion solution for 1 h. Glycerol was subsequently added, and the solution was stirred for 24 hrs. After preparation, the catalyst ink was painted on to decal Teflon blanks and dried in an oven. This process was repeated until the desired catalyst loading was achieved. Each membrane sample was cleaned and boiled in a dilute NaOH solution in order to ion exchange

the membrane to Na^+. After rinsing, the membrane was dried by hot pressing and then cooled prior to MEA fabrication. The MEA with an active electrode area of 5 cm^2 was obtained by pressing the cathode and anode onto each side of the recast Nafion or 10 wt. % F-GO/Nafion composite membrane at 210 °C and 110 lbs cm^{-2} for 5 min. Decals could then be removed, leaving the catalyst layers firmly attached to the membrane surface. The MEA was assembled into the fuel cell hardware for testing. Catalyst loading was 0.2 mg_{Pt} cm^{-2} for the cathode and 0.1 mg_{Pt} cm^{-2} for the anode and gas flow rates of 0.2 and 0.5 L min^{-1} were used for hydrogen and oxygen, respectively.

5.3 Results and Discussion

The nanosheet structure and morphology of GO was investigated by TEM and SEM imaging as displayed in Figure 1. TEM analysis (**Figure 5-2a-b**) showed that the pristine graphene oxide nanosheets appeared relatively flat with some wrinkles, consistent with the morphology typically reported in the literature [171, 184-187]. The SEM images of GO (**Figure 5-2c-d**) displayed the exfoliated layered structure of graphene oxide agglomerates [164].

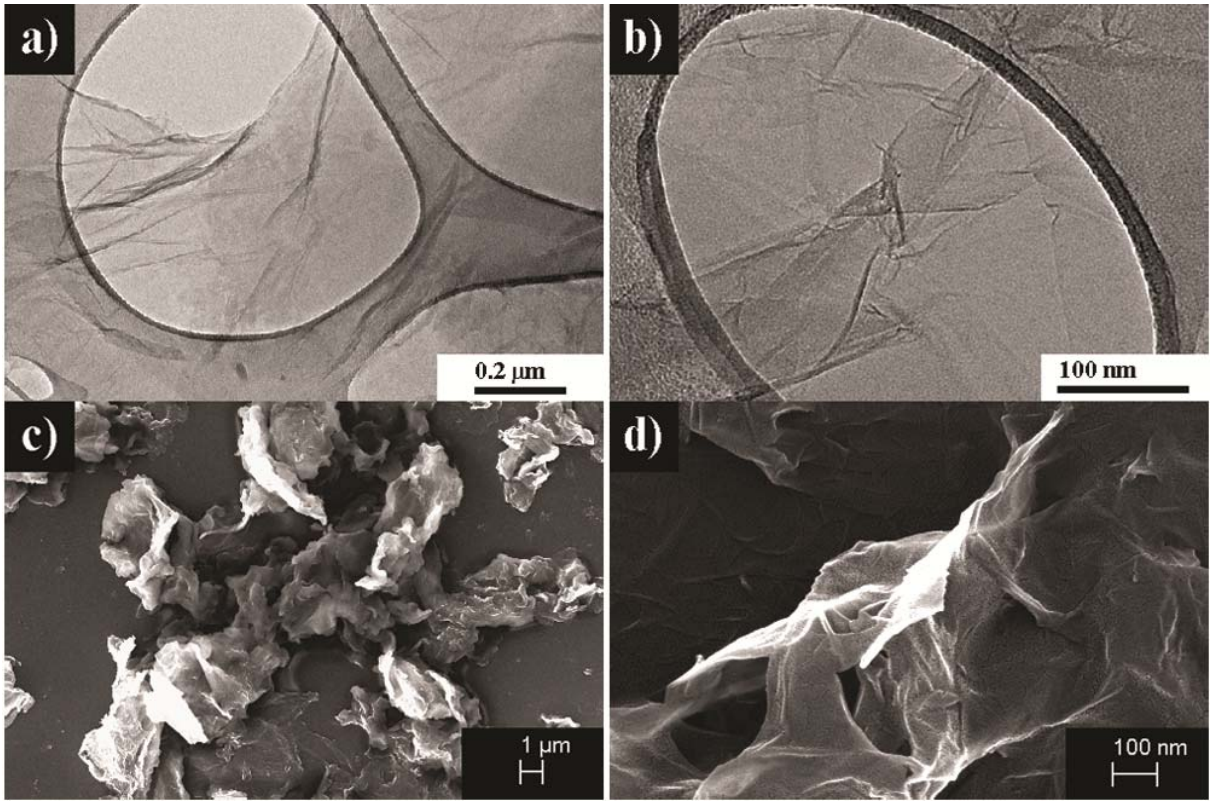

Figure 5-2. TEM of unmodified GO at (a) low magnification and (b) high magnification. SEM images of GO at (c) low magnification and (d) high magnification.

The chemical composition of both unmodified and functionalized GO were determined by XPS. Upon analysis of the wide range XPS patterns displayed in **Figure 5-3a-b**, two new peaks were observed for F-GO at binding energies of 169.48 and 104.28 eV, attributed to S 2p and Si 2p components, respectively. This confirms the successful attachment of the sulfonic acid containing precursor (MPTMS) onto the surface of the GO nanosheets. Furthermore, upon high resolution analysis, no S 2p peak at a binding energy of 164 eV (corresponding to –SH) was observed, confirming the complete oxidation of –SH to $–SO_3H$

functional groups [172]. In order to provide more insight regarding the surface decorated functional groups, deconvulated XPS spectra of the C 1s (**Figure 5-3c-d**) and O 1s (**Figure 5-3e-f**) signals are provided for both GO and F-GO. Comparison of the C 1s signal clearly indicates a change in the degree of surface oxidation before (**Figure 5-3c**) and after (Figure 5-3**d**) MPTMS functionalization. F-GO (**Figure 5-3d**) demonstrates three new peaks (283.7, 290 and 291.5 eV; **Table 5-1**) other than those assigned to the GO surface functional groups. Moreover, the peak intensities and binding energies observed for F-GO are slightly different than those in GO. This is because of the exposure of highly reactive hydroxyl and epoxy groups [188, 189] to the sulfonic acid containing precursor (MPTMS), leading to a decrease in the epoxy and hydroxyl components present on the surface and the addition of new C-O-Si and/or C-S bonds contributing to the peak observed at 285.4 eV.

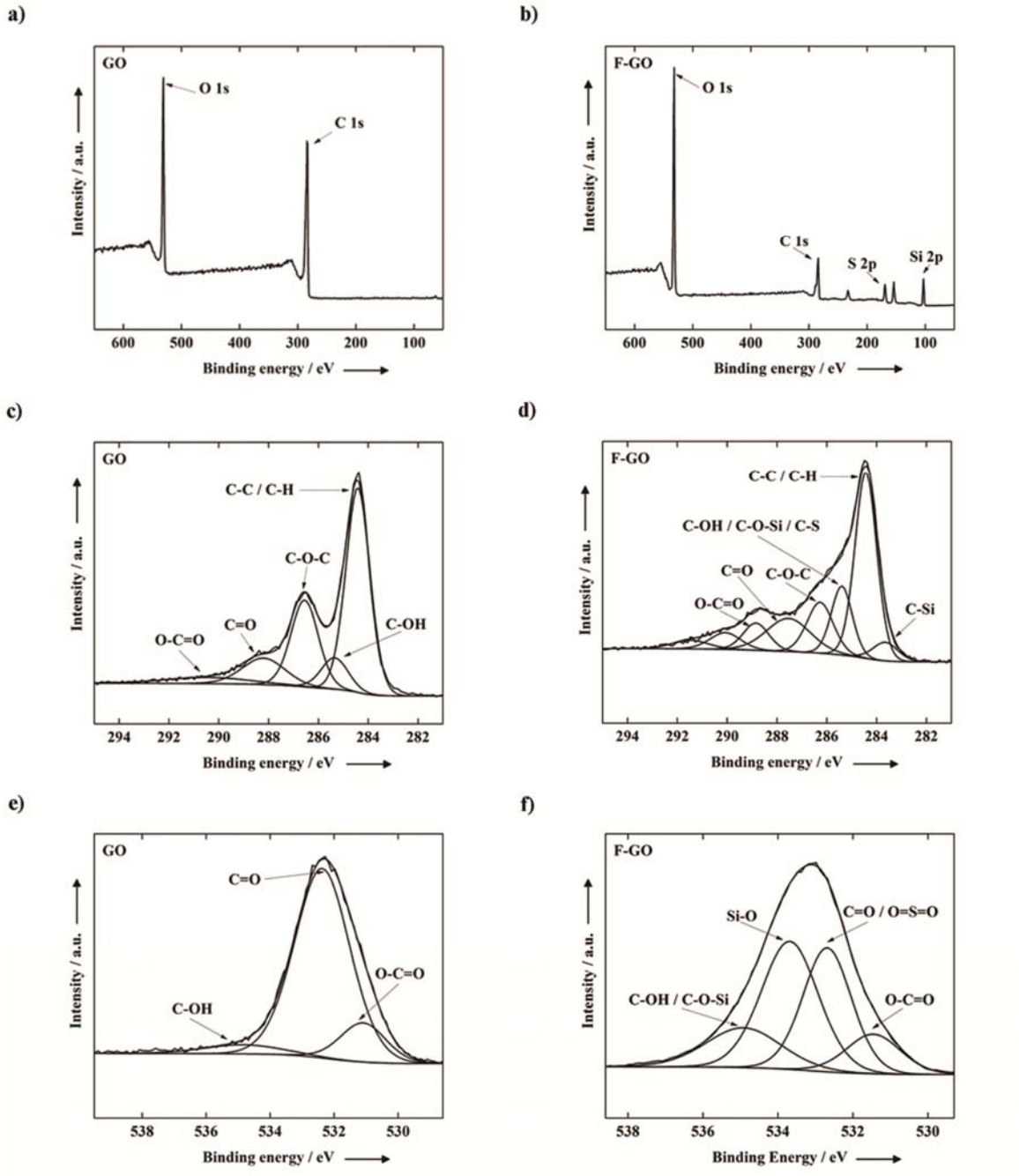

Figure 5-3. Wide region XPS spectra of (a) GO and (b) F-GO. Deconvoluted XPS spectra in the C1s region for (c) GO and (d) F-GO. Deconvoluted XPS spectra in the O1s region for (e) GO and (f) F-GO.

Table 5-1. Summary of C 1s and O 1s XPS Spectral Data.

	Sample	Binding energy [eV]	Assignment
C 1s	GO	284.4	sp2 and sp3 hybridized C–C/C–H
		285.4	C–OH
		286.6	C–O–C
		288.2	C=O
		290.0	O–C=O
	F-GO	283.7	C–Si
		284.4	sp2 and sp3 hybridized C–C/C–H
		285.4	C–OH/C–O–Si/C–S
		286.3	C–O–C
		287.6	C=O
		288.8	O–C=O
		290.1	π–π* shake up satellite of the sp2 hybridized C
		291.5	π–π* shake up satellite of the sp2- hybridized C
O 1s	GO	531.0	O–C=O
		532.4	C=O
		534.9	C–OH
	F-GO	531.5	O–C=O
		532.7	C=O/O=S=O
		533.7	Si–O
		534.9	C–OH/C–O–Si

The functionalized graphene oxide has shown a greater concentration of surface oxygen, 44.76 at. %, compared to pristine graphene oxide, 26.84 % (**Table 5-2**). The O 1s XPS peaks of GO in **Figure 5-3e** are composed of three components including O–C=O, C=O and C–OH with their binding energy at 531.0, 532.4 and 534.9 eV, respectively [185, 190]. These peaks are shifted to 531.5, 532.7 and 534. 9 eV in F-GO with a new peak appearing at 533.7 eV, indicating the creation of Si–O bonds due to the addition of sulfonic acid containing precursor, MPTMS (**Figure 5-3f**). Furthermore, the peak at 532.7 eV for F-GO has become more intense and shifted to slightly higher binding energies compared with that of GO (532.4 eV), assigned to a combination of C=O and O=S=O bonds, confirming the complete oxidation of –SH to $–SO_3H$ [172].

Table 5-2. Atomic Percentages of Pristine Graphene Oxide (GO) and Sulfonic Acid Functionalized Graphene Oxide (F-GO) Determined from XPS.

Sample	C [at. %]	O [at. %]	Si [at. %]	S [at. %]
GO	73.16	26.84	-	-
F-GO	36.03	44.76	3.73	15.48

The top view SEM images of recast Nafion and 10 wt. % F-GO/Nafion composite membranes were compared in **Figure 5-4a** and **Figure** 5-4**b** to determine the changes of the Nafion membrane surface after grafting F-GO nanofillers. It was observed that the bare recast Nafion has a smooth surface, while after the incorporation of F-GO nanosheets the surface became significantly rougher. Also, it was seen that the surface of Nafion was

uniformly covered with dark sheets of F-GO, indicating the successful grafting of sulfonated GO sheets onto the F-GO/Nafion electrolyte polymer surface. Cross-section SEM images of recast Nafion and 10 wt. % F-GO/Nafion nanocomposite membranes are shown in **Figure 5-4c** and **Figure** 5-4**d**, respectively. Distinct differences are observed, with the recast Nafion membrane presenting a relatively smooth cross section, whereas the F-GO/Nafion nanocomposite membrane displayed a very rough cross section. This is in agreement with the previous report by Lian et al [191]. **Figure 5-4e** provides visual comparison of the 10 wt. % F-GO/Nafion nanocomposite membrane to the transparent recast Nafion.

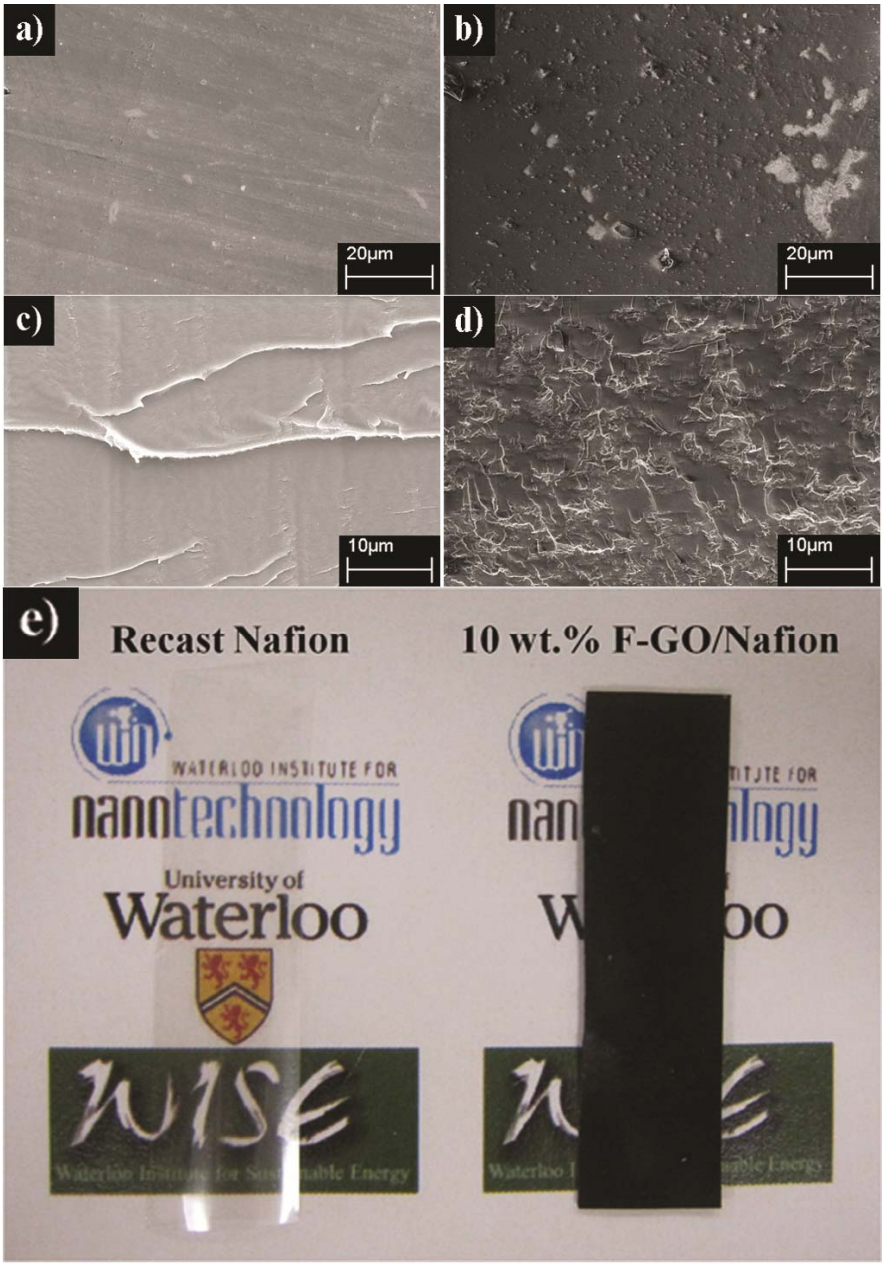

Figure 5-4. Top view SEM images of (a) recast Nafion and (b) 10 wt % F-GO/Nafion composite membrane. Cross section view of SEM images for (c) recast Nafion and (d) 10 wt % F-GO/Nafion composite membrane. (e) The pictures of recast Nafion and 10 wt%F-GO/Nafion composite membranes.

For elemental analysis of the membranes, the Fourier-transformed infrared (FT-IR) spectrum of F-GO/Nafion was compared to that of recast Nafion (**Figure 5-5**). The assignments of recast Nafion FT-IR spectrum was made by comparison with Nafion values obtained in the literature presented in **Table 5-3** [192-196]. The bands at 590, 793, 974, 1188 and 1354 cm^{-1} are typical of C–S, CF–CF_3, C–O, CF_2 and SO_3H groups which are in good agreement with previous reports [197, 198]. The two bending frequencies of 1626 and 1760 cm^{-1} could be possibly assigned to H_2O and $H_5O_2^+$ species [193, 199], since before FT-IR spectroscopy the membranes were not been completely dried and had low values of water content. The H-bonded OH stretching vibrations were in an extremely broad band region between 3178 and 3387 cm^{-1} and the free sharp OH groups band appeared at 3622 cm^{-1}.

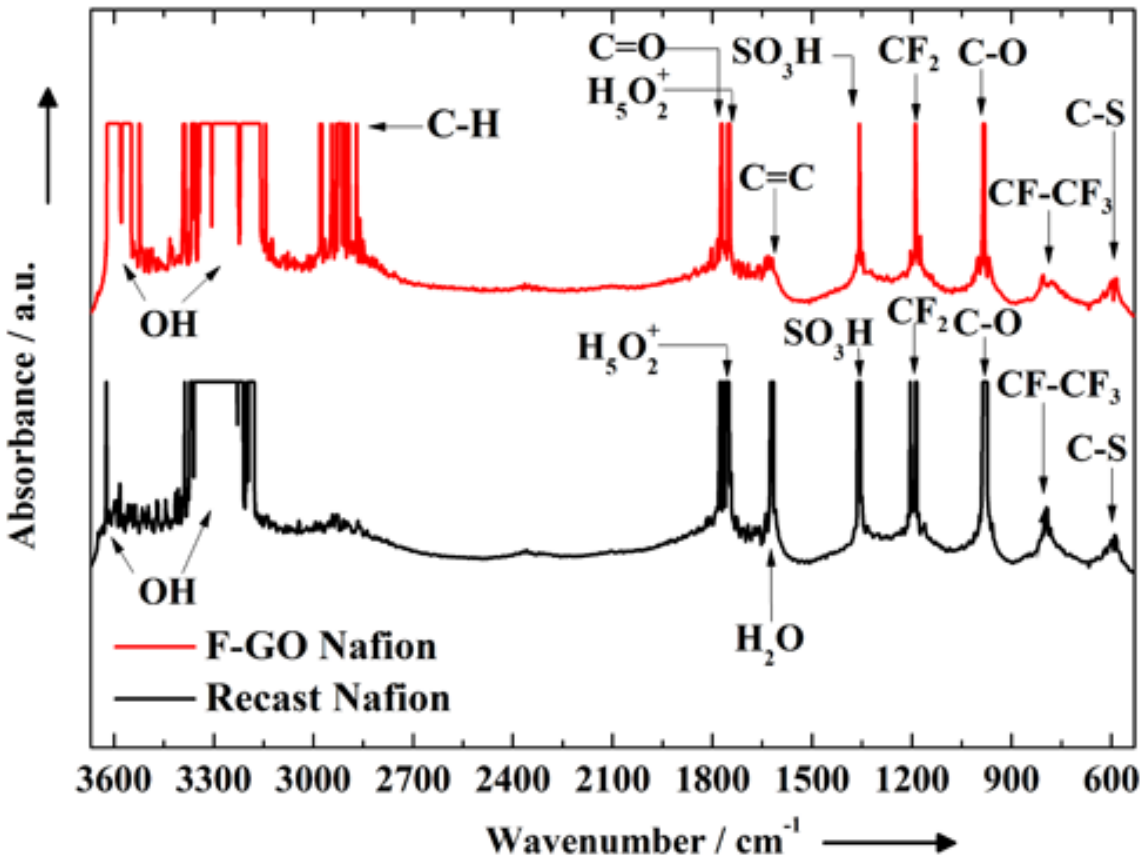

Figure 5-5. FT-IR spectra comparison between recast Nafion and 10 wt% F-GO/Nafion composite membranes.

In the F-GO/Nafion composite membrane, all of the expected functional groups of the Nafion backbone structure are observed (**Figure 5-5** and **Table 5-3**). The absence of peaks at 1060, 1250 and 1365 cm^{-1} indicates that all epoxide and hydroxyl groups attached to the basal pristine graphene layer have been removed [200], confirming that they have been attacked and sulfonated by MPTMS. However, $CF–CF_3$ and C–O functional groups are shifted to higher wave numbers of 801 and 982 cm^{-1}, respectively. This peak shift can be

attributed to changes of the chemical surroundings which may also affect the extinction coefficient of different functional groups [201, 202]. The absorption bands at 1620 and1748 cm^{-1} confirm the existence of aromatic C=C and carboxy C=O / $H_5O_2^+$, respectively. The presence of aliphatic C-H is indicated by the band stretching from 2893 to 3000 cm^{-1}, assigned to the $-(-CH_2-)-_3$ chains in the MPTMS sulfonic acid precursor [200]. Adjacent to this region, a peak at 3144 cm^{-1} was observed which refers to aromatic C–H stretching vibrations. In F-GO/Nafion membrane, the broad band of OH groups in the region between 3160 and 3368 cm^{-1} indicated the presence of both H-bonded and carboxy OH groups. Another broad band was also seen in the region between 3522 and 3620 cm^{-1} which is believed to be related to free OH groups.

Table 5-3. FT-IR Data Analysis for Recast Nafion and 10 wt % F-GO/Nafion Membranes.

Recast Nafion		**10 wt. % F-GO/Nafion**	
Wavenumber [cm^{-1}]	Assignment	Wavenumber [cm^{-1}]	Assignment
590	C–S	590	C–S
793	$CF–CF_3$	801	$CF–CF_3$
974	C–O	982	C–O
1188	CF_2	1188	CF_2
1354	SO_3H	1354	SO_3H
1626	H_2O	1620	C=C
1760	$H_5O_2^+$	1748	$C=O/H_5O_2^+$
3178-3387	H-bonded OH	2893-3000	Aliphatic $-(-CH_2-)-_3$
3622	Free OH	3144	Aromatic C–H
		3160-3368	H-bonded and carboxy OH
		3522-3620	Free OH

The water uptake (WU) and ion exchange capacity (IEC) of 5 % and 10 % F-GO/Nafion nanocomposite membranes are compared to that of react Nafion as displayed in **Figure 5-6**. It is seen that the WU of the F-GO/Nafion membranes are higher than that of recast Nafion, displaying WU values 2% and 6% higher for 5% F-GO/Nafion and 10 % F-GO/Nafion, respectively. Furthermore, the IEC of the membranes was found to increase with higher F-GO contents such that 0.96, 0.93 and 0.91 meq g^{-1} was determined for 10% F-GO/Nafion, 5% F-GO/Nafion and recast Nafion, respectively.

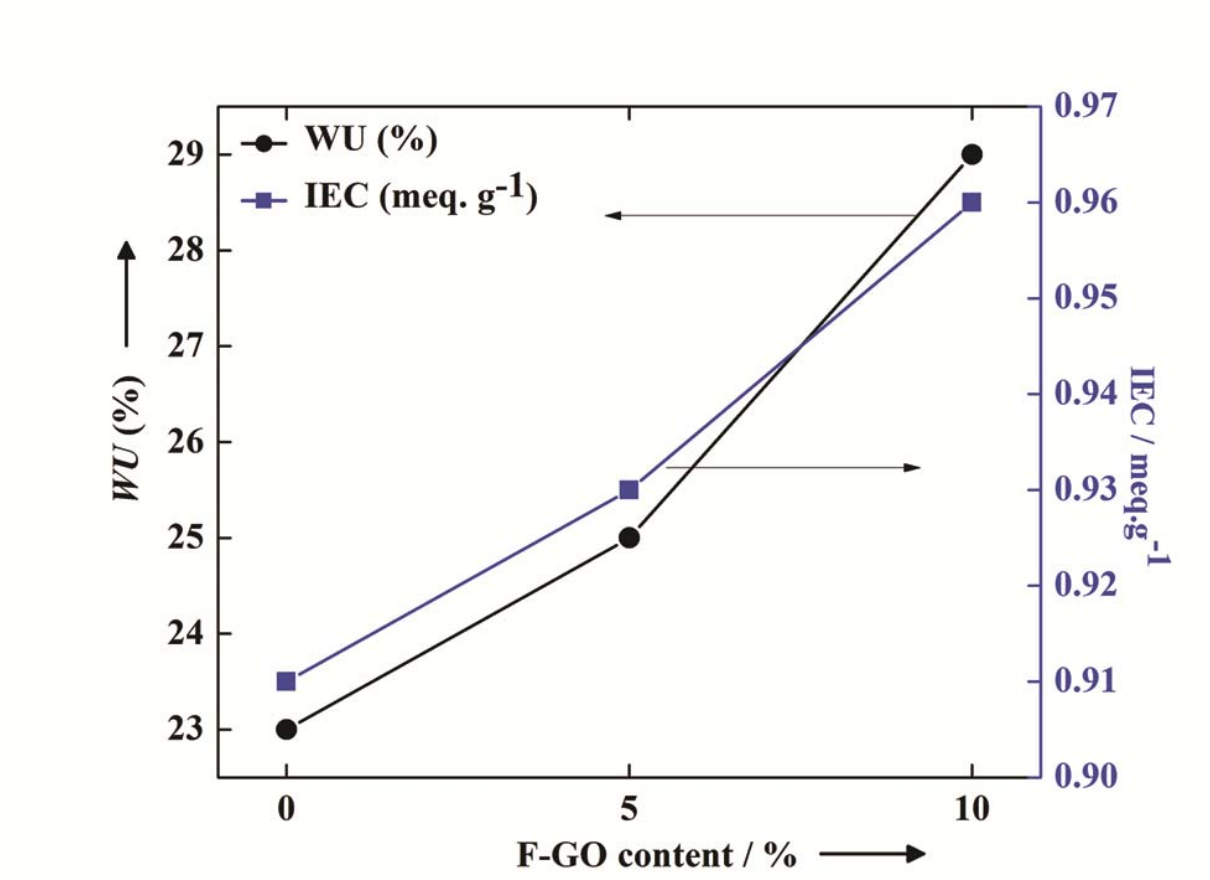

Figure 5-6. WU (%) and IEC (meq g^{-1}) of recast and composite Nafion membranes.

Figure 5-7a provides a comparison of the GO and F-GO powder ionic conductivity. The ionic conductivity of F-GO was found to be about three orders of magnitude higher at 20 °C and more than one order of magnitude higher at 80 °C than GO. This can be attributed to the higher sulfonic acid content of GO which helps the absorption and retention of more water, distinctively at high temperatures. In **Figure 5-7b-d**, the relative humidity dependence of the proton conductivity of the recast Nafion and the F-GO/Nafion composite membranes with 5

and 10 wt. % loadings of F-GO are determined at temperatures of 80, 100 and 120 °C, using a four-electrode AC impedance method [104, 154]. It can be observed that the incorporation of functionalized GO into the matrix of Nafion has significantly increased the proton conductivity, particularly at the high temperature of 120 °C with low relative humidity. **Figure 5-7b-d** clearly reveals that increasing the F-GO nanofiller content can effectively enhance the proton conductivity of the Nafion nanocomposite membranes, as at 120 ˚C and 30 % relative humidity, the proton conductivity of 10 wt. % F-GO/Nafion was 0.047 S cm^{-1}; an almost four-fold improvement over 0.012 S cm^{-1} for the recast Nafion membrane. This can be explained based on the Grotthuss mechanism [203], where protons diffuse through the hydrogen bond network of water molecules. Since F-GO has an extremely high surface area with an enormous amount of sulfonated functional groups, it holds more water and consequently could facilitate the transfer of more protons. The increase of F-GO nanofiller loading extends the number of available ion exchange sites per cluster, resulting in the increment of proton mobility in membrane at high temperatures and low humidity values.

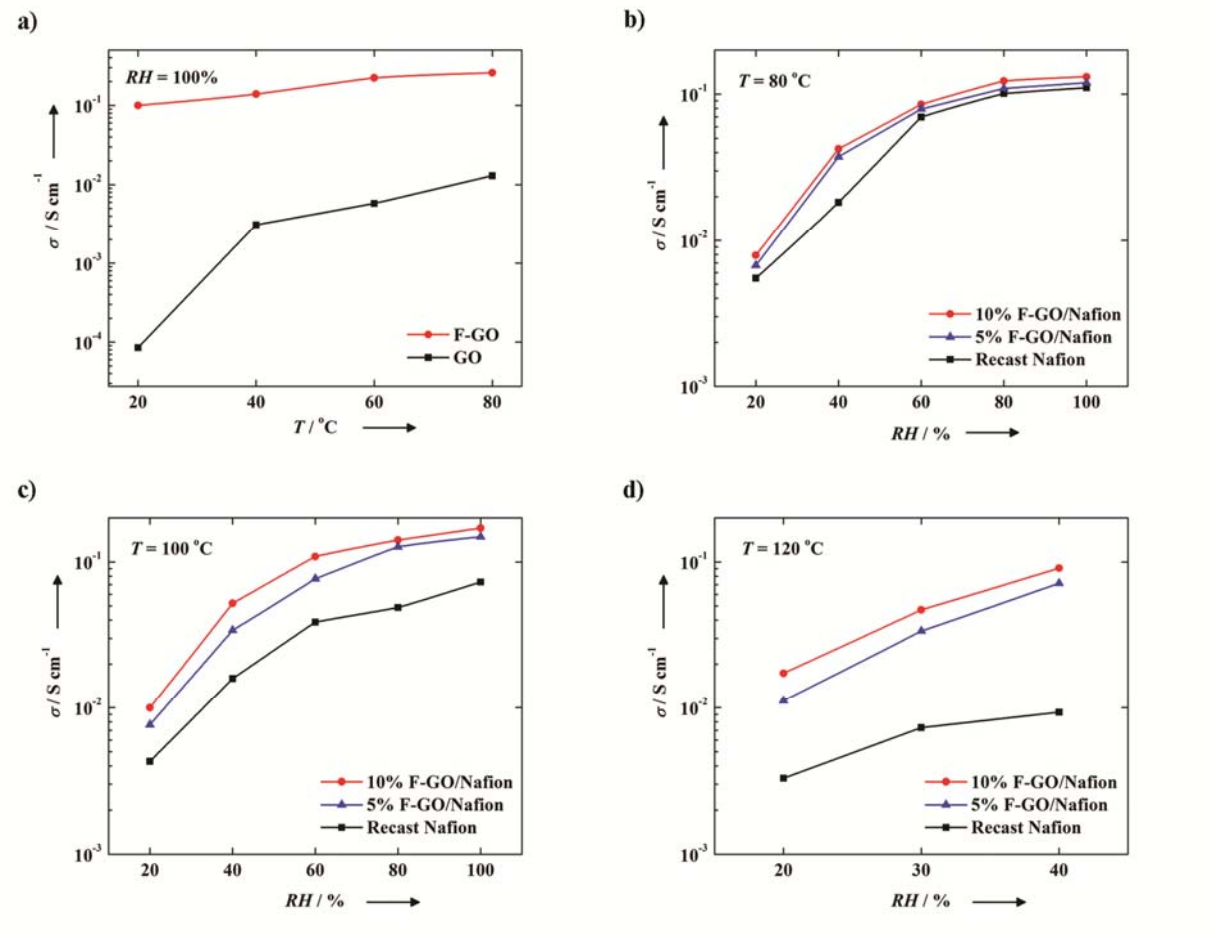

Figure 5-7. (a) Proton conductivity (σ) comparison between GO and F-GO powders. Proton conductivity of recast Nafion and F-GO composite membrane with doping levels of 5 and 10% at temperatures (T) of (b) 80 °C, (c) 100 °C, and (d) 120 °C at various relative humidities (RHs).

Figure 5-8 displays the polarization and power density curves for 10 wt. % F-GO/Nafion composite and recast Nafion in a single cell H_2/O_2 MEA system operating at 120 ° C and 25 % relative humidity. The peak power density for 10 wt. % F-GO/Nafion was 0.15 W cm^{-2}, approximately 3.6 times higher than that of recast Nafion (0.042 W cm^{-2}). At a cell voltage of

0.6 V, 10 wt. % F-GO/Nafion showed a current density of 0.16 A cm^{-2}, about 3.5 times higher than recast Nafion (0.046 A cm^{-2}). These results are in direct agreement with the membrane proton conductivity analysis, as 10 wt. % F-GO/Nafion displayed a substantial performance increase through MEA testing compared with recast Nafion under typical PEMFC conditions. Clearly, F-GO/Nafion nanocomposites offer significant promise as electrolyte membranes for PEMFC applications operating at elevated temperatures, owing to the beneficial structural and mechanical properties arising due to F-GO incorporation.

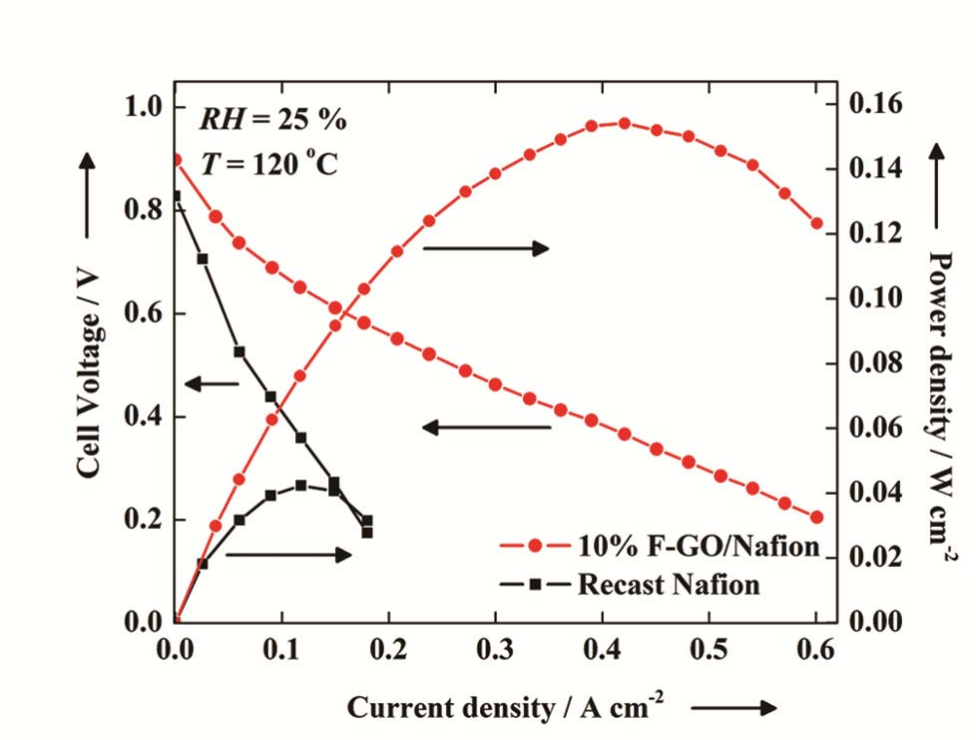

Figure 5-8. MEA polarization and power density curves for 10 wt % F-GO/Nafion and recast Nafion membranes, with commercial E-TEK 20 wt% Pt/C catalyst (anode 0.1 mg_{Pt} cm^{-2}, cathode 0.2 mg_{Pt} cm^{-2}) in a single-cell H_2/O_2 system at the temperature (T) of 120 °C and 25% relative humidity (RH).

5.4 Conclusion

In summary, a sulfonic acid-functionalized graphene oxide Nafion nanocomposite (F-GO/Nafion) has been presented as a potential proton exchange membrane replacement for low humidity and high temperature PEMFC applications. F-GO/Nafion nanocomposites demonstrated a significant proton conductivity improvement (4 times) over the unmodified one at a low humidity value of 30 % and high temperature of 120 °C. Under the similar operating conditions, single cell MEA testing also revealed a significantly higher performance of 10 wt. % F-GO/Nafion membrane than that of the recast Nafion, displaying peak power densities of 0.15 and 0.042 Wcm^{-2}, respectively. F-GO incorporation clearly offers substantial PEMFC performance improvements at elevated temperatures and further investigations are underway to optimize these composite membranes and determine their chemical and mechanical stabilities.

Chapter 6
High Durable PEK-based Anion Exchange Membrane for Elevated Temperature Alkaline Fuel Cells

Chapter 6 is based on published work by Zarrin et al. [33] and is reproduced with permission from the Journal of Membrane Science. The thesis author's specific contributions to this paper were to synthesize and fabricate the AEM, conduct EIS measurements, run all of physicochemical characterization tests, prepare all plots and results, write the final manuscript and respond to the comments of reviewers. This work and journal paper preparation was conducted with direction from the project supervisors who are co-authors on the publication. Jason Wu assisted in editing the manuscript.

6.1 Introduction

Anion exchange membrane fuel cells (AEMFCs) are attracting considerable interest relative to proton exchange membrane fuel cells (PEMFCs) in recent years, primarily due to the distinct advantages when operating in an alkaline environment such as cathode reaction kinetics and resistance polarization [15, 204]. The inherently faster and much easier kinetics of the oxygen reduction reaction (ORR) in alkaline environment than in acid medium leads to the use of non-noble and non-precious metal electrocatalysts such as silver (Ag) and nickel (Ni), making the AEMFC a potentially low cost technology compared to PEMFCs, which employ platinum (Pt) catalysts [1, 205]. Moreover, due to the less corrosive nature of an alkaline medium, higher durability is expected for AEMFCs. However, AEMFCs need to overcome strenuous technical and economic challenges which are specifically associated

with fabrication of a cost effective anion exchange membrane (AEM) possessing (i) high anionic conductivity and (ii) exemplary physico-chemical and temperature stability [15, 204, 206]. Due to the poor thermal, chemical and physical stability of current AEMs, the typical operating temperature of AEMFCs is limited to 50 or 60 °C [207]. However, AEMFC performance can be increased by operation at elevated temperatures which can be explained as follows. Increasing the operating temperature enhances both the charge (i.e., hydroxide) conduction within the membrane and the mass transfer, reducing the ohmic and mass transfer overpotentials, respectively. Moreover, the electrochemical kinetics of both the fuel oxidation reaction at the anode and the ORR at the cathode increase, resulting in minimized thermodynamic voltage losses and higher overall cell voltages. Thus, in order to successfully employ AEMFCs for applications such as vehicle propulsion, high temperature stable AEMs must be produced [68, 204, 208-211]. Accordingly, one of the primary challenges with AEMs is the membrane physico-chemical stability, especially at elevated temperatures.

Unlike polymer electrolyte membranes where highly chemically stable perfluorinated membranes such as perfluorosulfonic acid (DuPont™ Nafion®), control the market, commercially available AEMs are usually based on quaternary ammonium (QA) cross-linked polystyrene which albeit having been applied for water processing, cannot be used for AFCs due to low chemical and thermal stability, as well as weak mechanical property. Distinctively, the polystyrene backbone is too rigid to produce flexible thin films, and the QA functional group attached on polystyrene tends to degrade at 40–60 °C [206]. Furthermore, the blended aminated cross-linked polystyrene with other polymers limits the anion conductivity and may also reduce the chemical stability of the membrane [68]. So far, many

types of polymers, such as polybenzimidazole (PBI) [71], polyphenylene oxide (PPO) [72], cardo polyether ketone (PEK) [69], polyether sulfone (PES) [81], and radiation-grafted FEET [80] and FEFP [79] have been used to produce AEMs for application in alkaline fuel cells. Yet, the main problems stayed with many known AEMs, such as the low chemical stability in concentrated alkaline environments, due to the decay of the anion exchange groups (e.g., QA functional groups) in concentrated alkali solution; or the weak thermal stability which limits them to be used for elevated temperature alkaline fuel cells [212].

In this paper, in order to accomplish the aforementioned objectives, a modified quaternary ammonium polyetherketone (QAPEK) based block copolymer electrolyte has been developed through the chloromethylation and quaternization method, demonstrating the requirements for AEMs with improved thermal, chemical and mechanical stability for AEMFCs at elevated temperatures. Among different polymeric structures for AEMs, block copolymers possess higher water uptake and ion conductivity which can be assigned to their sequential hydrophilic/hydrophobic structure with ionic groups in the hydrophilic blocks, resulting in a helpful hydration effect [69, 72]. Since one of the requirements and a key challenge for AEMs is the satisfactory chemical stability, fully aromatic polymers are expected to have notably high chemical resistance, leading to the desirable durability for AEMFCs. Specifically, polyetherketones (PEKs) and their derivatives are the focus of many investigations, and the synthesis of these materials has been widely reported. This family of aromatic copolymers is attractive for use in AEMs because of their well-known chemical and hydrolytic stability under harsh conditions [213-215]. The reason for that behavior is a microphase separation between the chemically different and incompatible blocks which are

attached to each other by covalent bonds, and which does not occur in random copolymers or in blends (macrophase separation) of the same composition [216]. Moreover, AEMs containing QA functional groups as the cation exhibit higher thermal and chemical stability than other quaternary cations such as quaternary phosphonium (QP) or tertiary sulfonium (TS) groups [78, 217-219]. This is mainly due to the higher basicity of QA (pKa=31.9) than TS (pKa=17.8) and QP (pKa=17.4) compounds, respectively [220, 221]. For the obtained QAPEK copolymer, the water uptake, ion exchange capacity (IEC), ion conductivity, mechanical properties, thermal stability and chemical durability were investigated.

6.2 Experimental Methods

6.2.1 Materials

4,4'-Isopropylidenediphenol (Bisphenol A / BPA), 4,4'-Dihydroxylbenzophenone (DHBP) and 4,4'-Difluorobenzophenone (DFBP) were purchased from TCI America and used as received. Chloromethyl methyl ether (CMME), anhydrous zinc chloride ($ZnCl_2$), Triethylamine (TEA), N-Methylpyrrolidone (NMP) and 1,1,2,2-tetrachloroethane (TCE) were purchased from Sigma Aldrich and used as received. All other reagents such as toluene and potassium hydroxide (KOH) were obtained from other commercial sources and used as received.

6.2.2 Synthesis of PEK Block Copolymer via Polycondensation

The PEK block copolymer was synthesized through aromatic nucleophilic substitution polycondensation reaction of activated aromatic halide (DFBP) with BPA and DHBP in the presence of a weak base, potassium carbonate, and a dipolar aprotic solvent, NMP. In a 50

mL 3-necked round-bottomed flask Bisphenol A (7.5 mmol, 1.7122 g) and K_2CO_3 (8.25 mmol, 1.6585 g) were mixed in 6 mL of NMP and 6 mL toluene, equipped with a Dean-Stark receiver under nitrogen flow (**Figure 6-1**). The reaction temperature was maintained at 150 °C for 4 hrs until all the produced water was extracted and collected in the Dean-Stark trap via toluene. After cooling the solution to the room temperature, DFBP (10 mmol, 2.182 g) was added to the flask and then, the temperature was increased to 165 °C for 2 hrs to obtain the hydrophilic oligomer. In order to generate the hydrophobic oligomer block, DHBP (2.5 mmol, 0.5356 g) and K_2CO_3 (2.75 mmol, 0.3795 g) were added to the solution with 12 mL of Toluene and 6 mL of NMP, connected to the Dean-Stark trap under nitrogen flow. The temperature was kept at 150 °C for 4 hrs until the water was removed by toluene from the system. The reaction was continued under nitrogen flow at 175-180 °C for another 2 hrs until gaining a viscous co-polymer. The mixture was diluted with 12 mL of NMP at 100 °C and poured dropwise into a large excess of methanol with vigorously mechanical stirring. The precipitated PEK block co-polymer was washed and purified with double deionized (DDI) water and methanol three times. After being dried at 80 °C under vacuum, the white PEK co-polymer fibers were dissolved in 12 mL of NMP and then, re-precipitated in methanol, washed with DDI water and methanol several times, and finally vacuum dried at 80 °C in the oven.

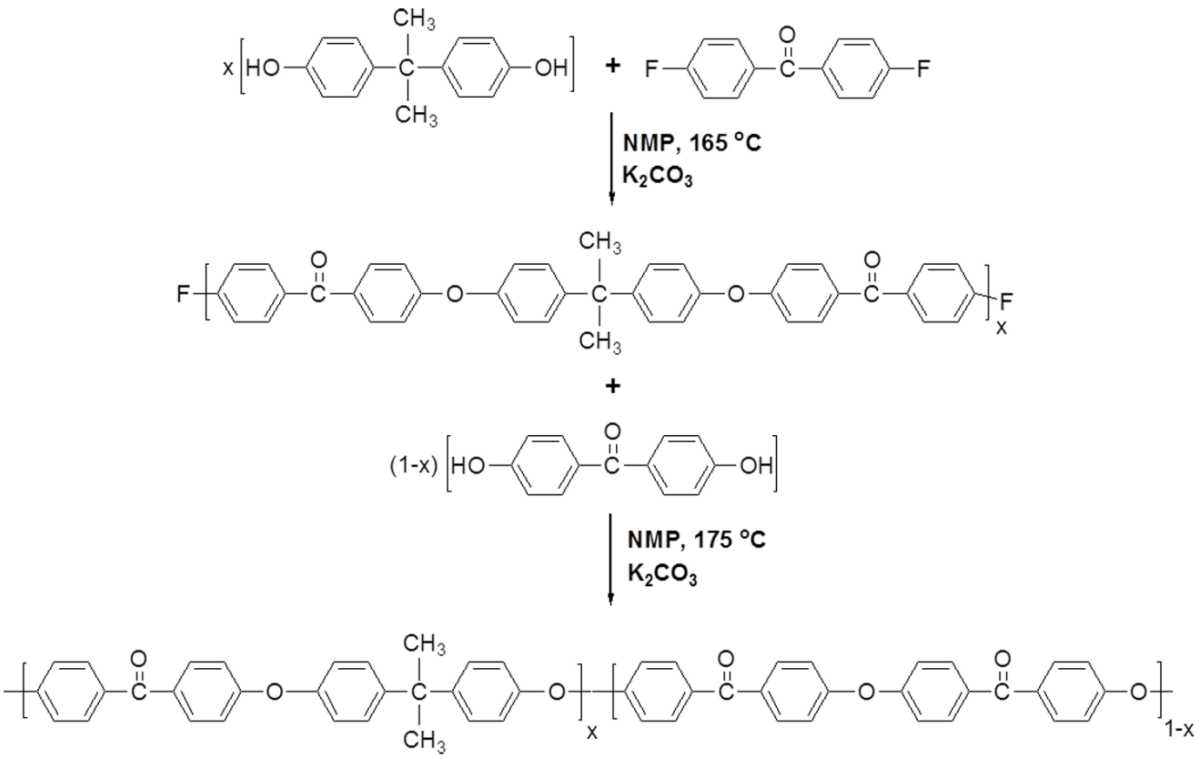

Figure 6-1. Synthesis of PEK block copolymer backbone by polycondensation.

6.2.3 Chloromethylation of PEK and Membrane Casting

According to **Figure 6-2**, the Friedel-Crafts chloromethylation reaction of the PEK occurs at the activated aryl ring between the isopropylidene and ether bond by adding CMME (ChloroMethyl Methyl Ether) and a Lewis acid catalyst (e.g., $ZnCl_2$). The product will be a halomethylated polymer. A 50 mL round-bottomed flask was charged with PEK block co-polymer (0.8 g) and 20 mL of 1,1,2,2-tetrachloroethane (TCE) as the solvent. After stirring the mixture under nitrogen at room temperature (until PEK is completely dissolved), a solution of CMME (29.28 mmol, 2.22 ml) and anhydrous $ZnCl_2$ (0.0998 g, 0.732 mmol) was added dropwise to the mixture and stirred at 35 °C for 48 hrs. The mixture was poured

slowly into a large excess of methanol, and washed with methanol three times. Then, the dried chloromethylated PEK (CMPEK) copolymer was dissolved in NMP and filtered via a fritted disk funnel. The filtrate was cast on a flat glass plate and heated at 80 °C for 1 day, resulted in a thin 35-40 μm thick, transparent and though membrane.

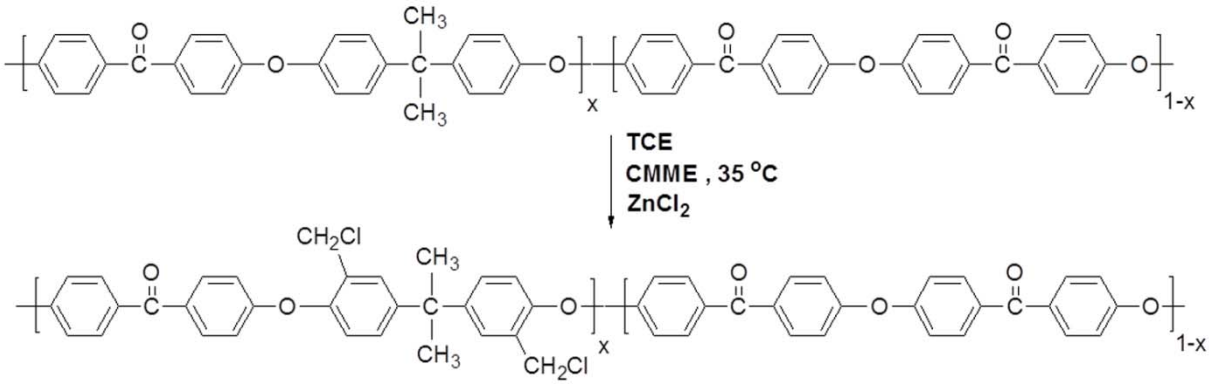

Figure 6-2. Chloromethylation process of PEK block copolymer through Friedel-Crafts reaction.

6.2.4 Quaternization and Alkalinization of CMPEK Membrane

The solid-state alkaline electrolytes are typically prepared by amination of halomethylated polymers with tertiary amines such as triethylamine (TEA). **Figure 6-3** clearly indicates the conversion from a chloromethyl group into a quaternary ammonium (QA) group by immersing the CMPEK membrane in a 35wt% TEA aqueous solution at room temperature for 48 hrs. The last step corresponds to the final product, i.e., QAPEK-OH. To replace the Cl- anion in the QAPEK with OH-, the membrane was placed in 1 M sodium hydroxide (KOH) aqueous solution at room temperature for 48 hrs, and then, washed with DDI water several

times. The obtained QAPEK-OH membrane was stored in a closed vessel filled with DDI water before being used for any performance test.

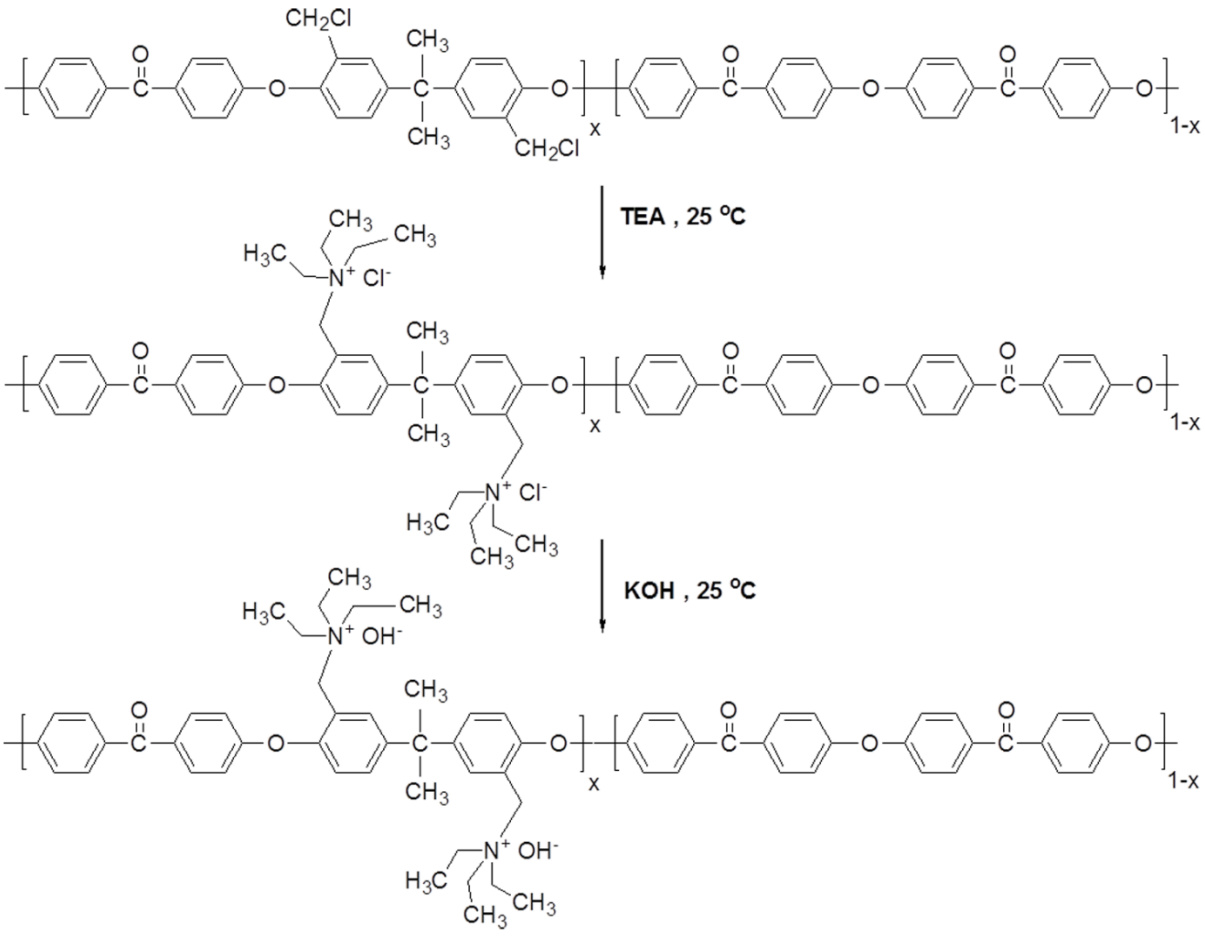

Figure 6-3. Quaternization/amination of CMPEK using TEA aqueous solution followed by alkalinization of the obtained QAPEK.

6.2.5 Measurements and Characterization Tests

Nuclear magnetic resonance (^{1}H NMR) spectra were measured at 500 MHz on a Bruker Analytik GmbH spectrometer. FT-IR spectra were recorded on 35-40 µm thick membrane

samples using a Avatar 320 FT-IR spectrometer. Thermogravimetric analysis (TGA) was performed under nitrogen with a TGA Q500 V20.10 instrument in the temperature range from 50 to 900 °C at the heating rate of 10 °C·min^{-1}. Differential scanning calorimetry (DSC) analysis was performed under nitrogen through the heating-cooling-heating cycle from 0 to 400 °C with a DSC Q2000 V24.4 Build 116 instrument. Tensile measurements were carried out with an UMT-CETR mechanical testing instrument at a speed of 0.05 mm min^{-1}.

6.2.5.1 Water Uptake (WU) and Ion Exchange Capacity (IEC)

The membrane was vacuum-dried at 80 °C for 10 hrs until constant weight for the dried membrane was obtained. They were then immersed in DDI water at given temperature for 4 hrs. After this time, the membranes were taken out, wiped with tissue paper, and quickly weighed on a microbalance. The water uptake of membranes was calculated according to **Equation 6-1**:

$$WU(\%) = \frac{W_{wet} - W_{dry}}{W_{dry}} \times 100 \qquad \textbf{Equation 6-1}$$

where WU (%), W_{wet} and W_{dry} are the water uptake by weight percentage, the weight of wet membrane and the weight of dry membrane, respectively.

The IEC of membrane samples was determined by using the back titration method. At first, the samples were dried until the weight was constant, after which each sample was immersed in DDI water overnight. Then, they were soaked in 0.01 M hydrochloric acid (HCl) for 48 hrs to exchange Cl^- ions with hydroxides. Back titration was then accomplished with 0.01 M

NaOH (aq.) standardized solution with phenolphthalein as an indicator. The IEC values were calculated using the **Equation 6-2:**

$$IEC = \frac{M_1 V_{1\,HCl} - M_2 V_{2\,NaOH}}{W_{dry}} \qquad \textbf{Equation 6-2}$$

where IEC is the ion exchange capacity ($meq \cdot g^{-1}$), M_1 (molar) and V_1 (mL) are the concentration and volume of HCl solution, respectively, before the titration; M_2 (molar) and V_2 (mL) are the concentration and volume of NaOH solution, respectively, used in the titration; W_{dry} (g) is the dry mass of the sample.

6.2.5.2 Anion Conductivity

The anion conductivities of all QAPEK-OH membrane samples were obtained by a four-electrode AC impedance spectroscopy [182] with a CHI760D potentiostat control model. The impedance was measured in the frequency range between 1 MHz and 0.1 Hz with perturbation voltage amplitude of 5 mV. The membranes and the electrodes were set in a Teflon cell, and the distance between the reference electrodes was 1 cm. The cell was placed in a thermo-controlled chamber in liquid water for measurement. Conductivity measurements under fully hydrated conditions were carried out with the cell immersed in liquid DDI water. All samples were equilibrated in water for at least 24 hrs prior to the conductivity measurement. At a given temperature, the samples were equilibrated for at least 30 min before any measurements. Repeated measurements (4 times) were then taken at that given temperature with 10 min interval until no more change in conductivity was observed. The anion conductivities (σ) of all samples were then determined along the longitudinal direction, using **Equation 6-3** [102, 154, 222].

$$\sigma = \frac{L}{AR}$$ **Equation 6-3**

where σ, L, R, and A denote the ionic conductivity, sample length (or distance between the reference electrodes in the membrane), the resistance of the membrane, and the cross-sectional area of the membrane, respectively.

6.2.5.3 Alkaline Stability

To measure the alkaline stability, the QAPEK-OH samples were kept in a stirred aqueous solution of 1 M KOH at 60 and 100 °C. Then, after different specific time, each sample was rinsed and stored in DDI water before re-testing the anion conductivity. Furthermore, the FT-IR and tensile strength tests were re-tested for samples after the stability test.

6.3 Results and Discusison

As shown in **Figure 6-2** and **Figure 6-3**, the AEM was prepared through three stages of chloromethylation, quaternization, and alkalinization chemical reactions. Among them, chloromethylation and quaternization are two chief reactions which demonstrate the anion conductivity [207]. The chloromethylation of polymer is a valuable procedure that was identified about four decades ago. Because of the high reactivity of the tethered chloromethyl group, chloromethylated polymer is the starting point for the synthesis of "polymer-bound reagents" for the ion-exchange polymer electrolytes [223].

The 1H NMR spectra of the PEK and CMPEK block co-polymers were well assigned to the supposed chemical structure (**Figure 6-4**). In the 1H NMR spectrum of CMPEK (denoted as **h** in **Figure 6-4**), a peak assignable to the methylene protons of the chloromethyl groups on the polymer main chain was observed at 4.6 ppm, which was absent in the 1H NMR

spectrum of the bare PEK. The signals with chemical shifts between 6.8-7.9 ppm were assigned to the aromatic protons of PEK and CMPEK co-polymers.

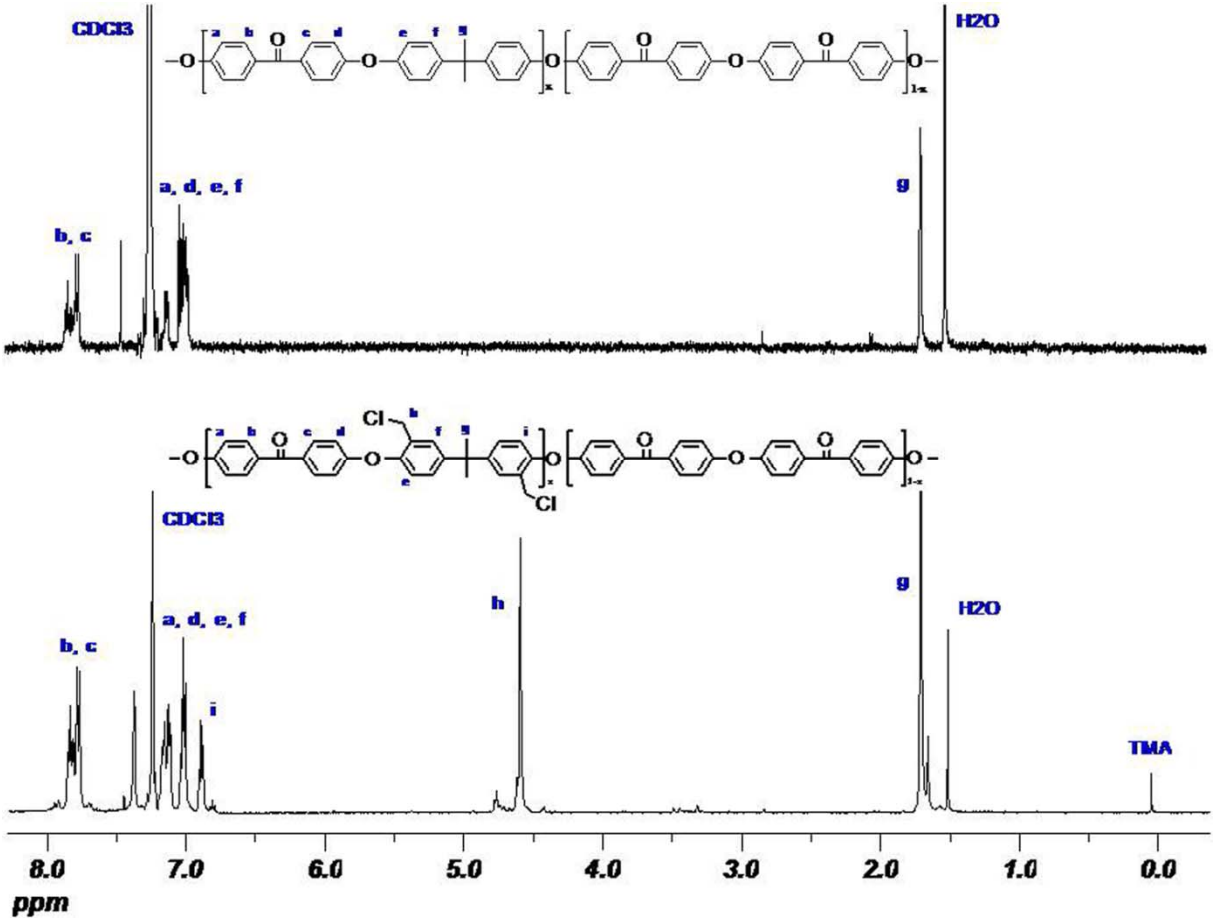

Figure 6-4. ^{1}H NMR spectra of PEK and CMPEK in deuterated chloroform ($CDCl_3$).

In order to demonstrate whether the quaternary ammonium (QA) groups are attached on the polymer chain, the elemental composition of QAPEK-OH membrane was investigated through the FT-IR spectroscopy (**Figure 6-5**). The absorption bands at 3290 and 2359 cm^{-1} were characteristic of QA groups [224, 225]. The absorption bands at 2873 and 2968 cm^{-1}

arise from the stretching vibrations of symmetric and asymmetric methylene (-CH_2-) groups, respectively [224-230].

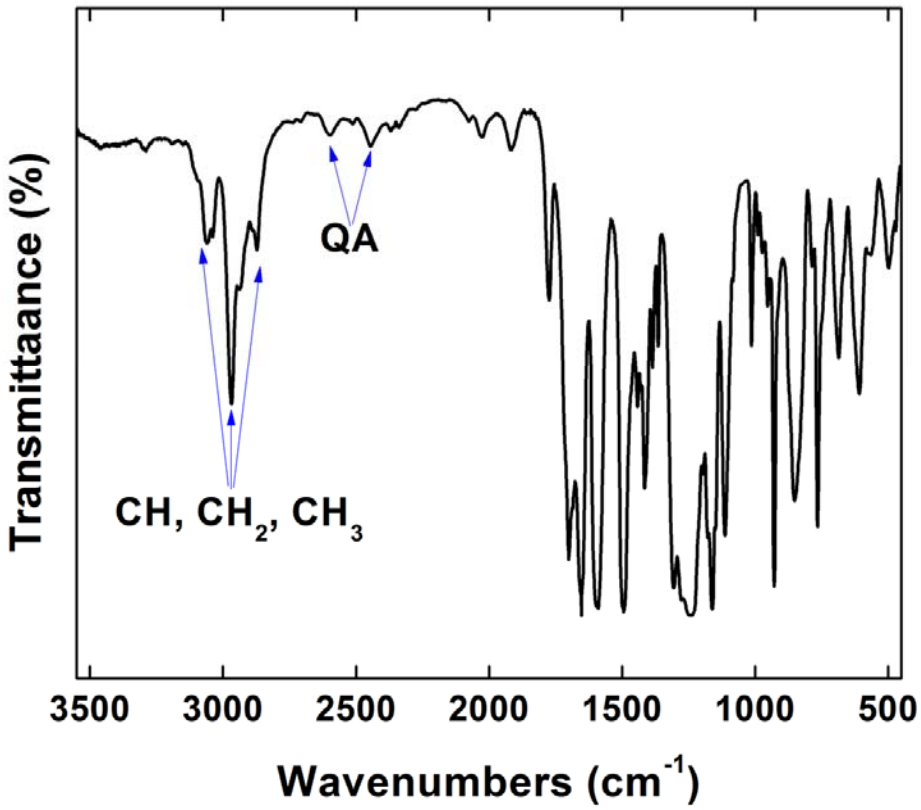

Figure 6-5. FT-IR spectrum of QAPEK-OH membrane.

The thermal stability of PEK, CMPEK and hydrated QAPEK-OH membrane were investigated by TGA curves, shown in **Figure 6-6**. The pure PEK copolymer started the degradation process around 461 °C. For CMPEK the weight loss (14 %) observed at 320 °C was attributed to the chloromethylene groups. In QAPEK-OH membrane, as a result of the

strong hydrophilicity of the quaternary ammonium groups and attracting water from the atmosphere, a slight weight loss (5.4 %) was observed between 150 and 180 °C, corresponding to the evaporation of absorbed water. This behavior has been commonly found in other polymeric ion-exchange membranes. The weight loss (9 %) observed for QAPEK-OH started at 200 °C was related to the degradation of QA groups and the one at 320 °C can be assigned to chloromethylene groups (18 %), satisfying alkaline fuel cell applications at high temperatures.

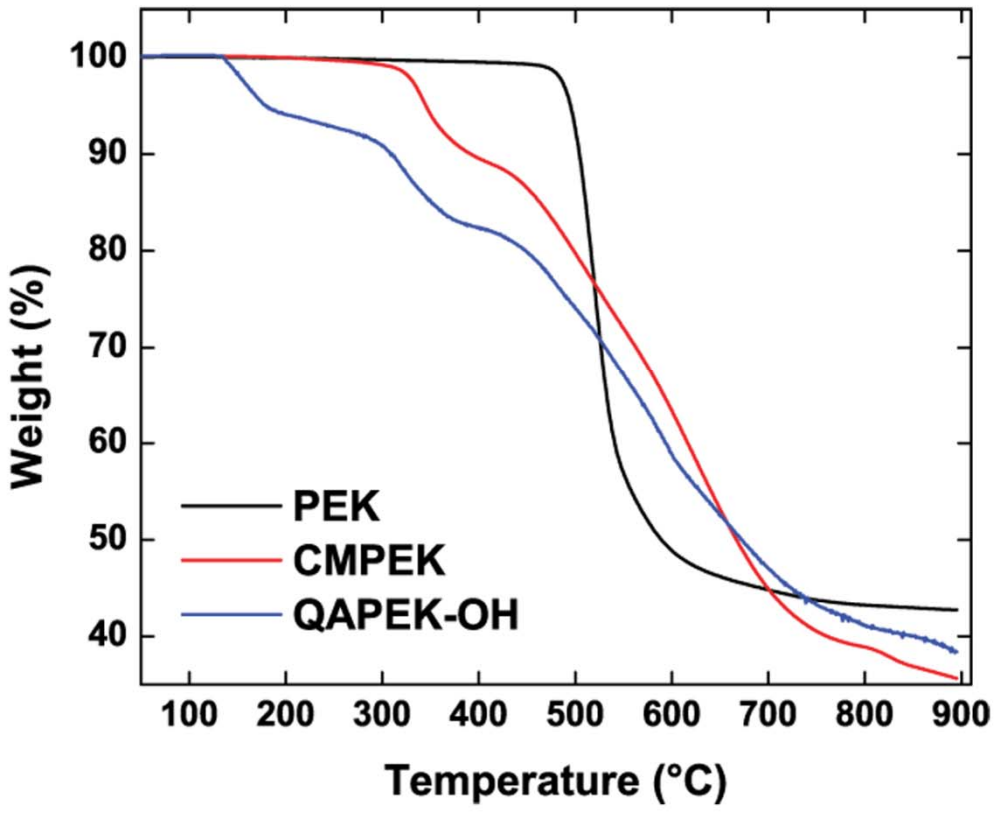

Figure 6-6. TGA curves for PEK, CMPEK and QAPEK-OH copolymers in N_2.

The DSC analysis was performed to identify their glass transition temperatures (T_g) of PEK, CMPEK and QAPEK-OH polymers (**Figure 6-7**). For unmodified PEK co-polymer, Tg was about 142 °C. It can be seen that the T_g for CMPEK and QAPEK-OH has been shifted to higher temperature of 155 and 167 °C, respectively. The increase of T_g for the CMPEK and QAPEK-OH, implies that they are thermo-mechanically more stable than unmodified PEK membrane. The membrane thus becomes more elastic in nature and can withstand higher temperatures. Thus, the results obtained from TGA and DSC shows the improved potential of the PEK based AEMs for high temperature operations of alkaline fuel cells applications.

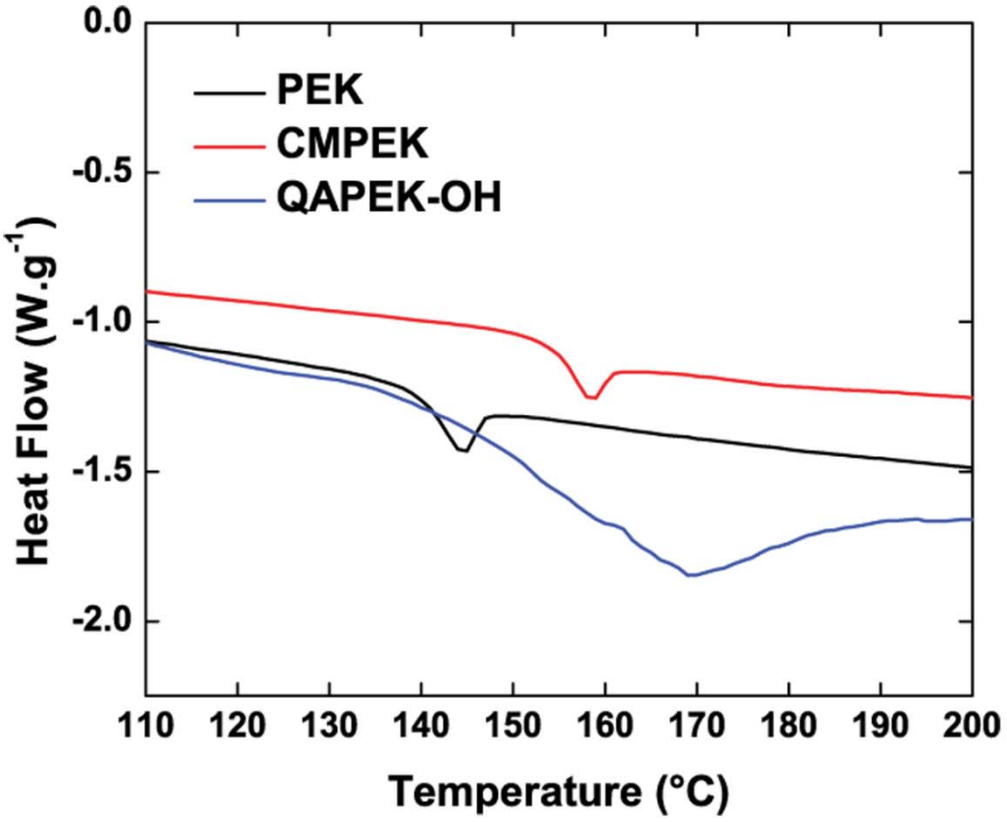

Figure 6-7. DSC curves for PEK, CMPEK and QAPEK-OH copolymers in N_2.

The water uptake of aminated polymers is known to have a profound effect on the anion conductivity and mechanical properties of AEMs. Water molecules dissociate the alkaline functionality and facilitate hydroxide transport. However, excessively high levels of water uptake can result in membrane fragility and dimensional change, which lead to the loss of mechanical properties [231]. Basically, the amount of water uptake of QAPEK-OH membrane is strongly dependent upon the amount of quaternary ammonium hydroxide

groups [232]. The deep effect of water uptake on the anion conductivity as well as the mechanical property of AEMs is remarkable. Basically, when the membrane absorbs higher amount of water, the number of available anion exchange sites increases, resulting in an increment in the anion conductivity. Although the higher water uptake leads to the higher anion conductivity, excessive uptake can also cause swelling and decrease the mechanical strength of the membrane [233-236]. The measured water uptake and IEC were 16.67 % (**Equation 6-1**) and 0.41 meq g^{-1} (**Equation 6-2**), respectively. To reach a high anion-conductive membrane, 16.67% water uptake was not enough for the developed QAPEK-OH membrane. The low water uptake value of the block QAPEK-OH membrane can be related to (i) low ion exchange capacity and (ii) the developed hydrophilic/hydrophobic phase-separated morphology [233, 235].

The anion conductivity of the QAPEK-OH membrane was compared to the commercial fumapem® FAA from FuMA-Tech GmbH (35–40 μm thickness, 0.59 Ω cm^2 at 20 °C), after the hydration in DDI water for 24 hrs at the room temperature. FAA is a hydrocarbon membrane-polymer of aminated polyarylene (polysulfone) chloride, hydroxide and carbonate salts anion exchange membrane, used for alkaline fuel cells without the need of liquid electrolyte. In **Figure 6-8**, the anion conductivity values of the membranes were shown and compared versus the temperature. In general, an anion conductivity above 10^{-2} S cm^{-1} is required for AEM materials used in fuel cells. As expected, an increase in temperature resulted in an increase in hydroxide conductivity based on the simplified diffusion mechanism and thermal motion of hydroxides within the membrane [227]. This is attributed to the increase of free volume in the membrane at elevated temperatures which expands the

required channels for ion conduction [69]. For the FAA membrane, the enhancement of the anion conductivity with the increase of the temperature was in a gradual fashion, whereas for the QAPEK-OH membrane the temperature had much higher effect on the improvement of the anion conductivity. The possible explanation is that at elevated temperature the hydrophilic domains of QAPEK-OH membrane would easily become continuous, leading to the expansion of overall hydrophilic domains [233]. This phenomenon results in the enhancement of anion conduction through the membrane by increasing the temperature. Moreover, as the temperature increased to 100 °C, the anion conductivity in FAA membrane started to decrease. This can be attributed to the degradation commencement of FAA membrane at temperatures higher than 80 °C, indicating its low thermal stability at elevated temperatures.

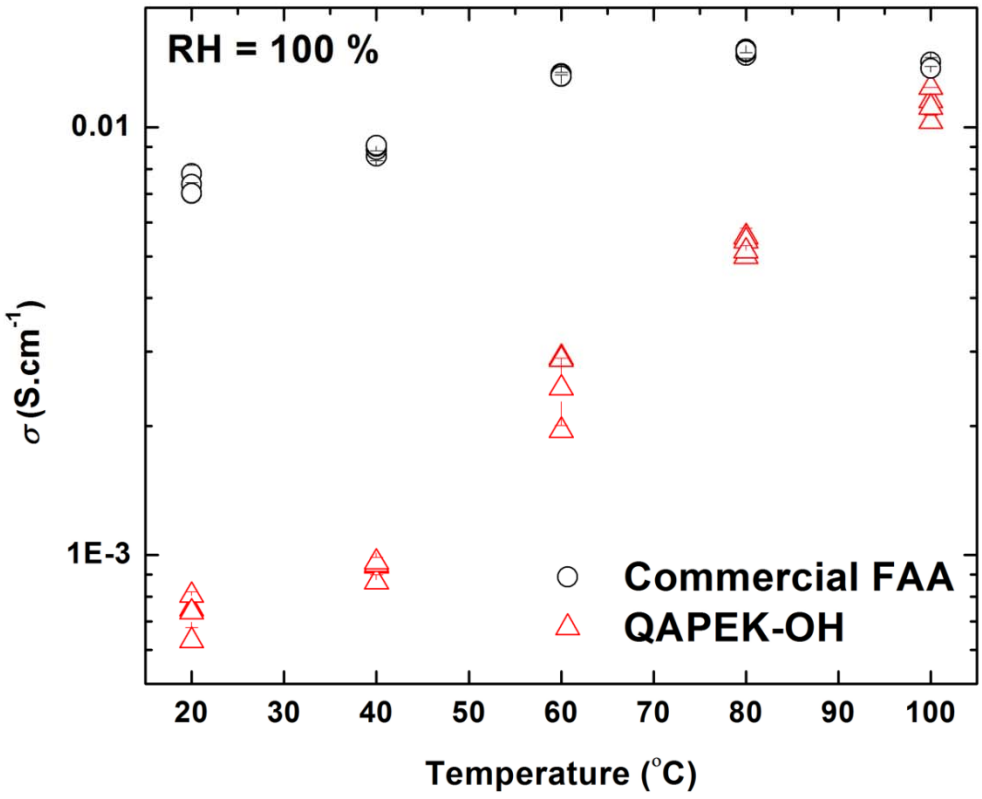

Figure 6-8. Anion conductivities of fully hydrated QAPEK-OH and commercial FAA membranes at different temperatures.

Besides the excellent thermal stability and satisfactory mechanical properties, QAPEK-OH also exhibited good alkaline stability at elevated temperatures. The alkaline stability was tested by immersing the samples in 1 M KOH at two different temperatures of 60 and 100 °C. In **Figure 6-9** the FT-IR spectroscopy of untreated QAPEK-OH membrane was compared to that after 24 and 48 hrs of chemical stability test at 100 °C. As the peaks assigned to QA and

methylene groups existed in alkaline treated QAPEK-OH membranes, it was concluded that the chemical stability of QAPEK-OH is good enough to keep its performance at elevated temperatures.

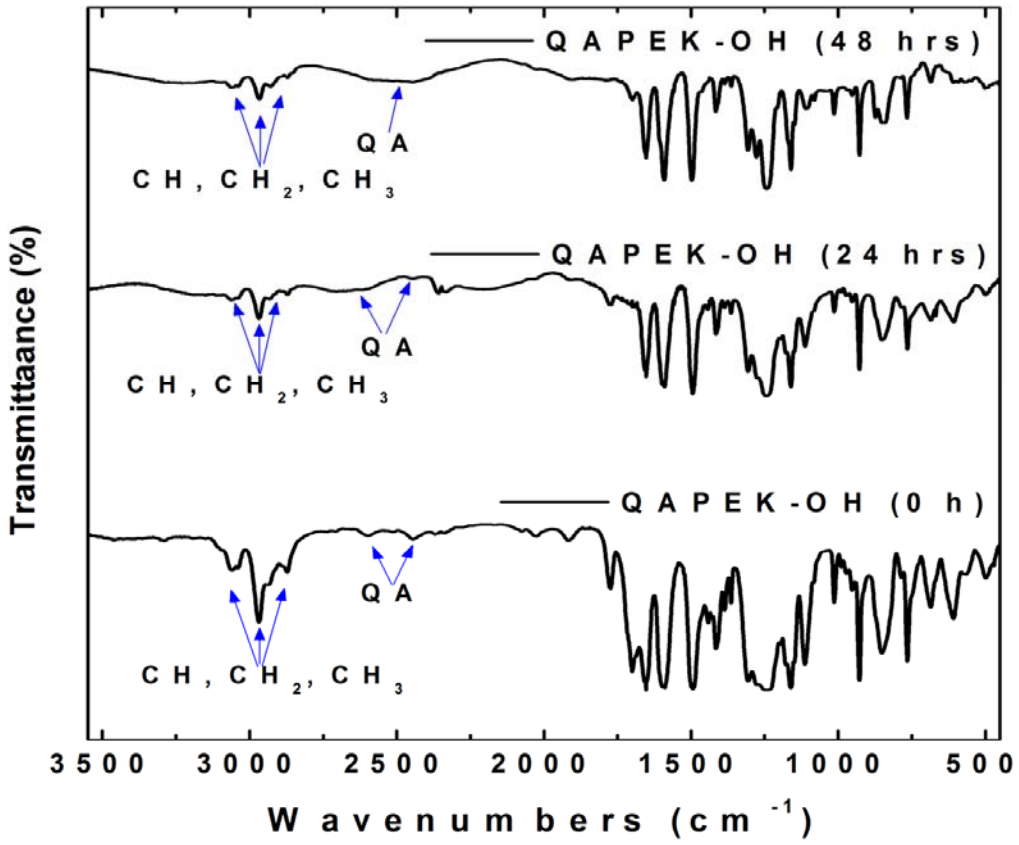

Figure 6-9. FT-IR spectrum of QAPEK-OH membranes treated in 1 M KOH solution at 100°C after 24 and 72 h.

The mechanical properties for the untreated QAPEK-OH membrane and the one after 48 hrs of the alkaline stability test at 100 °C are shown in **Figure 6-10**. For the untreated

QAPEK-OH membrane, the tensile strength, Young's modulus and the elongation at break were 17.16 MPa, 7.75 GPa and 10 %, respectively, showing that it possesses flexiblity, ductility and toughness to be applied in AFCs. The tensile strength, Young's modulus and the elongation at break of alkaline-treated QAPEK-OH at 100 °C were 18.81 MPa, 4.3 GPa and 5.64 %, respectively, exhibiting that the QAPEK-OH membrane kept its mechanical strength at elevated temperatures.

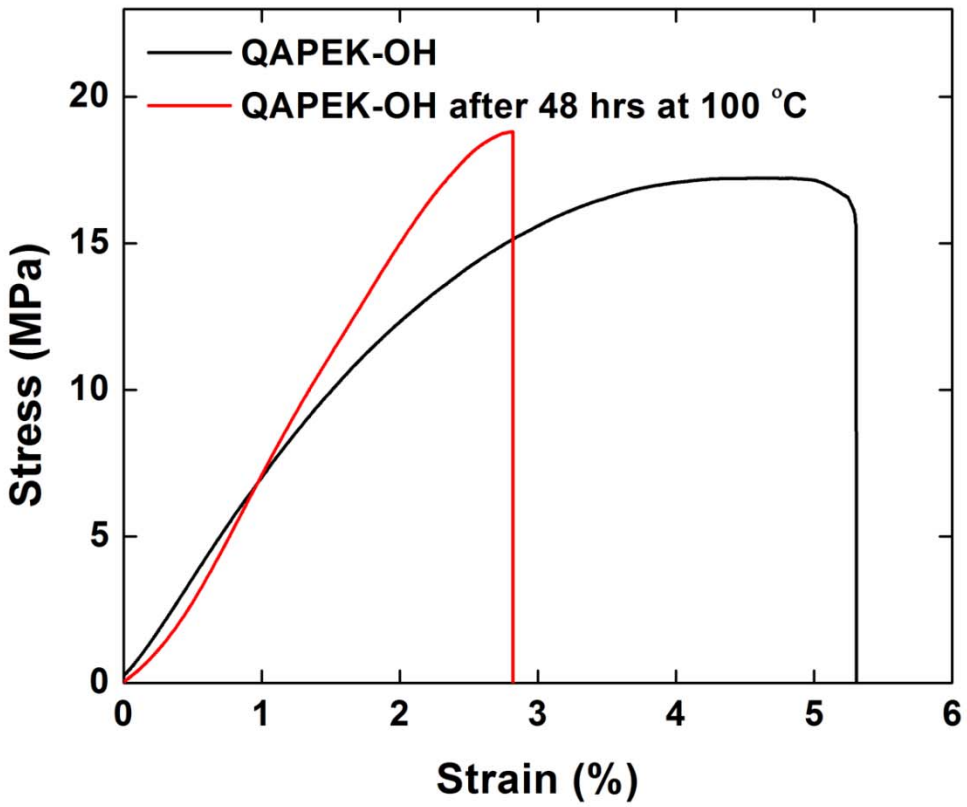

Figure 6-10. Stress–strain curves of the QAPEK-OH membranes under hydrated condition in ambient atmosphere (25 °C) before and after alkaline stability test at 100 °C.

The QAPEK-OH membranes also maintained their anion conductivity after immersion in 1 M KOH solution for more than 120 hrs at 60 °C (**Figure 6-11**) and 72 hrs at 100 °C (**Figure 6-12**). On the contrary, the FAA membrane started to degrade just after 24 hrs at 60 °C (**Figure 6-11**) and after 3 hrs at 100 °C (**Figure 6-12**) such that the ion conductivity was 15 times lower than that before the degradation test, indicating its very poor chemical stability at elevated temperatures (**Figure 6-13**).

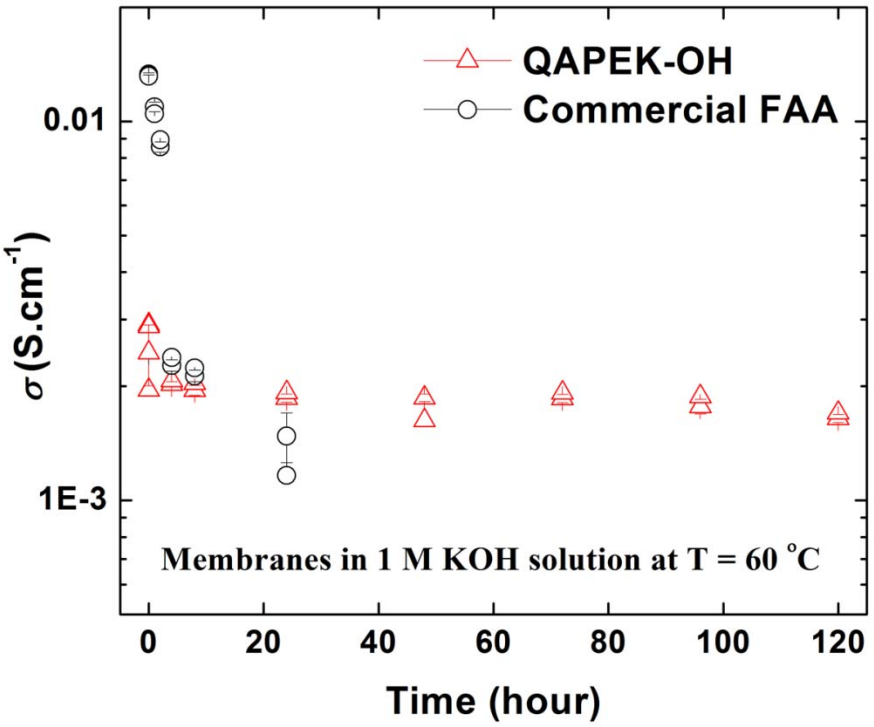

Figure 6-11. Anion conductivity after alkaline stability test of QAPEK-OH and commercial FAA in 1 M KOH at 60 °C.

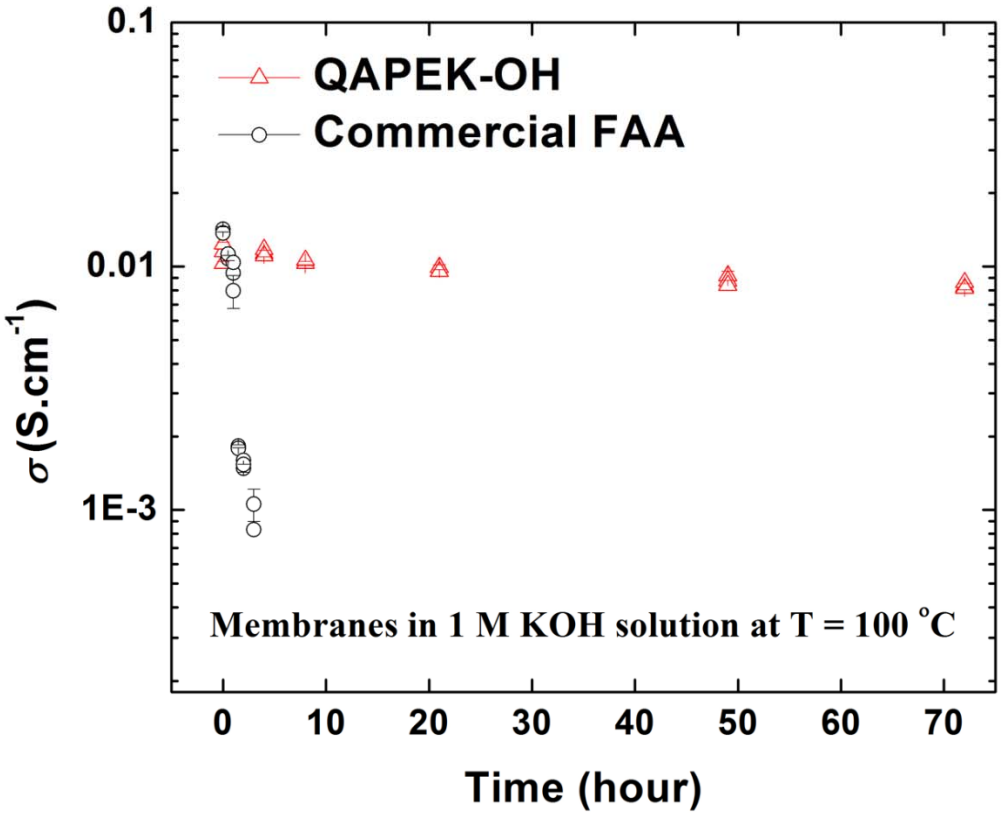

Figure 6-12. Anion conductivity after alkaline stability test of QAPEK-OH and commercial FAA in 1 M KOH at 100 °C.

Although the QAPEK-OH membrane exhibited high alkaline stability at elevated temperatures, their anion conductivity must be enhanced and increased to a satisfactory and desirable level by modifying the morphology and the ionomer structure of polymer electrolyte. For this purpose, large bulky substituents could be presented in the backbone of

polymer electrolyte, which prevent close packing of the polymer chains and can generate higher ionic conductivity [228, 237, 238].

Figure 6-13. Photographs of the QAPEK-OH and commercial FAA membranes before and after being treated with 1 M KOH solution at 100 °C.

6.4 Conclusions

In summary, polyetherketone (PEK) polymer backbone was successfully modified with quaternary ammonium groups through direct chloromethylation followed by reaction with triethylamine reagent. The obtained quaternized ionomers exhibited an excellent solubility

and formed flexible and tough membranes by casting from an NMP solution. These AEMs based on quaternary ammonium hydroxide groups, denoted QAPEK-OHs, presented excellent thermal stability, satisfactory mechanical property, and good alkaline stability. The preliminary properties have demonstrated their potential as electrolytes for high temperature anion exchange membrane fuel cells. The obtained results will aid in designing superior stable membranes for high temperature alkaline fuel cell application; yet, to enhance and increase the anion conductivity at high temperature AEMFCs, further modifications on the membrane morphology and ionomer structure must be performed.

Chapter 7
High Performance Porous Polybenzimidazole Membrane for Alkaline Fuel Cells

Chapter 7 is based on published work by Zarrin et al. [34] and is reproduced with permission from the International Journal of Hydrogen Energy. The thesis author's specific contributions to this paper were to synthesize and fabricate the AEM, conduct EIS measurements, run all of physicochemical characterization tests, prepare all plots and results, write the final manuscript and respond to the comments of reviewers. This work and journal paper preparation was conducted with direction from the project supervisors who are co-authors on the publication. Gaopeng Jiang aided with testing the single AEMFC performance. Grace Lam helped to conduct alkaline stability tests.

7.1 Introduction

Using alkaline medium instead of acidic in hydrogen fuel cells is preferred because the occurrence of corrosion is mitigated and cheaper construction materials can be used [239]. In anion exchange membrane fuel cells (AEMFCs), because of the alkaline environment, the reduction and oxidation kinetics of the oxidants and fuels (e.g., air and hydrogen) are inherently much faster for the cathode and anode electrodes, respectively, enabling higher power densities and energy conversion efficiency. Thereby, employing non-precious metal electro-catalysts such as nickel and silver are feasible in such systems, making them a potentially low-cost technology. Moreover, due to the less corrosive nature of an alkaline medium, longer lifetime is expected for AEMFCs [204, 206, 207, 240-242]. However, the

major barrier to commercialize AEMFCs is the anion exchange membrane (AEM) which suffers from low performance and physic-chemical stability. Thus, it is vitally required to develop a cost effective AEM, possessing excellent ionic conductivity and high thermo-physico-chemical stability [204, 243-246].

Generally, AEMs are categorized according to various types of polymeric backbones and ion-exchange groups [247-249]. Depending on ion-exchange groups, AEMs can be classified into (i) ion-doped membranes, in which the polymers are doped with electrolytic solutions (e.g., KOH, LiOH etc.); (ii) composite membranes, where the incorporated inorganic materials are in charge of ion transfer; and (iii) blended membranes, in which another polymer acts as the ion-exchange group. The most studied polymers, so far, are polybenzimidazole [242, 250-255], polyphenylene oxide [72, 256], polyetherketone [33], cardo polyetherketone [257], polyethersulfone [258, 259], poly(vinyl alcohol) [260], poly(ethylene-co- tetrafluoroethylene) [80, 81, 261, 262] and poly(arylene ether sulfone) [228]. However, at the current state of AEM technology, there are still major challenges that must be resolved, including low ion conductivities, chemical instabilities in concentrated alkaline environments, and fast thermal degradation.

In this study, the developed AEM is based on ion-doped membranes. Among the examined polymeric structures in literature, poly[2,2′-(m-phenylene)-5,5′-bibenzimidazole] (PBI) is an inexpensive amorphous homo-polymer, having outstanding physico-chemical and thermal stability [71, 241, 263-268], promising candidate for the backbone of ion-doped membranes [269-273]. An unmodified PBI is an ionic and electronic non-conductor [71, 274-277]. However, due to the existence of amine (–NH–) and imide (–N) groups in the imidazole rings

of PBI, it turns into an excellent ionic conductor by doping with strong alkaline (e.g., KOH) [71, 269, 270, 278] or acidic (e.g., phosphoric acid) [279-281] solutions, yet maintains its electronic non-conducting properties after doping. Xing *et al*. [71] have shown ionic conductivities between 5×10^{-5} $S\cdot cm^{-1}$ and 1×10^{-1} $S\cdot cm^{-1}$ for PBI using KOH with a concentration of 6 M at 70–90 °C. However, the reported high ionic conductivity for PBI was measured when the membrane was in the electrolytic solution at elevated temperatures. In this work, a unique approach has been taken to introduce porosity into the morphology of PBI and then dope it with KOH, which makes it to function without the requirement of being submerged in the electrolytic solution. The existence of pores can increase the uptake of KOH, leading to the increase of ionic conductivity [282, 283]. To the best of our knowledge, although there are a few examples of proton-conducting porous PBI membranes for proton exchange membrane fuel cells (PEMFCs) [251, 254, 255, 284-289], there are no reports on the development of KOH-doped porous PBI membranes for AEMFCs. In order to make the membrane porous, the synthesized PBI was mixed with an appropriate amount of a low molecular weight pore-forming agent (dibutyl phthalate, DBP), which could be removed after synthesis by immersion in methanol solution. DBP was selected among various phthalate-based porogens due to its aliphatic chains. It has been shown that aliphatic structure of phthalates exhibit more interconnected and larger pore size than fully aromatic ones such as diphenyl phthalate [251]. Accordingly, the authors chose dibutyl phthalate (DBP) as a candidate for porogen in their study.Then, the obtained porous membrane was doped with a highly concentrated KOH solution. The morphology, chemical analysis, mechanical properties, thermal stability, electrolyte absorption, hydroxide conductivity, alkaline

stability, and AEMFC performance of the KOH-doped PBI membranes with different porosities were characterized and compared to commercially available AEM (Fumapem® FAA from FuMA-Tech GmbH) using different spectroscopic and microscopic analysis methods, including proton nuclear magnetic resonance (^{1}H NMR), scanning electron microscopy (SEM), energy-dispersive X-ray (EDX) mapping, Fourier transform infrared (FT-IR), thermogravimetric analysis (TGA) and differential thermal analysis (DTA), tension testing, contact angle measurement, and electrochemical impedance spectroscopy (EIS).

7.2 Experimental Section

7.2.1 Synthesis of Polybenzimidazole (PBI)

The synthesis of PBI is well described in the literature [290]. In this study, according to **Figure 7-1**, 4.7 mmol of 3,3′-diaminobenzidine (DAB, Aldrich) with an equivalent molar amount of isophthalic acid (IPA, Aldrich) were dissolved into polyphosphoric acid (PPA, Alfa Aesar) in a round-bottom flask with a magnetic stirrer under a slow flow of nitrogen gas. After stirring for 7 h at 200 °C, the reaction mixture turned dark reddish brown and became viscous. The reaction was quenched by pouring the hot solution into a large amount of cold water. The formed PBI fibers were stirred and washed for 48 h in distilled deionized (DDI) water and subsequently for 7 h in 2 M KOH solution followed by drying in an oven at 100 °C overnight.

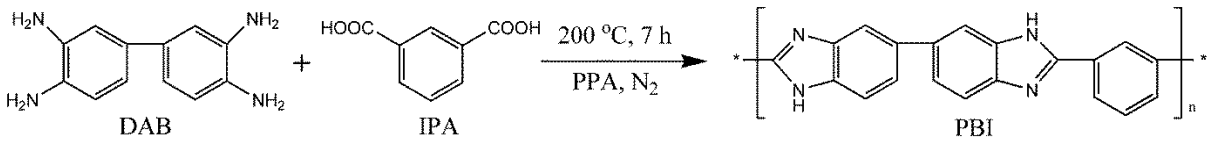

Figure 7-1. The synthesis and chemical structure of PBI.

7.2.2 Preparation of KOH-Doped Porous PBI Membranes

A schematic of fabricating KOH-doped porous PBI is displayed in **Figure 7-2**. As shown, 1 wt.% dried PBI polymer with different amounts of DBP (Aldrich) were dissolved in dimethyl sulfoxide (DMSO, Aldrich) under stirring and heating until an orange homogeneous solution was obtained. Then, it was spread onto a glass plate and placed in an oven. The temperature ramp was from 60 to 190 °C over 12 h in order to slowly evaporate the solvent. After the heating was finished, the glass plate was immersed in DDI water in order to detach the membrane from the plate. Then, DBP was extracted by immersing the membranes in methanol for 1 h. The porous PBI was dried at 80 °C until a constant weight was achieved. Then, all membranes were doped with KOH by keeping them in 6 M KOH solution for 2 days and finally stored in DDI water for future characterization tests. In this paper PBI and *x*-pPBI represent the bare PBI and porous PBI membrane with the porosity of *x* (=25, 50, 70), respectively.

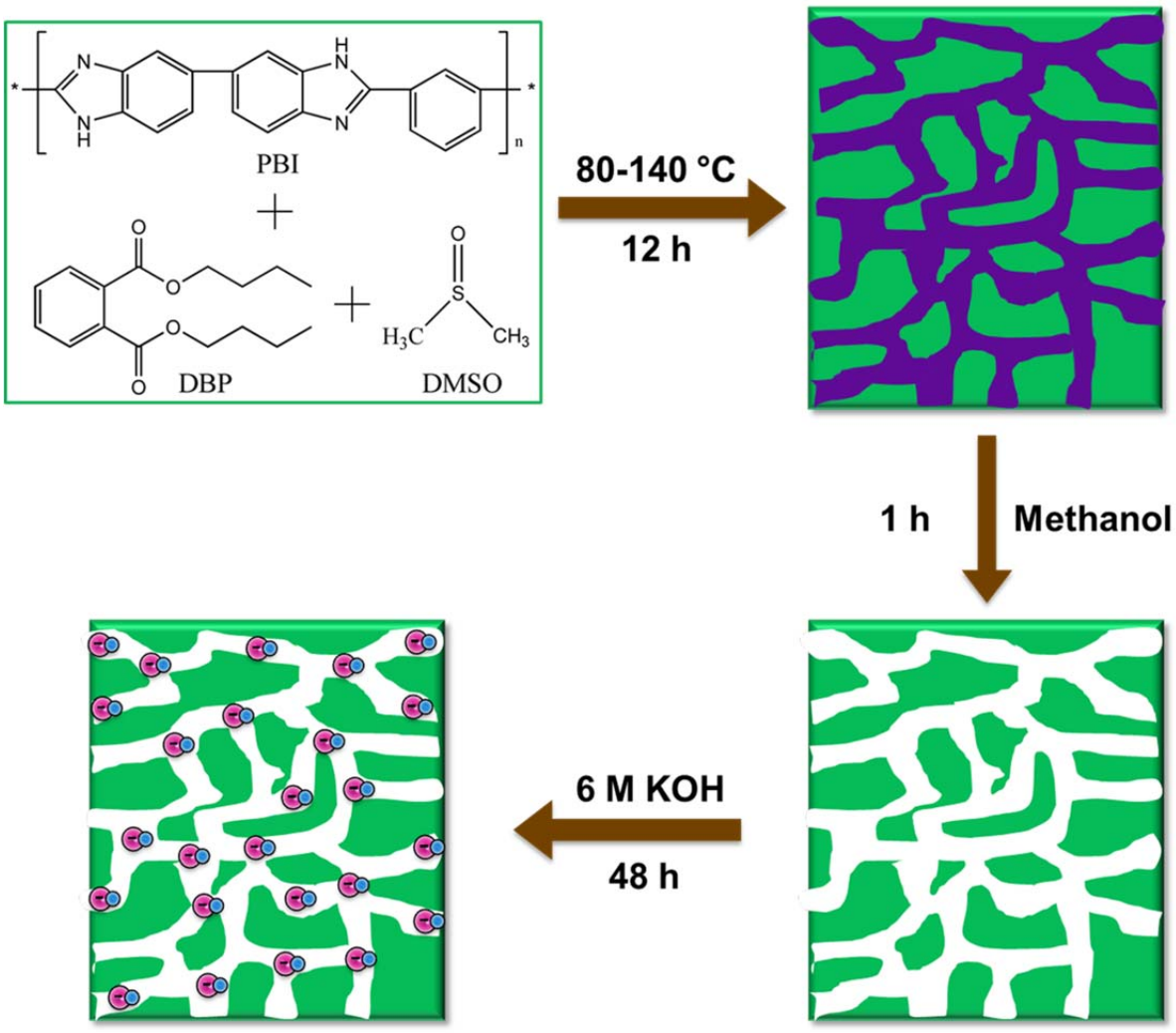

Figure 7-2. The fabrication of KOH-doped porous PBI membranes.

7.2.3 Thermal, Physical, and Chemical Characterization Tests

The presence of PBI was shown by ^{1}H NMR (500 MHz Bruker Analytik GmbH) and FT–IR (Avatar 320). The average molecular weight was measured by static light scattering (Malvern Instruments Ltd., Zetasizer Ver. 6.20). The overall morphology and EDX mapping of all samples was examined by using SEM (LEO FESEM 1530). TGA and DTA were performed

under nitrogen with a TGA Q500 V20.10 instrument in the temperature range from 25 to 900 °C at the heating rate of 10 °C·min^{-1}. The mechanical properties of all membranes were determined by a tension testing machine (ADMET 7603-5 kN) in ambient atmosphere at a tension speed of 5 mm·min^{-1}. The size of the species was 6 mm wide, 40 mm long, and 35 μm thick.

7.2.4 Porosity, KOH Uptake, Water Uptake, and Swelling Ratio

Two methods were applied to estimate the real porosity of the membranes. The first method was adapted from the work of Wang *et al.*[255] by measuring the weight of the porous membranes before and after filling the pores with DDI water for 48 h. Accordingly, the porosity (ε) can be calculated by the following equation:

$$\varepsilon_1 = \frac{W_w - W_d}{\rho_{H_2O} \times V_d} \qquad \textbf{Equation 7-1}$$

where W_w is the weight of the wet porous PBI membranes, W_d is the weight of dried membranes in a vacuum oven at 80 °C for 48 h after extracting the DBP, ρ_{H2O} is the density of DDI water, and V_d is the volume of dried porous membranes. The second method was taken from Mecerreyes *et al.* [251] research based on weight difference before and after leaching out the porogen from the membrane. According to this method, the percentage of weight loss after removing the porogen (i.e., DBP) was estimated as below:

$$\varepsilon_2 = \frac{W_{PBI+DBP} - W_{x-pPBI}}{W_{PBI+DBP}} \qquad \textbf{Equation 7-2}$$

where $W_{PBI+DBP}$ and $W_{x\text{-}pPBI}$ are the weight of dried membranes before and after removal of the DBP porogen, respectively.

To measure the KOH uptake (*KOH-U*), KOH-doped PBIs were removed from the concentrated KOH solution and wiped using a tissue paper to remove surface liquid. The weight of the KOH impregnated membrane (W_{KOH}) was measured and **Equation 7-3** was used to calculate the KOH uptake:

$$KOH-U\,(\%)=\frac{W_{KOH}-W_d}{W_d}\times 100 \qquad \textbf{Equation 7-3}$$

To calculate the water uptake and swelling ratio, the dried KOH-doped membranes were immersed in deionized water at room temperature for 48 h. After hydration, the surface water was wiped with tissue paper before weighing. Then, the membranes were fully dried in a vacuum oven at 80 °C for 48 h and weighed. The weight and dimensions of samples were measured several times until constant numbers were achieved. Then, the water uptake (*W-U*), lengthwise swelling ratio (*L-SWR*), and crosswise swelling ratio (*C-SWR*) were calculated by following equations:

$$WU\,(\%)=\frac{W_{w-KOH}-W_{d-KOH}}{W_{d-KOH}}\times 100 \qquad \textbf{Equation 7-4}$$

$$L-SWR\,(\%)=\frac{L_{w-KOH}-L_{d-KOH}}{L_{d-KOH}}\times 100 \qquad \textbf{Equation 7-5}$$

$$C-SWR\,(\%)=\frac{t_{w-KOH}-t_{d-KOH}}{t_{d-KOH}}\times 100 \qquad \textbf{Equation 7-6}$$

where $W_{w\text{-}KOH}$, $L_{w\text{-}KOH}$, and $t_{w\text{-}KOH}$ are the weight, length, and thickness of hydrated KOH-doped membranes and $W_{d\text{-}KOH}$, $L_{d\text{-}KOH}$, and $t_{d\text{-}KOH}$ are the weight, length, and thickness of dried KOH-doped films.

7.2.5 Water Contact Angle

VCA 2500 XE equipment and associated software (AST Products, Billerica, MA) were used to inspect how the hydrophilicity changes with the porosity by measuring the water contact angle on the surface of membranes. For this purpose, a droplet of water (about 7 μL) was laid onto the surface of all PBI samples and the images were captured using a CCD camera. Contact angles below 90 ° indicate the hydrophilic character of a sample describing the water-uptake capability.

7.2.6 Hydroxide Conductivity Measurement

The ion conductivity of all PBIs was characterized in both in-plane and through-plane directions of the membranes, using AC impedance spectroscopy in Princeton Versastat MC potentiostat. For in-plane, the membrane samples were sandwiched in a simple home-made four-point cell, made from four platinum strips and Teflon plates. For the through-plane conductivity, the membranes were sandwiched between two electrodes with 1.1304 cm^2 surface area. For both directions, the impedance was measured in the frequency range between 1 MHz and 0.1 kHz with perturbation voltage amplitude of 10 mV. The cells were placed in a thermo-controlled chamber in DDI water for measurement. All samples were equilibrated in water for at least 24 h prior to the conductivity measurement. At a given temperature, the samples were equilibrated for at least 30 min before any measurements. Repeated measurements (at least three times) were then taken at the given temperature with

10 min intervals until no more changes in conductivity were observed. The in-plane and through-plane ionic conductivities of all samples were then determined using **Equation 7-7**:

$$\sigma = \frac{L}{RA} \qquad \textbf{Equation 7-7}$$

where σ designates either the in-plane or through-plane hydroxide conductivity, L is either the distance between the reference electrodes in the four-probe cell or the thickness of membrane samples in the through-plane cell setup, R is the ionic resistance of the membrane, and A is either the cross-sectional area in the in-plane setup or the area of the electrodes in the through-plane cell.

7.2.7 Alkaline Stability Test

To measure the alkaline stability, all bare and porous KOH-doped PBI membranes were kept in a boiling solution of 6 M KOH. Then, after different specified times, each sample was rinsed and stored in DDI water before re-testing their ionic conductivity.

7.2.8 Membrane Electrode Assembly and Fuel Cell Testing

The performance of KOH-doped porous PBI, bare PBI, and FAA commercial in a fuel cell setup was determined using a single cell membrane electrode assembly (MEA) setup. The electrocatalyst used in the anode and cathode layers was Pt/C (28.2 wt.% Pt, TKK Corp.). Catalyst-containing inks were prepared by mixing and ultrasonicating the catalyst with isopropanol for 1 h. The inks were sprayed on gas diffusion layer (GDL, SIGRACET® GDL 10 BB) and dried in oven at 80 °C for 24 h. This process was repeated until the desired catalyst loading (0.5 $mg.cm^{-2}$) was achieved for both anode and cathode. The MEA with an active electrode area of 5 cm^2 was obtained by hot-pressing the cathode and anode onto each

side of the membranes at 110 °C and 2000 psi for 10 min. For FAA commercial, the MEA was fabricated by pressing the catalyst-coated GDLs onto the membrane at room temperature and 2000 psi for 10 min, due to its low thermal stability. For each sample, the MEA was assembled into the fuel cell hardware (850e Multi-Range Fuel Cell Test System, Scribner Associates) with gas flow rate of 0.2 $L.min^{-1}$ for both hydrogen and oxygen.

7.3 Results and Discussion

The average molecular weight of 104,167±1.898 $g{\cdot}mol^{-1}$ was calculated for PBI by the inverse of the intercept of the linear interpolation in the Zimm plot from static light scattering. **Figure 7-3** represents ^{1}H NMR spectra of PBI using deuterated dimethyl sulfoxide (DMSO-d6) solutions, which confirm the successful synthesis of the polymer. The proton chemical shifts (δ_H) are 9.14 (H_1), 8.28 (H_2), 7.85 (H_5), 7.8 (H_3), 7.67 (H_4), 7.53 (H_6) [291], which are assigned to the protons on the aromatic groups in PBI.

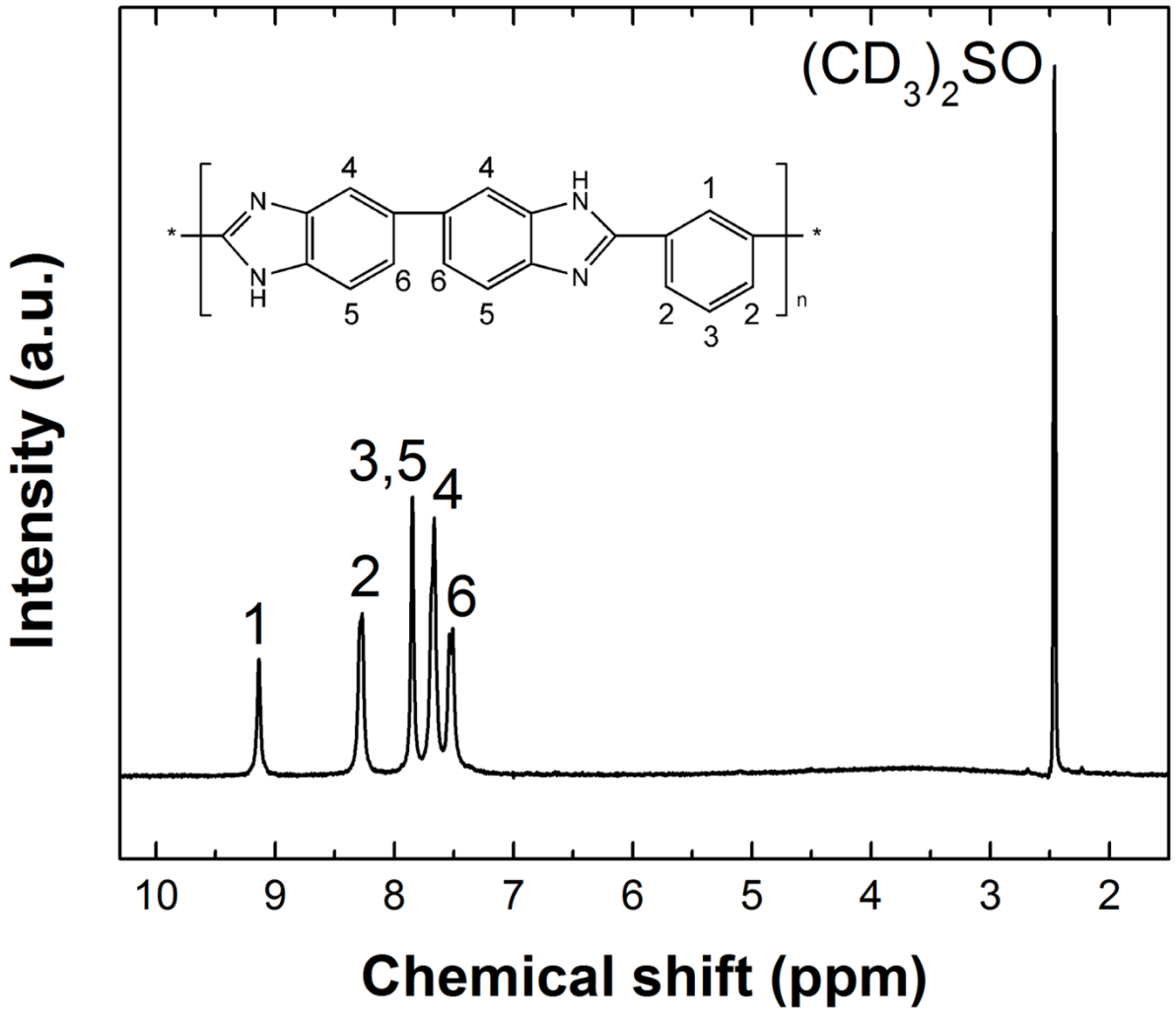

Figure 7-3. ^{1}H NMR spectrum of synthesized PBI.

Digital images of the bare and porous PBI membranes are provided in **Figure 7-4a**. As seen from left to right, the transparency of the PBI membrane reduces with an increase in porosity, where the 70-pPBI appeared as an opaque film. **Figure 7-4b** shows the FT-IR spectra of the developed PBI membrane, which was consistent to a previous report by Musto *et al*. [266, 292]. In this figure, the typical absorption peaks ascribed to the PBI membrane

were observed at 705 cm^{-1} (heterocyclic-ring vibration), 802 cm^{-1} (heterocyclic-ring vibration or C-H out-of-plane bending), 1284 cm^{-1} (imidazole ring breathing), 1444 cm^{-1} (in-plane ring vibration of phenyl benzimidazole), 1592 cm^{-1} (ring vibration of conjugation between benzene and imidazole rings), 1629 cm^{-1} (C=C/C=N stretching), and 3193 cm^{-1} (self-associated N–H stretching). **Figure 7-4c-e** compares the FT-IR spectra of all porous PBI membranes to the bare PBI and those containing the porogen, i.e., DBP. All of the porous PBI membranes exhibited the characteristic absorption peaks of bare PBI in **Figure 7-4b**, implying that the introduction of pores into the PBI membrane has not affected its compositional structure. The characteristic absorption peaks at around 1125 cm^{-1} and 1716 cm^{-1} appeared from the carboxylic stretching vibration of O–C–O and C=O bonds in DBP, respectively. The two peaks around 2873 cm^{-1} and 2959 cm^{-1} are assigned to stretching vibrations of CH_3, CH_2, and CH groups in the dibutyl chains of DBP. The disappearance of these four peaks in all KOH-doped porous PBI membranes indicated that DBP was completely extracted from the membranes and a porous structure was formed into the PBI membranes successfully.

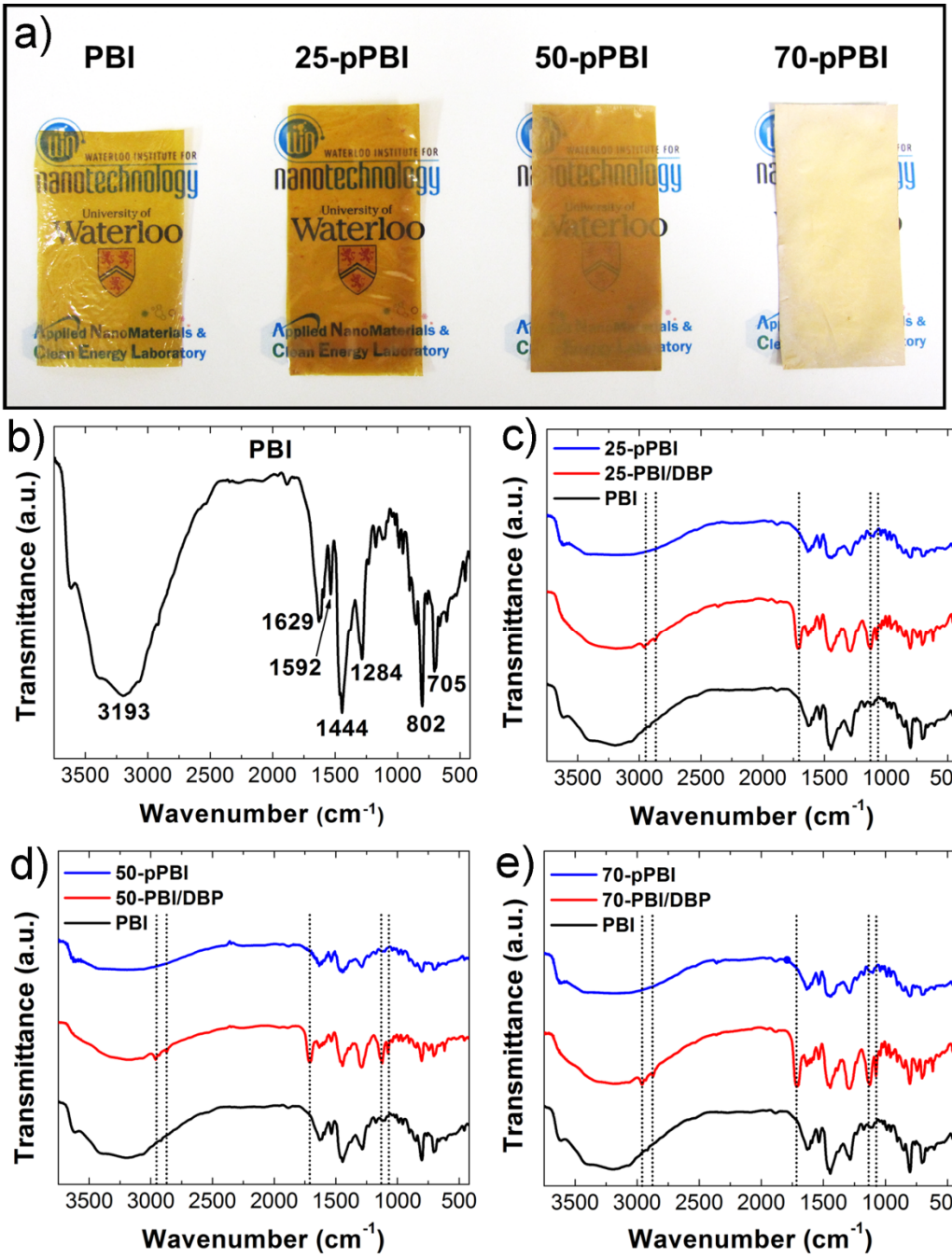

Figure 7-4. a) Digital images of all bare and porous PBI membranes. The FT-IR spectra of KOH-doped b) bare PBI, c) 25 wt.%, d) 50 wt.%, and e) 70 wt.% porous PBIs, compared to the spectra of bare and PBI/DBP membranes.

The cross-sectional images from SEM and EDX mapping of oxygen for the bare and porous PBI membranes with various porosities are shown in **Figure 7-5**. In **Figure 7-5a,c,e,g** the effect of the porogen amount on the morphology of the membranes was studied. The bare PBI possesses no pores; whereas the open pores could be observed in all of the porous membranes. The average pore size was measured using various cross-sectional, top-side, and bottom-side SEM images from different surfaces of the porous membranes. It is seen that higher amount of DBP led to larger pore size after its removal from the membrane such that at the porosity level of 25 wt.%, 50 wt.%, and 70 wt.% the pore size on average was about 253 nm, 300 nm, and 467 nm, respectively. **Figure 7-5b,d,f,h** illustrate the EDX mappings of oxygen. For all samples the EDX mapping was done with 10 frames and the exposed time for each frame was 30 seconds. Thus, all PBI membranes have had the same exposed time. It is clearly seen that the density of oxygen from KOH increases with increasing the porosity from 0 wt.% to 70 wt.% in the PBI membranes.

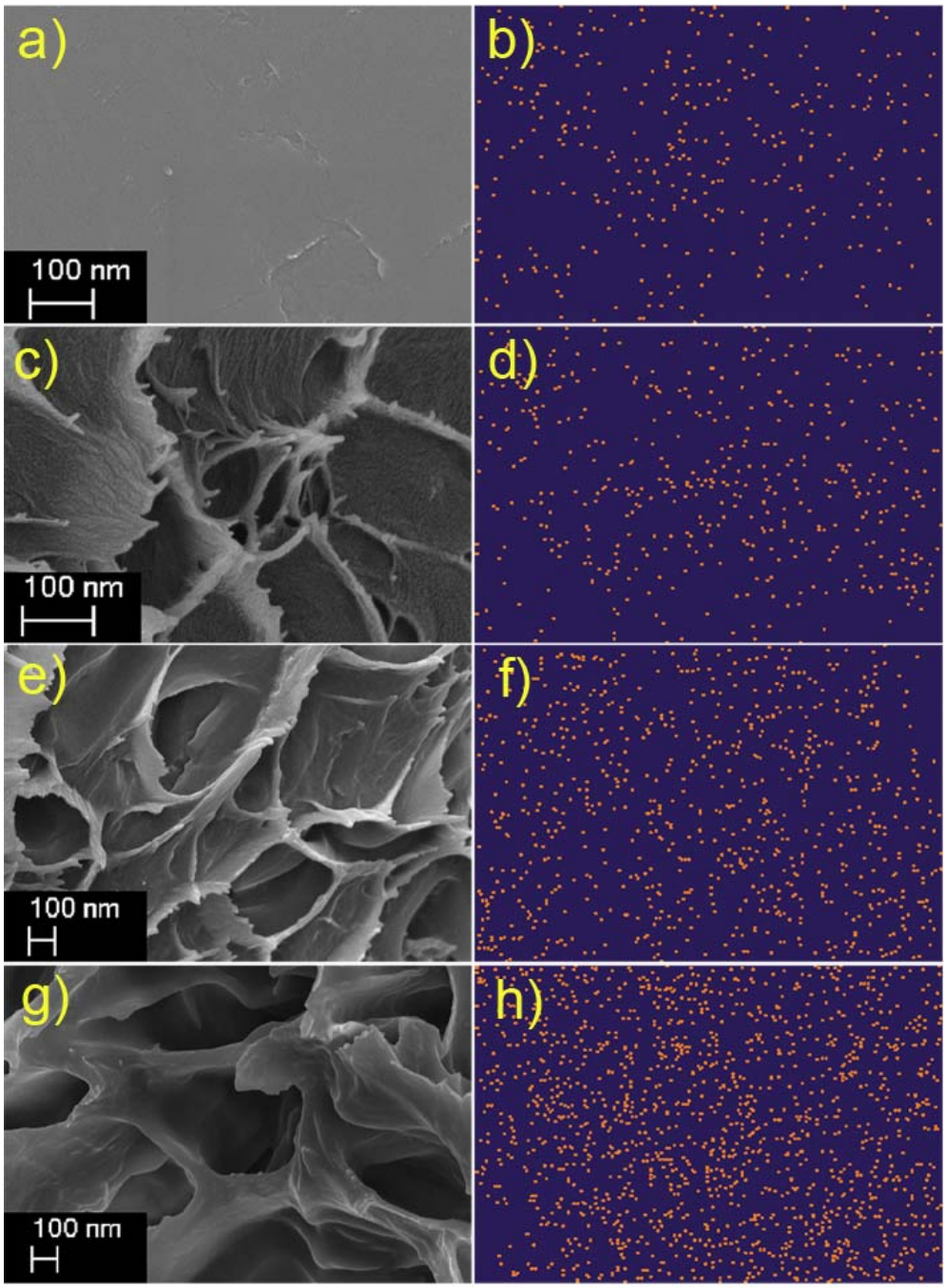

Figure 7-5. The cross-sectional images from SEM of a) bare PBI c) 25 wt.%, e) 50 wt.%, and g) 70 wt.% porous PBI membranes. The EDX mapping of oxygen element from KOH in b) bare PBI d) 25 wt.%, f) 50 wt.%, and h) 70 wt.% porous PBIs.

Figure 7-6a compares the TGA and DTA of the dry KOH-doped porous PBIs to that of the bare one. Generally, the increase of porosity has a slight effect on the thermal stability of the membrane. According to TGA-DTA curves, the initial weight loss below 200 °C can be attributed to the loss of unvaporized-bound water in PBI membranes, which changed from 2% to 5% by increasing the porosity from 0 wt.% to 70 wt.%. This indicated that because of the higher water affinity of porous PBI, more unvaporized-bound water existed in the membranes with higher porosity. From 200 °C to 500 °C the trend of weight change was almost close to a flat phase. The degradation temperature was started after 500 °C for all PBI membranes. Based on TGA-DTA curves, the increase of porosity from 0 wt.% to 70 wt.% caused the final weight loss to increase from 12 % to 20 % at 800 °C. In general, all porous PBI membranes exhibited excellent thermal stability.

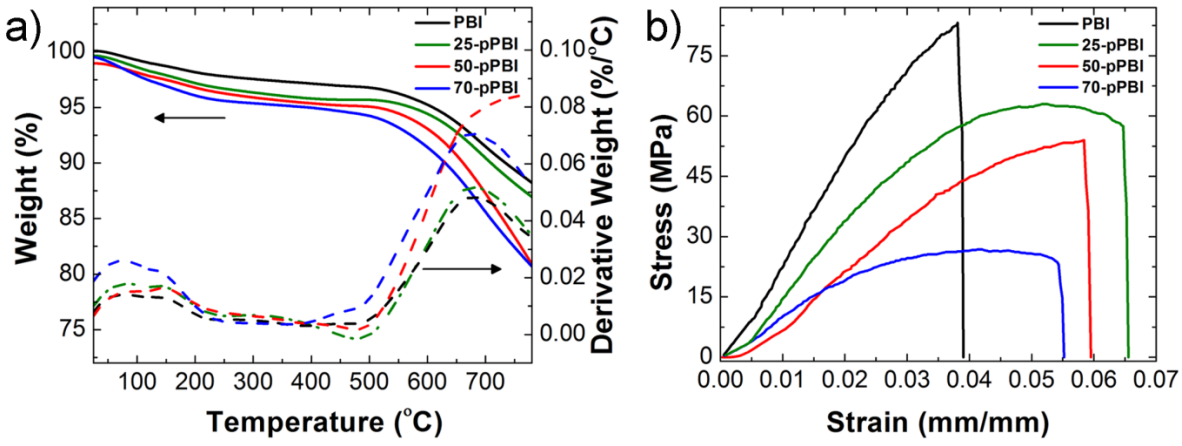

Figure 7-6. The TGA and DTA and b) The stress-strain curves of bare and porous PBIs.

The stress-strain curves and the mechanical properties of all bare and porous KOH-doped PBI membranes are displayed in **Figure 7-6b** and **Table 7-1**, respectively. The stress-strain curve of PBI membrane obeys the linear proportionality, whereas porous PBI films follow nonlinear trends, intensified by increasing the porosity, which could be attributed to the larger plasticity in the membrane. The plasticizing effect by increasing the porosity was further approved when the increase of porosity from 0 to 70 wt. % reduced the tensile strength and Young's modulus of the PBI membranes ca. 68 % and 45 %, respectively. The elongation at break didn't follow any regular ascending or descending trend with the introduction of porous structures. For instance, it was observed that the bare PBI exhibited the lowest elongation of 3.9 %, while the 25-pPBI had the highest elongation of 6.56 %. Generally, KOH-doped porous PBI membranes showed satisfactory mechanical properties to be used in alkaline electrochemical energy devices.

Table 7-1. The mechanical properties of PBI membranes.

Sample	Tensile Strength (MPa)	Young's Modulus (GPa)	Elongation at break (%)
PBI	84.29	1.88	3.90
25-pPBI	62.96	1.60	6.56
50-pPBI	54.44	1.16	5.96
70-pPBI	26.79	1.04	5.53

Table 7-2 represents the real porosity from two different methods, KOH uptake, water uptake, and swelling ratio of all PBI samples doped with KOH. According to both two different methods of calculations of real porosity, it can be concluded that the DBP porogen has been completely extracted from the PBI membrane. The results show that by increasing

the porosity from 0 to 70 wt.%, the KOH uptake and water uptake were increased about 60% and 53%, respectively. However, the enhancement of KOH and water affinity with the introduction of a porous structure has caused larger lengthwise and crosswise swelling ratios.

Table 7-2. Properties of KOH-doped porous PBI membranes.

Initial DBP [a] (wt.%)	ε_1 [b] (%)	ε_2 [c] (%)	KOH-U [d] (%)	W-U [e] (%)	L-SWR [f] (%)	C-SWR [g] (%)
0	0	0	23.38	28.8	5.56	5.89
25	22.03	20.54	43.89	46.11	20	9.68
50	48.19	49.07	54.18	56.03	23.08	10.53
70	69.03	68.62	57.90	60.82	24.15	13.33

[a] Based on $W_{DBP}/(W_{DBP}+ W_{PBI})$, where W_{DBP} and W_{PBI} are the weights of DBP and PBI, respectively. [b] Eq. (1). [c] Eq. (2). [d] Eq. (3). [e] Eq. (4). [f] Eq. (5). [g] Eq. (6).

To determine the changes in hydrophilicity, the water contact angle on the surface of all PBI membranes was measured, illustrated in **Figure 7-7a-e**. Digital images of water drops show that the increase of porosity has decreased the water contact angle, implying the increase of hydrophilicity of porous membranes. According to **Figure 7-7e** both left and right contact angles for all specimens were equal, decreasing from 62.7° to 54.2° by increasing the porosity from 0 to 70 wt.% of PBI.

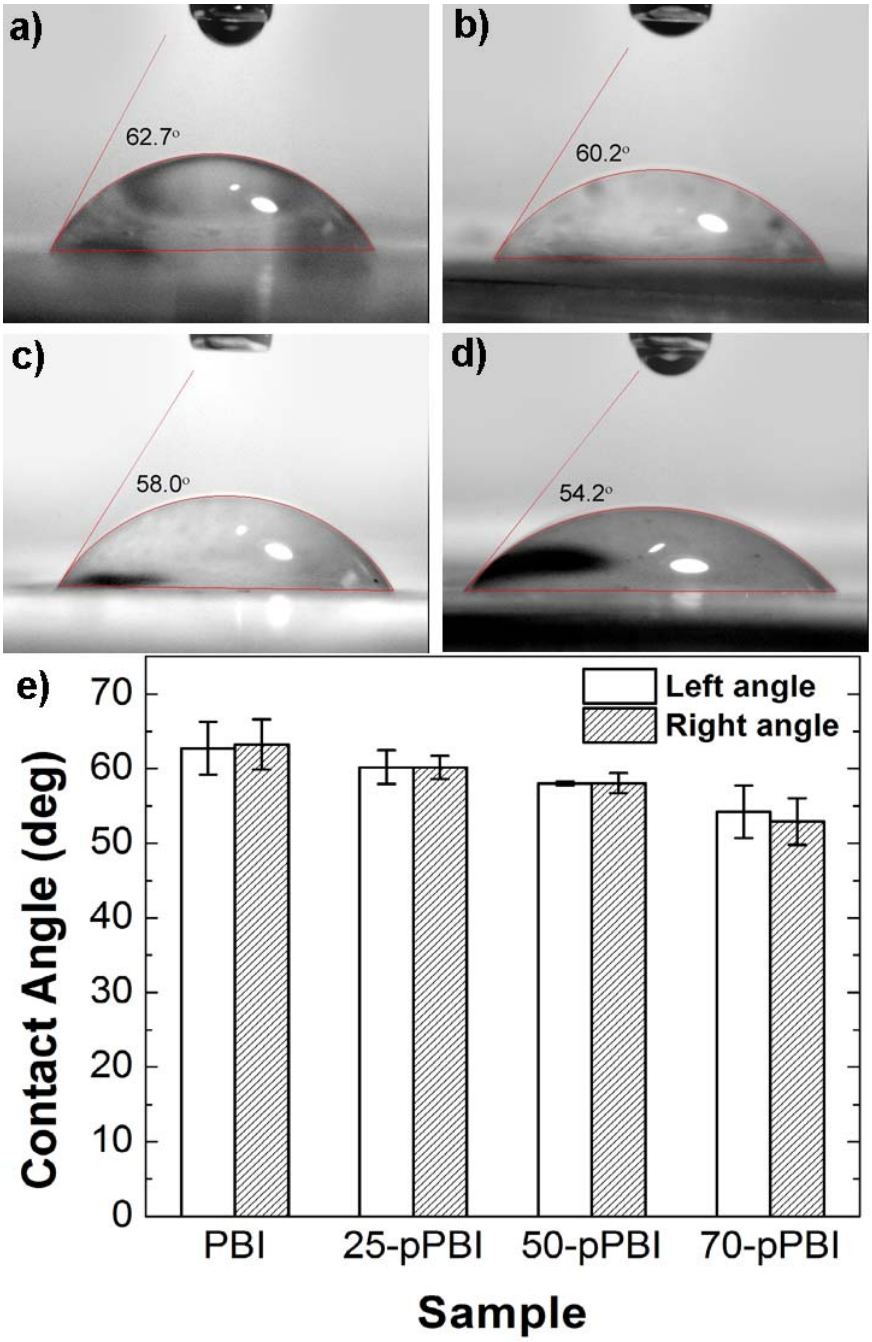

Figure 7-7. Digital images of water contact angle on the surface of a) bare, b) 25 wt.%, c) 50 wt.%, and d) 70 wt.% porous PBI membranes. e) The contact angle changes versus porosity.

Figure 7-8a-b illustrates the ionic conductivity of all the membranes under hydrous conditions at different temperatures and levels of porosity within the plane of sample (in-plane direction, IP) or through the thickness of them (through-plane, TP). The results are compared to the commercial FAA membrane. Fumapem® FAA from FuMA-Tech GmbH (35–40 μm thickness, resistivity of 0.59 $\Omega \cdot cm^2$ at 20 °C, IEC of 1.2 $mmol \cdot g^{-1}$) is an AEM made of aminated polyarylene (polysulfone) chloride, hydroxide and carbonate salts. The "FAA" is just the name of the membrane, coined by the producer (i.e., FuMA-Tech GmbH). In comparison to commercial FAA membrane, all bare and porous KOH-doped PBIs have exhibited higher ionic conductivity at all temperatures. At room temperature, the in-plane ionic conductivity has increased from 1.5×10^{-2} $S \cdot cm^{-1}$, obtained for the bare PBI, to 4.9×10^{-2} $S \cdot cm^{-1}$, measured for the KOH-doped 70 wt.% porous PBI. The maximum in-plane ionic conductivity was 1×10^{-1} $S \cdot cm^{-1}$ at 65 °C for 70 wt.% porous PBI, which was 2.9 times higher than that of commercial FAA. Generally, for both through-plane and in-plane directions it was observed that the highest ionic conductivity was at 65 °C for all types of PBI membranes, indicating high ion mobility at elevated temperature. It is clear that the increase of porosity introduction into the PBI has led to the larger absorption of concentrated KOH solution, resulting in higher water uptake and thus, superior ionic conductivity. The degree of anisotropy, expressed as the ratio of the in-plane to the through-plane conductivity (σ_{IP}/σ_{TP}), is presented in **Table 7-3**. All samples demonstrate a small degree of anisotropy in the through-plane direction. This behavior can be attributed to the anisotropic distribution of pore voids. However, on average it was observed that the degree of anisotropy was decreased

by increasing the porosity in PBI membranes. This is consistent with cross-sectional SEM images in **Figure 7-5**, where the increase of porosity favored the formation of more uniform and interconnected pores, and thus less anisotropic distribution of voids were occurred. Moreover, to examine the possibility of KOH leakage during ion-conductivity tests, the pH of water before and after immersion was measured. No change in pH of the water before and after immersion was observed, indicating that the leakage of KOH did not occur. This behavior could be explained by the fact that possibly KOH molecules are trapped in the pores because of possible anchor of KOH within the backbone of PBI by weak chemical bonds. According to Hou *et al.* [271] two possible chemical bondings can be presumed between PBI and KOH: one is the interaction between K^+ and –NH– in PBI chains due to neutralization between H in –NH– and OH^- in the medium; the other is the hydrogen bond between OH^- and –N= in the backbone of PBI, with K^+ as counter ion which might prevents the leakage of KOH from the matrix of porous PBI membranes.

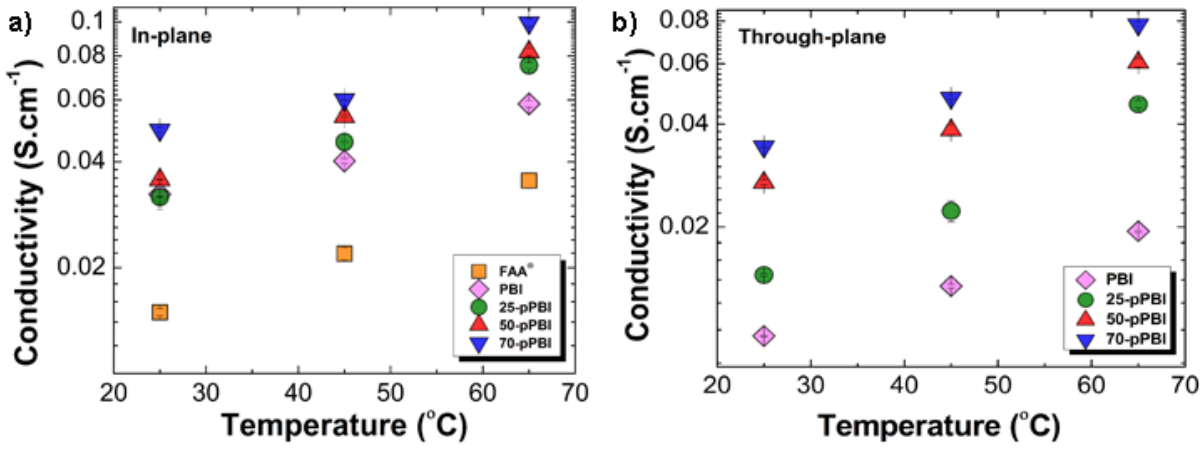

Figure 7-8. The ionic-conductivity of bare and porous PBIs, compared to the commercial FAA membrane in different temperatures at a) in-plane and b) through-plane directions.

Table 7-3. The degree of anisotropy of non-porous and porous PBI membranes.

Temperature (°C)	PBI	25-pPBI	50-pPBI	70-pPBI
25	1.56	2.19	1.32	1.44
45	1.63	2.05	1.40	1.26
65	1.82	1.65	1.36	1.27

Figure 7-9a shows the image of commercial FAA and 70 wt.% porous PBI membranes after being treated in a boiling 6 M KOH. It is observed that the commercial FAA has degraded after just 3 h, whereas 70-pPBI membrane is still unaltered. In **Figure 7-9b-d** the electrochemical stability of the pristine and all porous PBIs was compared to commercial FAA membrane. For commercial FAA, the membrane degradation resulted in a dramatic decrease in in-plane ionic conductivity at all temperatures. It is observed that for all PBI membranes, the in-plane ionic conductivity was first increased after the treatment in boiling 6 M KOH, indicating that prolonging the boiling and immersion time has resulted in higher absorption of KOH into the membrane, caused the improvement of ionic conductivity. However, after 24 h, the ionic conductivity of all specimens decreased slightly, but was maintained for 14 days.

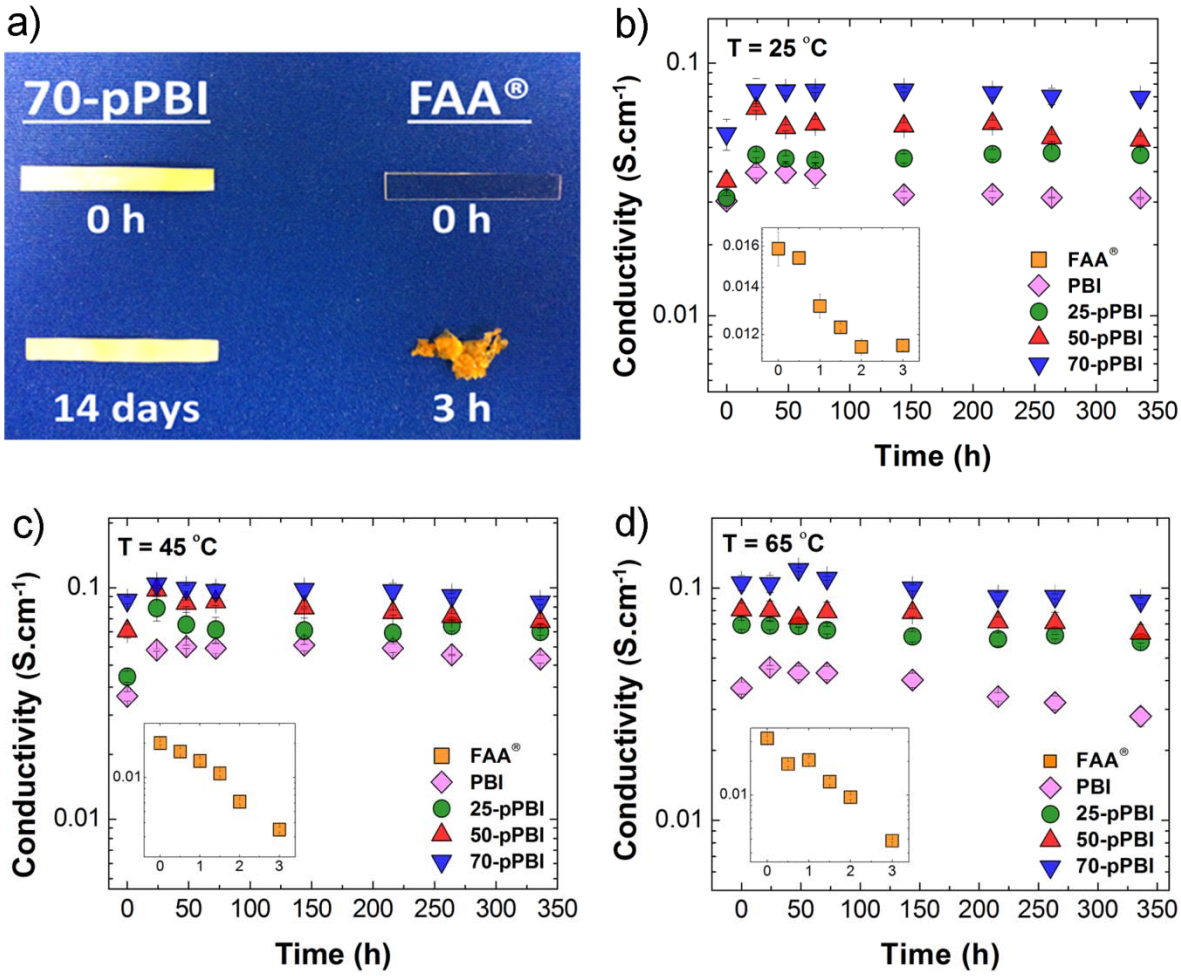

Figure 7-9.) The images of 70-pPBI and the commercial FAA after being treated in a boiling 6 M KOH solution for 14 days and 3 h, respectively. The changes of ionic conductivity at b) 25 °C, c) 45 °C, and d) 65 °C after testing the alkaline stability of all PBI membranes and the commercial FAA.

Figure 7-10 displays the polarization and power density plot of KOH-doped bare and 70-pPBI membranes in fully humidified H_2/O_2 MEA single-cell system, operating at 60 °C. In addition, the MEA performance of PBI membranes were compared to that with FAA

commercial, operated at same conditions. The peak power density for 70-pPBI was about 72.17 $mW.cm^{-2}$, 1.8 and 1.5 times higher than that of bare PBI (41.26 $mW.cm^{-2}$) and FAA commercial (45.36 $mW.cm^{-2}$), respectively. These results are in direct agreement with the membrane ionic conductivity analysis, as 70-pPBI displayed a substantial performance increase through MEA testing compared with FAA commercial under typical AEMFC conditions. Likewise, through determining the slope of ohmic region, the calculated ohmic resistance of FAA, PBI, and 70-pPBI was 4.94, 5.13, and 1.77 $\Omega \cdot cm^2$, respectively, indicating the fact that the porous morphology has favored higher ion transport through the membrane resulting in the reduction of ohmic losses comparing to FAA and bare PBI membranes. Clearly, KOH-doped porous membranes offer significant promise as electrolytic membranes for AEMFC applications, owing to their beneficial structure and electrochemical properties.

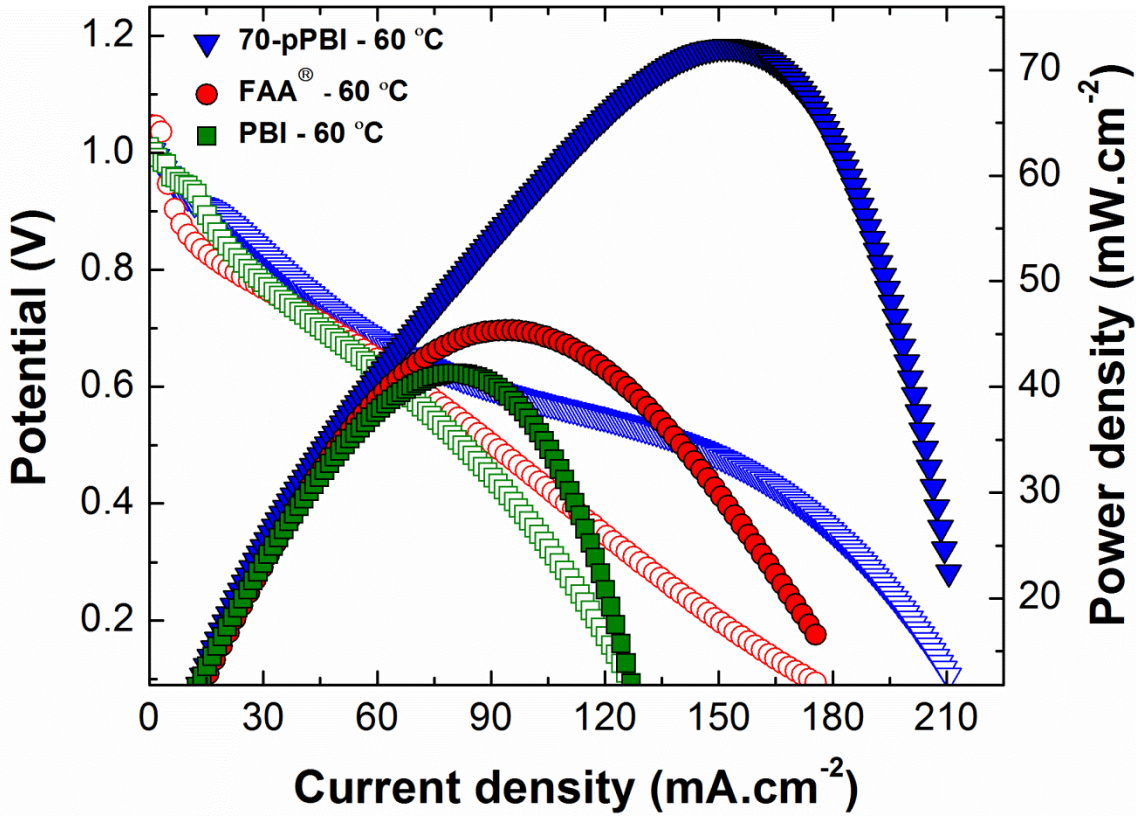

Figure 7-10. The single-cell polarization and power density curves employing FAA commercial, bare PBI, and 70-pPBI.

7.4 Conclusions

This study reports the fabrication and investigation of unique KOH-doped porous polymeric membranes for AEMFCs. The polymeric backbone of the membrane was based on PBI. The pores were introduced by leaching out a pore-forming agent, DBP after solution-casting the mixture of PBI and DBP. The introduction of a porous structure into the polymeric membrane created more open paths as well as higher surface area for ion transfer and the absorption of an electrolytic solution. The enhancement of electrolytic solution absorption

(e.g., KOH) and water uptake significantly helped the increase of ionic conductivity. It was observed that the in-plane ionic conductivity of 70-pPBI was 3 times higher than that of commercial FAA, approved by AEMFC performance results such that the MEA employing the porous PBI exhibited the highest peak power density and lower ohmic potential compared to bare PBI and FAA commercial membranes. All KOH-doped porous PBIs exhibited excellent thermal stability and satisfactory mechanical properties. The alkaline durability of all membranes was also tested in boiling KOH solutions up to 14 days and compared to the commercial FAA. All PBI films have almost maintained their ionic conductivity, while the commercial FAA degraded just after 3 h. The excellent performance and durability of KOH-doped porous PBI makes it a promising membrane material for alkaline electrochemical energy devices.

Chapter 8

Highly Anion-Conductive Graphene Oxide Nano-Composite Membrane for Alkaline Fuel Cells

Chapter 8 is based on submitted work by Zarrin et al. to ACS Nano Journal. The thesis author's specific contributions to this paper were to synthesize and fabricate the nano-composite AEM, conduct EIS measurements, run all of physicochemical characterization tests, prepare all plots and results, write the final manuscript and respond to the comments of reviewers. This work and journal paper preparation was conducted with direction from the project supervisors who are co-authors on the publication. Ms. Jing Fu aided with testing the single AEMFC performance. Mr. Gaopeng Jiang assisted in running some of physicochemical characterization tests. Ms. Skylar Yoo helped the first author to conduct EIS measurements for alkaline durability tests.

8.1 Introduction

In comparison to acidic polymer electrolyte membrane fuel cells (PEMFCs), alkaline anion exchange membrane fuel cells (AEMFCs) have attracted enormous attention by many researchers. Operating fuel cells in an alkaline medium results in (i) faster reaction kinetics, (ii) feasible use of non-noble metal catalysts, and (iii) mitigation of cell corrosion [204, 206, 207, 239-242]. However, due to the lack of high ionic conductivity and thermo-physico-chemical stability of anion exchange membrane (AEM) component, the commercialization of AEMFCs has been hindered. Thus, it is vitally required to develop a cost effective, well-designed and genuinely engineered material for AEM, possessing excellent ionic

conductivity and high durability [204, 243-246]. So far, different categories of homogeneous and heterogeneous AEMs [248, 249, 293] including (i) chemically/physically functionalized polymers [33, 73, 74, 79-81, 83, 227, 294-302], (ii) ion-solvating polymers (ISP) [71, 271, 303-306], (iii) inorganic-organic composites [31, 32, 72, 84, 225, 260, 307-313], and (iv) blended polymers [314-316] have been studied by different research groups. However, the dilemma between high ionic conductivity and physicochemical stability for AEMs is still remained as an important issue, i.e., maximizing one will minimize the other. Thus, it is highly required to develop an AEM material capable of maintaining both ion-conductivity and durability at the same time.

Among various classifications of AEMs, ISPs are believed to possess both high ion conductivity from the doped alkaline solution and good physicochemical stability from the polymeric backbone. Nonetheless, they have two critical disadvantages. First, a highly concentrated alkaline electrolyte (e.g., KOH) must be incorporated into ISPs to attain sufficient ion conductivity, causing undesirable degree of crystallinity when the relative humidity is reduced which diminishes the mechanical strength of the membrane [248]. Moreover, as KOH is in charge of conducting ions, in the humid operating conditions of AEMFCs, the generated K^+ and OH^- are greatly mobile. Consequently, the salt precipitation can occur due to the existence of CO_2 in the fed air, which damages the electrodes and reduces the ion conductivity after long-time AEMFC operations [271, 293]. Thus, it is highly demanded to upgrade the physicochemical configurations of ISPs to alleviate the aforementioned problems and maintain their desired advantages for AEMs.

The well-known polybenzimidazole (PBI) is a water-insoluble polymer applied to build the infrastructure of many acidic and alkaline ISPs [71, 250-252, 254, 255]. Containing electronegative atoms, PBIs are capable to coordinate with the cation in alkaline electrolytes. To further improve the electrolyte interaction with polymer framework, in the previous study performed by the author, Zarrin et al. [34], the porosity was introduced into the backbone of PBI membranes which provided higher surface area and efficient open paths for ions to be transferred. Formerly, in another investigation by Zarrin et al [32] it was perceived for the first time that Graphene oxide (GO) nanosheets were capable to be functionalized with stable ion-conductive groups and composed with Nafion which significantly increased the longevity of ion conductivity and PEMFC performance by 4 times in harsh operating conditions. Inspiring from the aforementioned successful studies, in this work a stable anion-conductive GO composed with porous PBI was designed and developed to improve AEMFC performance and durability. In order to induce durable anion-conductive groups on GO surface, dimethyloctadecyl [3-(trimethoxysilyl) propyl] ammonium chloride (DMAOP) is selected as the precursor which is an alkoxysilane having quaternary ammonium (QA) groups with a linear formula of $[(CH_3O)_3Si(CH_2)_3N(CH_3)_2(CH_2)_{17}CH_3]Cl$. The ion-conduction and the alkaline stability in the highly surface-active DMAOP is provided by quaternary ammonium groups and bulky hydrocarbon chains ($(CH_2)_{17}CH_3$) attached to ammonium cations, respectively [317-319]. As shown in **Figure 8-1**, the functionalization of GO nanosheets with QA-contained DMAOP (QAFGO) was accomplished through the coupling of trimethoxysilyl group ($(CH_3O)_3Si$) in DMAOP with oxygenated functional groups on GO. Then, the porous PBI was composed with different loadings of QAFGO,

denoted as *x*-QAFGO/pPBI in which *x* exhibited the weight percentage of QAFGO in the composite membrane. The porous PBI possesses a high surface area enabling the exfoliated QAFGO nanosheets to pass through the macropores and have effective interactions with the polymeric matrix. The morphology, elemental structure, and thermal stability of QAFGO and *x*-QAFGO/pPBI membranes were thoroughly characterized using different spectroscopic and microscopic methods, including, scanning electron microscopy (SEM), energy-dispersive X-ray (EDX) mapping, X-ray diffraction (XRD), X-ray photoelectron spectrometry (XPS), Fourier transform infrared (FT-IR), and thermogravimetric analysis (TGA). The ion conductivity, alkaline stability, and AEMFC performance of QAFGO and *x*-QAFGO/pPBI membranes were measured using electrochemical impedance spectroscopy (EIS) and polarization curves which were compared to commercially available AEM (Fumapem® FAA from FuMA- Tech GmbH).

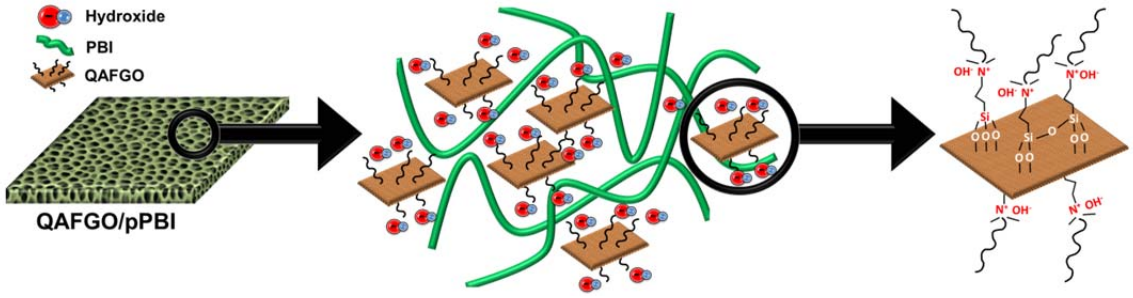

Figure 8-1. Schematic of hydroxide-conductive QAFGO/pPBI structure.

8.2 Experimental Section

8.2.1 Synthesis of GO

In this work the improved Hummers' method [320, 321] was employed for the synthesis of GO from natural graphite flakes which is the most commonly used approach at the present time. 2 g of Graphite powder was added to the mixture of 360 ml concentrated H_2SO_4 and 40 ml H_3PO_4 in a round- bottom flask. After 30 minutes stirring, 18 g $KMnO_4$ was added slowly as it was a strong oxidizing agent. The temperature of the mixture was increased to 50 °C, and the oxidative reaction of graphite last for 16 h. Afterwards, the solution was cooled down and 400 ml distilled deionized (DDI) water and then 20 mL H_2O_2 were added to it dropwise and stirred for 30 min to remove all impurities. In order to collect the produced GO nanosheets, the final mixture was washed and centrifuged with DDI, HCl, and ethanol, respectively. Finally, the GO was freeze-dried.

8.2.2 Functionalization of QAFGO

In order to alkali-functionalize GO nanosheets (QAFGO) with quaternary ammonium groups the DMAOP precursor was adopted. First, 0.1 g of GO fluffy powder was dispersed and exfoliated in 50 ml toluene by 2 h sonication to obtain a stable GO suspension. After adding 10 g DMAOP to GO, the reaction was carried out at room temperature for 2 days. Then, the product was centrifuged and washed several times with ethanol to remove the toluene and unreacted traces of DMAOP. The chlorine (Cl^-) counter ion in obtained QAFGO was exchanged with hydroxide (OH^-) by adding 1M KOH to it overnight. Finally, the product was washed and centrifuged several times with DDI water and then froze dried.

8.2.3 Synthesis of PBI

The detailed synthesis of PBI has been explained in the previous work [34]. In summary, 4.7 mmol of 3,3'-diaminobenzidine (DAB, Aldrich) with an equivalent molar amount of isophthalic acid (IPA, Aldrich) were dissolved into polyphosphoric acid (PPA, Alfa Aesar) and reacted for 7 h at 200 °C. The dark reddish brown and viscous product was quenched by pouring it into a large amount of cold water. The formed PBI fibers were stirred and washed for 48 h in DDI water and subsequently for 7 h in 2 M KOH solution followed by drying in an oven at 100 °C overnight.

8.2.4 Casting *x*-QAFGO/pPBI Membranes

x-QAFGO/pPBI nano-composite membranes were casted by mixing *x* (=3, 5, or 10) wt. % QAFGO with an appropriate amount of PBI dissolved in DMSO. Dibutylphthalate (DBP) was added to QAFGO/PBI mixture to produce 70 wt.% porous composite film. The final uniform solution was casted on a glass plate at 60 °C for 2 days, and then gradually heat treated from 100 °C to 190 °C for 4 h in order to fully evaporate the solvent. The obtained nano-composite membranes were immersed in methanol for 1 h to extract DBP and introduce porosity. After drying at 60 °C all *x*-QAFGO/pPBI composites were treated with 6 M KOH for 1 day and finally stored in DDI water for future physicochemical and electrochemical characterization tests.

8.2.5 Thermal, Physical, and Chemical Characterization Tests

The elemental and chemical-bonding analyses of QAFGO and *x*-QAFGO/pPBI membranes were determined via XPS (Thermo Scientific Al K-Alpha X-ray source) and FT_IR (Avatar 320). The presence and distribution degree of QAFGO inside the porous PBI were shown by

cross-sectional SEM images and EDX mapping of all samples using LEO FESEM 1530. To assess the thermal stability, TGA was performed under nitrogen with a TGAQ500 V20.10 instrument in the temperature range from 25 to 900 °C at the heating rate of 10 °C min^{-1}.

In order to calculate the water uptake and swelling ratio of *x*-QAFGO/pPBI nano-composite membranes, the samples were immersed in DDI water at room temperature for 48 h. After wiping out the water from the surface, the weight and thickness of membranes were immediately measured. Then, they were dried in a vacuum oven at 60 °C until a constant weight and thickness were achieved. Finally, the water uptake (WU) and crosswise swelling ratio (C-SWR) were calculated by following equations:

$$WU\,(\%) = \frac{W_w - W_d}{W_d} \times 100 \qquad \textbf{Equation 8-1}$$

$$C - SWR(\%) = \frac{t_w - t_d}{t_d} \times 100 \qquad \textbf{Equation 8-2}$$

where W_w and t_w are the weight and thickness of hydrated *x*-QAFGO/pPBI nano-composites and W_d and t_d are the weight and thickness of dried films.

8.2.6 Ion Conductivity Measurement

Both in-plane and through-plane hydroxide conductivities of QAFGO and *x*-QAFGO/pPBI nano-composite membranes were measured using AC electrochemical impedance spectroscopy (EIS) method in Princeton Versastat MC potentiostat. For in-plane direction, the membrane samples were sandwiched in a four-probe cell, made of platinum wires and Teflon plates. For the through-plane conductivity, the membranes were pressed between two copper strips with 1 cm^2 surface area. In order to acquire the ionic resistance at different

temperatures and fully hydrated conditions, the instruments were placed in a thermo-controlled chamber with DDI water. The real impedance for all samples was calculated in the frequency range between 1 MHz and 10 Hz with perturbation voltage amplitude of 10 mV. At a given temperature, the measurements were repeated at least four times with 10 min interval. The in-plane and through-plane hydroxide conductivities were then determined using Eq. (3):

$$\sigma = \frac{L}{RA}$$ **Equation 8-3**

where σ denotes either the in-plane (σ_{IP}) or through-plane (σ_{TP}) ionic conductivity, L is either the distance between the reference electrodes in the four-point cell or the thickness of membrane samples in case of through-plane setup, R the resistance of the membrane, and A the cross-sectional area in case of the in-plane setup and the area of the electrodes in case of the through-plane cell.

8.2.7 Alkaline Electrochemical Durability Test

In order to evaluate the alkaline electrochemical stability, all *x*-QAFGO/pPBI nano-composite membranes were held in a boiling solution of 6 M KOH. After different certain times, each sample was rinsed and stored in DDI water before re-measuring the hydroxide-conductivity stability.

8.2.8 MEA Preparation for AEMFC

The performance of 10-QAFGO/pPBI, pPBI, and FAA commercial in a fuel cell setup was determined using a single cell membrane electrode assembly (MEA) setup. The anode and

cathode catalyst layers were prepared by mixing and ultrasonicating appropriate amounts of Pt/C (45.7 wt.% Pt, TKK Corp.), AS-4 ionomer from Tokuyama Corp., and isopropanol as the solvent. The inks were sprayed on gas diffusion layers (GDL, SIGRACET® GDL10 BB) and then dried at room temperature overnight until the desired catalyst loading of 0.3 mg cm^{-2} was achieved for both anode and cathode. The MEA with an active electrode area of 5 cm^2 was obtained by pressing the catalyst-coated GDLs onto the membrane at room temperature with 3 metric tons loading for 3 min. For each sample, the MEA was assembled into the fuel cell hardware (850e Multi-Range Fuel Cell Test System, Scribner Associates) with gas flow rate of 0.2 L min^{-1} and back pressure of 6 psi for both hydrogen and oxygen.

8.3 Results and Discussion

The image of flexible 3-QAFGO-pPBI nano-composite membrane is illustrated in **Figure 8-2a**. Likewise, in all *x*-QAFGO-pPBI membranes, the QAFGO was uniformly dispersed and intercalated into pPBI backbone. In order to determine how QAFGO nanosheets were exfoliated and dispersed in pPBI, the XRD of GO, QAFGO, and *x*-QAFGO/pPBI membranes were studied in **Figure 8-2b**. The sharp and narrow diffraction-peak of GO appeared at 2θ=10.15°, exhibited a d-spacing of 8.7 Å [322-324]. When GO was functionalized with bulky QA groups, a much broader peak was observed at 2θ=10.70° and 2θ=20°. This indicated that DMAOP was successfully bonded to GO which expanded the distance of the nanosheets and generated defects on GO surface. The new broad peak 2θ=20° in QAFGO also revealed that the functionalized nanosheets had less tendency towards stacking and more free layers of QAFGO were produced [325]. After different loadings of QAFGO were incorporated into the matrix of pPBI, the XRD patterns of *x*-QAFGO/pPBI

membranes displayed same diffraction peaks at about 2θ=25.5°. The highly broad peak of *x*-QAFGO/pPBIs disclosed their amorphous structure. Moreover, the disappearance of the characteristic diffraction-peak of GO plainly explained the complete exfoliation and intercalation of QAFGO into pPBI backbone [326, 327].

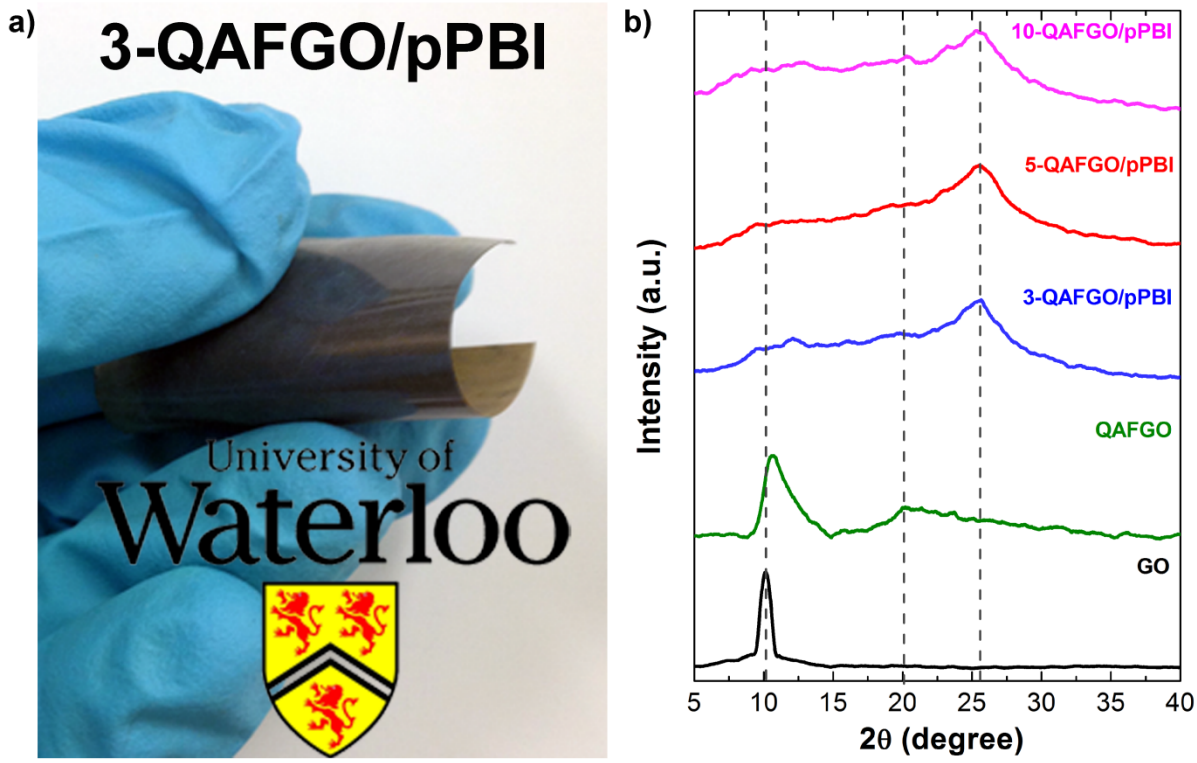

Figure 8-2. a) The image of 3-QAFGO/pPBI membrane. b) XRD patterns of GO, QAFGO, and *x*-QAFGO/pPBI membranes.

To confirm the successful alkaline functionalization of GO, FT-IR spectra of GO and QAFGO were compared in **Figure 8-3a**. In GO spectrum, the assigned peaks to epoxy (C-O), carbon-hydroxyl (C-OH), sp2 carbon (C=C), carbonyl (C=O), and free hydroxyl (OH) at 1053.96 cm^{-1}, 1411.74 cm^{-1}, 1627.71 cm^{-1}, 1741.49 cm^{-1}, and 3416.45 cm^{-1} were in

agreement with literature, respectively [32, 189, 326, 328-330]. In QAFGO spectrum, it was observed that the broad peak of epoxy at 1053.96 cm^{-1} in GO disappeared and alternatively, a new small peak emerged at 1233.32 cm^{-1} attributing to carbon-siloxane (C-O-Si) bond [331, 332]. This revealed that epoxy groups are clearly capable to react with trimethoxysilyl in DMAOP. Besides, two appeared small peaks at 2852.34 cm^{-1} and 2924.66 cm^{-1} are due to methyl and long chains of methylene groups in DMAOP [331, 332], supporting the effective reaction between DMAOP and GO.

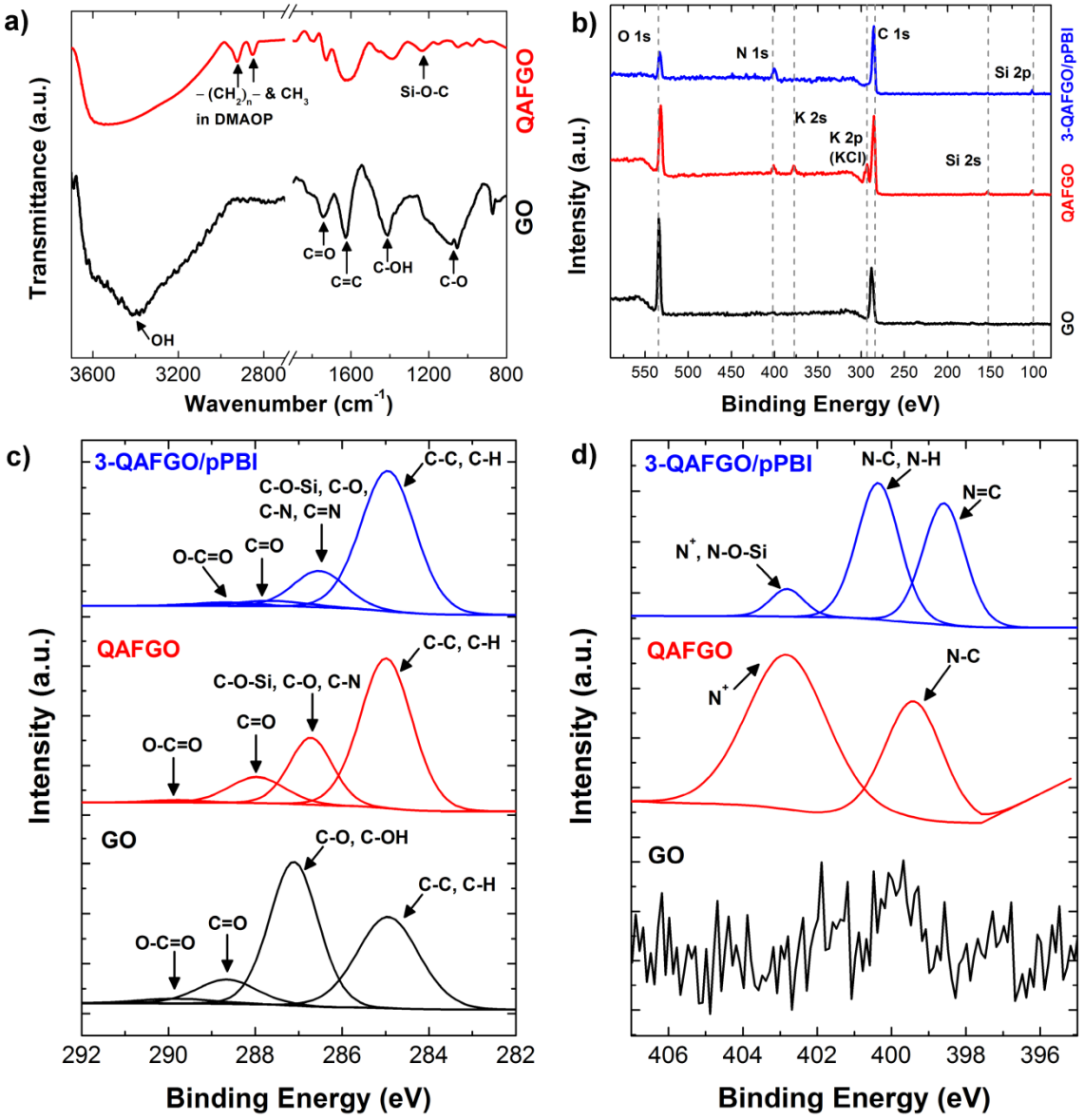

Figure 8-3. a) FT-IR spectra, b) wide region XPS spectra, c) deconvoluted XPS spectra in the C 1s region, and d) deconvoluted XPS spectra in the N 1s region of GO, QAFGO, and 3-QAFGO/pPBI membrane.

To supplementally approve the FT-IR results, the XPS analysis was carried out to thoroughly study the interactions between DMAOP and GO as well as QAFGO and pPBI. In the the wide-range XPS patterns displayed in **Figure 8-3b**, two new peaks other than C 1s and O 1s were observed for QAFGO and 3-QAFGO/pPBI at binding energies of 102.08 and 401.08 eV, attributed to Si 2p and N 1s components, respectively. This confirmed the successful coupling of QA-containing precursor (DMAOP) onto the surface of the GO nanosheets and QAFGO with pPBI. Comprehensive chemical-bonding analysis was carried out through deconvoluted XPS of C 1s (**Figure 8-3c**) and N 1s (**Figure 8-3d**) for GO, QAFGO, and 3-QAFGO/pPBI. The exhibited C 1s spectrum of GO were in compliance with many authorized references [32, 185, 189, 321, 326, 328, 330, 331, 333, 334] . According to C 1s spectra of QAFGO and 3-QAFGO/pPBI in **Figure 8-3c**, the peaks of oxygenated carbon groups in GO have shifted to lower binding energies, indicating a change in the degree of surface oxidation after DMAOP functionalization and pPBI composition. Compared to GO, it was seen that the peak intensity at 286.68 eV was significantly decreased in QAFGO and 3-QAFGO/pPBI composite, assigned to the higher reactivity of epoxy groups with trimethoxysilyl in DMAOP which is in accord with FT-IR results. In addition to carbon-siloxane bonds, the broad peak at 286.68 eV represents the carbon-ammonium in DMAOP and carbon-nitrogen peaks in 3-QAFGO/pPBI. Furthermore, the peak intensity increase of C-C/C-H bonds at 284.98 eV evidently demonstrated the existence of octadecyl and propyl chains coming from DMAOP in QAFGO as well as sp2 and sp3 hybrid orbitals in pPBI [185, 189, 326, 328, 330, 331, 334]. To further analyze the type of carbon-nitrogen bonds, the N 1s spectra of QAFGO and 3-QAFGO/pPBI in **Figure 8-3d** were studied. The displayed peaks at

399.38 eV and 402.88 eV were assigned to quaternary ammonium and ammonium cations in QAFGO, respectively. When composed with pPBI, the pyridinic N=C and pyrrolic N-C/N-H bonds were appeared at 398.58 eV and 400.38 eV, respectively, due to the existence of imidazole groups. At higher energy bond of 402.78 eV a small broad peak was seen which could be attributed to both ammonium cation in QAFGO and pyridinic nitrogen-siloxane bond in 3-QAFGO/pPBI [330, 335-337]. The latter might signify that some of the existent siloxane groups in QAFGO were bonded to pyridinic nitrogen of imidazole in pPBI. Such interactions can increase the chemical stability of *x*-QAFGO/pPBI composite membranes to a greater extent.

To investigate the morphology and elemental distribution, the cross-sectional SEM images and oxygen EDX mapping of *x*-QAFGO/pPBI membranes are exhibited in **Figure 8-4**. In **Figure 8-4a**, **c**, and **e** by increasing the loading of QAFGO, i.e., 3 wt.% to 10 wt.%, more exfoliated layers of QAFGO can be seen on the porous PBI. **Figure 8-4b**, **d**, and **f** illustrate the oxygen EDX mappings of *x*-QAFGO/pPBI samples which were taken after 20 frames with an exposed time of 30 s for each. The increase of QAFGO composition has resulted in more dense oxygen distribution on porous PBI, specifying more available ion-conductive sites in 10-QAFGO/pPBI.

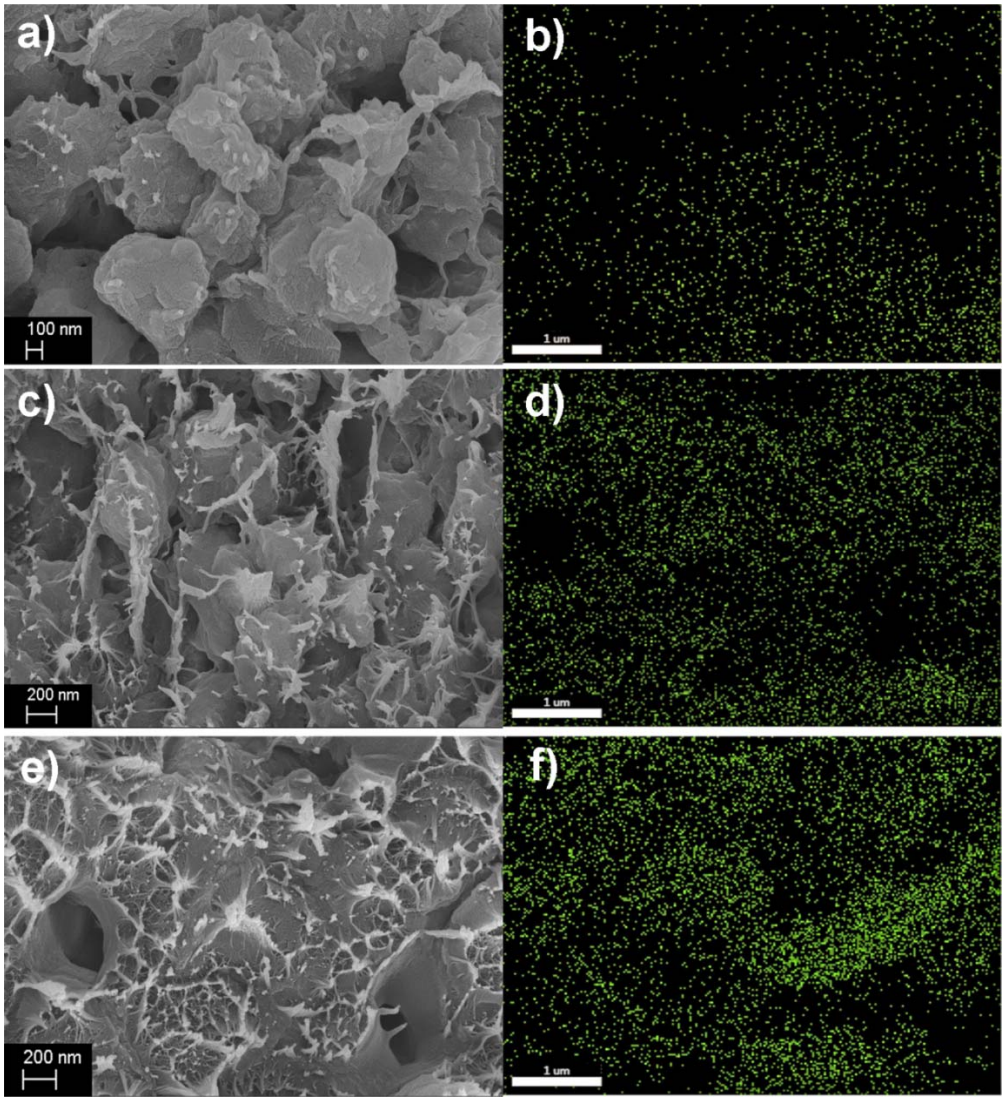

Figure 8-4. The cross-sectional images from SEM of a) 3-QAFGO/pPBI, c) 5-QAFGO/pPBI, and g) 10-QAFGO-pPBI membranes. The EDX mapping of oxygen element in b) 3-QAFGO/pPBI, d) 5-QAFGO/pPBI, and f) 10-QAFGO-pPBIs.

Figure 8-5a represents the water uptake and cross-wise swelling ratio of all *x*-QAFGO/pPBI membranes. The results showed that increasing the loading of QAFGO to 3

wt.% and 5 wt.% resulted in less water uptake compared to bare porous PBI. This could be due to the blockage of pores by QAFGO resulting in smaller water uptake due to less available ion-exchange sites. When the QAFGO composition was increased to 10 wt.% higher water uptake of 63.79% was achieved, indicating that higher loading of QAFGO enabled more accessible ion-exchange areas and thus, higher amount of water could be absorbed by the composite membrane. Among the nano-composite membranes the highest C-SWR of 11.46% was gained for 10-QAFGO/pPBI which was less than that of 13.33% for bare pPBI and higher than that of 3.51% and 9,7% for 3-QAFGO/pPBI and 5-QAFGO/pPBI, respectively. This demonstrated that the addition of QAFGO nano-filler has enhanced the mechanical properties of porous PBI by decreasing the membranes swelling.

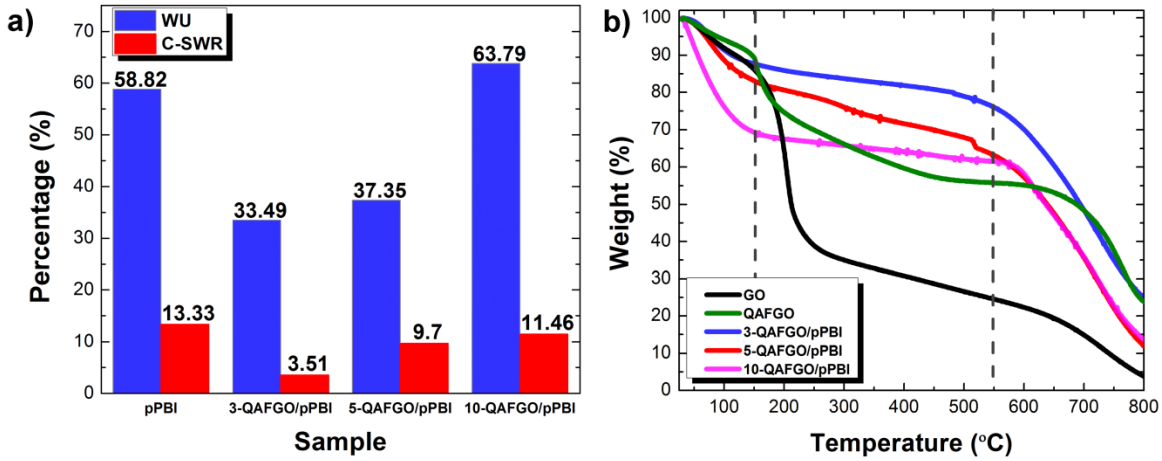

Figure 8-5. The water uptake and cross-wise swelling ratio of bare pPBI and x-QAFGO/pPBI composites. b) The TGA curves of GO, QAFGO, and x-QAFGO/pPBI membranes under nitrogen with 10 °C min-1 heating rate.

TGA was utilized to probe the influence of QAFGO on the thermal stability of composite pPBI membranes under nitrogen. The results are displayed in **Figure 8-5b**. Before running

the tests the samples were maintained at room temperature and 30% RH in a humidity chamber for 1 h. Compared to GO, the QAFGO exhibited remarkably higher thermal stability. The notable GO weight loss of 50 % from 150 °C to 250 °C was attributed to the decomposition of the oxygen-containing functional groups [338, 339]. Through the alkalization of GO with bulky organosiloxane precursor, the thermal stability of functional groups significantly increased from 150 °C to 700 °C with a weight loss of 38 %. The weight loss before 150 °C was assigned to the removal of unvaporized bound-water molecules, absorbed by all samples. It was seen that the increase of QAFGO loading in composite pPBIs has substantially improved the water retention since the water weight loss of 10-QAFGO/pPBI and 3-QAFGO/pPBI was approximately 30 % and 12 %, respectively. Considering the decomposition temperature of nano-composite pPBI membranes, 3-QAFGO/pPBI and 5-QAFGO/pPBI started to degrade at about 550 °C whereas 10-QAFGO/pPBI decomposition temperature was shifted to 600 °C. TGA results revealed the high potential of 10-QAFGO/pPBI as a stable and water-retentive AEM for alkaline fuel cells working at elevated temperatures.

Figure 8-6a-b illustrates the in-plane and through-plane ionic conductivities of *x*-QAFGO/pPBI membranes under hydrous conditions and different temperatures. The results were compared to the commercial Fumapem® FAA from FuMA-Tech GmbH (35–40 μm thickness, resistivity of 0.59 $\Omega \cdot cm^2$ at 20 °C, IEC of 1.2 $mmol \cdot g^{-1}$). In both through-plane and in-plane directions, the highest hydroxide conductivity accomplished at 65 °C for all membranes, indicating accelerated ion mobility at elevated temperatures. In **Figure 8-6a**, in comparison to commercial FAA membrane, the 3-QAFGO/pPBI exhibited smaller hydroxide

conductivity at all temperatures. However, as the loading of QAFGO increased to 5wt.% and 10 wt.% the hydroxide conductivity surpassed FAA. Such behavior was ascribed to more obtainable ion-exchange sites in nano-composite PBIs with greater amounts of QAFGO. The maximum in-plane ionic conductivity was 0.085 S cm^{-1} at 65 °C for 10-QAFGO/pPBI, which was 2.8 times higher than that of commercial FAA. In order to assess the genuine hydroxide conductivity in alkaline fuel cells, the conductivity in through-plane direction was measured. Based on the obtained results in **Figure 8-6b** the degree of anisotropy was measured, determined as the ratio of the in-plane to the through-plane conductivity. On average, for all nano-composite membranes, small degree of anisotropy of 1.55 was achieved, indicating that the interconnected pores in pPBI and uniform distribution of exfoliated QAFGO nanosheets aided faster ion-transfer through the thickness of composite membranes.

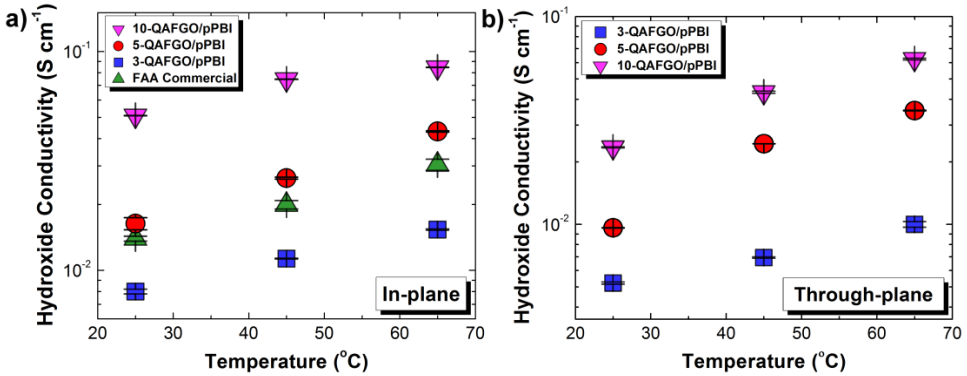

Figure 8-6. The hydroxide conductivity of x-QAFGO/pPBI membranes compared to the commercial FAA at different temperatures and hydrous conditions in a) in-plane and b) through-plane directions.

Figure 8-7a shows the alkaline electrochemical stability of all *x*-QAFGO/pPBIs compared to commercial FAA membrane. It was seen that the electrochemical stability of FAA was too

low such that after 3 h being exposed to boiling 6 M KOH, the membrane dramatically degraded. On the contrary, all *x*-QAFGO/pPBI membranes maintained their in-plane ionic conductivity for 21 days. The reduced conductivity of 3-QAFGO/pPBI, 5-QAFGO/pPBI, and 10-QAFGO/pPBI was 18 %, 11.9 %, and 10.01 %, respectively, indicating that increase of QAFGO loading in the nano-composite membrane resulted in more stable hydroxide conductivity. The relatively high alkaline-stability results were assigned to the bulky and long hydrocarbon chains attached to water-retentive ammonium groups on QAFGO nanosheets in nano-composite membranes.

In **Figure 8-7b** the single AEMFC performance of 10-QAFGO/pPBI membrane was compared to that of FAA commercial, evaluated in fully humidified H_2/O_2 system at 50 °C. The open circuit voltages (OCVs) were 1.025 V and 0.98 V for FAA and 10-QAFGO/pPBI, respectively, demonstrating that both had low hydrogen permeability. The peak power density of 86.68 mW cm^{-2} for 10-QAFGO/pPBI was about 2 times higher than that of 42.21 mW cm^{-2} for FAA commercial. The better performance was primarily attributed to the excellent hydroxide conductivity and strong water retention properties of the nano-composite membrane. In 10-QAFGO/pPBI the existing bulky quaternary ammonium groups on the large surface of exofoliated GO nanosheets provided more facile hopping of hydroxides to enhance the ionic conductivity. Clearly, alkaline-functionalized graphene oxide composed with porous PBI may be a significant potential AEM for AEMFCs due to its high hydroxide conductivity, alkaline electrochemical and thermal stability, and fuel cell performance.

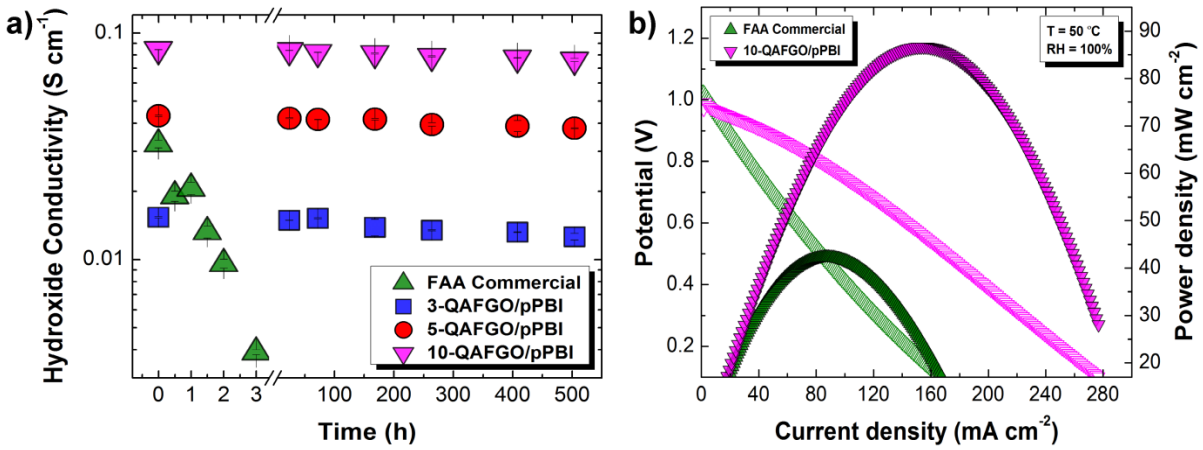

Figure 8-7. a) Alkaline electrochemical stability of FAA and x-QAFGO/pPBI membranes at 65 °C and hydrous conditions. b) The single-cell polarization and power density curves employing FAA commercial and 10-QAFGO/pPBI membranes.

8.4 Conclusions

In this work, first GO nanosheets were successfully functionalized with DMAOP containing bulky quaternary ammonium groups. The fabricated QAFGO was then incorporated into porous PBI to form an anion-conductive and stable nano-composite membrane for AEMFCs applications. The presence of bulky QA groups interacted with large surface areas of GO and pPBI significantly enhanced the hydroxide conductivity to 0.085 S cm^{-1} which was stable for 21 days whereas FAA commercial film degraded just after 3 h. The single MEA containing 10-QAFGO/pPBI revealed satisfactory fuel cell performance with a peak power density of 86.68 mW cm^{-2} when compared to FAA film. Apart from high performance, *x*-QAFGO/pPBI membranes also exhibited excellent physicochemical and thermal stability. The achieved results demonstrated that the porous PBI composites with QAFGO have the capability to be the potential AEMs for AEMFCs.

Chapter 9
Conclusions and Recommendations for Future Work

9.1 Conclusions

The main goal of this PhD work was the design and fabrication of advanced nano-engineered solid electrolyte membranes (PEMs and AEMs) for two important types of low temperature fuel cells, namely PEMFCs and AEMFCs. Concerning PEMFCs it is highly desired to operate them at temperatures higher than 80 °C to attain faster redox kinetics and better water management. However, the state of the art PEM, i.e., PFSA membrane, loses its functionality and physicochemical stability due to its poor water-retention at elevated temperatures. Thus, it is extremely required to substitute or modify PFSA membranes with the aim of maintenance and improvement of their performance at high-temperature PEMFCs. In the case of AEMFCs, in spite of extensive performed studies, no suitable AEM structure has been developed possessing both high ion-conduction and physicochemical stability in alkaline medium. Therefore, the fabrication of an AEM which can simultaneously maintain its ionic conductivity and durability is inevitable.

In this thesis, several approaches have been employed for improving the chemical structure and functionality of PEMs and AEMs to increase their ionic conductivity and operational stability in PEMFC and AEMFC systems. The first approach consisted of incorporating sulfunic-acid functionalized nano-fillers to enhance the water-retention and proton conductivity of PEMs at harsh operating conditions of PEMFCs (e.g., high temperature). The results of this approach were revealed in the first two works, elaborated in

Chapters Chapter 4 and **Chapter** 5. In the first work, a nano-composite membrane was developed, composed of sulfonic-acid functionalized titania nanotubes (F-TiO_2-NT) and commercial PFSA (i.e., Nafion^{TM}). At 120˚C and a relative humidity of 30%, the ion conductivity for the F-TiO_2-NT/Nafion nano-composite was about 5 times higher than that for Nafion [31]. The F-TiO_2-NT/Nafion composite membranes exhibited to be the potential PEM replacement for PEMFCs operating at temperatures higher than 80 °C and low relative humidity. As a result of the first work, the study of more effective and hygroscopic nano-fillers was initiated. It was discovered that the high surface area of GO nanosheets containing numerous oxygen-containing groups could be an excellent candidate for being efficiently functionalized with ion-conductive groups such as sulfunic acid. Thus, in the second work, for the first time the sulfonic-acid functionalized graphene oxide (F-GO) was composed with PFSA as the water-retentive filler. F-GO/PFSA nano-composites demonstrated a significant ion conductivity and single fuel cell performance improvement (4 times) over PFSA at the humidity of 30 % and temperature of 120 °C. F-GO incorporation into PFSA backbone clearly offered substantial PEMFC performance improvements at temperatures higher than 80 °C.[32]. The accomplished results of first approach revealed that the sulfunic-acid functionalization of either TiO_2 nanotubes or GO nanosheets have outstandingly increased the ionic-conductivity of the popular PFSA membrane in PEMFCs working at elevated temperatures and low relative humidity.

The second approach dealt with the design and fabrication of novel polymeric structures for AEMs endowed with both high ion-conduction and physicochemical stability. The outcomes of this approach were disclosed in the third and fourth works, expanded in

Chapters Chapter 6 and **Chapter** 7. In **Chapter 6**, a membrane based on polyetherketone structure, modified with quaternary ammonium hydroxide groups, has been developed for AEMFCs applications through direct chloromethylation followed by reaction with triethylamine reagent. The obtained membrane showed excellent thermal stability, satisfactory mechanical property, and good alkaline stability. However, the hydroxide conductivity of QAPEK-OH membranes was not high enough. Therefore, it was perceived that further modifications on the membrane morphology and ionomer structure must be performed [33]. To further increase the ion conductivity while maintaining the high physicochemical and thermal stability, in **Chapter 7**, porosity was introduced into polybenzimidazole (PBI) as a reliable polymeric backbone for AEMs. The introduction of a porous structure into the PBI-based membranes created more open paths as well as higher surface area for ion transfer and absorption of electrolytic solution. The enhancement of electrolytic solution absorption (e.g., KOH) significantly helped the increase of ionic conductivity and AEMFC performance by 70% and 40%, respectively, compared to commercial FAA membrane. Furthermore, the alkali-doped porous PBI exhibited excellent thermal stability, chemical durability and mechanical properties in opposition to comemrcial FAA [34]. Based on the achieved results, the porous PBI was selected as a physicochemically stable polymer backbone for AEMs capable of being interacted with ion-conductive groups.

The results of the first and second employed strategies, inspired the development of an alkaline nano-composite porous membrane to improve AEMFC performance and durability. In **Error! Reference source not found.** the GO nanosheets functionalized with quaternary

ammonium were nominated as the nano-sized fillers. The porous PBI was used to build the polymeric infrastructure of the alkaline nano-composite membrane. The presence of QA groups interacted with large surface area of GO significantly enhanced the hydroxide conductivity to 0.085 S cm^{-1} and revealed satisfactory fuel cell performance with a peak power density of 86.68 mW cm^{-2} when compared to FAA commercial film. Apart from high ionic conductivity, QAFGO/pPBI membranes also exhibited excellent physicochemical and thermal stability. The alkaline electrochemical stability of x-QAFGO/pPBI was 21 days whereas FAA degraded after 3 h. The achieved results demonstrated that the porous PBI composites with QAFGO have the capability to be the potential AEMs for AEMFCs.

9.2 Recommendations for Future Work

In this PhD work it was shown that the solid electrolyte membranes, as one of the key components in fuel cells, can be improved. Thus, the development of highly ion-conductive and durable PEM and AEM materials was substantially studied for PEMFCs and AEMFCs, respectively. In each application, the solid electrolyte required humidity to conduct the produced ions. The water-dependency of solid electrolytes caused many shortcomings including limited operating conditions. Therefore, alternative solid electrolytes with good water retention were developed via (i) incorporation of hydrophilic inorganic fillers into the conventional polymeric membranes or (ii) synthesis of more water-retentive polymeric backbones. Although significant improvements in water retention have been achieved, to some extent the water dependency of ion transfer still remains as a major issue. To address these issues, the development of an anhydrous solid electrolyte is extremely needed which is capable of ion conduction without the presence of water.

For the future work, it is recommended to design and fabricate water-independent and highly ionic-conductive solid electrolytes based on ionic liquids. Ionic liquids are room-temperature molten salts, composed mostly of organic ions which are non-volatile, non-flammable, anhydrous, and ion-conductive with high thermal and chemical stability. Various strategies can be examined for the preparation of ionic-liquid-based electrolytes as follow:

(1) *Polymerization of ionic-liquids*: In this method the unique properties of ionic liquids is combined with the flexibility and properties of macromolecular architectures and provide novel characteristics and functionalities.

(2) *Doping or functionalization of conventional polymeric membranes with ionic liquids*: Via this approach the water-dependent ion-exchange moieties on the polymeric backbones can be switched to anhydrous ionic liquids. This can be carried out by chemical or physical functionalization of polymer electrolytes with ionic liquids.

(3) *Functionalization of nano-sized inorganic fillers with ionic liquids*: Inspiring from the advantages of adding ion-conductive nano-sized fillers to polymeric infrastructure of membranes, they can be functionalized with ionic liquids. Then, the anhydrous ion-conductive nano-fillers are composed with desired polymeric structure and form a mechanically stable nano-composite electrolyte with high performance.

Based on the preliminary studies and results it is highly expected that novel anhydrous solid electrolytes can fulfill all the requirements for electrochemical cells including high ionic conductivity and physicochemical stability at various operational and environmental conditions. To accomplish this, understanding and combination of inorganic/organic

chemistry, electrochemistry, chemical engineering and nano-materials science are unavoidable. Consequently, all the involved companies in commercializing the fuel cell technology can benefit from this work.

References

[1] McLean G, Niet T, Prince-Richard S, Djilali N. An assessment of alkaline fuel cell technology. International Journal of Hydrogen Energy. 2002;27:507-26.
[2] Larminie J, Dicks A, McDonald MS. Fuel cell systems explained: Wiley New York; 2003.
[3] O'Hayre RP, Cha S-W, Colella W, Prinz FB. Fuel cell fundamentals. 2006.
[4] Basu S. Fuel Cell Science and Technology: Springer; 2007.
[5] Basu S. Future Directions of Fuel Cell Science and Technology. Recent Trends in Fuel Cell Science and Technology: Springer; 2007. p. 356-65.
[6] Lipp L, Patel P, Kopp R. High Temperature Membrane With Humidification-Independent Cluster Structure. 2008 DOE Hydrogen Program Merit Review and Peer Evaluation Meeting, Arlington, VA2008.
[7] Martin KE, Kopasz JP, McMurphy KW. Status of fuel cells and the challenges facing fuel cell technology today. Fuel Cell Chemistry and Operation (American Chemical Society Symposium Series)2010. p. 1-13.
[8] Spiegel C. PEM fuel cell modeling and simulation using MATLAB: Academic Press; 2011.
[9] Srinivasan S, Manko DJ, Koch H, Enayetullah MA, Appleby AJ. Recent advances in solid polymer electrolyte fuel cell technology with low platinum loading electrodes. Journal of power sources. 1990;29:367-87.
[10] Wang Y, Chen KS, Mishler J, Cho SC, Adroher XC. A review of polymer electrolyte membrane fuel cells: technology, applications, and needs on fundamental research. Applied Energy. 2011;88:981-1007.
[11] Gülzow E. Alkaline fuel cells: a critical view. Journal of power sources. 1996;61:99-104.
[12] Pintauro P, Mather PT. Nanocapillary network proton conducting membranes for high temperature hydrogen/air fuel cells. US DOE Hydrogen Program Annual Merit Review and Peer Evaluation; 2010.
[13] Li Q, He R, Jensen J, Bjerrum N. Approaches and recent development of polymer electrolyte membranes for fuel cells operating above 100 oC. Chem Mater. 2003;15:4896-915.
[14] Varcoe JR, Slade RC. Prospects for Alkaline Anion-Exchange Membranes in Low Temperature Fuel Cells. Fuel cells. 2005;5:187-200.
[15] Antolini E, Gonzalez E. Alkaline direct alcohol fuel cells. Journal of Power Sources. 2010;195:3431-50.
[16] Tang D, Pan J, Lu S, Zhuang L, Lu J. Alkaline polymer electrolyte fuel cells: principle, challenges, and recent progress. Science China Chemistry. 2010;53:357-64.
[17] Jalani N, Dunn K, Datta R. Synthesis and characterization of Nafion -MO2 (M= Zr, Si, Ti) nanocomposite membranes for higher temperature PEM fuel cells. Electrochimica Acta. 2005;51:553-60.
[18] Rodgers MP, Shi Z, Holdcroft S. Transport properties of composite membranes containing silicon dioxide and Nafion< sup>®</sup>. Journal of Membrane Science. 2008;325:346-56.
[19] Chalkovaa E, Wang C, Komarneni S, Lee J, Fedkin M, Lvov S. Composite proton conductive membranes for elevated temperature and reduced relative humidity PEMFC. ECS Transactions. 2009;25:1141-50.
[20] Chen Z, Holmberg B, Li W, Wang X, Deng W, Munoz R, et al. Nafion/zeolite nanocomposite membrane by in situ crystallization for a direct methanol fuel cell. Chemistry of Materials. 2006;18:5669-75.
[21] Tricoli V, Nannetti F. Zeolite–Nafion composites as ion conducting membrane materials. Electrochimica Acta. 2003;48:2625-33.

[22] Aksoy EA, Akata B, Bac N, Hasirci N. Preparation and characterization of zeolite beta–polyurethane composite membranes. Journal of applied polymer science. 2007;104:3378-87.
[23] Arico A, Baglio V, Di Blasi A, Creti P, Antonucci P, Antonucci V. Influence of the acid–base characteristics of inorganic fillers on the high temperature performance of composite membranes in direct methanol fuel cells. Solid State Ionics. 2003;161:251-65.
[24] Di Noto V, Gliubizzi R, Negro E, Pace G. Effect of SiO2 on relaxation phenomena and mechanism of ion conductivity of [Nafion/(SiO2) x] composite membranes. The Journal of Physical Chemistry B. 2006;110:24972-86.
[25] Jian-hua T, Peng-fei G, Zhi-yuan Z, Wen-hui L, Zhong-qiang S. Preparation and performance evaluation of a Nafion-TiO< sub> 2</sub> composite membrane for PEMFCs. International Journal of Hydrogen Energy. 2008;33:5686-90.
[26] Li Q, He R, Jensen JO, Bjerrum NJ. Approaches and recent development of polymer electrolyte membranes for fuel cells operating above 100 C. Chemistry of Materials. 2003;15:4896-915.
[27] Licoccia S, Traversa E. Increasing the operation temperature of polymer electrolyte membranes for fuel cells: From nanocomposites to hybrids. Journal of Power Sources. 2006;159:12-20.
[28] Savadogo O. Emerging membranes for electrochemical systems:(I) solid polymer electrolyte membranes for fuel cell systems. ChemInform. 1998;29.
[29] Li D, Honma I, Zhou H, Yamada M. A Self-Ordered, Crystalline Glass, Mesoporous Nanocomposite with High Proton Conductivity of 2 x 10-2 S cm-1 at Intermediate Temperature. Journal of the American Chemical Society: JACS. 2005;127:13092-3.
[30] Ladewig BP, Knott RB, Hill AJ, Riches JD, White JW, Martin DJ, et al. Physical and electrochemical characterization of nanocomposite membranes of Nafion and functionalized silicon oxide. Chemistry of Materials. 2007;19:2372-81.
[31] Jun Y, Zarrin H, Fowler M, Chen Z. Functionalized titania nanotube composite membranes for high temperature proton exchange membrane fuel cells. International Journal of Hydrogen Energy. 2011;36:6073-81.
[32] Zarrin H, Higgins D, Yu J, Fowler M, Chen Z. Functionalized Graphene Oxide Nanocomposite Membrane for Low Humidity and High Temperature Proton Exchange Membrane Fuel Cells. The Journal of Physical Chemistry C. 2011;115:20774.
[33] Zarrin H, Wu J, Fowler M, Chen Z. High durable PEK-based anion exchange membrane for elevated temperature alkaline fuel cells. Journal of Membrane Science. 2012;394-395:193.
[34] Zarrin H, Jiang G, Lam GY-Y, Fowler M, Chen Z. High performance porous polybenzimidazole membrane for alkaline fuel cells. International Journal of Hydrogen Energy. 2014;39:18405.
[35] Zarrin H, Chen Z, Fowler M. Highly Ion-Conductive Nano-Engineered Porous Electrolytic Composite Membrane For Alkaline Electrochemical Energy Systems. 2014.
[36] Adler SB. Fuel cells: current status and future challenges. Frontiers of Engineering: Reports on. 2006.
[37] Hoogers G. Fuel cell technology handbook: CRC press; 2002.
[38] Cook B. Introduction to fuel cells and hydrogen technology. Engineering Science & Education Journal. 2002;11:205-16.
[39] Wilson MS, Valerio JA, Gottesfeld S. Low platinum loading electrodes for polymer electrolyte fuel cells fabricated using thermoplastic ionomers. Electrochimica Acta. 1995;40:355-63.
[40] Wilson MS, Gottesfeld S. Thin-film catalyst layers for polymer electrolyte fuel cell electrodes. Journal of applied electrochemistry. 1992;22:1-7.
[41] Kinoshita K, Su Q, Tanaka Y, Togo T. Fuel cell powder generation method and system. Google Patents; 2001.
[42] Shah R. Introduction to fuel cells. Recent Trends in Fuel Cell Science and Technology: Springer; 2007. p. 1-9.

[43] Zhou C. Chemical Durability Studies of Ionomers and Model Compounds for Fuel Cell Applications: Case Western Reserve University; 2008.
[44] Donis WRM. Diagnosis of PEMFC Stack Failures via Electrochemical Impedance Spectroscopy: University of Victoria; 2002.
[45] Panha K. Accelerated Durability Testing via Reactants Relative Humidity Cycling on Polymer Electrolyte Membrane Fuel Cells. 2010.
[46] Yuan X-Z, Song C, Wang H, Zhang J. PEM fuel cells and their related electrochemical fundamentals. Electrochemical Impedance Spectroscopy in PEM Fuel Cells: Fundamentals and Applications. 2010:1-37.
[47] Smitha B, Sridhar S, Khan A. Solid polymer electrolyte membranes for fuel cell applications—a review. Journal of Membrane Science. 2005;259:10-26.
[48] Jiao K, Li X. Water transport in polymer electrolyte membrane fuel cells. Progress in Energy and Combustion Science. 2011;37:221-91.
[49] Dhathathreyan K, Sridhar P, Sasikumar G, Ghosh K, Velayutham G, Rajalakshmi N, et al. Development of polymer electrolyte membrane fuel cell stack. International Journal of Hydrogen Energy. 1999;24:1107-15.
[50] Carrette L, Friedrich K, Stimming U. Fuel cells–fundamentals and applications. Fuel cells. 2001;1:5-39.
[51] Shevchenko V, Gumennaya M. Synthesis and properties of anion-exchange membranes for fuel cells. Theoretical and Experimental Chemistry. 2010;46:139-52.
[52] Bae B, Ha HY, Kim D. Nafion< sup>®</sup>-< i> graft</i>-polystyrene sulfonic acid membranes for direct methanol fuel cells. Journal of Membrane Science. 2006;276:51-8.
[53] Jalani NH, Dunn K, Datta R. Synthesis and characterization of Nafion< sup>®</sup>-MO< sub> 2</sub>(M= Zr, Si, Ti) nanocomposite membranes for higher temperature PEM fuel cells. Electrochimica Acta. 2005;51:553-60.
[54] Kannan R, Kakade BA, Pillai VK. Polymer Electrolyte Fuel Cells Using Nafion-Based Composite Membranes with Functionalized Carbon Nanotubes. Angewandte Chemie International Edition. 2008;47:2653-6.
[55] Kumar B, Fellner J. Polymer–ceramic composite protonic conductors. Journal of power sources. 2003;123:132-6.
[56] Mauritz KA, Moore RB. State of understanding of Nafion. Chemical reviews. 2004;104:4535-86.
[57] Adjemian K, Lee S, Srinivasan S, Benziger J, Bocarsly A. Silicon oxide Nafion composite membranes for proton-exchange membrane fuel cell operation at 80-140 C. Journal of The Electrochemical Society. 2002;149:A256-A61.
[58] Peighambardoust S, Rowshanzamir S, Amjadi M. Review of the proton exchange membranes for fuel cell applications. International Journal of Hydrogen Energy. 2010;35:9349-84.
[59] Lin Y-F, Yen C-Y, Ma C-CM, Liao S-H, Lee C-H, Hsiao Y-H, et al. High proton-conducting Nafion< sup>®</sup>/–SO< sub> 3</sub> H functionalized mesoporous silica composite membranes. Journal of power sources. 2007;171:388-95.
[60] Sacca A, Gatto I, Carbone A, Pedicini R, Passalacqua E. ZrO< sub> 2</sub>–Nafion composite membranes for polymer electrolyte fuel cells (PEFCs) at intermediate temperature. Journal of power sources. 2006;163:47-51.
[61] Sahu A, Selvarani G, Pitchumani S, Sridhar P, Shukla A. A sol-gel modified alternative nafion-silica composite membrane for polymer electrolyte fuel cells. Journal of The Electrochemical Society. 2007;154:B123-B32.

[62] Uchida H, Ueno Y, Hagihara H, Watanabe M. Self-humidifying electrolyte membranes for fuel cells preparation of highly dispersed TiO 2 particles in Nafion 112. Journal of The Electrochemical Society. 2003;150:A57-A62.
[63] Tominaga Y, Hong I-C, Asai S, Sumita M. Proton conduction in Nafion composite membranes filled with mesoporous silica. Journal of power sources. 2007;171:530-4.
[64] McKeen JC, Yan YS, Davis ME. Proton conductivity of acid-functionalized zeolite beta, MCM-41, and MCM-48: effect of acid strength. Chemistry of Materials. 2008;20:5122-4.
[65] McKeen JC, Yan YS, Davis ME. Proton conductivity in sulfonic acid-functionalized zeolite beta: effect of hydroxyl group. Chemistry of Materials. 2008;20:3791-3.
[66] Gnana Kumar G, Kim A, Suk Nahm K, Elizabeth R. Nafion membranes modified with silica sulfuric acid for the elevated temperature and lower humidity operation of PEMFC. International Journal of Hydrogen Energy. 2009;34:9788-94.
[67] Hibbs MR, Fujimoto CH, Cornelius CJ. Synthesis and characterization of poly (phenylene)-based anion exchange membranes for alkaline fuel cells. Macromolecules. 2009;42:8316-21.
[68] Hibbs MR, Hickner MA, Alam TM, McIntyre SK, Fujimoto CH, Cornelius CJ. Transport properties of hydroxide and proton conducting membranes. Chemistry of Materials. 2008;20:2566-73.
[69] Xiong Y, Liu QL, Zeng QH. Quaternized cardo polyetherketone anion exchange membrane for direct methanol alkaline fuel cells. Journal of Power Sources. 2009;193:541-6.
[70] Wang G, Weng Y, Chu D, Xie D, Chen R. Preparation of alkaline anion exchange membranes based on functional poly (ether-imide) polymers for potential fuel cell applications. Journal of Membrane Science. 2009;326:4-8.
[71] Xing B, Savadogo O. Hydrogen/oxygen polymer electrolyte membrane fuel cells (PEMFCs) based on alkaline-doped polybenzimidazole (PBI). Electrochemistry communications. 2000;2:697-702.
[72] Wu L, Xu T, Wu D, Zheng X. Preparation and characterization of CPPO/BPPO blend membranes for potential application in alkaline direct methanol fuel cell. Journal of Membrane Science. 2008;310:577-85.
[73] Varcoe JR. Investigations of the ex situ ionic conductivities at 30 C of metal-cation-free quaternary ammonium alkaline anion-exchange membranes in static atmospheres of different relative humidities. Physical Chemistry Chemical Physics. 2007;9:1479-86.
[74] Zeng QH, Liu QL, Broadwell I, Zhu AM, Xiong Y, Tu XP. Anion exchange membranes based on quaternized polystyrene-block-poly (ethylene-ran-butylene)-block-polystyrene for direct methanol alkaline fuel cells. Journal of Membrane Science. 2010;349:237-43.
[75] Xiong Y, Fang J, Zeng QH, Liu QL. Preparation and characterization of cross-linked quaternized poly (vinyl alcohol) membranes for anion exchange membrane fuel cells. Journal of Membrane Science. 2008;311:319-25.
[76] Xiong Y, Liu QL, Zhang QG, Zhu AM. Synthesis and characterization of cross-linked quaternized poly (vinyl alcohol)/chitosan composite anion exchange membranes for fuel cells. Journal of Power Sources. 2008;183:447.
[77] Li L, Wang Y. Quaternized polyethersulfone Cardo anion exchange membranes for direct methanol alkaline fuel cells. Journal of Membrane Science. 2005;262:1-4.
[78] Stoica D, Ogier L, Akrour L, Alloin F, Fauvarque J. Anionic membrane based on polyepichlorhydrin matrix for alkaline fuel cell: Synthesis, physical and electrochemical properties. Electrochimica Acta. 2007;53:1596-603.
[79] Slade RCT, Varcoe JR. Investigations of conductivity in FEP-based radiation-grafted alkaline anion-exchange membranes. Solid State Ionics. 2005;176:585-97.
[80] Varcoe JR, Slade RCT. An electron-beam-grafted ETFE alkaline anion-exchange membrane in metal-cation-free solid-state alkaline fuel cells. Electrochemistry communications. 2006;8:839-43.

[81] Varcoe JR, Slade RCT, Yee ELH, Poynton SD, Driscoll DJ, Apperley DC. Poly (ethylene-co-tetrafluoroethylene)-derived radiation-grafted anion-exchange membrane with properties specifically tailored for application in metal-cation-free alkaline polymer electrolyte fuel cells. Chemistry of Materials. 2007;19:2686-93.
[82] Yi F, Yang X, Li Y, Fang S. Synthesis and ion conductivity of poly (oxyethylene) methacrylates containing a quaternary ammonium group. Polymers for Advanced Technologies. 1999;10:473-5.
[83] Danks TN, Slade RC, Varcoe JR. Alkaline anion-exchange radiation-grafted membranes for possible electrochemical application in fuel cells. Journal of Materials Chemistry. 2003;13:712-21.
[84] Wu Y, Wu C, Varcoe JR, Poynton SD, Xu T, Fu Y. Novel silica/poly (2, 6-dimethyl-1, 4-phenylene oxide) hybrid anion-exchange membranes for alkaline fuel cells: Effect of silica content and the single cell performance. Journal of Power Sources. 2010;195:3069-76.
[85] Holmberg BA, Wang X, Yan Y. Nanocomposite fuel cell membranes based on Nafion and acid functionalized zeolite beta nanocrystals. Journal of Membrane Science. 2008;320:86-92.
[86] Komkova E, Stamatialis D, Strathmann H, Wessling M. Anion-exchange membranes containing diamines: preparation and stability in alkaline solution. Journal of Membrane Science. 2004;244:25-34.
[87] Park J-S, Park S-H, Yim S-D, Yoon Y-G, Lee W-Y, Kim C-S. Performance of solid alkaline fuel cells employing anion-exchange membranes. Journal of power sources. 2008;178:620-6.
[88] Park JS, Park GG, Park SH, Yoon YG, Kim CS, Lee WY. Development of Solid-State Alkaline Electrolytes for Solid Alkaline Fuel Cells. Macromolecular Symposia: Wiley Online Library; 2007. p. 174-82.
[89] Fang J, Shen PK. Quaternized poly (phthalazinon ether sulfone ketone) membrane for anion exchange membrane fuel cells. Journal of Membrane Science. 2006;285:317-22.
[90] Young RJ, Lovell PA. Introduction to polymers: CRC press; 2011.
[91] Aronniemi M. Development of XPS data analysis and its application to gas sensor and catalyst surface studies: Helsinki University of Technology; 2007.
[92] Tong H-mH, Nguyen LT. New characterization techniques for thin polymer films: Wiley; 1990.
[93] Amelinckx S, van Dyck D, van Landuyt J, van Tendeloo G. Electron microscopy: principles and fundamentals: John Wiley & Sons; 2008.
[94] Majsztrik PW, Satterfield MB, Bocarsly AB, Benziger JB. Water sorption, desorption and transport in Nafion membranes. Journal of Membrane Science. 2007;301:93-106.
[95] Hensley JE, Way JD. The relationship between proton conductivity and water permeability in composite carboxylate/sulfonate perfluorinated ionomer membranes. Journal of power sources. 2007;172:57-66.
[96] D'Epifanio A, Navarra MA, Weise FC, Mecheri B, Farrington J, Licoccia S, et al. Composite Nafion/Sulfated Zirconia Membranes: Effect of the Filler Surface Properties on Proton Transport Characteristics†. Chemistry of Materials. 2009;22:813-21.
[97] Reich L, Levi DW. Dynamic thermogravimetric. Analysis in polymer degradation. Journal of Polymer Science: Macromolecular Reviews. 1967;1:173-275.
[98] Braun D, Cherdron H, Ritter H, Braun D, Cherdron H. Polymer synthesis: theory and practice: Springer; 2005.
[99] Macdonald JR. Impedance spectroscopy. Annals of biomedical engineering. 1992;20:289-305.
[100] Lasia A. Electrochemical impedance spectroscopy and its applications: Springer; 2002.
[101] Yuan X-Z, Song C, Wang H, Zhang J. Electrochemical impedance spectroscopy in PEM fuel cells. Fundamentals and ApplicationsSpringer-Verlag, London. 2010.
[102] Lee CH, Park HB, Lee YM, Lee RD. Importance of proton conductivity measurement in polymer electrolyte membrane for fuel cell application. Industrial & engineering chemistry research. 2005;44:7617-26.

[103] Park S-M, Yoo J-S. Peer reviewed: electrochemical impedance spectroscopy for better electrochemical measurements. Analytical chemistry. 2003;75:455 A-61 A.
[104] Mikhailenko S, Guiver M, Kaliaguine S. Measurements of PEM conductivity by impedance spectroscopy. Solid State Ionics. 2008;179:619-24.
[105] Sone Y, Ekdunge P, Simonsson D. Proton Conductivity of Nafion 117 as Measured by a Four-Electrode AC Impedance Method. Journal of The Electrochemical Society. 1996;143:1254-9.
[106] Yilanci A, Dincer I, Ozturk H. Performance analysis of a PEM fuel cell unit in a solar-hydrogen system. International Journal of Hydrogen Energy. 2008;33:7538-52.
[107] Vielstich W, Lamm A, Gasteiger H. Handbook of Fuel Cells: Fundamentals, Technology, Applications, 4-Volume Set. 2003.
[108] Peighambardoust S, Rowshanzamir S, Amjadi M. Review of the proton exchange membranes for fuel cell applications. International Journal of Hydrogen Energy.
[109] Savadogo O. Emerging membranes for electrochemical systems* 1:: Part II. High temperature composite membranes for polymer electrolyte fuel cell (PEFC) applications. Journal of Power Sources. 2004;127:135-61.
[110] Aksoy E, Akata B, Bac N, Hasirci N. Preparation and characterization of zeolite beta-polyurethane composite membranes. Journal of Applied Polymer Science. 2007;104:3378-87.
[111] Arico A, Baglio V, Di Blasi A, Creti P. ', PL Antonucci and V. Antonucci. Solid State Ionics. 2003;161:251.
[112] Adjemian K, Dominey R, Krishnan L, Ota H, Majsztrik P, Zhang T, et al. Function and Characterization of Metal Oxide- Nafion Composite Membranes for Elevated-Temperature H2/O2 PEM Fuel Cells. Chem Mater. 2006;18:2238-48.
[113] Nagarale R, Shin W, Singh P. Progress in ionic organic-inorganic composite membranes for fuel cell applications. Polymer Chemistry. 2009;1:388-408.
[114] Adjemian K, Lee S, Srinivasan S, Benziger J, Bocarsly A. Silicon oxide Nafion composite membranes for proton-exchange membrane fuel cell operation at 80-140 C. Journal of The Electrochemical Society. 2002;149:A256.
[115] Sacc A, Gatto I, Carbone A, Pedicini R, Passalacqua E. ZrO2-Nafion composite membranes for polymer electrolyte fuel cells (PEFCs) at intermediate temperature. Journal of Power Sources. 2006;163:47-51.
[116] Sahu A, Selvarani G, Pitchumani S, Sridhar P, Shukla A. A sol-gel modified alternative nafion-silica composite membrane for polymer electrolyte fuel cells. Journal of The Electrochemical Society. 2007;154:B123.
[117] Uchida H, Ueno Y, Hagihara H, Watanabe M. Self-humidifying electrolyte membranes for fuel cells. Journal of The Electrochemical Society. 2003;150:A57.
[118] Chen Z, Holmberg B, Li W, Wang X, Deng W, Munoz R, et al. Nafion/zeolite nanocomposite membrane by in situ crystallization for a direct methanol fuel cell. Chem Mater. 2006;18:5669-75.
[119] Lin Y, Yen C, Ma C, Liao S, Lee C, Hsiao Y, et al. High proton-conducting Nafion®/-SO3H functionalized mesoporous silica composite membranes. Journal of Power Sources. 2007;171:388-95.
[120] Tominaga Y, Hong I, Asai S, Sumita M. Proton conduction in Nafion composite membranes filled with mesoporous silica. Journal of Power Sources. 2007;171:530-4.
[121] Wilhelm M, Jeske M, Marschall R, Cavalcanti W, Tölle P, Köhler C, et al. New proton conducting hybrid membranes for HT-PEMFC systems based on polysiloxanes and SO3H-functionalized mesoporous Si-MCM-41 particles. Journal of Membrane Science. 2008;316:164-75.
[122] Tang H, Pan M. Synthesis and characterization of a self-assembled nafion/silica nanocomposite membrane for polymer electrolyte membrane fuel cells. The Journal of Physical Chemistry C. 2008;112:11556-68.

[123] D'Epifanio A, Navarra M, Weise F, Mecheri B, Farrington J, Licoccia S, et al. Composite Nafion/Sulfated Zirconia Membranes: Effect of the Filler Surface Properties on Proton Transport Characteristics†. Chemistry of Materials. 2009;22:813-21.
[124] Wang H, Holmberg B, Huang L, Wang Z, Mitra A, Norbeck J, et al. Nafion-bifunctional silica composite proton conductive membranes. Journal of Materials Chemistry. 2002;12:834-7.
[125] Jian-hua T, Peng-fei G, Zhi-yuan Z, Wen-hui L, Zhong-qiang S. Preparation and performance evaluation of a Nafion-TiO2 composite membrane for PEMFCs. International Journal of Hydrogen Energy. 2008;33:5686-90.
[126] Ke C, Li X, Shen Q, Qu S, Shao Z, Yi B. Investigation on sulfuric acid sulfonation of in-situ sol-gel derived Nafion/SiO2 composite membrane. International Journal of Hydrogen Energy.
[127] Pan J, Zhang H, Chen W, Pan M. Nafion-zirconia nanocomposite membranes formed via in situ sol-gel process. International Journal of Hydrogen Energy.35:2796-801.
[128] Baglio V, Di Blasi A, Aricò A, Antonucci V, Antonucci P, Trakanprapai C, et al. Composite mesoporous titania Nafion-based membranes for direct methanol fuel cell operation at high temperature. Journal of The Electrochemical Society. 2005;152:A1373.
[129] Li Y, Somorjai G. Nanoscale Advances in Catalysis and Energy Applications. Nano Letters. 2010:1.
[130] Shao Z, Xu H, Li M, Hsing I. Hybrid Nafion-inorganic oxides membrane doped with heteropolyacids for high temperature operation of proton exchange membrane fuel cell. Solid State Ionics. 2006;177:779-85.
[131] Chalkovaa E, Wang C, Komarneni S, Lee J, Fedkin M, Lvov S. Composite Proton Conductive Membranes for Elevated Temperature and Reduced Relative Humidity PEMFC. ECS; 2009.
[132] Kalappa P, Lee J. Proton conducting membranes based on sulfonated poly (ether ether ketone)/TiO2 nanocomposites for a direct methanol fuel cell. Polymer International. 2007;56:371-5.
[133] Gnana Kumar G, Kim A, Suk Nahm K, Elizabeth R. Nafion membranes modified with silica sulfuric acid for the elevated temperature and lower humidity operation of PEMFC. International Journal of Hydrogen Energy. 2009.
[134] Kannan R, Kakade B, Pillai V. Polymer Electrolyte Fuel Cells Using Nafion-Based Composite Membranes with Functionalized Carbon Nanotubes. Angewandte Chemie International Edition. 2008;47:2653-6.
[135] McKeen J, Yan Y, Davis M. Proton Conductivity in Sulfonic Acid-Functionalized Zeolite Beta: Effect of Hydroxyl Group. Chem Mater. 2008;20:3791-3.
[136] McKeen J, Yan Y, Davis M. Proton conductivity of acid-functionalized zeolite beta, MCM-41, and MCM-48: effect of acid strength. Chem Mater. 2008;20:5122-4.
[137] SUN X, LI R, ZHOU Y, CAI M, LIU H. ONE-DIMENSIONAL METAL AND METAL OXIDE NANOSTRUCTURES. WO Patent WO/2008/031,005; 2008.
[138] Kelarakis A, Alonso R, Lian H, Burgaz E, Estevez L, Giannelis E. Nanohybrid Nafion Membranes for Fuel Cells.
[139] Matos B, Aricó E, Linardi M, Ferlauto A, Santiago E, Fonseca F. Thermal properties of Nafion–TiO 2 composite electrolytes for PEM fuel cell. Journal of thermal analysis and calorimetry. 2009;97:591-4.
[140] Ou H, Lo S. Review of titania nanotubes synthesized via the hydrothermal treatment: Fabrication, modification, and application. Separation and Purification Technology. 2007;58:179-91.
[141] Yuan Z, Su B. Titanium oxide nanotubes, nanofibers and nanowires. Colloids and Surfaces A: Physicochemical and Engineering Aspects. 2004;241:173-83.
[142] Thorne A, Kruth A, Tunstall D, Irvine J, Zhou W. Formation, structure, and stability of titanate nanotubes and their proton conductivity. J Phys Chem B. 2005;109:5439-44.

[143] Chen W, Wu J, Kuo P. Poly (oxyalkylene) diamine-functionalized carbon nanotube/perfluorosulfonated polymer composites: synthesis, water state, and conductivity. Chemistry of Materials. 2008;20:5756-67.
[144] Kasuga T, Hiramatsu M, Hoson A, Sekino T, Niihara K. Formation of titanium oxide nanotube. Langmuir. 1998;14:3160-3.
[145] Wang L, Yang M, Shi Z, Chen Y, Feng J. Two-dimensional metal-organic framework constructed from 4, 4 0-bipyridine and 1, 2, 4-benzenetricarboxylate: synthesis, structure and magnetic properties. J Solid State Chem. 2005;178:3359.
[146] Lucky R, Sui R, Lo J, Charpentier P. Effect of Solvent on the Crystal Growth of One-Dimensional ZrO2- TiO2 Nanostructures. Crystal Growth & Design.10:1598-604.
[147] Matos B, Santiago E, Fonseca F, Linardi M, Lavayen V, Lacerda R, et al. Nafion–Titanate Nanotube Composite Membranes for PEMFC Operating at High Temperature. Journal of The Electrochemical Society. 2007;154:B1358.
[148] Park S, Yoo J. Peer Reviewed: Electrochemical Impedance Spectroscopy for Better Electrochemical Measurements. Analytical chemistry. 2003;75:455-61.
[149] Pavasupree S, Ngamsinlapasathian S, Suzuki Y, Yoshikawa S. One-dimensional Nanostructured TiO2 for Photocatalytic Activity and Dye-sensitized Solar Cells Applications.
[150] Morgado Jr E, de Abreu M, Moure G, Marinkovic B, Jardim P, Araujo A. Characterization of nanostructured titanates obtained by alkali treatment of TiO2-anatases with distinct crystal sizes. Chem Mater. 2007;19:665-76.
[151] Majsztrik P, Satterfield M, Bocarsly A, Benziger J. Water sorption, desorption and transport in Nafion membranes. Journal of Membrane Science. 2007;301:93-106.
[152] Hensley J, Way J. The relationship between proton conductivity and water permeability in composite carboxylate/sulfonate perfluorinated ionomer membranes. Journal of Power Sources. 2007;172:57-66.
[153] Holmberg B, Yan Y. An apparatus for direct proton conductivity measurement of powdered materials. Journal of The Electrochemical Society. 2006;153:A146.
[154] Sone Y, Ekdunge P, Simonsson D. Proton Conductivity of Nafion 117 as Measured by a Four Electrode AC Impedance Method. Journal of The Electrochemical Society. 1996;143:1254.
[155] Lee C, Park H, Lee Y, Lee R. Importance of proton conductivity measurement in polymer electrolyte membrane for fuel cell application. Ind Eng Chem Res. 2005;44:7617-26.
[156] Byrne M, McCarthy J, Bent M, Blake R, Gun'ko Y, Horvath E, et al. Chemical functionalisation of titania nanotubes and their utilisation for the fabrication of reinforced polystyrene composites. Journal of Materials Chemistry. 2007;17:2351-8.
[157] Lin Y, Wang L, Chiu W. Preparation and characterization of titania nanotubes and hybrid materials derived from them. Journal of Vacuum Science & Technology B: Microelectronics and Nanometer Structures. 2005;23:2398.
[158] Zawodzinski Jr T, Derouin C, Radzinski S, Sherman R, Smith V, Springer T, et al. Water uptake by and transport through Nafion 117 membranes. Journal of The Electrochemical Society. 1993;140:1041.
[159] Xu K, Chanthad C, Gadinski M, Hickner M, Wang Q. Acid-Functionalized Polysilsesquioxane-Nafion Composite Membranes with High Proton Conductivity and Enhanced Selectivity. ACS Applied Materials & Interfaces. 2009;1:2573-9.
[160] Yamada M, Li D, Honma I, Zhou H. A Self-Ordered, Crystalline Glass, Mesoporous Nanocomposite with High Proton Conductivity of 2× 10-2 S cm-1 at Intermediate Temperature. J Am Chem Soc. 2005;127:13092-3.

[161] Di Noto V, Gliubizzi R, Negro E, Pace G. Effect of SiO2 on Relaxation Phenomena and Mechanism of Ion Conductivity of [Nafion/(SiO2) x] Composite Membranes†. J Phys Chem B. 2006;110:24972-86.
[162] Ladewig B, Knott R, Hill A, Riches J, White J, Martin D, et al. Physical and electrochemical characterization of nanocomposite membranes of Nafion and functionalized silicon oxide. Chem Mater. 2007;19:2372-81.
[163] Li Q, He R, Jensen J, Bjerrum N. Approaches and recent development of polymer electrolyte membranes for fuel cells operating above 100 C. Chem Mater. 2003;15:4896-915.
[164] Bae B, Ha H, Kim D. Nafion®-graft-polystyrene sulfonic acid membranes for direct methanol fuel cells. Journal of membrane science. 2006;276:51-8.
[165] Kannan R, Kakade B, Pillai V. Polymer Electrolyte Fuel Cells Using Nafion Based Composite Membranes with Functionalized Carbon Nanotubes. Angewandte Chemie International Edition. 2008;47:2653-6.
[166] Kumar B, Fellner J. Polymer-ceramic composite protonic conductors. Journal of Power Sources. 2003;123:132-6.
[167] Mauritz K, Moore R. State of understanding of Nafion. Chem Rev. 2004;104:4535-86.
[168] Hickner M, Ghassemi H, Kim Y, Einsla B, McGrath J. Alternative polymer systems for proton exchange membranes (PEMs). Chem Rev. 2004;104:4587-612.
[169] Kim F, Cote L, Huang J. Graphene Oxide: Surface Activity and Two-Dimensional Assembly. Advanced Materials.22:1954-8.
[170] Tricoli V, Nannetti F. Zeolite-Nafion composites as ion conducting membrane materials. Electrochimica Acta. 2003;48:2625-33.
[171] Wilson N, Pandey P, Beanland R, Young R, Kinloch I, Gong L, et al. Graphene Oxide: Structural Analysis and Application as a Highly Transparent Support for Electron Microscopy. ACS nano. 2009;3:2547-56.
[172] Yang Q, Liu J, Yang J, Kapoor M, Inagaki S, Li C. Synthesis, characterization, and catalytic activity of sulfonic acid-functionalized periodic mesoporous organosilicas. Journal of Catalysis. 2004;228:265-72.
[173] Yang S, Feng X, Wang L, Tang K, Maier J, Müllen K. Graphene Based Nanosheets with a Sandwich Structure. Angewandte Chemie International Edition.49:4795-9.
[174] Dikin D, Stankovich S, Zimney E, Piner R, Dommett G, Evmenenko G, et al. Preparation and characterization of graphene oxide paper. Nature. 2007;448:457-60.
[175] Mkhoyan K, Contryman A, Silcox J, Stewart D, Eda G, Mattevi C, et al. Atomic and electronic structure of graphene-oxide. Nano Letters. 2009;9:1058-63.
[176] Yu A, Roes I, Davies A, Chen Z. Ultrathin, transparent, and flexible graphene films for supercapacitor application. Applied Physics Letters.96:253105.
[177] Stankovich S, Dikin D, Dommett G, Kohlhaas K, Zimney E, Stach E, et al. Graphene-based composite materials. Nature. 2006;442:282-6.
[178] Stankovich S, Piner R, Chen X, Wu N, Nguyen S, Ruoff R. Stable aqueous dispersions of graphitic nanoplatelets via the reduction of exfoliated graphite oxide in the presence of poly (sodium 4-styrenesulfonate). Journal of Materials Chemistry. 2006;16:155-8.
[179] Hummers Jr W, Offeman R. Preparation of graphitic oxide. Journal of the American Chemical Society. 1958;80:1339-.
[180] Lerf A, He H, Forster M, Klinowski J. Structure of Graphite Oxide Revisited. J Phys Chem B. 1998;102:4477-82.
[181] Wang Y, Yang D, Zheng X, Jiang Z, Li J. Zeolite beta-filled chitosan membrane with low methanol permeability for direct methanol fuel cell. Journal of Power Sources. 2008;183:454-63.

[182] Wu Z, Sun G, Jin W, Hou H, Wang S, Xin Q. Nafion® and nano-size TiO2-SO42-solid superacid composite membrane for direct methanol fuel cell. Journal of Membrane Science. 2008;313:336-43.
[183] Wilson M, Valerio J, Gottesfeld S. Low platinum loading electrodes for polymer electrolyte fuel cells fabricated using thermoplastic ionomers. Electrochimica Acta. 1995;40:355-63.
[184] Tian L, Meziani M, Lu F, Kong C, Cao L, Thorne T, et al. Graphene Oxides for Homogeneous Dispersion of Carbon Nanotubes. ACS Applied Materials & Interfaces.183.
[185] Wang H, Hao Q, Yang X, Lu L, Wang X. Effect of Graphene Oxide on the Properties of Its Composite with Polyaniline. ACS Applied Materials & Interfaces.2:821-8.
[186] Whitby R, Korobeinyk A, Glevatska K. Morphological changes and covalent reactivity assessment of single-layer graphene oxides under carboxylic group-targetted chemistry. Carbon.
[187] Xu L, Yang W, Neoh K, Kang E, Fu G. Dopamine-Induced Reduction and Functionalization of Graphene Oxide Nanosheets. Macromolecules.197-200.
[188] Haubner K, Murawski J, Olk P, Eng L, Ziegler C, Adolphi B, et al. The Route to Functional Graphene Oxide. ChemPhysChem.
[189] Park S, Dikin D, Nguyen S, Ruoff R. Graphene Oxide Sheets Chemically Cross-Linked by Polyallylamine. The Journal of Physical Chemistry C. 2009;113:15801-4.
[190] Wang G, Wang B, Park J, Yang J, Shen X, Yao J. Synthesis of enhanced hydrophilic and hydrophobic graphene oxide nanosheets by a solvothermal method. Carbon. 2009;47:68-72.
[191] Lian Y, Liu Y, Jiang T, Shu J, Lian H, Cao M. Enhanced Electromechanical Performance of Graphite Oxide-Nafion Nanocomposite Actuator. The Journal of Physical Chemistry C.114:9659-63.
[192] Chu D, Gervasio D, Razaq M, Yeager E. Infrared reflectance absorption spectroscopy (IRRAS). Study of the thermal stability of perfluorinated sulphonic acid ionomers on Pt. Journal of Applied Electrochemistry. 1990;20:157-62.
[193] Laporta M, Pegoraro M, Zanderighi L. Perfluorosulfonated membrane (Nafion): FT-IR study of the state of water with increasing humidity. Physical Chemistry Chemical Physics. 1999;1:4619-28.
[194] Lavorgna M, Mascia L, Mensitieri G, Gilbert M, Scherillo G, Palomba B. Hybridization of Nafion membranes by the infusion of functionalized siloxane precursors. Journal of membrane science. 2007;294:159-68.
[195] Ostrowska J, Narebska A. Infrared study of hydration and association of functional groups in a perfluorinated Nafion membrane, Part 1. Colloid & Polymer Science. 1983;261:93-8.
[196] Rieke P, Vanderborgh N. Temperature dependence of water content and proton conductivity in polyperfluorosulfonic acid membranes. Journal of membrane science. 1987;32:313-28.
[197] Hamwi A, Marchand V. Some chemical and electrochemical properties of graphite oxide. Journal of Physics and Chemistry of Solids. 1996;57:867-72.
[198] Mermoux M, Chabre Y, Rousseau A. FTIR and 13C NMR study of graphite oxide. Carbon. 1991;29:469-74.
[199] Leuchs M, Zundel G. Easily polarizable hydrogen bonds in aqueous solutions of acids. Perchloric acid and trifluoromethane sulphonic acid. Journal of the Chemical Society, Faraday Transactions 2. 1978;74:2256-67.
[200] Si Y, Samulski E. Synthesis of water soluble graphene. Nano Letters. 2008;8:1679-82.
[201] Liang Z, Chen W, Liu J, Wang S, Zhou Z, Li W, et al. FT-IR study of the microstructure of Nafion® membrane. Journal of membrane science. 2004;233:39-44.
[202] Wool R. Mechanisms of frequency shifting in the infrared spectrum of stressed polymer. Journal of Polymer Science: Polymer Physics Edition. 1975;13:1795-808.
[203] Agmon N. The grotthuss mechanism. Chemical Physics Letters. 1995;244:456-62.
[204] Varcoe JR, Slade RCT. Prospects for Alkaline Anion Exchange Membranes in Low Temperature Fuel Cells. Fuel cells. 2005;5:187-200.

[205] Markovic N, Gasteiger H, Ross PN. Kinetics of oxygen reduction on Pt (hkl) electrodes: Implications for the crystallite size effect with supported Pt electrocatalysts. Journal of the Electrochemical Society. 1997;144:1591.
[206] Tang DP, Pan J, Lu SF, Zhuang L, Lu JT. Alkaline polymer electrolyte fuel cells: Principle, challenges, and recent progress. SCIENCE CHINA Chemistry. 2010;53:357-64.
[207] Gu S, Cai R, Luo T, Chen Z, Sun M, Liu Y, et al. A Soluble and Highly Conductive Ionomer for High Performance Hydroxide Exchange Membrane Fuel Cells. Angewandte Chemie International Edition. 2009;48:6499-502.
[208] Ilie A, Simoes M, Baranton S, Coutanceau C, Martemianov S. Influence of operational parameters and of catalytic materials on electrical performance of Direct Glycerol Solid Alkaline Membrane Fuel Cells. Journal of Power Sources. 2011.
[209] Li Y, Zhao T. A high-performance integrated electrode for anion-exchange membrane direct ethanol fuel cells. International Journal of Hydrogen Energy. 2011.
[210] Neagu V, Bunia I. Acrylic weak base anion exchangers and their chemical stability in aggressive media. Polymer degradation and stability. 2004;83:133-8.
[211] Zagorodni AA, Kotova DL, Selemenev VF. Infrared spectroscopy of ion exchange resins: chemical deterioration of the resins. Reactive and Functional Polymers. 2002;53:157-71.
[212] Browning DJ, Lovell KV, Horsfall JA, Waring SC. ANION EXCHANGE MEMBRANES. Google Patents; 2008.
[213] Wang S, McGrath J. Synthesis of Poly (arylene ether) s. Synthetic Methods in Step-Growth Polymers: Wiley: New York; 2003. p. 327-74.
[214] Capodanno V, Petrillo E, Romano G, Russo R, Vittoria V. Effect of physical aging on the properties of films of amorphous poly (ether ether ketone)(PEEK). Journal of Applied Polymer Science. 1997;65:2635-41.
[215] Cassidy P, Aminabhavi T, Farley J. Macromol. Sci, Rev. Macromol Chem Phys, C. 1989;29:365.
[216] Meier-Haack J, Taeger A, Vogel C, Schlenstedt K, Lenk W, Lehmann D. Membranes from sulfonated block copolymers for use in fuel cells. Separation and purification technology. 2005;41:207-20.
[217] Abuin GC, Nonjola P, Franceschini EA, Izraelevitch FH, Mathe MK, Corti HR. Characterization of an anionic-exchange membranes for direct methanol alkaline fuel cells. International Journal of Hydrogen Energy. 2010;35:5849-54.
[218] Bauer B, Strathmann H, Effenberger F. Anion-exchange membranes with improved alkaline stability. Desalination. 1990;79:125-44.
[219] Trostyanskaya E, Makarova S. Anion exchangers onium class of compounds. Zhurnal Prikladnoi Khimii. 1966;39:1754.
[220] Cheng JP, Liu B, Zhang XM. Radical Substituent Effects of Î±-Sulfonium Groups. The Journal of Organic Chemistry. 1998;63:7574-5.
[221] Zhang XM, Bordwell FG. Equilibrium acidities and homolytic bond dissociation energies of the acidic carbon-hydrogen bonds in P-substituted triphenylphosphonium cations. Journal of the American Chemical Society. 1994;116:968-72.
[222] Mikhailenko S, Guiver M, Kaliaguine S. Measurements of PEM conductivity by impedance spectroscopy. Solid State Ionics. 2008;179:619-24.
[223] Wright ME, Toplikar EG, Svejda SA. Details concerning the chloromethylation of soluble high-molecular-weight polystyrene using dimethoxymethane, thionyl chloride, and a Lewis acid: a full analysis. Macromolecules. 1991;24:5879-80.
[224] Li L, Wang Y. Quaternized polyethersulfone Cardo anion exchange membranes for direct methanol alkaline fuel cells. Journal of Membrane Science. 2005;262:1-4.

[225] Tripathi BP, Kumar M, Shahi VK. Organic-inorganic hybrid alkaline membranes by epoxide ring opening for direct methanol fuel cell applications. Journal of Membrane Science. 2010;360:90-101.
[226] Guo M, Fang J, Xu H, Li W, Lu X, Lan C, et al. Synthesis and characterization of novel anion exchange membranes based on imidazolium-type ionic liquid for alkaline fuel cells. Journal of Membrane Science. 2010;362:97-104.
[227] Vinodh R, Ilakkiya A, Elamathi S, Sangeetha D. A novel anion exchange membrane from polystyrene (ethylene butylene) polystyrene: Synthesis and characterization. Materials Science and Engineering: B. 2010;167:43-50.
[228] Wang J, Li S, Zhang S. Novel hydroxide-conducting polyelectrolyte composed of an poly (arylene ether sulfone) containing pendant quaternary guanidinium groups for alkaline fuel cell applications. Macromolecules. 2010;43:3890-6.
[229] Xu H, Fang J, Guo M, Lu X, Wei X, Tu S. Novel anion exchange membrane based on copolymer of methyl methacrylate, vinylbenzyl chloride and ethyl acrylate for alkaline fuel cells. Journal of Membrane Science. 2010;354:206-11.
[230] Hind A, Bhargava S, Grocott S. Adsorption of quaternary ammonium compounds on the surface of sodium oxalate: FTIR/ATR investigation under high-ionic-strength, highly alkaline conditions. Langmuir. 1997;13:6255-9.
[231] Goh YT, Patel R, Im SJ, Kim JH, Min BR. Synthesis and characterization of poly (ether sulfone) grafted poly (styrene sulfonic acid) for proton conducting membranes. Korean Journal of Chemical Engineering. 2009;26:518-22.
[232] Wang J, Zhao Z, Gong F, Li S, Zhang S. Synthesis of Soluble Poly (arylene ether sulfone) Ionomers with Pendant Quaternary Ammonium Groups for Anion Exchange Membranes. Macromolecules. 2009;42:8711-7.
[233] Gu S, He G, Wu X, Li C, Liu H, Lin C, et al. Synthesis and characteristics of sulfonated poly (phthalazinone ether sulfone ketone)(SPPESK) for direct methanol fuel cell (DMFC). Journal of Membrane Science. 2006;281:121-9.
[234] Jun Y, Zarrin H, Fowler M, Chen Z. Functionalized titania nanotube composite membranes for high temperature proton exchange membrane fuel cells. International Journal of Hydrogen Energy. 2011.
[235] Tanaka M, Fukasawa K, Nishino E, Yamaguchi S, Yamada K, Tanaka H, et al. Anion Conductive Block Poly (arylene ether) s: Synthesis, Properties, and Application in Alkaline Fuel Cells. Journal of the American Chemical Society. 2011.
[236] Zawodzinski Jr TA, Derouin C, Radzinski S, Sherman RJ, Smith VT, Springer TE, et al. Water uptake by and transport through Nafion 117 membranes. Journal of the Electrochemical Society. 1993;140:1041.
[237] Pan J, Lu S, Li Y, Huang A, Zhuang L, Lu J. High-Performance Alkaline Polymer Electrolyte for Fuel Cell Applications. Advanced Functional Materials. 2010;20:312-9.
[238] Shevchenko V, Gumennaya M. Synthesis and properties of anion-exchange membranes for fuel cells. Theoretical and Experimental Chemistry. 2010:1-14.
[239] Dopp RB, Stein SZ. Electrochemical Devices, Systems, and Methods. 0114496 ed. US2011. p. 0114496.
[240] Antolini E, Gonzalez E. Alkaline direct alcohol fuel cells. Journal of Power Sources. 2010;195:3431.
[241] Luo H, Vaivars G, Agboola B, Mathe M. Anion exchange membrane based on alkali doped poly (2, 5-benzimidazole) for fuel cell. Solid State Ionics. 2011;208:52.

[242] Xia Z, Yuan S, Jiang G, Guo X, Fang J, Liu L, et al. Polybenzimidazoles with pendant quaternary ammonium groups as potential anion exchange membranes for fuel cells. Journal of Membrane Science. 2012;390-391:152.
[243] Adams LA, Poynton SD, Tamain C, Slade RCT, Varcoe JR. A Carbon Dioxide Tolerant Aqueous-Electrolyte-Free Anion-Exchange Membrane Alkaline Fuel Cell. ChemSusChem. 2008;1:79.
[244] Gülzow E. Alkaline fuel cells: a critical view. Journal of Power Sources. 1996;61:99.
[245] Hoogers G. Fuel cell technology handbook. United States of America: CRC Press LLC; 2003.
[246] McLean G, Niet T, Prince-Richard S, Djilali N. An assessment of alkaline fuel cell technology. International Journal of Hydrogen Energy. 2002;27:507.
[247] Couture G, Alaaeddine A, Boschet F, Ameduri B. Polymeric materials as anion-exchange membranes for alkaline fuel cells. Progress in Polymer Science. 2011;36:1521.
[248] Merle G, Wessling M, Nijmeijer K. Anion exchange membranes for alkaline fuel cells: A review. Journal of Membrane Science. 2011;377:1.
[249] Wang Y-J, Qiao J, Baker R, Zhang J. Alkaline polymer electrolyte membranes for fuel cell applications. Chemical Society Reviews. 2013.
[250] Li Q, He R, Jensen J, Bjerrum N. PBI-Based Polymer Membranes for High Temperature Fuel Cells–Preparation, Characterization and Fuel Cell Demonstration. Fuel cells. 2004;4:147.
[251] Mecerreyes D, Grande H, Miguel O, Ochoteco E, Marcilla R, Cantero I. Porous polybenzimidazole membranes doped with phosphoric acid: highly proton-conducting solid electrolytes. Chemistry of Materials. 2004;16:604.
[252] Mustarelli P. Polymer fuel cells based on polybenzimidazole/H3PO4. Energy Environ Sci. 2012;5:6436.
[253] Quartarone E, Mustarelli P, Carollo A, Grandi S, Magistris A. PBI composite and nanocomposite membranes for PEMFCs: the role of the filler. Fuel cells. 2009;9:231.
[254] Shen CH, Jheng L, Hsu SL, Wang JTW. Phosphoric acid-doped cross-linked porous polybenzimidazole membranes for proton exchange membrane fuel cells. J Mater Chem. 2011;21:15660.
[255] Wang S, Zhao C, Ma W, Zhang G, Liu Z, Ni J, et al. Preparation and properties of epoxy-cross-linked porous polybenzimidazole for high temperature proton exchange membrane fuel cells. Journal of Membrane Science. 2012;411-412:54.
[256] Li N, Yan T, Li Z, Thurn-Albrecht T, Binder WH. Comb-shaped polymers to enhance hydroxide transport in anion exchange membranes. Energy & Environmental Science. 2012;5:7888.
[257] Xiong Y, Liu QL, Zeng QH. Quaternized cardo polyetherketone anion exchange membrane for direct methanol alkaline fuel cells. Journal of Power Sources. 2009;193:541.
[258] Fang J, Shen PK. Quaternized poly (phthalazinon ether sulfone ketone) membrane for anion exchange membrane fuel cells. Journal of Membrane Science. 2006;285:317.
[259] Unlu M, Zhou J, Kohl PA. Anion exchange membrane fuel cells: experimental comparison of hydroxide and carbonate conductive ions. Electrochemical and Solid-State Letters. 2009;12:B27.
[260] Wang E, Zhao T, Yang W. Poly (vinyl alcohol)/3-(trimethylammonium) propyl-functionalized silica hybrid membranes for alkaline direct ethanol fuel cells. International Journal of Hydrogen Energy. 2010;35:2183-9.
[261] Deavin OI, Murphy S, Ong AL, Poynton SD, Zeng R, Herman H, et al. Anion-exchange membranes for alkaline polymer electrolyte fuel cells: Comparison of pendent benzyltrimethylammonium-and benzylmethylimidazolium-head-groups. Energy & Environmental Science. 2012:DOI: 10.1039/c2ee22466f.

[262] Wang Y, Qiu J, Peng J, Xu L, Li J, Zhai M. Study on the chemical stability of the anion exchange membrane of grafting dimethylaminoethyl methacrylate. Journal of Membrane Science. 2011;376:70.
[263] Chatfield DA, Einhorn IN. Stepwise thermal degradation of a polybenzimidazole foam. Journal of Polymer Science: Polymer Chemistry Edition. 1981;19:601.
[264] Gieselman MB, Reynolds JR. Aramid and imidazole based polyelectrolytes: physical properties and ternary phase behavior with poly (benzobisthiazole) in methanesulfonic acid. Macromolecules. 1993;26:5633.
[265] Gray D, Shulman GP, Conley R. The Mechanism of Polybenzimidazole Formation by Condensation of Aromatic Tetramines and Esters and the Structure of the Resulting Polycondensates. Journal of Macromolecular Science—Chemistry. 1967;1:395.
[266] Musto P, Karasz F, MacKnight W. Fourier transform infra-red spectroscopy on the thermo-oxidative degradation of polybenzimidazole and of a polybenzimidazole/polyetherimide blend. Polymer. 1993;34:2934.
[267] Shulman GP, Lochte W. Thermal Degradation of Polymers. IV. Poly-2, 2′-(m-phenylene)-5, 5′-bibenzimidazole. Journal of Macromolecular Science—Chemistry. 1967;1:413.
[268] Weng D, Wainright J, Landau U, Savinell R. Electro-osmotic Drag Coefficient of Water and Methanol in Polymer Electrolytes at Elevated Temperatures. Journal of the Electrochemical Society. 1996;143:1260.
[269] Hou H, Sun G, He R, Sun B, Jin W, Liu H, et al. Alkali doped polybenzimidazole membrane for alkaline direct methanol fuel cell. International Journal of Hydrogen Energy. 2008;33:7172.
[270] Hou H, Sun G, He R, Wu Z, Sun B. Alkali doped polybenzimidazole membrane for high performance alkaline direct ethanol fuel cell. Journal of Power Sources. 2008;182:95.
[271] Hou H, Wang S, Jiang Q, Jin W, Jiang L, Sun G. Durability study of KOH doped polybenzimidazole membrane for air-breathing alkaline direct ethanol fuel cell. Journal of Power Sources. 2011;196:3244-8.
[272] Modestov A, Tarasevich M, Leykin AY, Filimonov VY. MEA for alkaline direct ethanol fuel cell with alkali doped PBI membrane and non-platinum electrodes. Journal of Power Sources. 2009;188:502.
[273] Nores-Pondal FJ, Buera MP, Corti HR. Thermal properties of phosphoric acid-doped polybenzimidazole membranes in water and methanol–water mixtures. Journal of Power Sources. 2010;195:6389-97.
[274] Aharoni SM, Litt MH. Synthesis and some properties of poly-(2, 5-trimethylene benzimidazole) and poly-(2, 5-trimethylene benzimidazole hydrochloride). Journal of Polymer Science: Polymer Chemistry Edition. 1974;12:639.
[275] Aharoni SM, Signorelli AJ. Electrical resistivity and ESCA studies on neutral poly (alkylbenzimidazoles), their salts, and complexes. Journal of applied polymer science. 1979;23:2653.
[276] Hoel D, Grunwald E. High protonic conduction of polybenzimidazole films. The Journal of Physical Chemistry. 1977;81:2135.
[277] Pohl HA, Chartoff RP. Carriers and unpaired spins in some organic semiconductors. Journal of Polymer Science Part A: General Papers. 1964;2:2787.
[278] Tomlin D, Fratini A, Hunsaker M, Wade Adams W. The role of hydrogen bonding in rigid-rod polymers: the crystal structure of a polybenzobisimidazole model compound. Polymer. 2000;41:9003.
[279] Cheddie DF, Munroe NDH. A two-phase model of an intermediate temperature PEM fuel cell. International Journal of Hydrogen Energy. 2007;32:832.
[280] Hu J, Zhang H, Zhai Y, Liu G, Yi B. Performance degradation studies on PBI/H3PO4 high temperature PEMFC and one-dimensional numerical analysis. Electrochimica acta. 2006;52:394-401.

[281] Pasupathi S, Ji S, Jan Bladergroen B, Linkov V. High DMFC performance output using modified acid–base polymer blend. International Journal of Hydrogen Energy. 2008;33:3132.
[282] Quartarone E, Mustarelli P, Magistris A. Transport properties of porous PVDF membranes. The Journal of Physical Chemistry B. 2002;106:10828.
[283] Saito Y, Kataoka H, Capiglia C, Yamamoto H. Ionic conduction properties of PVDF-HFP type gel polymer electrolytes with lithium imide salts. The Journal of Physical Chemistry B. 2000;104:2189.
[284] Eguizábal A, Lemus J, Urbiztondo M, Garrido O, Soler J, Blazquez J, et al. Novel hybrid membranes based on polybenzimidazole and ETS-10 titanosilicate type material for high temperature proton exchange membrane fuel cells: A comprehensive study on dense and porous systems. Journal of Power Sources. 2011;196:8994-9007.
[285] van de Ven E, Chairuna A, Merle G, Benito SP, Borneman Z, Nijmeijer K. Ionic liquid doped polybenzimidazole membranes for high temperature Proton Exchange Membrane fuel cell applications. Journal of Power Sources. 2013;222:202-9.
[286] Li J, Li X, Yu S, Hao J, Lu W, Shao Z, et al. Porous polybenzimidazole membranes doped with phosphoric acid: Preparation and application in high-temperature proton-exchange-membrane fuel cells. Energy Conversion and Management. 2014;85:323-7.
[287] Eguizábal A, Sgroi M, Pullini D, Ferain E, Pina M. Nanoporous PBI membranes by track etching for high temperature PEMs. Journal of Membrane Science. 2014;454:243-52.
[288] Merle G, Chairuna A, Ven EVd, Nijmeijer K. An easy method for the preparation of anion exchange membranes: Graft-polymerization of ionic liquids in porous supports. Journal of applied polymer science. 2013;129:1143-50.
[289] Jheng L-C, Hsu SL-C, Tsai T-Y, Chang WJ-Y. A novel asymmetric polybenzimidazole membrane for high temperature proton exchange membrane fuel cells. Journal of Materials Chemistry A. 2014;2:4225-33.
[290] Yu S, Zhang H, Xiao L, Choe EW, Benicewicz B. Synthesis of Poly (2, 2′-(1, 4-phenylene) 5, 5′-bibenzimidazole)(para-PBI) and Phosphoric Acid Doped Membrane for Fuel Cells. Fuel cells. 2009;9:318-24.
[291] Ainla A, Brandell D. Nafion®–polybenzimidazole (PBI) composite membranes for DMFC applications. Solid State Ionics. 2007;178:581.
[292] Musto P, Karasz F, MacKnight W. Hydrogen bonding in polybenzimidazole/polyimide systems: a Fourier-transform infra-red investigation using low-molecular-weight monofunctional probes. Polymer. 1989;30:1012.
[293] Pan J, Chen C, Zhuang L. Membranes for Alkaline Polyelectrolyte Fuel Cells. Non-Noble Metal Fuel Cell Catalysts. 2014:243-70.
[294] Danks TN, Slade RC, Varcoe JR. Comparison of PVDF-and FEP-based radiation-grafted alkaline anion-exchange membranes for use in low temperature portable DMFCs. Journal of Materials Chemistry. 2002;12:3371-3.
[295] Herman H, Slade RC, Varcoe JR. The radiation-grafting of vinylbenzyl chloride onto poly (hexafluoropropylene-co-tetrafluoroethylene) films with subsequent conversion to alkaline anion-exchange membranes: optimisation of the experimental conditions and characterisation. Journal of Membrane Science. 2003;218:147-63.
[296] Tzanetakis N, Varcoe J, Slade R, Scott K. Radiation-grafted PVDF anion exchange membrane for salt splitting. Desalination. 2005;174:257-65.
[297] Fang J, Yang Y, Lu X, Ye M, Li W, Zhang Y. Cross-linked, ETFE-derived and radiation grafted membranes for anion exchange membrane fuel cell applications. International Journal of Hydrogen Energy. 2012;37:594-602.

[298] Liu H, Yang S, Wang S, Fang J, Jiang L, Sun G. Preparation and characterization of radiation-grafted poly (tetrafluoroethylene-co-perfluoropropyl vinyl ether) membranes for alkaline anion-exchange membrane fuel cells. Journal of Membrane Science. 2011;369:277-83.
[299] Wan Y, Peppley B, Creber KA, Bui VT. Anion-exchange membranes composed of quaternized-chitosan derivatives for alkaline fuel cells. Journal of power sources. 2010;195:3785-93.
[300] Li N, Zhang Q, Wang C, Lee YM, Guiver MD. Phenyltrimethylammonium Functionalized Polysulfone Anion Exchange Membranes†. Macromolecules. 2012;45:2411-9.
[301] Zhang F, Zhang H, Qu C. Imidazolium functionalized polysulfone anion exchange membrane for fuel cell application. Journal of Materials Chemistry. 2011;21:12744-52.
[302] Arges CG, Kulkarni S, Baranek A, Pan K-J, Jung M-S, Patton D, et al. Quarternary Ammonium and Phosphonium Based Anion Exchange Membranes for Alkaline Fuel Cells. ECS Transactions. 2010;33:1903-13.
[303] Fu J, Qiao J, Lv H, Ma J, Yuan X-Z, Wang H. Alkali doped poly (vinyl alcohol)(PVA) for anion-exchange membrane fuel cells: Ionic conductivity, chemical stability and FT-IR characterizations. ECS Transactions. 2010;25:15-23.
[304] Lewandowski A, Skorupska K, Malinska J. Novel poly (vinyl alcohol)–KOH–H< sub> 2</sub> O alkaline polymer electrolyte. Solid State Ionics. 2000;133:265-71.
[305] Nikolić VM, Žugić DL, Maksić AD, Šaponjić DP, Marčeta Kaninski MP. Performance comparison of modified poly (vinyl alcohol) based membranes in alkaline fuel cells. International Journal of Hydrogen Energy. 2011;36:11004-10.
[306] Sang S, Wu Q, Gan Z. Influences of doping approach on conductivity of composite alkaline solid polymer electrolyte PVA–HA–KOH–H< sub> 2</sub> O. Electrochimica Acta. 2008;53:5065-70.
[307] Vinodh R, Sangeetha D. A Novel Composite Membrane from QPSU and SiO2 for Solid Alkaline Fuel Cell Applications. International Journal of Green Energy. 2012.
[308] Wu C, Xu T, Yang W. Synthesis and characterizations of novel, positively charged poly (methyl acrylate)–SiO< sub> 2</sub> nanocomposites. European polymer journal. 2005;41:1901-8.
[309] Wu Y, Wu C, Yu F, Xu T, Fu Y. Free-standing anion-exchange PEO–SiO< sub> 2</sub> hybrid membranes. Journal of Membrane Science. 2008;307:28-36.
[310] Xu T. Ion exchange membranes: state of their development and perspective. Journal of Membrane Science. 2005;263:1-29.
[311] Zhang S, Wu C, Xu T, Gong M, Xu X. Synthesis and characterizations of anion exchange organic–inorganic hybrid materials based on poly (2, 6-dimethyl-1, 4-phenylene oxide)(PPO). Journal of Solid State Chemistry. 2005;178:2292-300.
[312] Zhang S, Xu T, Wu C. Synthesis and characterizations of novel, positively charged hybrid membranes from poly (2, 6-dimethyl-1, 4-phenylene oxide). Journal of Membrane Science. 2006;269:142-51.
[313] Wu Y, Wu C, Li Y, Xu T, Fu Y. PVA-silica anion-exchange hybrid membranes prepared through a copolymer crosslinking agent. Journal of Membrane Science. 2010;350:322.
[314] Guo TY, Zeng QH, Zhao CH, Liu QL, Zhu AM, Broadwell I. Quaternized polyepichlorohydrin/PTFE composite anion exchange membranes for direct methanol alkaline fuel cells. Journal of Membrane Science. 2011;371:268-75.
[315] Qu C, Zhang H, Zhang F, Liu B. A high-performance anion exchange membrane based on bi-guanidinium bridged polysilsesquioxane for alkaline fuel cell application. Journal of Materials Chemistry. 2012;22:8203.
[316] Zhang F, Zhang H, Ren J, Qu C. PTFE based composite anion exchange membranes: thermally induced in situ polymerization and direct hydrazine hydrate fuel cell application. Journal of Materials Chemistry. 2010;20:8139-46.

[317] Voigt WV. Water stable, antimicrobial active nanofibres generated by electrospinning from aqueous spinning solutions: Universitätsbibliothek; 2009.
[318] Szczepanowicz K, Para G, Bouzga AM, Simon C, Yang J, Warszynski P. Hydrolysis of silica sources: APS and DTSACl in microencapsulation processes. Fizykochemiczne Problemy Mineralurgii. 2012;48:403-12.
[319] Walcarius A, Ganesan V. Ion-exchange properties and electrochemical characterization of quaternary ammonium-functionalized silica microspheres obtained by the surfactant template route. Langmuir. 2006;22:469-77.
[320] Hummers Jr WS, Offeman RE. Preparation of graphitic oxide. Journal of the American Chemical Society. 1958;80:1339-.
[321] Marcano DC, Kosynkin DV, Berlin JM, Sinitskii A, Sun Z, Slesarev A, et al. Improved synthesis of graphene oxide. ACS nano. 2010;4:4806-14.
[322] Li Z, Lu C, Xia Z, Zhou Y, Luo Z. X-ray diffraction patterns of graphite and turbostratic carbon. Carbon. 2007;45:1686-95.
[323] Huh SH. Thermal reduction of graphene oxide. Physics and Applications of Graphene—Experiments, edited by S Mikhailov (InTech, New York, 2011). 2011.
[324] Jeong H-K, Lee YP, Lahaye RJ, Park M-H, An KH, Kim IJ, et al. Evidence of graphitic AB stacking order of graphite oxides. Journal of the American Chemical Society. 2008;130:1362-6.
[325] He H, Gao C. General approach to individually dispersed, highly soluble, and conductive graphene nanosheets functionalized by nitrene chemistry. Chemistry of Materials. 2010;22:5054-64.
[326] Wang Y, Shi Z, Fang J, Xu H, Yin J. Graphene oxide/polybenzimidazole composites fabricated by a solvent-exchange method. Carbon. 2011;49:1199-207.
[327] Xu C, Cao Y, Kumar R, Wu X, Wang X, Scott K. A polybenzimidazole/sulfonated graphite oxide composite membrane for high temperature polymer electrolyte membrane fuel cells. Journal of Materials Chemistry. 2011;21:11359-64.
[328] Haubner K, Murawski J, Olk P, Eng LM, Ziegler C, Adolphi B, et al. The route to functional graphene oxide. ChemPhysChem. 2010;11:2131-9.
[329] Yan W, Huang Y, Xu Y, Huang L, Chen Y. Rapid and Effective Functionalization of Graphene Oxide by Ionic Liquid. Journal of nanoscience and nanotechnology. 2012;12:2270-7.
[330] Compton OC, Dikin DA, Putz KW, Brinson LC, Nguyen ST. Electrically conductive "alkylated" graphene paper via chemical reduction of amine-functionalized graphene oxide paper. Advanced Materials. 2010;22:892-6.
[331] Tang X-Z, Li W, Yu Z-Z, Rafiee MA, Rafiee J, Yavari F, et al. Enhanced thermal stability in graphene oxide covalently functionalized with 2-amino-4, 6-didodecylamino-1, 3, 5-triazine. Carbon. 2011;49:1258-65.
[332] Launer PJ. Infrared analysis of organosilicon compounds: spectra-structure correlations. Silicone Compounds Register and Review. 1987:100-3.
[333] Wang SJ, Geng Y, Zheng Q, Kim J-K. Fabrication of highly conducting and transparent graphene films. Carbon. 2010;48:1815-23.
[334] Xue Y, Liu Y, Lu F, Qu J, Chen H, Dai L. Functionalization of graphene oxide with polyhedral oligomeric silsesquioxane (POSS) for multifunctional applications. The Journal of Physical Chemistry Letters. 2012;3:1607-12.
[335] Yang WJ, Neoh K-G, Kang E-T, Teo SL-M, Rittschof D. Stainless steel surfaces with thiol-terminated hyperbranched polymers for functionalization via thiol-based chemistry. Polymer Chemistry. 2013;4:3105-15.
[336] Liu G, Li X, Lee J-W, Popov BN. A review of the development of nitrogen-modified carbon-based catalysts for oxygen reduction at USC. Catalysis Science & Technology. 2011;1:207-17.

[337] Yang X, Tu Y, Li L, Shang S, Tao X-m. Well-dispersed chitosan/graphene oxide nanocomposites. ACS Applied Materials & Interfaces. 2010;2:1707-13.
[338] Zhang WL, Choi HJ. Silica-graphene oxide hybrid composite particles and their electroresponsive characteristics. Langmuir. 2012;28:7055-62.
[339] Stankovich S, Dikin DA, Piner RD, Kohlhaas KA, Kleinhammes A, Jia Y, et al. Synthesis of graphene-based nanosheets via chemical reduction of exfoliated graphite oxide. Carbon. 2007;45:1558-65.